Zhengyu Jin

Functional Starch and Applications in Food

Springer

Functional Starch and Applications in Food

Zhengyu Jin
Editor

Functional Starch and Applications in Food

Springer

Editor
Zhengyu Jin
School of Food Science and Technology
Jiangnan University
Wuxi, Jiangsu, China

ISBN 978-981-13-1076-8 ISBN 978-981-13-1077-5 (eBook)
https://doi.org/10.1007/978-981-13-1077-5

Library of Congress Control Number: 2018952231

This Springer imprint is published by the registered company Springer Nature Singapore Pte Ltd.
The registered company address is: 152 Beach Road, #21-01/04 Gateway East, Singapore 189721, Singapore

Contents

Chapter 1
The Overview of Functional Starch

Chunsen Wu and Xing Zhou

1.1 Introduction

Starch is the most abundant reserve carbohydrate which can be found in different plant organs such as tubers, roots, leaves, fruits, and seeds. In the human diet, the grains of rice, wheat, and maize, or the tubers of potato and cassava, are staple foodstuffs and a major source of energy [1]. Most naturally occurring starch granules consist of two principal polysaccharides that are α-D-glucoses linked together in two different forms. Amylopectin, the major macromolecular component in most starch granules (comprising 70–80%), is an extensively branched molecule that consists of α-1→4-linked short α-D-glucosyl chains connected at their reducing ends by α-1→6 linkages [2]. The percentage of α-1→6 branches of amylopectin in most starches is about 4–6% [2]. Amylose is the minor fraction present in starch granules, which is traditionally defined as a linear molecule of only α-D-glucose connected by α-1→4 linkages; but, it is well established that some amylose molecules possess low levels of α-1→6 branches (<1%) [3]. It has also been proposed that the presence of branches does not significantly alter the solution behavior of amylose chains, which remain identical to that of strict linear chains [4]. Starch is biosynthesized as semicrystalline granules with varying polymorphic types and degrees of crystallinity [5]. The complex organization of the α-1→6 branches is assumed to support the semicrystalline dense packing regions in the starch granules [6]. Amylose cannot adopt a semicrystalline structure independently and is therefore not amenable to common testing methods. Nowadays, it is still unclear how the amylose interacts with amylopectin, as well as the respective contribution to

C. Wu
College of Food Science and Engineering, Yangzhou University, Yangzhou, Jiangsu, China
e-mail: wuchunsen@yzu.edu.cn

X. Zhou (✉)
School of Food Science and Technology, Jiangnan University, Wuxi, Jiangsu, China
e-mail: zhouxing@jiangnan.edu.cn

Z. Jin (ed.), *Functional Starch and Applications in Food*,
https://doi.org/10.1007/978-981-13-1077-5_1

crystallinity in starch granules. It is universally recognized that the organization of starch granules is very complicated and depends strongly on the botanical origin, which gives the different structure, functionality, processability, and palatability of starches [7].

The starches from different sources differ significantly in their physicochemical, rheological, thermal, and retrogradation properties, and there has been a great increase in demand for starch with specific functionality as additives in food systems. Potato starch granules are smooth-surfaced, oval, and irregular or cuboidal-shaped, are rich in esterified phosphorus, and exhibit higher swelling power, solubility, paste clarity, and viscosity [8]. Cereal starches such as corn, rice, and wheat starches are smaller in granule size, possessing less phospholipids and a higher tendency toward retrogradation when compared with potato starch [8]. In practice, starch with desirable functional properties can play an important role as a good texture stabilizer and regulator in food systems, whereas starch in its native form lacks the versatility to function adequately in the whole range of food product, due to its relatively low solubility, shear resistance, thermal resistance, and pH (acid) resistance and high tendency toward retrogradation.

Food processing industries and consumers require starches to have better behavior characteristics than that provided by native starches. Fortunately, shortcomings of native starches can be overcome by chemical, physical, or enzymatical modification. Functional starch is designated as modified starch with specific functional properties such as physiological function, healthy benefits, absorption function, sustained slow energy release, and other functions endowed via different modification methods. There has been intense interest among researchers to develop novel methods for functional starch preparation, with more emphasis on enzymatic and physical modifications. The multiscale structures of the physicochemical properties of functional starch have been well evaluated by modern analytical techniques. Based on these, this chapter will briefly introduce the variety, preparation, characterization, and application of functional starch in the food industry.

1.2 Characterization of Functional Starch

Modified starches have been the subject of intensive research over many decades, resulting in a vast body of published studies on functional starch with newly developed functionalities. The preparation of functional starch is an ongoing process as there are numerous possibilities, resulting from an evolution of new processing technologies and market trends. Slowly digestible starch, resistant starch, porous starch, starch microemulsions, nano-sized starch, and starch copolymers are the major varieties of functional starches that can be used in the food industry.

1.2.1 Slowly Digestible Starch (SDS)

Slowly digestible starch (SDS) is defined as the starch fraction that is slowly digested throughout the small intestine, resulting in a low initial glycemia and, subsequently, a slow and prolonged release of glucose into the blood steam, coupled to a low glycemic response in humans [9, 10]. Unlike most starch components, SDS is indigested by salivary α-amylase in the oral cavity and gastric acid in the stomach, or through the vigorous grinding action resulting from gastric mobility [9]. The healthy benefits of SDS are linked to a stable postprandial glucose metabolism [11], reduced meal-associated hyperglycemia of diabetes [12], and better mental performance of the brain [13, 14]. There are two fundamental metabolic mechanisms for SDS benefits based on its starch structure: the physical structure of the starch granule that limits the accessibility of digestive enzymes and the chemical structures that restrict the rate of digestive enzyme actions. Native starch granules are ideal SDS due to their semicrystalline physical structure with slow digestibility [15]. However, SDS will lose its slow digestible property if added in thermally processed starch food. In this regard, amylopectin is another important component of SDS, where the molecular structure itself, or the branching pattern, is key to the formation of starch molecules with slow digestibility [16]. Controlled enzymatic treatments of starch with debranching enzyme [17], amylosucrase [18], 4-α-glucanotransferase [19], α-amylase [20], and/or β-amylase [21] are successful in producing special molecular structures of starch with slow digestibility. However, all these tailor-made starches merely partially retain the slow digestibility after thermal processing. Therefore, the challenges for applications of SDS in the food industry are to improve the current stability issues by introducing new product designs or novel processing methods into the preparation of SDS.

1.2.2 Resistant Starch (RS)

Resistant starch (RS) is designated as the fraction of starch that escapes digestion in the small digestion of healthy individuals and may be fermented in the colon [22]. It has been classified into five general types depending on the structural characteristics and indigestible mechanisms of RS. RS1 is physically inaccessible starch in the food matrix, RS2 is native granular starch, RS3 is retrograded or crystalline non-granular starch formed through the reorganization of starch chains, RS4 is chemically modified or re-polymerized starch, and RS5 is amylose-lipid complexed starch [23]. RS can be fermented by the probiotic bacteria in the colon into short-chain fatty acids (principally acetate, propionate, butyrate, and lactate), along with a small quantity of gasses such as carbon dioxide, methane, and hydrogen [24].

Its physiological effects include colonic cancer prevention, hypoglycemic/hypocholesterolemia effects, prebiotic functions, as well as the inhibition of fat accumulation and bile stone formation, which contribute to the health effects of RS [25]. Thermal processing and retrogradation treatment, in combination with enzymatic and/or chemical treatment, are frequently used procedures in RS preparation. The unique properties of RS, such as its white color, bland favor, fine particle size, and high resistance in processing make it widely used in food products. In the future, novel processing methods should be developed regarding the preparation of new RS products from natural sources, to help lower the production costs of RS.

1.2.3 Porous Starch

Porous starch is a novel functionally modified starch with abundant micro-sized pores extending from the surface to the interior of the starch granules [26]. The pores covering the granule surface are approximately 1 μm in diameter, and their volume constitutes about half of the starch granule [26]. Amylase, with the ability to act on the surface of native starch granules at a temperature below that of starch gelatinization, can be used in porous starch preparation, where α-amylase and/or amyloglucosidase is the most often used enzymes [26]. Porous starch can also be prepared, when starch granules have been completely destroyed by replacing ice crystals in a frozen starch gel with selected solvents, using a solvent exchange technique [27, 28]. Porous starches effectively increase the specific surface area and serve as excellent natural absorbents [29]. In the food industry, porous starch can be used as carriers of sweeteners, flavorings, and colorants and also for the protection of sensitive elements such as phenolics, oils, minerals, vitamins, and probiotics [29–33]. Currently, chemical treatments are frequently introduced into porous starch preparations to improve the adsorption, stability, and controllability. Jiang et al. developed a porous chitosan-modified starch to improve the adsorption of procyanidins, which were fabricated by facile surface modification of chitosan on porous rice starch [34]. Chemical modifications, such as using succinic ester, citric acid, and/or xanthate combined with the solvent exchange technique, have been successful in improving the absorption behavior and stability of porous starch in aqueous solutions [27, 35, 36]. Further attempts should be encouraged to solve the processing stability of porous starch applicated in the food industry.

1.2.4 Starch Microemulsion

Microemulsions are clear, isotropic or translucent, thermodynamically stable dispersions comprised of oil, water, surfactant, cosurfactant, and ethanol [37, 38]. The microemulsion possesses special properties such as ultralow interfacial tension and

large interfacial tension with the capability to stabilize and solubilize otherwise immiscible liquids [39]. The most important use of starch microemulsion is as a medium for polymerization reactions [39]. Starch microemulsion is prepared by dropwise addition of a starch solution into an oil phase under mechanical stirring. There are several procedures developed to prepare starch microemulsions, such as solvent evaporation, spray drying, precipitation, and emulsion cross-linking techniques [40–42]. Starch microemulsion is normally designed to prepare starch microspheres and nanoparticles in the food industry.

1.2.5 Nano-sized Starch

Nano-sized starch, also called starch nanoparticles (SNs), is a kind of organic nanoparticle of 50–200 nm prepared from starch using chemical, enzymatic, and/or physical methods. During the previous decade, studies have been focused on nano-sized starch, due to its availability in nature, low cost, renewability, biocompatibility, biodegradability, and nontoxicity [43]. The native starch granules are micro-sized and can be broken down into nano-sized particles using different nanotechnology methods, which are grouped into "top-down" and "bottom-top" processes [44]. In the "top-down" process, nano-sized starch is prepared from structure and size refinement by the breakdown of larger starch particles [44]. In the "bottom-top" approach, nano-sized starch is produced from a buildup of atoms or molecules in a controlled manner, such as by self-assembly and nanoprecipitation from dropwise starch paste solutions [45, 46]. Currently, the "top-down" approach is the most employed method in nano-sized starch preparation. Acid hydrolysis, regeneration, and mechanical treatments are widely used for the preparation of nano-sized starch, and acid hydrolysis is the most commonly used protocol [44]. It is still difficult for scientists and food producers to obtain uniform nano-sized starch using a simple, economic, and high-yielding method at a commercial/industrial level. In the food industries, nano-sized starch can be used as a unique component for the regulation of physicochemical and rheological properties of processed foods, which are also found to have applications as emulsion stabilizers [47, 48], fat replacers [44], and nanocomposite agents in the food packaging industry [49, 50]. Innovative processing/modification approaches should be developed in order to solve the aggregation problem of nano-sized starch, thus greatly improving its application in the future.

1.2.6 Starch-Lipid and Starch-Protein Systems

Molecular inclusion is a superior technique for effective protection of sensitive substances, compared to conventional encapsulation procedures such as freeze drying, spray drying, conservation, and liposome entrapment because of the difficulty of

these methods in achieving the ideal process conditions to ensure effective coating of the compound to be protected [51]. Starch is nonallergenic, safe, and cheap; it provides a highly attractive alternative for use as a delivery system for the protection of sensitive and unstable substances [52]. There has been increasing interest in starch use in native and modified forms to encapsulate food ingredients such as flavones, lipids, polyphenols, carotenoids, vitamins, enzymes, and probiotics [53]. Starch in granular or amorphous forms are treated using chemical, physical, and/or enzymatic methods to confer the required properties for targeted encapsulation. The starch-based encapsulation of food ingredients is developed using various methods such as freeze drying, physical trapping, precipitation, spray drying, extrusion, complexation, electrospinning, emulsification, and electrostatic interaction [53]. Amylose inclusion is usually carried out at rather high temperatures of over 100 °C, but Vasiliadou et al. discovered that the production of crystallites of amylose complexed with lipids can be quantitatively achieved at temperature as low as 75 °C [51]. Therefore, it is possible to produce complexes under milder processing conditions where the substances will not suffer significant losses during complexation. The linear component of starch, especially amylose, can develop a helical structure with a hydrophobic cavity that can form inclusion complexes with hydrophobic ligands such as lipids, phenolics, and flavors [54, 55]. By forming an inclusion complex with amylose or starch, these active ingredients can be protected from the acidic environment of the stomach for targeting absorption in the small intestine, and in this manner, their bioavailability may be increased [56, 57]. Briefly, two methods, including coprecipitation and acidification of an alkaline solution, are commonly employed in starch-lipid complexation, while electrospinning-based complexation was recently reported [58]. Amylose-omega-3 fatty acid complexes can be incorporated into bread formulations and can then be reduced by lipid oxidation and the formation of nonanal and hexanal during the baking [59].

Proteins and starch interact with each other in foods when brought together, and the interactions may be repulsive (repel each other) or associative (attract one another) [60]. It has also been reported that protein-starch interactions are driven by the attraction of opposite changes between the macromolecules, but there may be significant influences of the gelatinization parameters (increase in onset and peak temperatures and decrease in the delta H) and water evaporation of the starch [61]. Starch and protein interactions have also been known to significantly alter macroscopic properties, such as flow, stability, texture, and "mouthfeel" of the food products [62, 63]. The development of starch-protein complexes is complicated; therefore, the reaction processes and end products are determined by many internal and external factors. The starch-protein complexes function to improve the solubility, viscosity, gelation, emulsification, foam-forming ability, and inoxidizability of the starch and/or protein. The starch-protein complexes can be used in starch gels [64], in snacks [65], for a clean food contact surface [66], in yogurt [67], and as an emulsifier [68]. Shah A. et al. have developed a soluble self-assembled complex from starch, proteins, and free fatty acids for healthy nutrient delivery as a nanoparticle carrier for hydrophobic small molecules [62, 63].

1.3 Preparation of Functional Starch

1.3.1 Chemical Modification

Chemical modification is a widely used method that involves the polymer molecules of the starch granule in its native form and enables the enhancement and/or introduction of functionality into the modified starch [69]. The common chemical modifications used in the food industry involve oxidation, cross-linking, stabilization, and depolymerization, as well as changes in the pasting properties, freeze-thaw stability, shear resistance, solubility, and digestibility [70]. The chemical treatments used for starch modification can be classified as depolymerization or derivatization reactions based on the molecule weight of the modified starch. Acid and oxidative modifications are depolymerization procedures used to produce thinned starch with decreased paste viscosity, lower gelatinization and pasting temperature, improved emulsification, increased solubility, and improved film properties (i.e., stiffness and water vapor permeability) [70, 71]. The chemical modifications of starch are generally achieved through derivatizations such as etherification, esterification, cross-linking, oxidation, cationization, grafting of starch, and chemical derivatization. In the US market, food starches are modified by using hydroxypropyl, acetate, phosphate, octenyl succinate, and adipate compounds [70, 72]. The consumer safety of chemically modified starch and the resulting pollution of the processing environment are not optimal and are therefore major drawbacks for chemical modification of starch. Thus, there is a considerable need to develop novel and cleaner methods for functional starch preparation with more emphasis on enzymatic, physical, and genetic modifications.

1.3.2 Physical Modification

Physical modification can be safely used in the preparation of functional starch because it usually does not involve any chemicals. Recently, novel physical modification methods have been introduced into this field [72].

1.3.2.1 Plasma Modification

Plasma is a medium that contains both negatively and positively charged particles with an overall electrical charge of zero. These include electrons, protons, negative and positive ions, free radicals, atoms, and non-excited or excited molecules [72, 73]. Plasma modification, which is a physical treatment that induces chemical changes, can be divided into two types, thermal and non-thermal, based on different generated conditions. Thermal plasma is generated at high pressure (up to 10^5 Pa)

and/or high temperature ($\geq 2 \times 10^4$ K) [74]. In contrast, nonthermal plasma processing is an emerging green technology that uses lower pressures with much less power input without generating industrial waste, resulting in a greater potential to improve the quality and microbial safety of various food materials [74]. There has been increasing interest in utilizing plasma to modify the functionalities of starch through interactions with reactive molecules. A range of techniques and instruments, such as coronal discharge, a gliding arc, and a plasma jet, have been used to generate nonthermal plasma. Plasma modification induces various chemical changes to the starch, which include depolymerization, cross-linking, and the formation and addition of new functional groups [75]. Plasma modification has been used to change the surface properties of various starch-based materials, including thermoplastic films and biocomposites [76], and the compatibility of starch-based biocomposites with proteins and cells [77]. The desired surface properties of starch can be obtained through carefully manipulating these factors, including the type of plasma, treatment conditions, and starch/composite type [72, 73]. Plasma treatment coupled with multiple starch modification should be further explored to create a range of starch functionalities in the future.

1.3.2.2 Hydrothermal Treatment

Annealing (ANN) and heat-moisture treatment (HMT) are two hydrothermal treatment procedures, which alter the physicochemical properties of starch without destroying its granular structure [78]. These two related processes differ in the amount of water and the temperatures used. ANN is carried out with excess water and relatively low temperatures (below the starch gelatinization temperature), while HMT uses heat at temperatures above the gelatinization temperatures (90–120 °C), but with insufficient water (10–30%) for gelatinization [79, 80]. Regardless of the origin, ANN improves the physicochemical properties of starch by improving the crystalline qualities and facilitating interactions between the starch chains to reorganize the starch molecules [80, 81]. HMT allows for the control of molecular mobility at high temperatures by limiting the amount of water used to promote a change in the structural arrangement of the starch chains within the amorphous and crystalline areas of the granules [82, 83]. The granular swelling, crystallinity, gelatinization, retrogradation, thermal stability, amylose leaching parameters, and paste properties are modulated by HMT [82, 83]. ANN- and HMT-modified starches are suitable for utilization in canned foods, noodle manufacturing, and frozen foods [79].

1.3.2.3 Ultrasonic Treatment

Ultrasonic treatment is a physical method employing high-frequency ultrasound (>15–20 kHz), which creates strong shear force, high temperatures and free radicals, and may result in changes in the structures and functions of starch in a starch-water system [84]. Ultrasound causes many pores and fissures in the starch granules, inducing either degradation or having little effect on the starch chain on the

molecular level [85]. New pores in the range of 1.7–300 nm may be existed during the ultrasonic treatment of starch [86]. Ultrasound could significantly change the thermal stability, retrogradation, and gel properties of starch, causing depressions on the surface of the starch granules [85]. The resulting cracks and pores in the starch granules greatly enhance the reaction efficiency of other chemical, physical, or enzymatic agents [84].

1.3.2.4 High-Pressure Treatment/Homogenization

High-pressure treatments (HPTs), such as ultrahigh-pressure and high hydrostatic pressure treatment, are nonthermal processing technologies suitable for the production of minimally processed foods. In the food industry, HPT is carried out at 100–1000 MPa and room temperature to modify and sterilize food packed materials in vessels [87]. At present, HPT has been successfully used for gelatinization of various types of starches while maintaining the integrity of the granules [88]. Compared with the conventional heat-gelatinized starches, HPT-gelatinized starches show dissimilar properties, such as lower swelling indices, lower rates of retrogradation, lower susceptibilities to amylolytic enzymes, and increased creaming stabilities [87, 89–92].

High-pressure homogenization (HPH) is different from static HPT, where liquid samples undergo cavitation, high shear, turbulence, and velocity gradients induced by a rapid change in pressure [93, 94]. In industry, homogenization pressure usually occurs between 20 and 50 MPa, and for ultra-HPH, the pressure can be above 100 MPa [95]. In the food industry, HPH is extensively used to disperse, emulsify, mix, and process the food substances [96, 97]. Starches are frequently processed by HPH with the purpose of imparting novel functional properties, producing new products, and/or isolating starch from other constituents [96]. HPH induces an inside-out disruption of starch granules, occurring close to the linkage among blocklets [96]. There have been increased applications of HPH in the field of starch-lipid complex preparation. HPH facilitated the rapid dispersion of lipids with lower water solubility and enhanced the chances of reactions between lipids and amylose [54, 98]. In addition, HPH has been used recently as an efficient emulsification technique to provide mechanical energy to produce miniemulsions for preparing nanoparticles [99].

1.3.2.5 Extrusion Processing

Extrusion cooking is a commercially promising technique used to process and produce large numbers of starch-based foods of varying shapes, sizes, tastes, and textures; it is a barothermal treatment that involves shear energy, pressure, and heating [100]. The main advantages of extrusion cooking are the ability to process highly viscous polymers in the presence of plasticizers and the promotion of significant structural qualities in the starch molecule. Changes for starch during extrusion include gelatinization, melting, degradation, and fragmentation [101]. The

disruption of molecular, supramolecular, and granular structure of starch depends on the barrel temperature, plasticizer content, screw speed, feeding rate, die size, and screw configuration used during the extrusion cooking process [102]. The intense shear force used during extrusion can cleave both α-1→6 and α-1→4 linkages of starch molecules and the starch ordered structures such as the double helical and crystalline structures. Amylopectin with short branch lengths is associated with higher susceptibility to shear degradation than the linear and smaller molecular weight amylose [103]. Extrusion degradation prefers cleavage of longer branches when the starch polymers are in a semicrystalline granular formation [103]. Moreover, the rigid crystal structure in amylopectin is more sensitive to shear treatments than the flexible amorphous structure of amylose [104]. Extrusion processing lowers the retrogradation degree [105], improves the freeze-thaw stability [106], and decreases the digestibility [100] of starches. Extrusion processing techniques have been successful in producing starch-based films [107], resistant starch [100], thermoplastic starch [108], starch-lipid complexes [109], and noodles [110] as well as preparing chemically modified starch as an initial reactant [111].

1.3.2.6 Microwave Irradiation

Microwaves are electromagnetic waves of 300 MHz to 300 GHz. For domestic food applications, the microwave usually operates at a frequency of 2.45 GHz, and industrial applications operate at frequencies of 915 MHz and 2.45 GHz [112]. Microwave irradiation has many applications in the food processing field, including drying, pasteurization, sterilization, thawing, tempering, and baking of food materials [112]. Microwaves create heat deep inside the materials being processed as a result of rapid alterations in the electromagnetic field at high frequency, thus achieving shorter processing time, higher yields, and better quality when compared with conventional processing techniques [113]. Microwave irradiation induces the rearrangement of crystalline structures within the starch granule leading to changes in the molecular structure and physicochemical properties, such as water absorption ability, swelling power, and viscosity [113, 114]. In addition, the advantages of microwave technology in promoting chemical reactions include lower energy use, improved reaction rates, simplification of procedures, and significantly reduced waste by-products from the chemical reaction production process [115]. Based on these properties, microwave irradiation was used to prepare insoluble starch composite foams [116], starch ester films [117], starch acetate [115], and resistant starch [118].

1.3.3 Enzymatic Modification

Enzymatic modification has been increasingly explored as an alternative technique to modify the granular and/or molecular structure to produce functional starches. The main advantages are the mild reaction conditions, high selectivity, and less

undesirable by-products than that of chemical processes that require harsh conditions and highly reactive compounds [119].

1.3.3.1 Acylation

Acylation reactions are performed by lipases and proteases to increase the hydrophobicity, reduce the viscosity, and decrease the digestibility of starch. Unlike chemical esterification modification, the enzymatic technique is an environmentally friendly method, which is operated under milder conditions with less by-products [120]. Regiospecific and stereospecific esterification of starch can be easily performed using enzymes [119]. The esterification of starch palmitic acid was catalyzed by Novozyme 435 lipase in a micro-solvent or solvent-free system to produce functional starches with emulsifying properties [120]. The esterification of starch catalyzed by lipase was also feasible on starch nanoparticles [121] and in aqueous gel systems [122].

1.3.3.2 Copolymerization

Copolymer preparation with specific structural and functional properties can be catalyzed by specific enzymes to achieve the coupling of starch with another polymer. Starch is rather difficult to substitute with aromatic or phenolic compounds by conventional chemical modification methods, because there are few reactive functional groups such as the hydroxyl groups [119]. Waxy maize starch is produced by sodium lignosulfonate using laccase, resulting in starch-sodium lignosulfonate copolymers with good antioxidant activity and cation binding properties [123].

1.3.3.3 Debranching Reaction

Pullulanase and isoamylase are two debranching enzymes that selectively hydrolyze the α-1→6 glycosidic bonds of starch in granular and gelatinized forms. Debranching reactions are normally performed by treating starch paste with pullulanase or isoamylase, leading to the formation of linear short chains and recrystallization under different storage conditions [124]. The modification of starch through debranching reactions introduces new properties and functionalities into the starch molecules, providing promising applications in the food industry attributed to the recrystallization and gel-forming properties of the debranched starches [124]. Debranched starches have shown great potential in the food industry as hypoglycemic foods [125], fat replacers [126], coating materials in ready-to-eat cereals [127], and tableting excipients [128], due mainly to their gelling properties. The molecular inclusion properties of debranched starch drive the formation of inclusion complexes, self-assembling spheroids, and nanoparticles [124].

1.3.3.4 Branching Reaction

The α-glucan branching enzymes are the only enzymes that catalyze transglycosylation reactions to form α-1→6 glucosidic bonds in amylopectin or glycogen, by breaking an α-1→4 glucosidic bond in starch and creating an α-1→6 glucosidic bond within a linear α-1→4 segment [129]. Branching enzymes can catalyze various substrates, thus activating different action mechanisms and subsequently producing different products, such as highly branched cyclic α-glucan and cluster dextrin [130]. The transfer activities of branching enzymes are activated and are higher in amylose-containing starch compared with that of amylose-free starch [131]. Branching reactions are widely used in tailoring starch into highly branched structures with slow digestion properties and improved three-dimensional embedding [17, 132, 133].

1.3.3.5 Hydrolyzing Reaction

Enzymatic modification systems have also been used (hydrolyzing enzymes) for the modification of starch to prepare starches with various functional qualities. The α-amylases and/or amyloglucosidases have the ability to attack the surface of raw granular starch at a temperature below the gelatinization temperature of starch and have been widely used in the preparation of granular starch [26]. There are more hydrolyzing enzymes now being tested for use in the modification of starch in gelatinized form. The use of amylomaltase to modify starch is expected to help to form thermo-reversible gels [134], fat replacers, and enhancers of creaminess in yogurt [135]. Further applications include its use in the food industry as a plant and chemical-free alternative to gelatin [136]. Amylosucrase is used to modify waxy cornstarch, to significantly elongate the chain length of the starches, resulting in the formation of precipitates [137]. In addition, several amylases, such as β-amylase [138], maltogenic α-amylase [138], cyclodextrin glycosyltransferase [139], and maltotriohydrolase [140], are used to improve the branch density of starches to produce functional starches with slow digestibility.

1.3.4 Multiple Modifications

For specific applications in the food industry, functional starches are always tailor-made with a combination of two or more modifications. Dual enzymatic modifications such as those catalyzed by branching enzymes and amylosucrase are employed for modification of starch to promote the formation of SDS and RS in sweet potato starch [141]. Cassava starch prepared by carboxymethyl modification and thermal α-amylase hydrolysis is an ideal fat replacer in low-fat and energy sausages [142]. Maize starches with different amylose contents are modified by acid-ethanol

treatment, followed by enzymatic debranching and then recrystallization through temperature cycling to produce resistant starch [143]. Moreover, rice starches are subjected to acid and heat-moisture treatments to produce resistant starch [144]. Studies on the optimal combinations of modification procedures used in preparing functional starch are ongoing and merit further research using new technologies.

1.4 Characterization of Functional Starch

1.4.1 Electron Microscopy

Electron microscopy uses electrons instead of light to image samples. It is a highly specific method to analyze the structural characteristics of functional starch granules [145, 146]. The electrons are focused and collected after the beam passes through the specimen, and a two-dimensional projected image of the three-dimensional sample structure is obtained [146]. The resolving power of an electron microscope has a linear relationship with the wavelength. There are three types of electron microscopy used in the analysis of functional starch granules: scanning electron microscopy (SEM), transmission electron microscopy (TEM), and atomic force microscopy (AFM).

With SEM, the sample images are formed by scanning a focused electron beam across the surface of the functional starch; the electrons are deflected by elastic scattering phenomena [146]. The energy spectra of the electrons that pass through the specimen are processed by the detector, resulting in two types of contrast images [146, 147]. Topographical contrast images result from the secondary electron signal and allow the image to acquire a quasi-three-dimensional surface topography [146]. The main advantage of SEM is the pronounced depth of focus and particular method of image projection, as some areas cast shadows, while recessed areas appeared dark [146]. SEM is frequently used to qualitatively observe the microstructural damage on the functional starch granules after drying and directly mounting the specimen stubs with a thin layer of gold [145]. The diameter of the starch granule ranges from 5 to 50 nm; thus, SEM is suitable for the characterization of changes in starch granules after physical, chemical, and/or enzymatic treatments.

TEM analysis of functional starch granules is initiated by projecting a high-voltage electron beam to create an image, where the electrons are emitted by an electron gun, commonly fitted with a tungsten filament cathode as the electron source [146]. The electron beam is focused by electrostatic and electromagnetic lenses and transmitted through the specimen that is, in part, transparent to electrons and, in part, scatters electrons out of the beam. The electrons are collected, focused, and magnified by lenses to produce a projected image. TEM has been widely used to characterize the morphology, crystalline structure, and elemental information of modified starch granules. The two basic modes of TEM are the bright-field mode and dark-field mode [148, 149].

AFM is operated at a constant setting when working in the tapping scanning mode to analyze the topography of surface granules on a microscale or nanoscale. AFM provides quantitative parameters regarding the surface roughness through height parameters, roughness average, and root mean square roughness descriptors. However, AFM provides only qualitative information regarding the food microstructure [145]. AFM provides molecular or supermolecular resolution by scanning with a sharp stylus attached to a flexible cantilever across a sample surface [150].

1.4.2 Differential Scanning Calorimetry (DSC)

DSC is a thermoanalytical technique that determines the difference in the amount of heat flow or the differences in temperatures between a test sample and an inert reference as a function of programmed raised and/or lowered temperatures at a designated constant rate [151]. There are two types of DSC instruments used for the analysis of samples, including heat flux DSC and power compensation DSC. For functional starch analyses, power compensation DSC is commonly used with the sample and an inert reference sealed independently in different pans. The difference of power input between these two specimens is measured as a function of time and recorded as the sample temperature is increased at a constant rate [151]. In general analyses, the temperature scanning program is designed and input by the operator as the sample holder temperature increases linearly as a function of time [151]. The gelatinization, retrogradation, glass transition, and starch-lipid complexation of starch samples can be determined using DSC [152–155].

1.4.3 X-Ray Powder Diffraction (XRD)

XRD is a technique developed to analyze the atomic and molecular structure of the crystalline and semicrystalline structure of samples, in which the crystalline atoms cause a beam of incident X-rays to diffract into many directions. Crystals are regular arrays of atoms, and X-rays can be considered waves of electromagnetic radiation, primarily generated through the electrons of atoms. The X-ray wavelength is from 10 to 0.01 nm, which is on the scale of covalent chemical bonds and within the radius of a single atom. There are three different XRD patterns for starches designated as A-type (A-type polymorph), B-type (B-type polymorph), and C-type (C-type polymorph) [156]. A-type starch exists in a close-packed arrangement with water molecules between the double helical structures; it is associated mainly with cereal starches [157]. The B-type starch is usually obtained from high-amylose starch and tuber starch, is more open, and has more water molecules located in a central cavity surrounded by six double helices [157]. The packing of these double helices within the A-type structure is relatively compact with lower water content, while the B-type starch has loosely packed double helices containing a hydrated

helical core [158, 159]. The C-type starch, including pea starch and some bean starches, is now believed to represent a mixture of A-type and B-type polymorphic structures [159]. In addition, the V-type conformation is a result of amylose being complexed with molecules such as fatty acids, emulsifiers, butanol, and iodine [157]. The XRD technique has been successfully used to determine the crystalline polymorphic structures of functional starches during the preparing and processing stages.

The starch structure as a unit is organized into four different lengths as follows: the whole granule (μm), growth rings (about 0.1 μm), lamellar structure (8–11 nm), and molecular scale (about 0.1 nm) [160]. The small-angle X-ray scattering (SAXS) technique offers the unique potential to quantify the lamellar architecture of semi-crystalline growth rings in starch granules, where the lamellae of starch are structurally formed by side chains of amylopectin interspersed with amylose. Their behavior upon contact with water and varying temperature has been explained using a widely accepted "liquid crystalline" model for starch [160]. SAXS is able to probe structures over a size range from approximately 1 to 100 nm, which is useful for structural determination at low resolution for systems that do not necessarily possess long-range or crystalline order. Currently, the SAXS technique is widely used in lamellar structure characterization of functional starch, because the alternating amorphous and crystalline lamellae exhibit different electron densities [161, 162].

1.4.4 Nuclear Magnetic Resonance (NMR) Imaging

NMR imaging measures nuclei in a magnetic field that can absorb and reemit electromagnetic radiation; it involves the energy exchange between at least two nuclei (resonance) [163]. Several different atoms, including ^{1}H, ^{13}C, and ^{31}P, are used to study the different aspects of samples under natural or industrial conditions [164]. Starch has been analyzed by NMR for chemical composition, degree of molecular order, degree of branching, physical structure of V-type amylose inclusion complexes, and extents and positions of modifications [164]. The degree of branching and amylose content of starch is determined by ^{1}H-NMR more efficiently and with less time than by the conventional methods. NMR imaging is based on anomeric protons involved in the α-1→4 and α-1→6 linkages giving rise to different signals in the NMR spectrum [165]. Solid-state ^{13}C cross-polarization magic angle spinning (CP/MAS) NMR has been used to quantify the molecular order of granular starch, where the corresponding NMR spectra of A-type starch differs from that of B-type starch [166]. Amylose complexed with small molecules both in solution and in solid states to form V-type inclusion complexes is also analyzed by solid-state ^{13}C CP/MAS NMR [167]. The nature and composition of phosphorus-containing compounds such as phosphate monoester, inorganic phosphate, and phospholipids are also characterized by ^{31}P NMR. The position and degree of phosphorylation on starch chains can also be determined [168, 169]. The chemical, physical, and starch-grafted copolymer structures of functional starch preparations have also been analyzed by NMR.

1.4.5 Rheometry

The rheometer is a laboratory instrument used to determine the way in which a liquid, suspension, or slurry flows in response to an applied force. Rotational and shear rheometries are two methods based on controlling the applied shear stress or shear strain, respectively. The rheological properties of starch are governed by the structure, especially amylose content, granule size distribution, granule shape, granule-granule interaction, granule volume fraction, and the continuous phase viscosity [170, 171]. Dynamic rheometry enables the continuous evaluation of dynamic conditions, including temperature and frequency sweep testing of the starch suspensions. The storage dynamic modulus (G′) is a determination of the energy stored in a sample and its recovery per cycle, while the loss modulus (G″) is a determination of the energy dissipated or lost per cycle of sinusoidal deformation [172]. The tan δ is defined as the ratio of G″ to G′ for each cycle, where the loss of tan δ is the phase difference between the applied and resulting sinusoidal stress [172]. For starch in a dynamic rheometer setting, G′ gradually increases to a maximum (peak G′) at a certain temperature (TG′) because of granule swelling [173]. Following continued heating, G′ decreases in the rheometer, which indicates that the gel structure is destroyed by melting of the crystalline regions remaining in the swollen granules [173]. Shah et al. discovered that dual enzyme-modified oat starch exhibited shear thinning as reflected from the convex-shaped graph. The sample is used as an additive in food products because the food required less energy to masticate and the gel was swallowed easily [174]. The dynamic rheological properties of chemically modified starch pastes were not affected by post gelatinization time, while native starch pastes developed a more rigid structure during storage [175]. Fan Zhu and Ya-Jane Wang reported that starch/α-naphthol complexes greatly increased the consistency coefficient and decreased the flow behavior indices of wheat starch [176].

1.4.6 Size Exclusion Chromatography

The molecular size characterization of starches is difficult to determine due to difficulties in solubilization, size separation without degradation, and the broad size distribution of starch molecules. The common techniques for size separation of starch molecules, for molecular size characterization, are analytical ultracentrifugation, size exclusion chromatography (SEC), and field-flow fractionation [177]. SEC is frequently selected as a separation technique for functional starch evaluation; it is sometimes also termed gel filtration chromatography (GFC) or gel permeation chromatography (GPC). SEC separation of starch molecules is accompanied by the use of single or multiple detection systems, including differential refractive index (DRI) and multiple-angle laser light scattering (MALLS) systems. There is no unique relationship between the size of a molecule and its molar mass and the size uniformity of the starch molecules, which may contain a range of molar masses [177]. SEC can

be divided into the following steps: dissolution, separation, detection, and data processing. Starches are not readily solubilized in aqueous solution unless they are of low molecular weight [178]. The purpose of dissolution is to dissolve the starch sample without further degradation or aggregation, which would result in an incorrect apparent size distribution [177]. Dimethyl sulfoxide (DMSO) with the addition of small amounts of water and salt is commonly used to dissolve starch, followed by ethanol addition to remove lipids and proteins [179, 180]. The starch solution is then redissolved in an organic solvent (DMSO) or an aqueous solution with a salt and further separated on different types of size exclusion columns. For SEC-DRI, the hydrodynamic volume distributions are obtained if the universal calibration assumption is valid [177]. The SEC-MALL-DRI system detects small amounts of large molecules with good signal-to-noise, and the analyses of the MALLS data use the formula d_n/d_c [177]. In this manner, the molecular structure of functional starch molecules can be determined using size exclusion chromatography.

1.5 Functional Starch Applications

1.5.1 Fat Replacers

Studies have shown that the overconsumption of dietary fat contributes to various chronic diseases, and this has promoted attempts to develop and consume low-fat foods [181]. Starch with granular sizes similar to those of fat emulsions is potential fat replacers [182]. Cross-linked (thermally or chemically) starches with low digestibility have be used as fat replacers [183]. Sodium octenyl succinate (OSA)-modified starches have emulsifying properties for the starch granules to better simulate the behavior of lipids in food systems [184]. Dextrozyme is an efficient enzyme used to digest granules of cornstarch into fine particles that act as fat mimetics for generating a fatty mouthfeel [185]. Moreover, these modified starches have lipophilic flavors and nutrients and interact with other food components such as proteins to further improve the quality of low-fat products [186]. Modified starch-based replacers have been used in a wide variety of low-fat food products such as cheese, frozen dessert, yogurt, sausage, and mayonnaise [181].

1.5.2 Food Ingredient Capsules

Functional ingredients can be encapsulated by various materials for controlled release into food and digestion systems. There has been a growing interest in using modified starches to encapsulate food ingredients such as lipids, polyphenols, vitamins, enzymes, lipids, carotenoids, and probiotics [53]. OSA starch-stabilized Pickering emulsions have been fabricated for encapsulating food ingredients [187].

Porous starch was developed to encapsulate many food ingredients such as sweeteners, flavorings and colorants, phenolics, oils, minerals, vitamins, and probiotics [29–33]. Starch nanoparticles can also be loaded with vitamin D_3 and curcumin. Various types of nanoparticles enhance the absorption of food ingredients through the epithelial cells and increase their bioavailability after absorption [188]. Amylose from partially gelatinized starch or debranched starches encapsulates small molecules such as polyphenols and unsaturated fatty acids by forming inclusion complexes [53]. The encapsulation procedures are developed to promote starch-based systems to encapsulate food ingredients; these include extrusion, freeze drying, anti-solvent precipitation, physical trapping, complexation, spray drying, and emulsification [53]. The functional starch-based encapsulation systems positively modulate the controlled release of food ingredients in food and for nutritional applications.

1.5.3 Edible Films and Coatings

Packaging materials play an important role in containing and preserving food through the supply chain. For this purpose, starch is considered as one of the most promising candidates due to its biodegradability, low price, abundance, and thermoplastic behavior [189]. Starch films have been shown to be odorless, tasteless, colorless, transparent, low cost, biocompatible, and biodegradable but are inherently hydrophilic in nature and have a tendency to absorb water in conditions of elevated relative humidity [190]. The mobile starch chains in starch films suffer retrogradation and crystallization during storage, resulting in undesirable changes of the thermomechanical properties [191]. Furthermore, there are still many drawbacks to this approach, such as poor solubility, uncontrollable paste consistency, low freeze-thaw stability, and poor mechanical properties for the developed starch films [192]. Functional starches have drawn attention at the research and industrial level, because these films exhibit dramatic improvement in filming properties without involving any significant increase in cost of production [192]. Functional starches such as cross-linked, substituted, oxidized, or acid-hydrolyzed starches are produced as a result of chemical modification to improve the film properties, including enhanced solubility, improved mechanical properties, and heat-sealing capacity [192]. In the future, multiple modifications should be examined to produce starch films with more desirable properties.

References

1. Jobling S. Improving starch for food and industrial applications. Curr Opin Plant Biol. 2004;7(2):210–8.
2. Bertoft E. Composition of clusters and their arrangement in potato amylopectin. Carbohydr Polym. 2007;68(3):433–46.
3. Ball SG, van de Wal MHBJ, Visser RGF. Progress in understanding the biosynthesis of amylose. Trends Plant Sci. 1998;3(12):462–7.
4. Roger P, Colonna P. Molecular weight distribution of amylose fractions obtained by aqueous leaching of corn starch. Int J Biol Macromol. 1996;19(1):51.
5. Buléon A, et al. Starch granules: structure and biosynthesis. Int J Biol Macromol. 1998;23(2):85–112.
6. Manners DJ. Recent developments in our understanding of amylopectin structure. Carbohydr Polym. 1989;11(2):87–112.
7. Jane J, et al. Effects of amylopectin branch chain length and amylose content on the gelatinization and pasting properties of starch. Cereal Chem. 1999;76(5):629–37.
8. Jenkins S. Morphological, thermal and rheological properties of starches from different botanical sources. Food Chem. 2003;81(2):219–31.
9. Miao M, et al. Slowly digestible starch: a review. Crit Rev Food Sci Nutr. 2015;55(12):1642–57.
10. Zhang G, Hamaker BR. Slowly digestible starch: concept, mechanism, and proposed extended glycemic index. Crit Rev Food Sci Nutr. 2009;49(10):852.
11. A H, et al. Glycemic and insulinemic meal responses modulate postprandial hepatic and intestinal lipoprotein accumulation in obese, insulin-resistant subjects. Am J Clin Nutr. 2004;80(4):896–902.
12. Axelsen M, et al. Breakfast glycaemic response in patients with type 2 diabetes: effects of bedtime dietary carbohydrates. Eur J Clin Nutr. 1999;53(9):706.
13. Benton D, Nabb S. Carbohydrate, memory, and mood. Nutr Rev. 2003;61(2):61–7.
14. Benton D, et al. The delivery rate of dietary carbohydrates affects cognitive performance in both rats and humans. Psychopharmacology., 2003. 2003;166(1):86–90.
15. Zhang G, Venkatachalam M, Hamaker BR. Structural basis for the slow digestion property of native cereal starches. Biomacromolecules. 2006;7(11):3259–66.
16. Zhang G, Ao Z, Hamaker BR. Nutritional property of endosperm starches from maize mutants: a parabolic relationship between slowly digestible starch and amylopectin fine structure. J Agric Food Chem. 2008;56(12):4686.
17. Li X, et al. Partial branching enzyme treatment increases the low glycaemic property and α-1,6 branching ratio of maize starch. Food Chem., 2014. 2014;164:502–9.
18. Kim BK, et al. Branch chain elongation by amylosucrase: production of waxy corn starch with a slow digestion property. Food Chem. 2014;152:113–20.
19. Jiang H, et al. Enzymatic modification of corn starch with 4-α-glucanotransferase results in increasing slow digestible and resistant starch. Int J Biol Macromol. 2014;65:208–14.
20. Miao M, et al. Development of maize starch with a slow digestion property using maltogenic α-amylase. Carbohydr Polym. 2014;103:164–9.
21. Miao M, et al. Improved the slow digestion property of maize starch using partially β-amylolysis. Food Chem. 2014;152:128–32.
22. Englyst HN, et al. Measurement of resistant starch in vitro and in vivo. Br J Nutr. 1996;75(5):749.
23. Fuentes-Zaragoza E, et al. Resistant starch as prebiotic: a review. Starch-Stärke. 2011;63(7):406–15.
24. Cummings JH, Englyst HN. Measurement of starch fermentation in the human large intestine. Can J Physiol Pharmacol. 1991;69(1):121.
25. Ashwar BA, et al. Preparation, health benefits and applications of resistant starch—a review. Starch-Stärke. 2016;68(3–4):287–301.

26. Zhang B, et al. Corn porous starch: preparation, characterization and adsorption property. Int J Biol Macromol. 2012;50(1):250–6.
27. Chang PR, Yu J, Ma X. Preparation of porous starch and its use as a structure-directing agent for production of porous zinc oxide. Carbohydr Polym. 2011;83(2):1016–9.
28. Qian D, Chang PR, Ma X. Preparation of controllable porous starch with different starch concentrations by the single or dual freezing process. Carbohydr Polym. 2011;86(3):1181–6.
29. Benavent-Gil Y, Rosell CM. Comparison of porous starches obtained from different enzyme types and levels. Carbohydr Polym. 2017;157:533–40.
30. Li H, et al. Encapsulation of Lactobacillus plantarum in porous maize starch. LWT Food Sci Technol. 2016;74:542–9.
31. Belingheri C, et al. Oxidative stability of high-oleic sunflower oil in a porous starch carrier. Food Chem. 2015;166:346–51.
32. Belingheri C, Ferrillo A, Vittadini E. Porous starch for flavor delivery in a tomato-based food application. LWT Food Sci Technol. 2015;60(1):593–7.
33. Wang H, et al. Preparation and characterization of porous corn starch and its adsorption toward grape seed proanthocyanidins. Starch-Stärke. 2016;68(11–12):1254–63.
34. Jiang S, et al. Adsorption of procyanidins onto chitosan-modified porous rice starch. LWT Food Sci Technol. 2017;84:10–7.
35. Chang R, et al. Preparation and properties of the succinic ester of porous starch. Carbohydr Polym. 2012;88(2):604–8.
36. Ma X, et al. Modification of porous starch for the adsorption of heavy metal ions from aqueous solution. Food Chem. 2015;181:133–9.
37. Acosta E, et al. Net-average curvature model for solubilization and supersolubilization in surfactant microemulsions. Langmuir., 2003. 2003;19(1):186–95.
38. Moulik SP, et al. Studies on the interfacial composition and thermodynamic properties of W/O microemulsions. Langmuir. 2000;16(7):3101–6.
39. Wang X, et al. Preparation of starch nanoparticles in water in oil microemulsion system and their drug delivery properties. Carbohydr Polym. 2016;138:192.
40. Bezemer JM, et al. Microspheres for protein delivery prepared from amphiphilic multiblock copolymers: 2. Modulation of release rate. J Control Release. 2000;67(2–3):249–60.
41. Kawashita M, et al. Preparation of ferrimagnetic magnetite microspheres for in situ hyperthermic treatment of cancer. Biomaterials. 2005;26(15):2231–8.
42. Sturesson C, Carlfors J. Incorporation of protein in PLG-microspheres with retention of bioactivity. J Control Release. 2000;67(2–3):171–8.
43. Sandhu KS, Nain V. Starch nanoparticles: their preparation and applications. In: Gahlawat SK, et al., editors. Plant biotechnology: recent advancements and developments. Singapore: Springer Singapore; 2017. p. 213–32.
44. Kim H-Y, Park SS, Lim S-T. Preparation, characterization and utilization of starch nanoparticles. Colloids Surf B: Biointerfaces. 2015;126:607–20.
45. Ma X, et al. Fabrication and characterization of citric acid-modified starch nanoparticles/plasticized-starch composites. Biomacromolecules. 2008;9(11):3314–20.
46. Qin Y, et al. Characterization of starch nanoparticles prepared by nanoprecipitation: influence of amylose content and starch type. Ind Crop Prod. 2016;87:182–90.
47. Li C, Sun P, Yang C. Emulsion stabilized by starch nanocrystals. Starch-Stärke. 2012;64(6):497–502.
48. Ge S, et al. Characterizations of Pickering emulsions stabilized by starch nanoparticles: influence of starch variety and particle size. Food Chem. 2017;234:339–47.
49. Kristo E, Biliaderis CG. Physical properties of starch nanocrystal-reinforced pullulan films. Carbohydr Polym. 2007;68(1):146–58.
50. Orsuwan A, Sothornvit R. Development and characterization of banana flour film incorporated with montmorillonite and banana starch nanoparticles. Carbohydr Polym. 2017;174:235–42.

51. Vasiliadou E, Raphaelides SN, Papastergiadis E. Effect of heating time and temperature on partially gelatinized starch-fatty acid interactions. LWT Food Sci Technol. 2015;60(2):698–707.
52. Raphaelides SN, et al. A process designed for the continuous production of starch inclusion complexes on an industrial scale. Food Bioprod Process. 2015;96:245–55.
53. Zhu F. Encapsulation and delivery of food ingredients using starch based systems. Food Chem. 2017;229:542–52.
54. Chen B, et al. Properties of lotus seed starch-glycerin monostearin complexes formed by high pressure homogenization. Food Chem. 2017;226:119–27.
55. Conde-Petit B, Escher F, Nuessli J. Structural features of starch-flavor complexation in food model systems. Trends Food Sci Technol. 2006;17(5):227–35.
56. Ying Y, Gu ZB, Zhang GY. Delivery of bioactive conjugated linoleic acid with self-assembled amylose-CLA complex. J Agric Food Chem. 2009;57(15):7125–30.
57. Arijaje EO, et al. Effects of chemical and enzymatic modifications on starch–stearic acid complex formation. J Agric Food Chem. 2014;62(13):2963–72.
58. Kong L, Ziegler GR. Formation of starch-guest inclusion complexes in electrospun starch fibers. Food Hydrocoll. 2014;38(3):211–9.
59. Gökmen V, et al. Development of functional bread containing nanoencapsulated omega-3 fatty acids. J Food Eng. 2011;105(4):585–91.
60. de Kruif CG, Tuinier R. Polysaccharide protein interactions. Food Hydrocoll. 2001;15(4):555–63.
61. Mohamed AA, Rayas-Duarte P. The effect of mixing and wheat protein/gluten on the gelatinization of wheat starch. Food Chem. 2003;81(4):533–45.
62. Shah A, et al. Rheological properties of a soluble self-assembled complex from starch, protein and free fatty acids. J Food Eng. 2011;105(3):444–52.
63. Zhang G, et al. Self-assembly of amylose, protein, and lipid as a nanoparticle carrier of hydrophobic small molecules. Chichester: Wiley; 2015. p. 263–71.
64. Fan M, et al. Gel characteristics and microstructure of fish myofibrillar protein/cassava starch composites. Food Chem. 2017;218:221–30.
65. Philipp C, et al. Impact of protein content on physical and microstructural properties of extruded rice starch-pea protein snacks. J Food Eng. 2017;212:165–73.
66. Otto C, et al. Comparative cleaning tests with modified protein and starch residues. J Food Eng. 2016;178:145–50.
67. Sun N-x, et al. Interaction of starch and casein. Food Hydrocoll. 2016;60:572–9.
68. Qu B, Zhong Q. Casein-maltodextrin conjugate as an emulsifier for fabrication of structured calcium carbonate particles as dispersible fat globule mimetics. Food Hydrocoll. 2017;66:61–70.
69. Masina N, et al. A review of the chemical modification techniques of starch. Carbohydr Polym. 2017;157:1226–36.
70. Kaur L, Singh J. Starch: modified starches. In: Caballero B, Finglas PM, Toldrá F, editors. Encyclopedia of food and health. Oxford: Academic; 2016. p. 152–9.
71. Biduski B, et al. Impact of acid and oxidative modifications, single or dual, of sorghum starch on biodegradable films. Food Chem. 2017;214:53–60.
72. Kaur B, et al. Progress in starch modification in the last decade. Food Hydrocoll. 2012;26(2):398–404.
73. Moreau M, Orange N, Feuilloley MGJ. Non-thermal plasma technologies: new tools for bio-decontamination. Biotechnol Adv. 2008;26(6):610–7.
74. Mir SA, Shah MA, Mir MM. Understanding the role of plasma technology in food industry. Food Bioprocess Technol. 2015;9(5):1–17.
75. Zhu F. Plasma modification of starch. Food Chem. 2017;232:476–86.
76. Andrade CT, et al. Surface modification of maize starch films by low-pressure glow 1-butene plasma. Carbohydr Polym. 2005;61(4):407–13.
77. Alves CM, et al. Modulating bone cells response onto starch-based biomaterials by surface plasma treatment and protein adsorption. Biomaterials. 2007;28(2):307–15.

78. Jacobs H, Delcour JA. Hydrothermal modifications of granular starch, with retention of the granular structure: a review. J Agric Food Chem. 1998;46(8):2895–905.
79. Zavareze EdR, Dias ARG. Impact of heat-moisture treatment and annealing in starches: a review. Carbohydr Polym. 2011;83(2):317–28.
80. Jayakody L, Hoover R. Effect of annealing on the molecular structure and physicochemical properties of starches from different botanical origins-a review. Carbohydr Polym. 2008;74(3):691–703.
81. Gomes AMM, Mendes da Silva CE, Ricardo NMS. Effects of annealing on the physicochemical properties of fermented cassava starch (polvilho azedo). Carbohydr Polym. 2005;60(1):1–6.
82. Chung H-J, Hoover R, Liu Q. The impact of single and dual hydrothermal modifications on the molecular structure and physicochemical properties of normal corn starch. Int J Biol Macromol. 2009;44(2):203–10.
83. Hoover R. The impact of heat-moisture treatment on molecular structures and properties of starches isolated from different botanical sources. Crit Rev Food Sci Nutr. 2010;50(9):835.
84. Zhu F. Impact of ultrasound on structure, physicochemical properties, modifications, and applications of starch. Trends Food Sci Technol. 2015;43(1):1–17.
85. Hu A, et al. Ultrasonic frequency effect on corn starch and its cavitation. LWT Food Sci Technol. 2015;60(2):941–7.
86. Sujka M. Ultrasonic modification of starch-impact on granules porosity. Ultrason Sonochem. 2017;37:424–9.
87. Tian Y, et al. Effect of high hydrostatic pressure (HHP) on slowly digestible properties of rice starches. Food Chem. 2014;152:225–9.
88. Ahmed J, et al. Impact of high pressure treatment on functional, rheological, pasting, and structural properties of lentil starch dispersions. Carbohydr Polym. 2016;152:639–47.
89. Błaszczak W, Valverde S, Fornal J. Effect of high pressure on the structure of potato starch. Carbohydr Polym. 2005;59(3):377–83.
90. Hu X-P, et al. Effect of high hydrostatic pressure and retrogradation treatments on structural and physicochemical properties of waxy wheat starch. Food Chem. 2017;232:560–5.
91. Li W, et al. Recrystallization characteristics of high hydrostatic pressure gelatinized normal and waxy corn starch. Int J Biol Macromol. 2016;83:171–7.
92. Villamonte G, Jury V, de Lamballerie M. Stabilizing emulsions using high-pressure-treated corn starch. Food Hydrocoll. 2016;52:581–9.
93. Paquin P. Technological properties of high pressure homogenizers: the effect of fat globules, milk proteins, and polysaccharides. Int Dairy J. 1999;9(3–6):329–35.
94. Brookman JSG. Mechanism of cell disintegration in a high pressure homogenizer. Biotechnol Bioeng. 1974;16(3):371–83.
95. Tribst AAL, Franchi MA, Cristianini M. Ultra-high pressure homogenization treatment combined with lysozyme for controlling Lactobacillus brevis contamination in model system. Innovative Food Sci Emerg Technol. 2008;9(3):265–71.
96. Wei B, et al. Disruption and molecule degradation of waxy maize starch granules during high pressure homogenization process. Food Chem. 2018;240:165–73.
97. Floury J, et al. Degradation of methylcellulose during ultra-high pressure homogenisation. Food Hydrocoll. 2002;16(1):47–53.
98. Meng S, et al. Preparation of corn starch–fatty acid complexes by high-pressure homogenization. Starch-Stärke. 2015;66(9–10):809–17.
99. Antonietti M, Landfester K. Polyreactions in miniemulsions. Macromol Rapid Commun. 2001;22(12):689–757.
100. Masatcioglu TM, Sumer Z, Koksel H. An innovative approach for significantly increasing enzyme resistant starch type 3 content in high amylose starches by using extrusion cooking. J Cereal Sci. 2017;74:95–102.
101. Lai LS, Kokini JL. Physicochemical changes and rheological properties of starch during extrusion (a review). Biotechnol Prog. 1991;7(3):251–66.

102. Zhang B, et al. Extrusion induced low-order starch matrices: enzymatic hydrolysis and structure. Carbohydr Polym. 2015;134:485–96.
103. Liu W-C, Halley PJ, Gilbert RG. Mechanism of degradation of starch, a highly branched polymer, during extrusion. Macromolecules. 2010;43(6):2855–64.
104. Liu X, et al. Shear degradation of corn starches with different amylose contents. Food Hydrocoll. 2017;66:199–205.
105. Zhang Y, et al. Retrogradation behaviour of high-amylose rice starch prepared by improved extrusion cooking technology. Food Chem. 2014;158:255–61.
106. Ye J, et al. Freeze-thaw stability of rice starch modified by improved extrusion cooking technology. Carbohydr Polym. 2016;151:113–8.
107. Li M, et al. Extrusion processing and characterization of edible starch films with different amylose contents. J Food Eng. 2011;106(1):95–101.
108. Mościcki L, et al. Application of extrusion-cooking for processing of thermoplastic starch (TPS). Food Res Int. 2012;47(2):291–9.
109. De Pilli T, et al. Study of starch-lipid complexes in model system and real food produced using extrusion-cooking technology. Innovative Food Sci Emerg Technol. 2011;12(4):610–6.
110. Rathod RP, Annapure US. Physicochemical properties, protein and starch digestibility of lentil based noodle prepared by using extrusion processing. LWT Food Sci Technol. 2017;80:121–30.
111. Tian Y, et al. Starch sodium dodecenyl succinate prepared by one-step extrusion and its properties. Carbohydr Polym. 2015;133:90–3.
112. Chandrasekaran S, Ramanathan S, Basak T. Microwave food processing-a review. Food Res Int. 2013;52(1):243–61.
113. Yang Q, et al. Effect of microwave irradiation on internal molecular structure and physical properties of waxy maize starch. Food Hydrocoll. 2017;69:473–82.
114. Bra M, et al. Behaviour of starch exposed to microwave radiation treatment. Starch-Stärke. 2014;66(1–2):3–14.
115. Lin D, et al. Study on the synthesis and physicochemical properties of starch acetate with low substitution under microwave assistance. Int J Biol Macromol. 2017;103:316–26.
116. Deng Y, J.M. Catchmark, insoluble starch composite foams produced through microwave expansion. Carbohydr Polym. 2014;111:864–9.
117. Zhu J, et al. Multi-scale structural changes of starch-based material during microwave and conventional heating. Int J Biol Macromol. 2016;92:270–7.
118. Mutlu S, Kahraman K, Öztürk S. Optimization of resistant starch formation from high amylose corn starch by microwave irradiation treatments and characterization of starch preparations. Int J Biol Macromol. 2017;95:635–42.
119. Gübitz GM, Paulo AC. New substrates for reliable enzymes: enzymatic modification of polymers. Curr Opin Biotechnol. 2003;14(6):577–82.
120. Xin J-Y, et al. Biosynthesis of corn starch palmitate by Lipase Novozym 435. Int J Mol Sci. 2012;13(6):7226.
121. Chakraborty S, et al. Enzyme-catalyzed regioselective modification of starch nanoparticles. Macromolecules. 2005;38(1):61–8.
122. Alissandratos A, et al. Lipase-catalysed acylation of starch and determination of the degree of substitution by methanolysis and GC. BMC Biotechnol. 2010;10(1):82.
123. Shogren RL, Biswas A. Preparation of starch–sodium lignosulfonate graft copolymers via laccase catalysis and characterization of antioxidant activity. Carbohydr Polym. 2013;91(2):581–5.
124. Liu G, et al. Structure, functionality and applications of debranched starch: a review. Trends Food Sci Technol. 2017;63:70–9.
125. Cai L, Shi Y-C. Self-assembly of short linear chains to A- and B-type starch spherulites and their enzymatic digestibility. J Agric Food Chem. 2013;61(45):10787–97.
126. Chiu CW, Mason WR. Method of replacing fats with short chain amylose. 1998. U.S. Patent 5711986.

127. Luckett CR, Wang YJ. Application of enzyme-treated corn starches in breakfast cereal coating. J Food Sci. 2012;77(8):901–6.
128. Liu G, et al. Preparation and characterization of pullulanase debranched starches and their properties for drug controlled-release. RSC Adv. 2015;5(117):97066–75.
129. Roussel X, et al. Characterization of substrate and product specificity of the purified recombinant glycogen branching enzyme of Rhodothermus obamensis. Biochim Biophys Acta Gen Subj. 2013;1830(1):2167–77.
130. Takata H, et al. Industrial production of branching enzyme, and its application for producing a highly branched cyclic dextrin, Cluster DextrinTM. Seibutsu-kogaku Kaishi. 2006;84(2):61–6.
131. Tian Y, et al. Highly branched dextrin prepared from high-amylose maize starch using waxy rice branching enzyme (WRBE). Food Chem. 2016;203:530.
132. Lee B-H, et al. Enzyme-synthesized highly branched maltodextrins have slow glucose generation at the mucosal α-glucosidase level and are slowly digestible in vivo. PLoS One. 2013;8(4):e59745.
133. Kawabata Y, et al. Preparation of highly branched starch by glycogen branching enzyme from Neurospora crassa N2-44 and its characterization. J Appl Glycosci., 2002. 2002;49(3):273–9.
134. Kaper T, et al. Exploring and exploiting starch-modifying amylomaltases from thermophiles. Biochem Soc Trans. 2004;32(2):279–82.
135. Arnoc A, et al. Improved creaminess of low-fat yoghurt: the impact of amylomaltase-treated starch domains. Food Hydrocoll. 2009;23(3):980–7.
136. Euverink GJW, Binnema DJ. Use of modified starch as an agent for forming a thermoreversible gel. 2005. US.
137. Zhang H, et al. Enzymatically modified waxy corn starch with amylosucrase: the effect of branch chain elongation on structural and physicochemical properties. Food Hydrocoll. 2017;63:518–24.
138. Z A, et al. Starch with a slow digestion property produced by altering its chain length, branch density, and crystalline structure. J Agric Food Chem. 2007;55(11):4540–7.
139. Dura A, Rosell CM. Physico-chemical properties of corn starch modified with cyclodextrin glycosyltransferase. Int J Biol Macromol. 2016;87:466–72.
140. Wu CS, et al. Molecular characterization and in vitro digestibility of normal maize starch hydrolyzed by maltotriohydrolase. Int J Biol Macromol. 2015;74:283–8.
141. Jo AR, et al. Preparation of slowly digestible sweet potato Daeyumi starch by dual enzyme modification. Carbohydr Polym. 2016;143:164–71.
142. Luo Z, Xu Z. Characteristics and application of enzyme-modified carboxymethyl starch in sausages. LWT Food Sci Technol. 2011;44(10):1993–8.
143. Sun B, et al. Effect of acid-ethanol treatment and debranching on the structural characteristics and digestible properties of maize starches with different amylose contents. Food Hydrocoll. 2017;69:229–35.
144. Hung PV, Vien NL, Lan Phi NT. Resistant starch improvement of rice starches under a combination of acid and heat-moisture treatments. Food Chem. 2016;191:67–73.
145. Barrera GN, et al. Evaluation of the mechanical damage on wheat starch granules by SEM, ESEM, AFM and texture image analysis. Carbohydr Polym. 2013;98(2):1449–57.
146. Klang V, Valenta C, Matsko NB. Electron microscopy of pharmaceutical systems. Micron. 2013;44:45–74.
147. Reimer L. Image formation in low-voltage scanning electron microscopy. Washington: SPIE Opt Eng Press; 1993. p. 89–96.
148. Tang CY, Yang Z. Transmission electron microscopy (TEM). In: Hilal N, Ismail A, Matsuura T, Oatley-Radcliffe D, editors. Membrane characterization. Amesterdan: Elsevier; 2017. p. 145–59.
149. Yang J, et al. Fabrication and characterization of hollow starch nanoparticles by gelation process for drug delivery application. Carbohydr Polym. 2017;173:223–32.
150. Meyer E. Atomic force microscopy. Prog Surf Sci. 1992;41(1):3–49.

151. Zhou P, Labuza TP. Analytical methods | differential scanning calorimetry A2 – Fuquay, John W. In: Encyclopedia of dairy sciences (2nd edn). San Diego: Academic; 2011. p. 256–63.
152. Jenkins PJ, Donald AM. Gelatinisation of starch: a combined SAXS/WAXS/DSC and SANS study. Carbohydr Res. 1998;308(2):133–47.
153. Eliasson AC. Interactions between starch and lipids studied by DSC. Thermochim Acta. 1994;246(2):343–56.
154. Fisher DK, Thompson DB. Retrogradation of maize starch after thermal treatment within and above the gelatinization temperature range. Cereal Chem. 2007;74(3):344–51.
155. And KT, Reid DS. Differential scanning calorimetry study of glass transition in frozen starch gels. J Agric Food Chem. 2004;52(13):4308–17.
156. Sarko A, Wu HC. The crystal structures of A-, B- and C-polymorphs of amylose and starch. Starch-Stärke. 1978;30(3):73–8.
157. Cheetham NWH, Tao L. Variation in crystalline type with amylose content in maize starch granules: an X-ray powder diffraction study. Carbohydr Polym. 1998;36(4):277–84.
158. Liu PL, Hu XS, Shen Q. Effect of high hydrostatic pressure on starches: a review. Starch-Stärke. 2010;62(12):615–28.
159. Tester RF, Karkalas J, Qi X. Starch-composition, fine structure and architecture. J Cereal Sci. 2004;39(2):151–65.
160. Pérez S, Bertoft E. The molecular structures of starch components and their contribution to the architecture of starch granules: a comprehensive review. Starch-Stärke., 2010. 2010;62(8):389–420.
161. Kuang Q, et al. Lamellar structure change of waxy corn starch during gelatinization by time-resolved synchrotron SAXS. Food Hydrocoll. 2017;62:43–8.
162. Blazek J, Gilbert EP. Application of small-angle X-ray and neutron scattering techniques to the characterisation of starch structure: a review. Carbohydr Polym. 2011;85(2):281–93.
163. Gidley MJ. Quantification of the structural features of starch polysaccharides by N.M.R. spectroscopy. Carbohydr Res. 1985;139:85–93.
164. Zhu F. NMR spectroscopy of starch systems. Food Hydrocoll. 2017;63:611–24.
165. Dunn LB, Krueger WJ. Branching ratios of starch via proton nuclear magnetic resonance and their use in determining amylose/amylopectin content: evidence for three types of amylopectin. Macromol Symp. 1999;140(1):179–86.
166. Flanagan BM, Gidley MJ, Warren FJ. Rapid quantification of starch molecular order through multivariate modelling of ^{13}C CP/MAS NMR spectra. Chem Commun. 2015;51(80):14856–8.
167. Le Bail P, Rondeau C, Buléon A. Structural investigation of amylose complexes with small ligands: helical conformation, crystalline structure and thermostability. Int J Biol Macromol. 2005;35(1):1–7.
168. Muhrbeck P, Tellier C. Determination of the phosphorylation of starch from native potato varieties by ^{31}P NMR. Starch-Stärke. 1991;43(1):25–7.
169. Genkina NK, Kurkovskaya LN. A novel method for the determination of phospholipids in starch matrixes. J Anal Chem. 2013;68(2):170–2.
170. Kaur L, Singh N, Sodhi NS. Some properties of potatoes and their starches II. Morphological, thermal and rheological properties of starches. Food Chem. 2002;79(2):183–92.
171. Kaur L, et al. Some properties of potatoes and their starches I. Cooking, textural and rheological properties of potatoes. Food Chem. 2002;79(2):177–81.
172. Singh N, et al. Morphological, thermal and rheological properties of starches from different botanical sources. Food Chem. 2003;81(2):219–31.
173. Singh J, Kaur L, Mccarthy OJ. Factors influencing the physico-chemical, morphological, thermal and rheological properties of some chemically modified starches for food applications – a review. Food Hydrocoll. 2007;21(1):1–22.
174. Shah A, et al. Dual enzyme modified oat starch: structural characterisation, rheological properties, and digestibility in simulated GI tract. Int J Biol Macromol. 2017. in press.

175. López OV, Zaritzky NE, García MA. Physicochemical characterization of chemically modified corn starches related to rheological behavior, retrogradation and film forming capacity. J Food Eng. 2010;100(1):160–8.
176. Zhu F, Wang Y-J. Characterization of modified high-amylose maize starch-α-naphthol complexes and their influence on rheological properties of wheat starch. Food Chem. 2013;138(1):256–62.
177. Gidley MJ, et al. Reliable measurements of the size distributions of starch molecules in solution: current dilemmas and recommendations. Carbohydr Polym. 2010;79(2):255–61.
178. Harding SE, Adams GG, Gillis RB. Molecular weight analysis of starches: which technique? Starch-Stärke. 2016;68(9–10):846–53.
179. Li C, Godwin ID, Gilbert RG. Diurnal changes in Sorghum leaf starch molecular structure. Plant Sci. 2015;239:147–54.
180. Zhong F, et al. Rice starch, amylopectin, and amylose: molecular weight and solubility in dimethyl sulfoxide-based solvents. J Agric Food Chem. 2006;54(6):2320–6.
181. Peng X, Yao Y. Carbohydrates as fat replacers. Annu Rev Food Sci Technol. 2017;8(1):331.
182. Malinski E, et al. Isolation of small starch granules and determination of their fat mimic characteristics. Cereal Chem. 2007;80(1):1–4.
183. Radi M, Niakousari M, Amiri S. Physicochemical, textural and sensory properties of low-fat yogurt produced by using modified wheat starch as a fat replacer. J Appl Sci. 2009;9(11):2194–7.
184. Tesch S, Gerhards C, Schubert H. Stabilization of emulsions by OSA starches. J Food Eng. 2002;54(2):167–74.
185. Ma Y, et al. Enzymatic hydrolysis of corn starch for producing fat mimetics. J Food Eng. 2006;73(3):297–303.
186. Lobato-Calleros C, et al. Impact of native and chemically modified starches addition as fat replacers in the viscoelasticity of reduced-fat stirred yogurt. J Food Eng. 2014;131(3):110–5.
187. Qi Z, Xu A. Starch-based ingredients for flavor encapsulation. Cereal Foods World., 1999. 1999;44:460–5.
188. Li Z, et al. A review: using nanoparticles to enhance absorption and bioavailability of phenolic phytochemicals. Food Hydrocoll. 2015;43:153–64.
189. López-Córdoba A, et al. Cassava starch films containing rosemary nanoparticles produced by solvent displacement method. Food Hydrocoll. 2017;71:26–34.
190. Jiménez A, et al. Edible and biodegradable starch films: a review. Food Bioprocess Technol. 2012;5(6):2058–76.
191. Mukurumbira AR, Mellem JJ, Amonsou EO. Effects of amadumbe starch nanocrystals on the physicochemical properties of starch biocomposite films. Carbohydr Polym. 2017;165:142–8.
192. Shah U, et al. Art and science behind modified starch edible films and coatings: a review. Compr Rev Food Sci Food Saf. 2004;15(3):568–80.

Chapter 2
Slowly Digestible Starch

Junrong Huang, Qi Yang, and Huayin Pu

2.1 Introduction

Starch is the main carbohydrate in human nutrition and is probably the second most abundant natural biopolymer on earth after cellulose. It is a major component of staple foods and plays important roles in bodily health by helping to maintain proper metabolic energy levels. Based on the rate and extent of its digestibility, starch has been classified into rapidly digestible starch (RDS), slowly digestible starch (SDS), and resistant starch (RS). The starch fraction digested within 20 min of incubation is classified as RDS; the starch fraction digested within 20–120 min corresponds to SDS; and the remaining fraction, which is not digested further, is RS (Fig. 2.1a) [1–3].

RDS induces a fast increase in blood glucose and insulin levels, which may cause a series of health complications, such as diabetes and cardiovascular diseases. SDS is slowly digested throughout the small intestine, resulting in the slow and prolonged release of glucose into the bloodstream, coupled to a low glycemic response. This type of starch may be helpful in controlling and preventing hyperglycemia-related diseases. RS is a type of starch that cannot be digested in the small intestine (Fig. 2.1b) [3].

The accurate determination of the bioavailable carbohydrates in a given product allows the manufacturer to predict and communicate the glycemic response to each serving of the food, which is especially important for therapeutic foods consumed by diabetics, and the management of diabetes and disorders of carbohydrate metabolism. The concept of the glycemic index (GI) was introduced to classify foods on the basis of the postprandial blood glucose response they induce. GI is defined as the postprandial increment in the glycemic area under the glycemic dose–response

J. Huang (✉) · Q. Yang · H. Pu
School of Food and Biological Engineering, Shaanxi University of Science and Technology, Xi'an, Shaanxi, China
e-mail: huangjunrong@sust.edu.cn; shmym4@sust.edu.cn; puhuayin@sust.edu.cn

Z. Jin (ed.), *Functional Starch and Applications in Food*,
https://doi.org/10.1007/978-981-13-1077-5_2

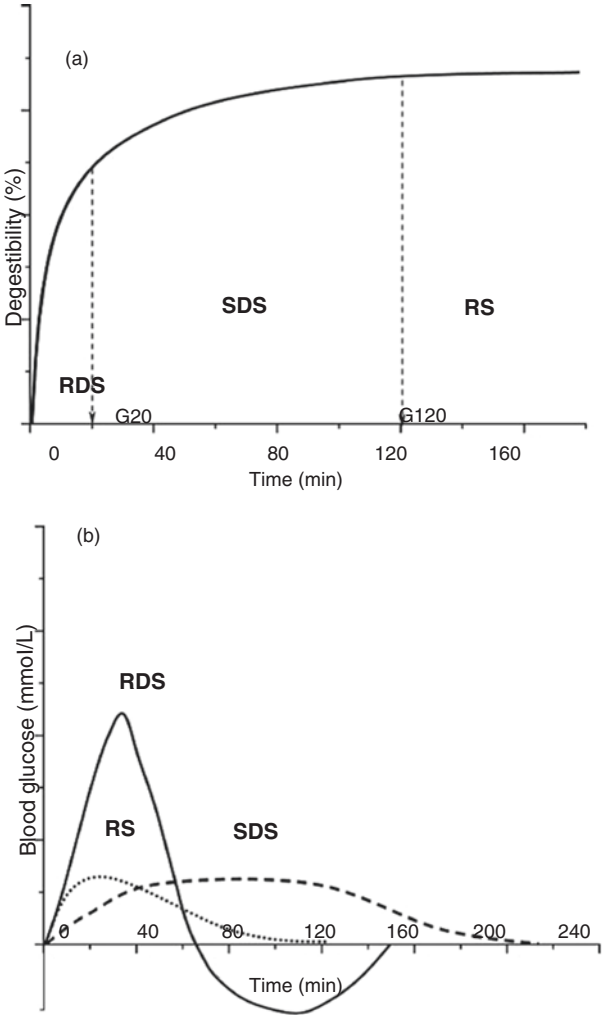

Fig. 2.1 Classification of the bioavailability of nutritional starch fractions. (**a**) In vitro digestion and (**b**) in vivo glycemic responses to RDS, SDS, and RS [3]. *RDS* rapidly digestible starch, *SDS* slowly digestible starch, *RS* resistant starch

curve after a test meal, expressed as a percentage of the corresponding area after an equi-carbohydrate portion of a reference food, such as glucose or white bread [4, 5]. Several researchers have demonstrated a strong relationship between the rate of in vitro digestion and the glycemic response to food. Such studies can be used to identify foods with potential utility in the diets of individuals with diabetes.

The digestibility of starch is determined by several factors. The important factors are the starch characteristics, the physical access of enzymes to the starch, the

availability of the water required for the hydrolysis of glycosidic linkages, and the rate of diffusion and the viscosity of the substrate.

The plant source of starch affects its digestibility. The digestibility of cereal starches, such as wheat starch, barley starch, oat starch, cornstarch, and sorghum starch, decreases in that order, and the digestibility of legume starch is lower than that of cereal starches [6]. The granule size of a starch is directly related to its digestibility, and studies of debranched cooked rice starch have shown that larger granules reduce the rate of digestion.

On the basis of X-ray diffraction scattering studies, native starch is classified into A, B, C, and V types. The crystallization of the starch granule structure also affects starch digestibility. X-ray diffraction scattering studies of three different starches (cereal starch, tuber starch, and bean starch) showed that cereal starch has a type A pattern, and its digestion rate is highest; tuber starch, such as potato starch, has a type B pattern, and its digestion rate is lowest; and bean starch has a type C pattern, and its digestion rate is between those of cereal starch and tuber starch [7].

Obesity and diabetes have become major public health concerns worldwide, and the number of cases has increased exponentially in recent years. New discoveries in food and nutrition science imply that slowing the rate of digestion of the glucose derived from ingested carbohydrate sources blunts glycemia, reduces the insulin required, and induces satiety [6]. Some examples of commercially available products that slow the rate of glucose digestion include isomaltulose, trehalose, pullulan, and sucromalt, together with other slow-release energy beverages, fodders, and medicines [8]. All these products claim to slow and extend the postprandial level of glucose after intake, although they differ in their molecular structures, functional properties, and potential applications in conjunction with SDS.

SDS food products are currently very limited in food markets [1, 9, 10]. However, a new slow-digesting rice starch (Ricemic), developed by the US Department of Agriculture (USDA), and a kind of starch-based cereal food, EDP® (“energy delivered progressively”), are available in markets [11]. This chapter focuses on the preparation, structures, physicochemical properties, functions, and potential applications of SDS.

2.2 Preparation of SDS

Native starch is a good texture stabilizer and regulator of food systems, but factors such as its low shear resistance, thermal resistance, and high tendency to retrogradation restrict its use in some food applications. Starch is commonly modified both chemically and physically to generate starches with special functional properties. However, most industries (especially the food and pharmaceutical industries) prefer starches that have been physically altered, to ensure their relative safety. SDS can also be prepared with enzymatic methods or several of these methods.

2.2.1 Physical Modification Methods

The advantages of using physical methods to prepare SDS are that these methods are considered more natural and are very safe [12]. The physical modification methods used to produce SDS include hydrothermal, malleablization, autoclaving, microwaving, and polymer entrapment methods (Table 2.1) [13–20]. The SDS content of pea starch is the highest of the native starches. Heat–moisture treatment (HMT) markedly improves the SDS content of waxy potato, potato, waxy corn, rice, yam, and banana starches, whereas it has little obvious effect on pea starch.

A higher percentage of SDS is mainly attributed to the facts that intact starch granules are retained during physical modification treatments and that intact granules are less susceptible to amylolytic enzymes. Some treatments cause the formation of amylose–lipid complexes in the starch granules, which can lower the susceptibility of SDS products to enzymatic degradation. In other words, any physical modification of the starch structure that affects enzyme binding and therefore the rate of its digestion can be used to modulate starch digestibility and form SDS [18].

On the other hand, a higher percentage of SDS can involve a higher ratio of imperfect crystallites to perfect crystallites. Most SDSs consist of amorphous regions and weak crystallites, with a high proportion of dextrin, with a degree of polymerization (DP) ≥ 25. This structural information can be used to develop low-digestibility food products.

Table 2.1 Physical modification methods for preparing SDS

Modified method	Native starch	Preparation condition	Content of SDS/%		References
			Native starch	Modified starch	
HMT	Waxy potato	Water 25.7%, 120 °C, 5.3 h	8.1	41.8	[13]
HMT	Pea	Water 30%, 120 °C, 24 h	40.3	45.3	[14]
HMT	Potato	Water 30%, 30 °C, 12 h	5.4	37.5	[15]
HMT	Waxy corn	Water 35%, 120 °C, 10 h	0.8	9.3	[16]
HMT	Germinated brown rice	Water 30%, 100 °C, 1 h	39.1	46.3	[17]
HMT	Rice	Water 16%, 121 °C, 1 h	38.2	43.3	[18]
Malleableize	Pea	Water 70%, 50 °C, 24 h	40.3	43.2	[14]
Autoclaving	Yam	Water 83%, 121 °C, 1 h	15.0	34.1	[19]
Parboiling	Corn	Water 83%, 60 °C water bath 2 h	22.2	35.5	[19]
Microwave	Banana	Water 83%, 20 min	9.9	18.3	[19]
β-Cyclodextrin	Rice	Water 80%, 25 °C, *β*-CD 3%	18.1	52.1	[20]

HMT heat–moisture treatment

Figure 2.2 [13] shows the surface features and cross-sectional views of HMT waxy potato starch granules. Scanning electron micrographs of the native starch granules show round or oval shapes, with no evidence of fissures or cracks (Fig. 2.2a1), and the cross sections show no hollow internal structures (Fig. 2.2a2). However, the surfaces of all the HMT samples show signs of cracking and dents (Fig. 2.2b1–f1), and the cross section of each starch granule shows a large hollow in

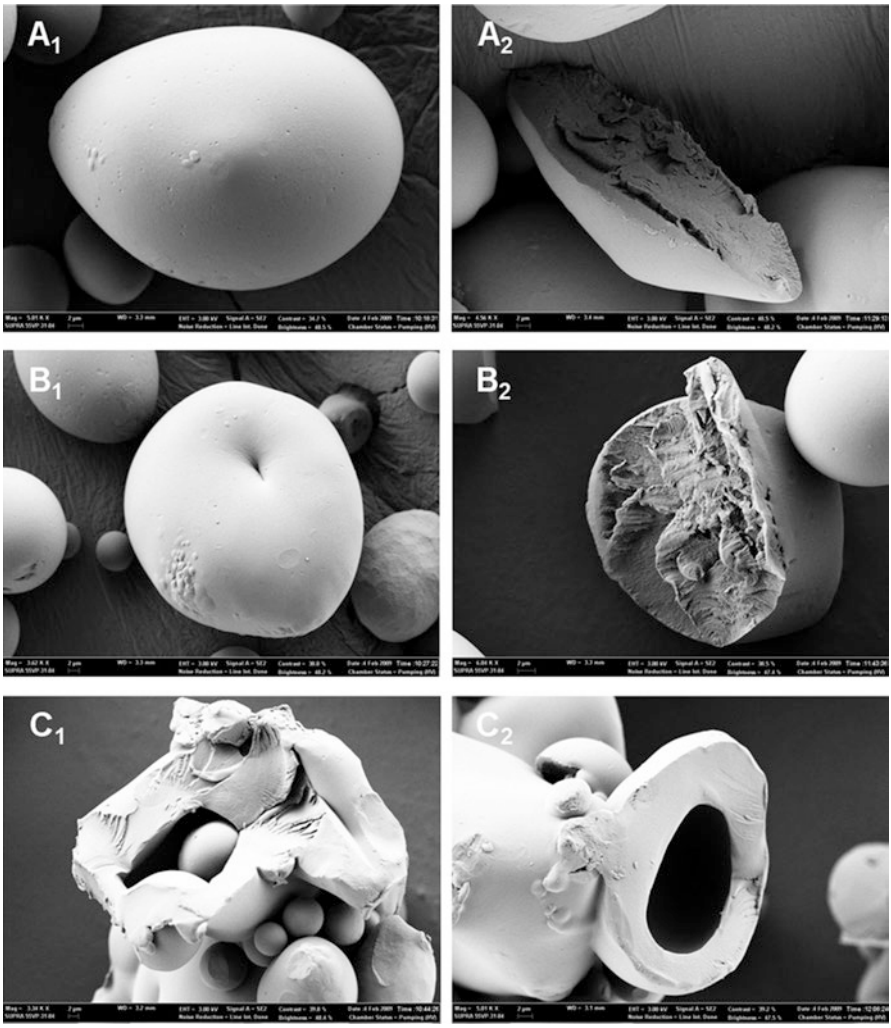

Fig. 2.2 Scanning electron micrographs of heat–moisture-treated (HMT) waxy potato starch: (**a**) native starch; (**b**) sample B (20%, 110 °C, 5 h); (**c**) sample C (30%, 130 °C, 1 h); (**d**) sample D (20%, 130 °C, 9 h); (**e**) sample E (30%, 150 °C, 5 h); (**f**) sample F (25.7%, 120 °C, 5.3 h). (1) SEM images of the surfaces of the starch granules; (2) SEM images of the cross section of the starch granules [13]

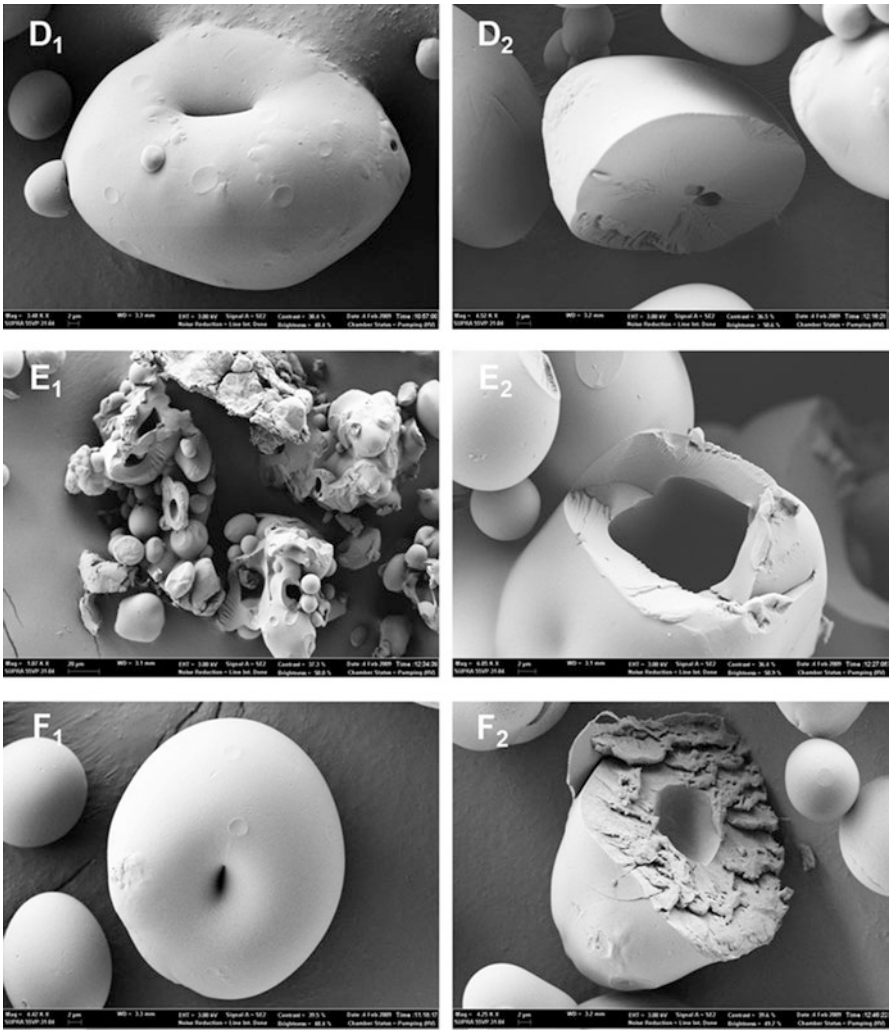

Fig. 2.2 (continued)

the central region, the size of which is probably proportional to the moisture level. These results may be attributable to the partial swelling and disruption of the starch granules by the abundant water molecules. The hollow structures at the centers of the HMT starch granules may have resulted from the rearrangement of the molecular structure and the disintegration of the central tissue during HMT. At a high moisture level (30%), the hollow region was large and readily visible.

Both samples B and D were treated with 20% moisture. No hollow region was observed in the cross section of starch sample B (110 °C, 5 h), but a small hollow region was observed in sample D (130 °C, 9 h). Therefore, this difference is attributable to the higher treatment temperature and longer treatment time. Samples C

(130 °C, 1 h) and E (150 °C, 5 h) were both treated with 30% moisture and showed the largest hollow regions. Overall, the size of the hollow region increased as the moisture level, temperature, and time of treatment increased. Among these three factors, the moisture level had the most significant effect on the size of the hollow region [13].

The development of new crystallites in the amorphous region through the interactions between amylose chains or the formation of crystalline amylose–lipid complexes may contribute to the reduction in enzyme sensitivity of HMT starches [16]. Recent studies have demonstrated that the hydrophobic section of some lipids is preferentially introduced into the central axis of the amylose helix to form an amylose–lipid complex during interactions between amylose and lipids [21, 22]. The amylose chain of starch has a natural twist, producing a helical conformation with six anhydroglucose units per turn [7]. Amylose has a helical conformation and can form inclusion complexes with small hydrophobic molecules. Complexes between fatty acids, such as lauric acid, and amylose can form rapidly under physiological conditions and contribute to the formation of both SDS and RS [23]. The formation of such complexes with lipids can cause significant changes in the behavior of starch, reducing its solubility, increasing its gelatinization temperature, delaying its retrogradation, and increasing its resistance to digestive enzymes.

The complex formed has an unstable V-type crystalline structure and inhibits the formation of B-type recrystallized starch. The stability of the V-type complex to amylolytic and lipolytic enzymes has been estimated, and its melting temperature is above 100 °C [22]. This resistance to high temperature protects SDS from dissociation during food processing. However, the lipid content added during the formation of amylose–lipid complexes often exceeds 10% and contributes a lot of additional energy.

Zhan et al. demonstrated that β-cyclodextrin (β-CD) interacts with paddy starch to increase the yield of SDS. Under the optimum conditions for modification (β-CD, 3%; water, 80%; and equilibrium temperature, 25 °C), the maximum SDS yield was 52.1%. The basic rule for conferring slow digestibility is the formation of starch–β-CD non-inclusion complexes with a partial V-type structure and weak resistance to enzymes. Starch–β-CD non-inclusion complexes were found more suitable for improving the SDS yield than starch–lipid complexes [20]. In vivo data have suggested that potato amylose–lipid complexes (weight ratio, amylose/lipid = 5:1, 60 °C) are hydrolyzed and absorbed within 120 min of ingestion to the same extent, but somewhat more slowly, than uncomplexed starch, with a 12% lower digestion rate [24].

Figure 2.3 [25] presents SEM images of a rice SDS product prepared with single-retrogradation or dual-retrogradation treatments over different time intervals. In that study, rice starch (5.0 g) was dispersed with two volumes of distilled water and heated in a boiling water bath for 30 min. The resultant gel was hermetically sealed and stored at 4 °C for 24, 36, or 48 h to analyze its retrogradation. The retrograded samples were regelatinized in a boiling water bath for 20 min and subjected to a dual-retrogradation treatment for periods of 24, 36, and 48 h. Each of the resulting gels was dried at 40 °C for 8 h. The SEM images revealed that the SDS products that

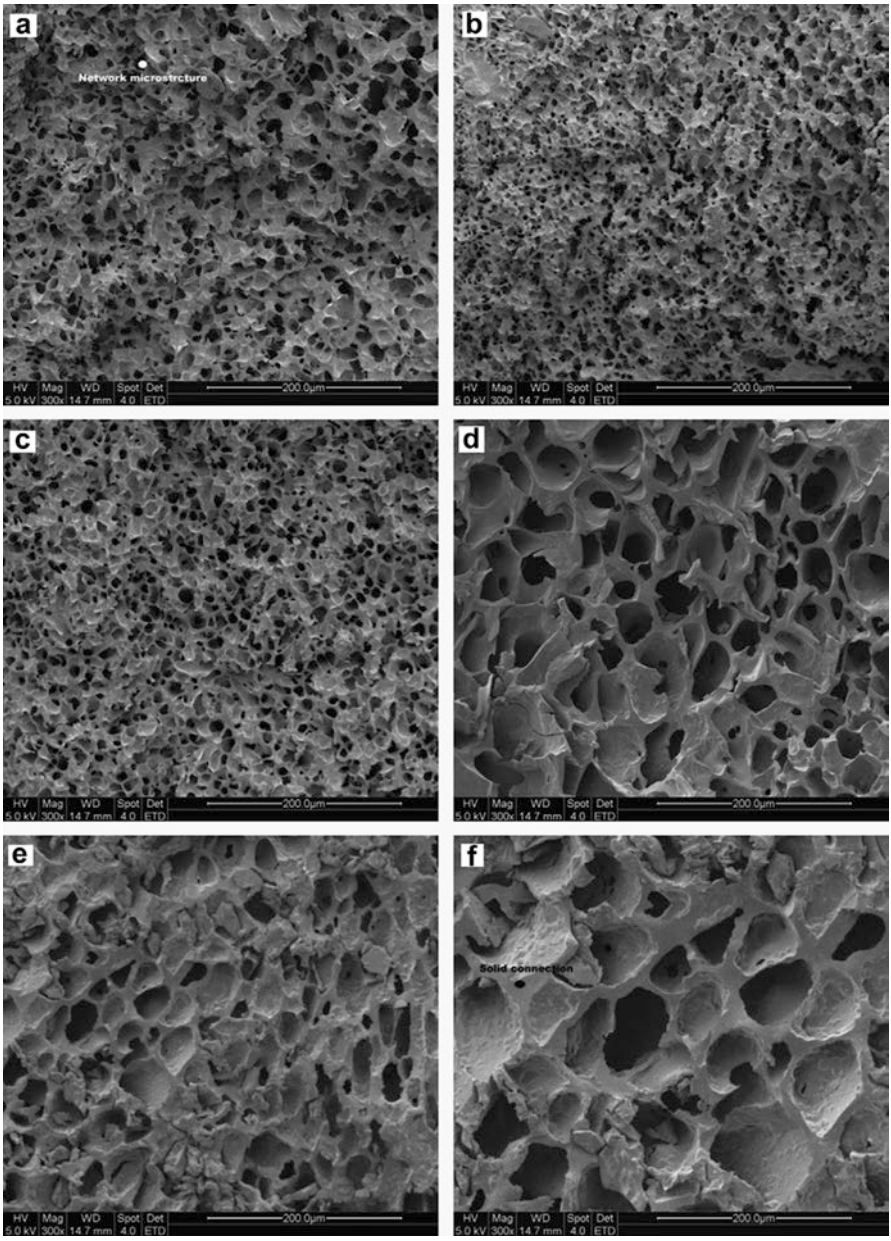

Fig. 2.3 Scanning electron micrographs of SDS products prepared from rice starch by (**a**) single retrogradation with a time interval of 24 h, (**b**) single retrogradation with a time interval of 36 h, (**c**) single retrogradation with a time interval of 48 h, (**d**) dual retrogradation with a time interval of 24 h, (**e**) dual retrogradation with a time interval of 36 h, and (**f**) dual retrogradation with a time interval of 48 h [25]

underwent single retrogradation had network microstructures with smaller cavities than those observed in SDS after dual retrogradation. This morphological conformation was produced by starch gelatinization, but was not affected by the retrogradation time (Fig. 2.3a, e, c). However, larger holes and more solid connecting parts were observed in the SDS products subjected to dual retrogradation (Fig. 2.3). The larger cavities reduced the contact area between the starch and amylase molecules. Furthermore, the solid connecting parts formed during the dual-retrogradation treatment prevented the starch molecules leaching out and produced moderate retrogradation, resulting in a higher SDS yield. Compared with single retrogradation, dual retrogradation generated larger cavities and more solid connection parts in the SDS products. This internal microstructure increased the degree of slow digestibility. These findings suggest that dual retrogradation can be used to increase the yield of SDS in starchy products.

2.2.2 Chemical Modification Methods

Starches are modified by chemical methods to improve their functionality and increase their commercial value. Several key structural properties of starches can be modified to functionalize the copolymer to meet specific requirements and to confer a variety of physicochemical benefits.

Many modified starches made for food use contain only small amounts of substituent groups and are used as safe food ingredients. Legislative approval for the use of novel starch derivatives in processed food formulations is still under debate, but several tailor-made starch derivatives with multiple modifications are being prepared and characterized [7]. Some chemically modified starches are increasingly used as fat replacements or fat substitutes in different food systems. These starches are either partially or totally undigested and therefore contribute few calories to the food [7].

The chemical modification of starch is generally achieved through its derivatization, including the etherification, cross-linking, oxidation, substitution, and grafting of the starch molecule. Chemical modification involves the introduction of functional groups into the starch molecule, which markedly alters its functional properties. These modifications of native granular starches profoundly alter their gelatinization, pasting, and retrogradation behaviors [26].

Some chemical methods used to prepare SDS are shown in Table 2.2 [19, 27–29]. After treatment with acid or esterification, the SDS content of the modified starch is significantly greater than that of the native starch.

Chemical reagents provide nonionic, cationic, hydrophobic, or covalently reactive substituent groups. These modifications generally alter the gelatinization and pasting properties of starch [30]. Citric acid, a polyfunctional carboxylic acid, can be used to esterify the hydroxyl groups on starch, resulting in the formation of cross-links and improving the starch properties or SDS content [27].

Table 2.2 Chemical modification methods for preparing SDS

Reagents	Native starch	Preparation condition	Content of SDS/%		References
			Native starch	Modified starch	
Citric acid	Paddy rice	2.62 mmol acid/20 g starch, 128.4 °C, 13.8 h	9.8	23.0	[27]
Citric acid	Mung bean	Citric acid 30%, starch 20%, pH 2.0, 120 °C, 1 h	15.1	23.3	[19]
Hydrochloric	Mung bean	Hydrochloric 1.0 mol/L, starch 20%, pH 5.0, 120 °C, 1 h	15.1	23.3	[19]
Vitriol	Mung bean	Vitriol 0.3 mol/L, starch 20%, pH 2.0, 120 °C, 1 h	15.1	23.3	[19]
OSA	Waxy corn	OSA 3%, starch 40%, pH 8.4, 35 °C, 2.3 h	15.0	25.0	[28]
OSA	Waxy corn	OSA 3%, starch 57%, pH 8.5, 20 °C, 6 h	15.3	28.1	[29]

OSA octenyl succinic anhydride

A study of paddy rice starch treated with citric acid (2.62 mmol acid/20 g starch, 128.4 °C for 13.8 h) showed an increase in the apparent amylose content from 21.1% to 30.3%, indicating that it contained more linear chains, derived from the amylopectin side chains and acid-hydrolyzed amylose. The reduced molecular weight caused by the acid treatment allowed a greater freedom of polymer motion and enhanced its ability to form more stable structures that better resisted enzymatic hydrolysis [27].

Esterification with octenyl succinic anhydride (OSA) is one of the modifications that most effectively increase SDS. OSA-modified starch showed an extremely low glycemic response during human trials, consistent with the extended glucose release profile of SDS [28]. The SDS (42.8%) produced by subjecting OSA-treated waxy corn starch to HMT (10% moisture, 120 °C for 4 h) was higher than that produced by treating OSA-modified starch with the Englyst test method (28.3%). The modified starch products with attached OSA molecules may act as noncompetitive inhibitors of digestive enzymes, reducing enzyme activity and thereby slowing digestion [28, 29]. As these studies show, chemical modification can be used to prepare SDS, but clinical and toxicological trials are required to evaluate the safety and nutritional efficacy of consuming this SDS.

2.2.3 Enzymatic Modification Methods

The enzymatic processing of starch is a commonly used and effective modification technique. Enzymatic treatments of starch with pullulanase, isoamylase, α-amylase, β-amylase, or transglucosidase can change the chain lengths of starch, thus achieving the appropriate digestibility and glycemic response [31, 32].

After treatment with different kinds of enzymes, the structures and physicochemical properties of starches change. Some enzymatic methods used to prepare SDS are shown in Table 2.3 [33–35]. After treatment with enzymes, the SDS contents of most starches clearly increase. After treatment with pullulanase, the SDS content of native waxy rice starch reached a high level but decreased to 24.9% after cooking [33].

Xiong studied the SDS content of normal corn starch after *β*-amylase, transglucosidase, or maltogenic amylase treatment. The product obtained after processing with *β*-amylase showed an increased SDS content, with an average chain length of DP 16.16 and a branch density of 6.19%. After treatment with a combination of enzymes (*β*-amylase and transglucosidase), the product had a higher SDS content, with an average chain length of DP 14.36 and a branch density of 6.96%. After treatment with maltogenic amylase, the product had the highest SDS content, with an average chain length of DP 10.95 and a branch density of 9.13%. These results sug-

Table 2.3 Enzymatic modification methods for preparing SDS

Enzymes	Native starch	Preparation condition	Content of SDS/%		References
			Native starch	Modified starch	
Pullulanase	Waxy rice	Starch (10% w/v) boiled with continuous stirred for 30 min, adjust temperature to 58 °C, pullulanase 60 ASPU/g, 12 h	45.5	57.8	[33]
Amylosucrase	Waxy rice	Starch (2%, w/w) and sucrose (100 mM) in 100 mM in sodium citrate buffer (pH 6.0), boil suspension for 10 min. Adjust temperature to 30 °C, add amylosucrase (40,000 U), 40 h	4.9	29.1	[34]
Amylosucrase	Waxy corn	Ditto	5.2	30.2	[34]
Amylosucrase	Waxy potato	Ditto	4.4	24.2	[34]
β-Amylase	Normal corn	Starch (8% w/v) shake for 20 min in 95 °C, adjust temperature 55 °C, pH 5.2, adding 0.032% *β*-amylase, shake for 12 h	15.2	22.4	[35]
β-Amylase+ transglucosidase	Normal corn	Starch (8% w/v) shake for 20 min in 95 °C, adjust temperature 57 °C, pH 5.2, adding mixed enzyme (composited ratio, 0.032%:8 TGU), shake for 8 h	15.2	33.5	[35]
Maltogenic amylase	Normal corn	Starch (8% w/v) shake for 20 min in 95 °C, adjust temperature 60 °C, pH 4.8, adding 40 mg/kg maltogenic amylase shake 16 h	15.2	38.1	[35]

ASPU enzyme activity, *TGU* enzyme activity

gest that enzymatic treatments can increase SDS contents and that treatment with maltogenic amylase is most effective [35].

The molecular weight of most starches decreases rapidly during enzymatic treatment. According to BeMiller and Whistler, a native starch formed two fractions with different molecular weight: amylopectin, which is a larger molecule (10^7–10^8), and amylose, which is a smaller molecule (10^4–10^6) [36].

The addition of enzymes reduced the contents and molecule weights of both amylose and amylopectin. According to Christophersen, maltogenic α-amylase quickly reduced the peak DP of amylose, with the formation of only minor glucose, maltose, and other low-molecular-weight oligosaccharides. They reported that only 3% of other low-molecular-weight oligosaccharides were produced, but the DP was dramatically reduced from DP 350 to DP 123 [37]. Bijttebier et al. reported that the maltogenic α-amylase from *Bacillus stearothermophilus* preferentially hydrolyzed the exterior chains of amylopectin during the early stages of hydrolysis but also hydrolyzed the inner chains, with high multiple attack action, during the later stages [38]. These data suggest that the endomechanism of maltogenic α-amylase is consistent with the reduced molecular weight of the starch molecule. It is generally known that amylopectin consists of multiple clusters connected by long linear chains. Based on the enzymatic properties of the branching enzyme, the α-1,6-linked segments between the amylopectin clusters are hydrolyzed to release the cluster units. Similar findings have been reported by the others [39]. The action of enzymes on the linear chain of amylose can also form branched linkages and a cyclic amylose, and these reactions may change the physical structure of the substrate, slowing its digestion time [40, 41].

According to the Hizukuri cluster model, amylopectin molecules have A, B (B1–B4), and C chains, and the fractions DP < 13 and DP 13–30 together constitute the short chains, corresponding to the A + B1 chains. The other longer-chain fractions correspond to the B2–B4 chains [42]. It has been reported that maltogenic α-amylase has a marked effect on the side-chain distribution of starch and especially reduces the number of short B chains [43]. In that study, maltogenic α-amylase reduced the levels of the outer chains (primarily A and B1) by 50% compared with the control sample, with little effect on the internal chain length. Based on these observations, it can be concluded that the addition of maltogenic α-amylase reduced the molecular weight of amylopectin, and significantly affected the side-chain distribution of the residual amylopectin, increasing the relative numbers of short chains. The reduced proportion of short chains could lead to the formation of more perfect crystallites, increasing the starch's resistance to starch-digesting enzymes [43].

In the study by Miao et al., gelatinized cornstarch (10% w/v, pH 5.0) was treated with maltogenic α-amylase (5 U/g dry weight of starch, 55 °C). The product had a higher proportion of short chains than the native cornstarch (44.2% and 23.7%, respectively), which maximized the SDS content (19.6%) [44]. A starch debranching analysis (mutant cornstarch debranched with isoamylase) revealed a parabolic relationship between the SDS content and the weight ratio of amylopectin short chains (DP < 13) to long chains (DP > 13). Amylopectin with higher amounts of either short chains or long chains can contain relatively large amounts of SDS [45].

2.2.4 Composite Modification Methods

Compared with the modification methods discussed above, the composite modification methods have several advantages in the preparation of SDS, including greater efficiency and cost-effectiveness. Some composite modification methods used to prepare SDS are shown in Table 2.4 [46–50], including different combinations of physical, chemical, and enzymatic methods. The combination of different kinds of modification methods has several advantages, including a great increase in the SDS content compared with the native starch.

Dual modification methods combining debranching modification and other types of modification can be used to prepare SDS with various properties and functionalities. Debranched-acetylated starch and debranched-octenyl succinylated (OSA) starch have shown great potential utility in starch–lipid complexes, low-fat salad dressings, and emulsion stabilizers [51–53]. Recently, there has been increasing interest in the preparation of micro- and nanocomposites [54–57]. These new composites, with slow digestibility and barrier properties, can be used to design economic and biocompatible delivery systems for bioactive agents in foods, beverages, and pharmaceutical agents.

In general, the physical modification methods for SDS have several disadvantages, including lower yield. Moreover, the equipment required to produce SDS products is always expensive and cannot meet the requirements for continuous production. However, it is the safest way to generate SDS because no hazardous substances are incorporated into the products during processing. Chemical production methods for SDS are widely used in industry, but the use of chemical reagents in the production process is not environmentally friendly, and their application to food products is restricted. Enzymatic methods are suitable for producing many SDS products, but the cost is so high that they cannot meet the demands of industrial production. Together with the several other advantages of composite methods, the SDS produced with composite methods is more stable to heat than that produced by other methods.

2.3 Digestibility of SDS

An apparent direct negative relationship between large granules and starch digestibility was reported in 1922. Many studies have since confirmed this relationship [58]. Lindeboom reported that small barley and wheat starch granules are hydrolyzed faster than large granules [59]. Singh et al. observed significant differences between the enzymatic hydrolysis of different native potato starches when fractionated according to small, medium, and large granules [26].

The lower susceptibility of large granule starches to enzymatic hydrolysis has been attributed to the smaller specific surface area of the granules, which may reduce the extent of enzyme binding and ultimately result in less hydrolysis that occurs in small granules [60].

Table 2.4 Composite modification methods for preparing SDS

Modified method	Native starch	Preparation condition	Content of SDS/%		References
			Native starch	Modified starch	
Pullulanase – retrogradation	Waxy corn	Native starch samples hydrolyzing with pullulanase (20 U/g) for 6 h and then cooled at 4 °C for 2 days	–	45.1	[46]
Pullulanase – lipid	High amylose corn	Native starch slurry (10% w/v, pH 4.4) cooked in boiling water bath with stirring for 30 min. Adjusted temperature to 60 °C, add pullulanase 40 ASPU/g of starch for 2 h; mix with lauric acid (10% w/w, db), boiling water bath for 30 min	6.6	11.2	[47]
Emulsifier – alcohol	High amylose corn	Native starch 5 g, glycerin monostearate 0.5 g, 40% ethyl alcohol 35 mL, KOH (3 M) 25 mL cooked in 35 °C water bath for 15 min	–	67.4	[48]
Cross-link – esterification	Waxy rice	Native starch slurry (35% w/v, pH 9) with STMP 6.5% cooked in 35 °C water bath for 4.5 h; adjusted to pH 8, add OSA 5.3%, cooked for 15 h	13.8	33.8	[49]
Ultrasonic wave – pullulanase	Corn	Native starch slurry (10%) cooked in 70 °C water bath for 20 min; adjusted to 40 °C, add 14% pullulanase, ultrasonic wave (300 W) for 40 min	25.3	43.1	[50]
Microwave – HMT	Corn	Water 60%, 50 °C, microwave 300 W for 25 min	25.3	38.3	[50]

ASPU enzyme activity, *db* dry starch base, *HMT* heat–moisture treatment, *STMP* sodium trimetaphosphate, *OSA* octenyl succinic anhydride; "–" means not mentioned

How the structural aspects of SDS are related to the mechanisms of its digestion and their health implications have been investigated and reported [21, 61]. Based on current data, the slow digestibility of SDS is caused by two factors, its physical structure and chemical construction, both of which reduce the contact between enzymes and SDS.

2.3.1 Physical Structure of SDS and Its Digestibility

The digestion of starch granules is a complex process that includes different phases: the diffusion of the enzyme toward the substrate, which is affected by the porosity of the substrate; the adsorption of the enzyme to the starchy material; and the

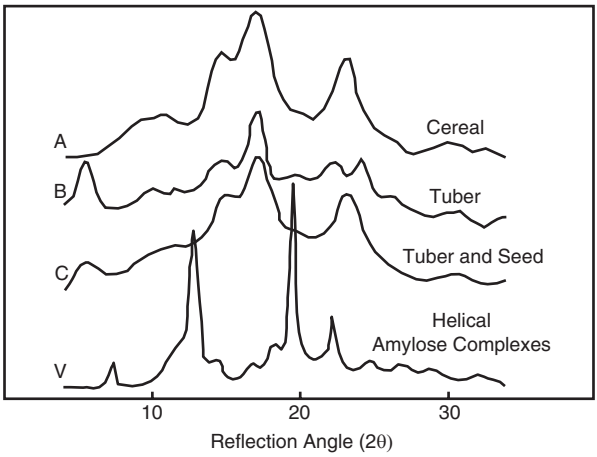

Fig. 2.4 X-ray diffraction patterns of different starches [7]. A, B, C, V: types of crystal structures in starch

hydrolytic event [62]. A large amount of starch is protected from the protein and other components of food, and is not contacted by digestive enzymes, which is why pasta contains so much SDS.

X-ray diffraction scattering studies have classified native starches into types A, B, C, and V (Fig. 2.4) [7]. The molecular structure of the starch granules, especially the arrangements in A-type and B-type crystallites, influences the hydrolysis of the starches. A-type polymers are less resistant to amylase hydrolysis than B-type polymers. The shorter double helices and interior crystallites present in A-type starches are more susceptible, whereas long chains form longer and more stable helices and are more resistant to enzymatic hydrolysis [21]. The structural arrangements of the A-type or B-type crystallites markedly influence their digestibility. Generally, a higher susceptibility to hydrolysis has been reported for the A-type crystallites than the B-type crystallites [63]. A-type and B-type starches differ in the packing of their double helices and in their water content [64]. The shorter double helices and interior crystallites of the A-type starches are more readily digestible and contain larger amounts of RDS and SDS than the B-type starches [65].

A comprehensive account of the enzymatic digestibility of native uncooked starches from different sources has been given by Dreher et al. [66–68]. The authors suggest that cereal starches are more digestible than tuber and legume starches, which may be attributable to the presence of numerous pinholes in the surface layers of the granules and pores, which penetrate toward the interior of the granules from cereal sources, such as corn. These pores in the granules facilitate the entry of amylases, allowing the digestion of the granules.

Huber et al. demonstrated that both the crystalline and amorphous regions in cereal starch granules have the same granule center, as shown in Fig. 2.5 [69]. Enzymatic digestion begins at the surface pores and interior channels, and then digestion gradually enlarges the channel by simultaneously digesting the crystalline

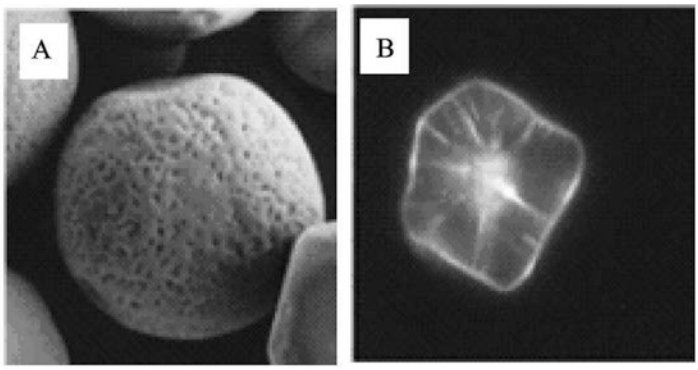

Fig. 2.5 (**a**) (SEM) Surface pores of a cereal starch granule; (**b**) (micrograph) the interior channels and cavity revealed with an aqueous solution of merbromin [69]

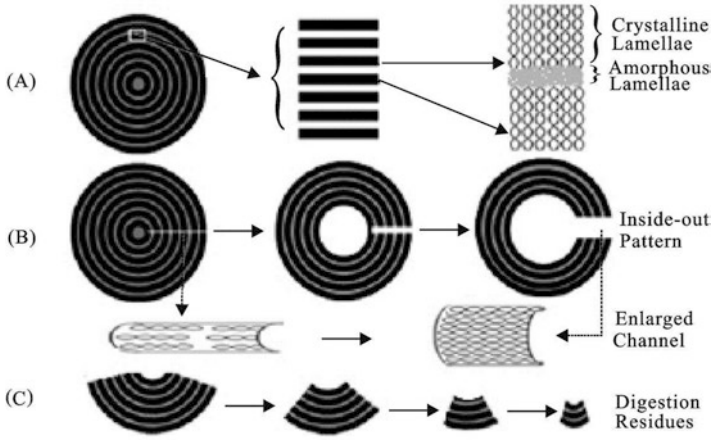

Fig. 2.6 Schematic representation of the dynamic side-by-side digestion mechanism and resulting static inside-out digestion pattern [70]

and amorphous regions. This explains this slow digestion process. Figure 2.6 [70] shows that the digestion of the starch granules starts at the interior channels.

In general, starch is consumed after it is processed. An excess of water and high temperatures during processing cause starch gelatinization and destroy its granular structure. However, the granular structure of starch is retained in several low-moisture food products, such as biscuits [71].

The hydrolysis of native starches can vary greatly, depending on the interplay of a range of factors, but it is usually determined by the botanical origin of the starch, which determines its morphology and crystalline organization [72]. This offers a way to influence starch digestibility with breeding research and the selection of suitable crop varieties.

The diffusion of α-amylase into the substrate is considered an important step in hydrolysis. The interactions of starch with fiber, protein, and other food components can prevent the effective diffusion and adsorption of α-amylase [62]. The hydrolysis of starch was previously considered to start from the surface of the granule. However, native cereal starches, such as corn and sorghum starches, contain peripheral pores and channels that allow the penetration of α-amylase, resulting in an inside-out hydrolysis mechanism [70]. In contrast, potato starch and other B-type starches are digested from the surface of the starch granule [73], explaining the higher digestibility of cereal starches compared with tuber starches, such as potato starch [74, 75]. Tuber starches are generally more resistant to enzymatic hydrolysis than cereal starches, because of their larger granules, their surface properties, and their supramolecular arrangement. The large amounts of resistant starch in tubers, particularly the potato, and in fruits such as the banana have been reported both in vitro and in vivo [1], whereas cereal starches, such as rice, wheat, and barley starches, are highly digestible [76]. Native normal cornstarch, waxy starches, millet starches, sorghum starches, and legume starch reportedly display intermediate digestibility because they contain medium-to-high amounts of SDS [74, 77–79]. Part of the lower digestibility of millet, sorghum, and legume starches can be attributed to their interactions with protein, which forms a protective network around the granule.

2.3.2 Fine Structure of SDS and Its Digestibility

When starch is processed for use in food, the starch is gelatinized. At this time, the molecular structure of the starch is the only factor determining its functionality and nutritive peculiarities. The molecular structure of starch includes the ratio of amylose and amylopectin and the fine structure of amylopectin [80].

At the molecular level, the crystallite structure and the packing of the amorphous phase influence the enzymatic susceptibility of starch [73]. The unit chain length of amylopectin correlates with its digestibility, and the proportion of the amylopectin unit chain length with DP 8–12 or DP 16–26 correlates positively and negatively, respectively, with its hydrolysis [81]. Longer chains form longer and more stable helices, which are further stabilized by hydrogen bonds distributed throughout the entire crystalline region, which further reduce its digestibility.

The nature of starch also influences its digestibility and the postprandial glucose response. Starches high in amylopectin have been shown to be digested more quickly than those high in amylose [82], probably because amylopectin has many more nonreducing chain ends than amylose, to which digestive enzymes can attach [83].

Some researchers have shown that the fine structure of amylopectin, with its high branching density and either long or short internal chains, causes its slow digestion. Therefore, the inherent molecular structure of amylopectin is responsible for its

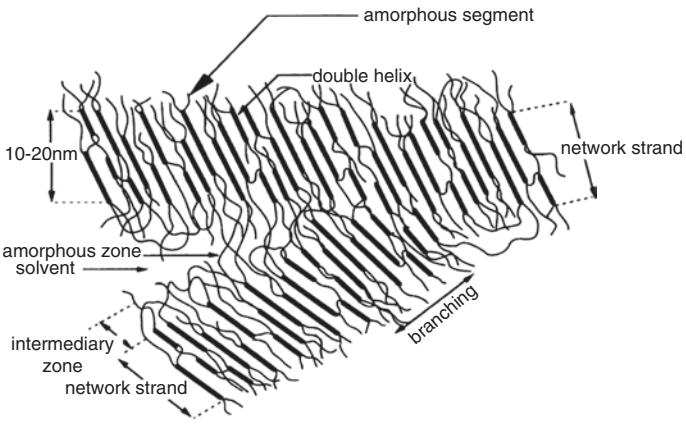

Fig. 2.7 Structure of amylose gel, a structural feature of recrystallized SDS [85]

slow digestion [63, 84]. The structure of SDS may include imperfect crystallites and amylopectin, with a high branching density, which probably cause its slow digestion [3].

An illustration of retrograded starch chains and the arrangement of the amorphous material that determine the formation of SDS is presented in Fig. 2.7. It is proposed that amylose chains aggregate in an infinite three-dimensional network, linking the microstructure and the macromolecular organization of starch. The chain segments inside the crystallites are disposed obliquely relative to the microfiber axis. Therefore, the network of strands consists of contiguous associated blocks aligned along the length axis of the microfiber. Double helices are then linked to other helices by loops of amorphous amylose segments, dangling in the gel pores. This fraction is responsible for the hydrodynamic behavior of amylose gels [85].

2.4 Physicochemical Properties of SDS

2.4.1 Postprandial Glycemic Response

The slow digestion property of SDS products can be confirmed with a postprandial glycemia test. The microencapsulation of normal cornstarch by zein protein was investigated, and the starch capsules displayed a significant increase in SDS [86]. In a further in vivo study using a mouse model, both the cornstarch material and the encapsulated starch material showed slow digestion profiles, with the prolonged and sustained elevation of blood glucose, confirming that microencapsulation did not alter the inherent slow digestion property of native normal cornstarch.

Dietary carbohydrates are the main source of energy in the human diet and are also the main determinant of postprandial blood glucose levels. In recent decades, the effects of carbohydrate-rich diets on human health have been debated because of

their potential untoward effects on glycemic control and plasma lipid concentrations. A high intake of refined carbohydrate foods has been particularly associated with increased plasma glucose and insulin levels in the postprandial period, the elevation of fasting and postprandial plasma triglycerides, and a reduction in high-density lipoprotein (HDL)–cholesterol levels [87–89]. A large body of evidence indicates that blood glucose concentrations are an important and independent risk factor for cardiovascular diseases, not only in diabetic patients but also in individuals with normal fasting glucose levels.

Delayed dietary carbohydrate digestion and absorption may have significant beneficial implications for the prevention and treatment of metabolic disorders. Many factors influence the digestion of carbohydrates in the small intestine, including their viscosity, the physical form of the food, the cooking and processing methods, the type of starch (amylose or amylopectin), the presence of antinutrients, and the amounts of fiber, fat, and protein present [89].

The postprandial glycemic and lipid responses are linked to the risk of chronic diseases. The rate of digestion of dietary carbohydrates in the intestine plays a clinically relevant role in the regulation of the postprandial metabolism. After a meal, glucose levels are modulated by the rate of carbohydrate digestion in the small intestine and by the fermentation of undigested carbohydrates in the colon. Moreover, when the carbohydrate reaches the colon, it has a beneficial effect on the composition of the colonic microbiota and on short-chain fatty acid production, which improves the metabolism of glucose and lipids. This explains why a diet based on legumes, vegetables, fruits, and high amounts of SDS can significantly improve an individual's cardiovascular risk profile, particularly in type 2 diabetic patients, and can substantially reduce the overall risk of cardiometabolic diseases [90].

2.4.2 Gelatinization Parameters

When heated in excess water, starch granules undergo gelatinization in three distinct stages: the granule swelling, the disruption of the ordered (crystalline and molecular) structures, and the solubilization of the starch molecules [91]. Gelatinization causes irreversible changes in the starch properties, including its water uptake, granule swelling, crystal melting, birefringence, solubility, and viscosity. These changes greatly affect the functional properties of starch and its digestion. These changes also involve a sequence of thermal events that results in the phase transition of the starch granules. When starches are heated in limited water, biphasic endotherms are often observed with differential scanning calorimetry (DSC), which is related to the gelatinization and melting of the starch crystallites [92].

In the SDS gelatinization studies mentioned above [13, 14, 28, 29], the thermal parameters of modified and native starches were determined with DSC, and the results showed that the gelatinization parameters of starch differ considerably before and after modification.

2.4.3 Starch Pasting Properties

Pasting involves the swelling of the starch granules, the leaching of carbohydrates, the formation of a three-dimensional network of leached molecules, and the interactions between the granule remnants and the leached material. It is determined by the botanical origin of the starch, its amylose content, the distribution of amylopectin chain lengths, the swelling power, the starch concentration, and the processing conditions, such as the shearing and heating rates.

The determination of starch pasting profiles with a rapid visco analyzer (RVA) was originally proposed by Charles (Chuck) Walker in rain-damaged wheat [93]. RVA starch pasting profiles are currently used extensively in the human food industry, e.g., to determine the different parameters related to the starch pasting properties of cereals and starchy foods [86].

The typical profile of a starch sample analyzed with RVA indicates the main parameters measured during the analysis. The pasting temperature provides information about the minimum temperature required to cook a given sample [94]. Other parameters, such as the rate of breakdown in viscosity and the hot paste viscosity or trough, depend upon the temperature and degree of mixing [94]. The reassociation of the starch molecules during cooling is commonly referred to as the "setback." It involves the retrogradation of the starch molecules and has been correlated with the texture of various products. The final viscosity of the starch is the parameter most commonly used to define the pasting properties of a given sample.

In recent years, several authors have evaluated the use of multivariate data analysis techniques to better interpret RVA profiles and have obtained further information about the starch pasting properties of a sample [95, 96].

The RVA results of Xu and Zhang [86] showed that encapsulated starch was considerably altered. In that study, the microencapsulation of normal cornstarch with zein protein and its slow digestion property were investigated. A significant increase in SDS was detected in the starch capsules (weight ratio of zein to starch, 1:6) containing plasticizers (glycerol and oleic acid) after high-temperature (70 °C) treatment. The temperature at peak viscosity increased, and the peak viscosity of the microencapsulated starch was substantially reduced, indicating improved thermal resistance after microencapsulation. These data suggest that the starch granules were densely packed in the zein matrix after the high-temperature treatment, which may slow the enzymatic digestion and generate a relatively high amount of SDS.

2.5 Functions of Slowly Digestible Starch

Studies of the benefits of SDS are limited. The potential health benefits of SDS are linked to stable glucose metabolism, diabetes management, mental performance, and satiety.

2.5.1 SDS and the Metabolic Response

The metabolic effects of carbohydrates, particularly glucose, are related to the rate of carbohydrate absorption after a meal. A common measurement that assesses these effects is the GI. Positive associations have been established between the dietary GI and the risk of colon and breast cancer [97]. SDS has a medium-to-low GI and therefore reduces the glycemic load of a food product compared with that of RDS, which has a high GI [10].

The limited research available in humans suggests that SDS blunts the postprandial increase and subsequent decline in the plasma glucose and insulin concentrations, leading to prolonged energy availability and satiety, compared with more rapidly digestible starch.

There have been few reports of the effects of SDS on glucose tolerance or energy expenditure. The ingestion of 35 g of available carbohydrate as cornstarch or waxy cornstarch (both SDS) resulted in a smaller and more sustained increase in plasma glucose than did maltodextrin (an RDS) [98]. In healthy young women, a meal containing slowly digestible waxy cornstarch resulted in lower peak concentrations of plasma glucose and insulin than a meal containing cooked, rapidly digestible cornstarch [99]. In young men, the consumption of uncooked cornstarch (an SDS) blunted their plasma glucose and insulin responses. During the first 120 min after consumption, the area under the glycemic dose–response curve for the SDS was smaller than that after the consumption of glucose, whereas after 120 min, there was no difference between the two areas [100].

Sands et al. examined the effects of uncooked waxy cornstarch (an SDS) on postprandial plasma insulin and glucose and on the whole-body energy expenditure and appetites of men and women. The consumption of uncooked waxy cornstarch led to lower postprandial glucose and insulin concentrations but had no effect on postprandial energy expenditure or appetite compared with the consumption of cooked, rapidly digested waxy cornstarch [101]. These findings are similar to those of Wachters, who reported that the consumption of 50 g of available carbohydrate from an SDS, uncooked cornstarch, led to smaller glucose and insulin areas than the consumption of 50 g of glucose [99]. In conclusion, these results establish that the consumption of native waxy cornstarch blunts the postprandial glucose and insulin responses in humans, potentially providing a steadier supply and release of energy over a specific period than the RDS maltodextrin.

The digestion of alginate-entrapped starch microspheres as a source of SDS generates short-chain fatty acids in the alimentary canal, including propionic, acetic, and n-butyric acids, which help to prevent colon cancer but produce little energy [102].

The intake of slowly available glucose improved the metabolic profiles of obese insulin-resistant subjects [103], particularly reducing postprandial insulinemia and lowering the levels of circulating triacylglycerols and the apolipoproteins in triacylglycerol-rich lipoproteins. RDS and SDS also differ in their ability to stimulate the secretion of the gut incretin hormones.

2.5.2 SDS and Diabetes

Postprandial hyperglycemia leads to insulin resistance and ultimate pancreatic β-cell failure. This results in noninsulin-dependent diabetes mellitus, which accounts for 90% of all diabetes cases.

The occurrence of obesity-related problems is currently increasing in response to modern lifestyles, the consumption of excessive dietary fat, and a reduction in physical activity. Obesity-related problems also lead to complications such as hyperlipidemia, nonalcoholic fatty liver disease, various cardiovascular diseases, and diabetes in humans. In general, diabetes is a form of metabolic disorder that occurs with the dietary intake of excessive carbohydrates and lipids [104].

Type 2 diabetes mellitus (T2DM) is a common endocrine and metabolic disease caused by an absolute or relative lack of insulin in the blood, resulting in metabolic abnormalities such as obesity, hypertension, low levels of HDL, elevated triglyceride levels, hyperglycemia, and resistance to insulin [105]. The complications of T2DM are associated with obesity, oxidative damage, dysfunction of metabolism, and eventual organ failure [106, 107].

Apart from genetic causes, the dietary pattern of an individual plays a key role in the occurrence of metabolic syndrome, which is often attributed to the increasing influence of the western diet, which contains an excessive fat content and is poor in minerals and fiber [108].

With the increased occurrence of diabetes in humans, current research has focused on the development of drugs to treat and control T2DM. Various drugs have been developed, but the long-term use of antidiabetic drugs can have considerable adverse effects, with symptoms of hypoglycemia and kidney or liver malfunction [107, 109]. Because no medication is yet effective in the treatment of T2DM, current research is concentrated on the prevention or delayed onset of diabetes by exploring the functional adjuncts responsible for it.

This increase in metabolic syndrome has challenged food scientists to develop innovative food products that combine dietary satisfaction with disease management. Therefore, reducing meal-associated hyperglycemia is one goal in the prevention of diabetes mellitus. SDS has a beneficial metabolic effect on diabetes and is recommended for its prevention and management [10, 110]. Several processes are used to produce either components that remain undigested in the upper intestinal tract or an intermediate starch, which is digested slowly in the small intestine. In this way, the release of glucose is slowed, which is advantageous for diabetic patients.

SDS-containing breakfast foods also improve carbohydrate metabolism and reduce the insulin requirements of insulin-treated T2DM patients [111]. Because there is a lack of suitable sources, uncooked cornstarch is recommended as a source of SDS for those suffering diabetes. This can improve the glycemic response at the next meal and prevent evening hypoglycemia in diabetic patients who are treated with insulin [77].

2.5.3 SDS and Mental Performance

The consumption of foods containing high levels of sugar correlates with risk factors for cardiovascular disease, including impaired glucose metabolism, obesity, dyslipidemia, T2DM, and hypertension [112]. Many biological pathways are involved in these adverse outcomes, including the glucose-related dysregulation of vascular biology and vascular functions. Most studies of sugar intake and cardiovascular risk have been cross-sectional and based on patients' self-reported usual dietary habits [113].

A previous investigation of the effects of acute glucose ingestion on the resting cardiovascular function demonstrated its potent hemodynamic effects, which are characterized by increased cardiac output, heart rate, systolic blood pressure, and superior mesenteric artery flow and reductions in diastolic blood pressure and total peripheral resistance [114]. These glucose-induced hemodynamic changes reflect, at least in part, the increased demand of the gut for blood to maintain its digestive activities [115].

Evidence suggests that the acute ingestion of glucose increases the mental challenge-induced activity of the hypothalamic–pituitary–adrenal axis [116, 117] and the total peripheral resistance and that prolonged challenge increases the cardiac output [114]. The ingestion of a gelatin-based drink containing "complex carbohydrates" is associated with increases in cardiac output and systolic blood pressure, reduced total peripheral resistance at baseline, and an increased heart rate in response to mental challenge [118]. These studies are clinically important because elevated autonomic nervous system and cardiovascular responses to mental challenge and delayed recovery have been identified as risk factors for cardiovascular disease [119].

Previous studies have made mental efforts using indices of psychophysiology, particularly cardiovascular measures. Metabolic measures represent a complementary approach by which the investment in mental effort is explicitly linked to the process of energy mobilization [120]. Glucose provides energy for our brains. One study showed that glucose levels in the blood can influence mental performance, especially higher mental activities [121], and studies using glucose drinks have also demonstrated the positive effect of glucose, which tended to improve attentional performance by 8% ($P < 0.07$) [122]. When the specific effects of macronutrients on performance are evaluated, the effects of meals are less consistent. A limited amount of data is available on the effects of the carbohydrate absorption rate on cognitive performance.

Glucose regulation has been associated with cognitive performance in elderly subjects with normal glucose tolerance, and dietary carbohydrates enhance cognition in subjects with poor memories [123]. A literature review that focused on the physiological effects of starches concluded that glucose may influence both memory and mood [124].

2.5.4 SDS and Satiety

Most mammals, including humans, prefer foods and liquids rich in sugar [125, 126]. A preference for this macronutrient stems from both its sensory and postingestive properties and is regulated at the brain level [126]. Several central mechanisms underlie the drive to consume sucrose. For example, multiple studies assessing operant behavior have shown increased motivation to obtain sweet foods. Furthermore, sucrose intake, especially chronic intake, activates components of the central reward circuitry, for example, by modifying the expression of genes encoding opioid peptides and their receptors or by affecting the release of neuropeptides and neurotransmitters, such as dopamine and opioids [112].

Satiety is a complex phenomenon controlled by social, physiological, and psychological factors. The ability to balance energy intake and expenditure is critical to survival, and sophisticated physiological mechanisms have evolved to do this, including appetite control. Satiation and satiety are part of the body's appetite control system and are involved in limiting energy intake. Satiation is the process that causes one to stop eating, whereas satiety is the feeling of fullness that persists after eating, suppressing further consumption, and both are important in determining the total energy intake [113]. Satiation and satiety are controlled by a cascade of factors that is initiated when a food or drink is consumed and continues as the ingesta enters the gastrointestinal tract and is digested and absorbed. Signals of the ingestion of food energy are transmitted to specific areas of the brain that are involved in the regulation of energy intake, in response to the sensory and cognitive perceptions of the food or drink consumed and the distension of the stomach. These signals are integrated by the brain, and satiation is induced. When nutrients reach the intestine and are absorbed, a number of hormonal signals are released that are also integrated in the brain to induce satiety. In addition to these episodic signals, satiety is also induced by fluctuations in hormones, such as leptin and insulin, which indicate the level of fat stored in the body [113, 127].

The concept that blood glucose levels, determined by the carbohydrate intake, are the central regulator of satiety is based on the glucostatic theory of food intake regulation [128]. This theory maintains that low blood glucose can cause high blood insulin levels, which signal satiety. Campfield and Smith [129] reviewed our current knowledge of the complex regulatory mechanisms mediating the dynamics of blood glucose and meal initiation, which supported the proposition that transient declines in blood glucose promote hunger. A stable and low insulin response after a meal also seems to be important for the regulation of satiety, which supports the hypothesis that SDS has a beneficial effect on satiety. A study that compared slowly digested barley kernels with a white bread control reported similar results [130]. In terms of appetite, the ingestion of slowly digested barley kernels is reported to cause greater satiety over a 3-h period than white bread.

It can be concluded that SDS affects satiety-influencing factors, such as postprandial blood glucose and insulin levels. However, further study of the mechanisms of satiety is required, including gut hormones and meal composition.

2.6 Applications of SDS

As a new functional component or ingredient in novel product development, SDS can be widely used in solid or liquid processed food products, nutritional supplements, and drug preparations (tablets, emulsions, and suspensions). The amount of SDS added is selected to confer the desired functional properties, digestibility, and glucose release rate or some desirable balance of these parameters.

2.6.1 Applications in Foods

A wide range of techniques is used by the food industry to process various food materials. Processing changes the food structure and also influences the nutritional characteristics of the food, including its starch digestibility. SDS can be added to many food products in the form of a powdered ingredient to help control energy release, including in cakes, bread, cookies, pastries, pasta, pizza, cereals, chips, fries, candy, muesli, dressings, fillings, icing, sauces, syrups, soups, gravies, puddings, custards, cheese, yogurts, creams, beverages, dietary supplements, and diabetic products [131–133].

Oral glucose can be taken before prolonged vigorous exercise to increase endurance and to avoid the exhaustion associated with endurance sporting activities. SDS products, which can extend glucose release, may therefore provide athletes with necessary energy [134].

High-fat foods contain more calories than low-fat foods, and in light of the epidemiological link between fat intake and health, they increase health risks. The caloric content of fat is higher than that of carbohydrates, and the replacement of fats in typical foods with carbohydrates should reduce the calorie-associated health hazards [135]. Several essential requirements must be considered when carbohydrates are used as fat replacements in food, such as their unique flavors, mouthfeel, viscosity, and other functional and organoleptic properties.

Most SDSs that contain linear short chains are fat-like carbohydrates and may effectively replace one or more fats in foods. These starches are either partially or totally undigested and therefore contribute zero calories to food. Some SDSs provide a variety of fat-like textures in aqueous dispersions, ranging from oily to creamy to waxy. These fat replacements offer significant advantages in food applications, including the high-strength gels or thermo-reversible gels provided by SDS dispersions.

Microencapsulation is often used to preserve food components that are volatile or sensitive to oxidation, light, or temperature. Park et al. used this method to preserve some heat-sensitive SDSs and RSs. They encapsulated native and amylosucrase-treated waxy cornstarches with three different concentrations of sodium alginate: 0.5%, 0.7%, or 1.0%. The SDS and RS fractions constituted 57.5% and 97.7% of the encapsulated starch, respectively. After cooking, the proportions

of these fractions still ranged from 55.7% to 96.1%, depending on the type of starch and the concentration of sodium alginate added, whereas the unencapsulated starch contained between 2.9% and 48.3% SDS and RS after cooking. Therefore, replacing amylosucrase-treated waxy cornstarch with an encapsulated form allowed the development of new products with high SDS levels and different functional properties [136].

2.6.1.1 Functional Foods

A new slow-digesting rice starch (Ricemic) has been developed at the US Department of Agriculture (USDA) Southern Regional Research Center and is used to maintain stable blood sugar levels in diabetics and to provide athletes with a steady energy supply to maintain their endurance [11].

Starch-based cereal foods and whole kernel foods have been developed with low GIs and high SDS loads. For example, EDP® ("energy delivered progressively") can be found in both European and Chinese markets [11].

2.6.1.2 Slow-Release Energy Beverages

The satiating power of foods is related to their energy and volume [137] and might also be related to their fiber content. The Institute of Medicine (Kathmandu, Nepal) defined dietary fiber as those indigestible or weakly digestible carbohydrates that occur naturally in plants, so SDS can be considered a kind of dietary fiber [138]. The addition of fiber to foods and beverages can provide volume and reduce the energy density of the food and can increase the viscosity of liquid or semiliquid foods. Both dietary and functional fibers have been shown to promote physiological processes that are associated with satiety. For example, fiber can slow gastric emptying, reduce the GI of foods, modify the release of gastrointestinal hormones, and alter the absorption of other nutrients [139, 140].

Jolly-Zarrouk et al. investigated extended energy beverages containing a high level of SDS (1.5%) prepared with a hydrothermal treatment (35% moisture, 100 °C for 60 min), such as Milo®, Nesquik®, and Migros® [141].

2.6.2 Applications in Medicine

Starch, a natural carbohydrate polymer, is cheap, abundant, and renewable, and its biodegradability, biocompatibility, and bioabsorbability make it suitable for pharmaceutical applications [142]. Starch can be thoroughly absorbed by the human body without any allergic or toxic effects [143]. The interactions between the functional groups in the starch matrix and those in other compounds strengthen the capacity of starch to bind and entrap wide ranges of hydrophilic and hydrophobic

compounds. In contrast to lipid- or protein-based carriers, starch-based delivery systems provide a better protective shell for bioactive compounds at high processing temperatures because they are thermally stable [144]. These advantages of starch materials, together with the diversity of starch modifications, make starch and its derivatives ideal candidates for use in drug delivery, tissue engineering, and wound dressing.

Recent studies have focused on the modification of starch for its use in drug delivery systems. For instance, starch nanoparticles synthesized from cornstarch (modified and unmodified) have been used to formulate two different types of nanoparticles used in drug delivery systems [145].

Given the characteristics of the enzymatic digestion that occurs in the upper gastrointestinal tract, SDS can be used in medicines as a novel, starch-based biodegradable carrier, which may prove useful in oral drug delivery systems that specifically target the small intestine [133]. For example, SDS can be used as a biomacromolecular film to coat pharmaceuticals to ensure that the medicines are released in the small intestine. SDS can also be used for the treatment of certain medical modalities. Wolf and Bauer reported its utility in treating glycogen storage disease and diabetes mellitus [146].

2.6.3 Application to Fodder

Starch is the main source of energy in poultry diets, comprising approximately 40% of the diet and contributing more than half of the metabolizable energy intake [147]. Therefore, variations in starch digestibility strongly affect the energy value of poultry diets. Despite this, starch digestion in poultry has received little attention until recently because it is seldom a problem in poultry fed a corn-based diet. Several studies have indicated that the starch in corn is almost completely digested by broiler chickens. The secretion of pancreatic amylase by chickens also increases as their ingestion of starch increases [148]. However, accumulating evidence suggests that starch is not fully digested by poultry and that its digestibility varies considerably among cereal species and cultivars within those species. Therefore, the factors that reduce starch digestibility in the total gastrointestinal tract or the ileum in poultry are critically relevant to the development of practical feed formulations [149].

Perhaps the most important factor affecting starch digestibility in poultry, at the total gastrointestinal tract or ileal level, is the accessibility to the starch fraction by digestive enzymes. This accessibility is determined by several factors, including granule size, shape, and surface area and the amylose-to-amylopectin ratio [21]. Briefly, the lower susceptibility of large granule starches to enzymatic hydrolysis has been attributed to their smaller granule-specific surface area, which may reduce the extent of enzyme binding and ultimately result in less hydrolysis than small granules [59].

Its excellent properties make SDS a suitable feedstuff or fodder material. Based on a patent of Winowiski [150], feed for ruminants that is rich in SDS may reduce

the rate of digestion by rumen microbes, thereby reducing the effect that the rapid consumption of fermentable grains can have on the rumen pH and the digestion of fiber. This may provide a more even flow of fermentable starch to support the microbial metabolism and may increase the proportion of starch from cereal grain consumption that ultimately arrives in the small intestine.

The consumption of SDS improves protein and energy utilization in broiler chickens, including superior feed conversion at the amino acid level [3]. The results of Weurding et al. suggest that the starch digestion rate is an important feed characteristic in broiler chickens. Broiler chickens grew faster and more efficiently on a diet containing SDS than on a diet containing RDS [151].

2.7 Conclusions and Future Directions

Because of its many functions, SDS has shown great potential utility as a fat replacement, in slow-release energy beverages, as a medicinal carrier, and in the preparation of fodder. The linear short chains released from amylopectin endow SDS with the mobility required for molecular alignment and aggregation, leading to the formation of gel networks and crystalline structures. SDS is hydrophilic and can hold water to form a gel network, and its use in controlled-release medicines is based on this property. A gel layer can immediately form on the surface of SDS-based tablets, which retards drug release. The retrogradation and recrystallization of these starches also contribute to the formation of SDS products. SDS can be used to prepare low-calorie foods and improve the fermentation processes of the gut flora in the colon.

SDS is an important kind of modified starch, with potential utility in a wide range of applications. Future research should focus on the various aspects of recent advances. These include the stabilization and protection of flavors, lipids, bioactive agents, and drugs from oxidation and enzyme hydrolysis. The accurate regulation of SDS fabrication with specifically designed components is another essential research focus. The functionality of vague SDS mixtures is highly variable, according to the preparation conditions. A most important aspect of future research is the rigorous evaluation of the health effects of consuming any SDS product. More industrial-scale applications of SDS in both the food and nonfood sectors should be thoroughly investigated. SDS should have extensive applications in foods, beverages, pharmaceuticals, cosmetics, fodder, and so on.

References

1. Englyst HN, Kingman SM, Cummings JH. Classification and measurement of nutritionally important starch fractions. Eur J Clin Nutr. 1992;46(Suppl 2):S33.
2. Englyst KN, Englyst H. Classification and measurement of nutritionally important starch fractions N. Carbohydrate bioavailability: review. Br J Nutr. 2005;94(1):1–11.

3. Miao M, Jiang B, Cui SW, Zhang T, Jin Z. Slowly digestible starch-a review. Crit Rev Food Sci Nutr. 2015;55(12):1642–57.
4. Goñi I, Garcia-Alonso A, Saura-Calixto F. A starch hydrolysis procedure to estimate glycemic index. Nutr Res. 1997;17(3):427–37.
5. Jenkins DJ, Thorne MJ, Wolever TM, Jenkins AL, Rao AV, Thompson LU. The effect of starch-protein interaction in wheat on the glycemic response and rate of in vitro digestion. Am J Clin Nutr. 1987;45(5):946–51.
6. Hoover R, Zhou Y. In vitro and in vivo hydrolysis of legume starches by α-amylase and resistant starch formation in legumes-a review. Carbohydr Polym. 2003;54(4):401–17.
7. Zobel HF. Starch crystal transformations and their industrial importance. Starch-Stärke. 1988;40(1):1–7.
8. Ness A. Diet, nutrition and the prevention of chronic diseases. WHO technical report series 916. Report of a joint WHO/FSA expert consultation. Int J Epidemiol. 2004;33(4):914–5.
9. Björck I, Östman HLE. Low glycaemic-index foods. Br J Nutr. 2000;83(Suppl 1):S149.
10. Ells LJ, Seal CB, Bal W, Mathers JC. Postprandial glycaemic, lipaemic and haemostatic responses to ingestion of rapidly and slowly digested starches in healthy young women. Br J Nutr. 2005;94(6):948–55.
11. Lee J. Surprising new uses for rice. Agric Res. 1997;45(1):22.
12. Bemiller JN, Huber KC. Physical modification of food starch functionalities. Rev Food Sci Technol. 2015;6(1):19–69.
13. Lee CJ, Kim Y, Choi SJ, Moon TW. Slowly digestible starch from heat-moisture treated waxy potato starch: preparation, structural characteristics, and glucose response in mice. Food Chem. 2012;133(4):1222–9.
14. Chung HJ, Liu Q, Hoover R. Effect of single and dual hydrothermal treatments on the crystalline structure, thermal properties, and nutritional fractions of pea, lentil, and navy bean starches. Food Res Int. 2010;43(2):501–8.
15. Chang JL, Sang IS, Yang K, Choi SJ, Moon TW. Structural characteristics and glucose response in mice of potato starch modified by hydrothermal treatments. Carbohydr Polym. 2011;83(4):1879–86.
16. Zhang EJ, Xiao-Wei HE. Study on preparation of slowly digestible starch by heat-moisture treatment and its properties. Sci Technol Food Ind. 2010;31(5):121–3. (In Chinese)
17. Chung HJ, Cho DW, Park JD, Kweon DK, Lim ST. In vitro, starch digestibility and pasting properties of germinated brown rice after hydrothermal treatments. J Cereal Sci. 2012;56(2):451–6.
18. Silva WM, Biduski B, Lima KO, Pinto VZ, Hoffmann JF, Vanier NL, Dias AR. Starch digestibility and molecular weight distribution of proteins in rice grains subjected to heat-moisture treatment. Food Chem. 2017;219(15):260–7.
19. Niba LL. Processing effects on susceptibility of starch to digestion in some dietary starch sources. Int J Food Sci Nutr. 2009;54(1):97–109.
20. Zhan J, Tian Y, Tong Q. Preparation and slowly digestible properties of *β*-cyclodextrins (*β*-CDs)-modified starches. Carbohydr Polym. 2013;91(2):609–12.
21. Lehmann U, Robin F. Slowly digestible starch-its structure and health implications: a review. Trends Food Sci Technol. 2007;18(7):346–55.
22. Nebesny E, Rosicka J, Tkaczyk M. Influence of selected parameters of starch gelatinization and hydrolysis on stability of amylose-lipid complexes. Starch-Stärke. 2005;57(7):325–31.
23. Tang MC, Copeland L. Analysis of complexes between lipids and wheat starch. Carbohydr Polym. 2007;67(1):80–5.
24. Holm J, Björck I, Ostrowska S, Eliasson AC, Asp NG, Larsson K, Lundquist I. Digestibility of amylose-lipid complexes in-vitro and in-vivo. Starch-Stärke. 1983;35(9):294–7.
25. Tian Y, Zhan J, Zhao J, Xie Z, Xu C, Jin Z. Preparation of products rich in slowly digestible starch (SDS) from rice starch by a dual-retrogradation treatment. Food Hydrocoll. 2013;31(1):1–4.

26. Singh J, Kaur L, Mccarthy OJ. Factors influencing the physico-chemical, morphological, thermal and rheological properties of some chemically modified starches for food applications-a review. Food Hydrocoll. 2007;21(9):1–22.
27. Kim DI, Lee HA, Cheong JJ, Chuagn KM. Formation, characterization, and glucose response in mice to rice starch with low digestibility produced by citric acid treatment. J Cereal Sci. 2007;45(1):24–33.
28. He JH, Zhang GY. Preparation and digestibility of octenyl succinic anhydride starch. J Chines Cereals Oils Assoc. 2007;22(4):71–4. (In Chinese)
29. He J, Liu J, Zhang G. Slowly digestible waxy corn starch prepared by octenyl succinic anhydride esterification and heat-moisture treatment: glycemic response and mechanism. Biomacromolecules. 2008;9(1):175–84.
30. Jeon YS, Lowell AV, Gross RA. Studies of starch esterification: reactions with Alkenylsuccinates in aqueous slurry systems. Starch-Stärke. 1999;51(2–3):90–3.
31. Park EY, Baik BK, Lim ST. Influences of temperature-cycled storage on retrogradation and in vitro, digestibility of waxy corn starch gel. J Cereal Sci. 2009;50(1):43–8.
32. Zhang L, Hu X, Xu X, Jin Z, Tian Y. Slowly digestible starch prepared from rice starches by temperature-cycled retrogradation. Carbohydr Polym. 2011;84(3):970–4.
33. Feng Z, Chen F, Kong F, Gao Q, Aadil RM, Yu S. Structure and digestibility of debranched and repeatedly crystallized waxy rice starch. Food Chem. 2015;187:348–53.
34. Shin HJ, Choi SJ, Park CS, Moon TW. Preparation of starches with low glycaemic response using amylosucrase and their physicochemical properties. Carbohydr Polym. 2010;82(2):489–97.
35. Xiong SS. The study on enzymatic preparation of slowly digestible starch. Wuxi: Jiangnan University; 2012. (In Chinese)
36. BeMiller JN, Whistler RL. Starch: chemistry and technology. Elsevier Inc; 2009:28
37. Christophersen C, Otzen DE, Norman BE, Christensen S, Schaefer T. Enzymatic characterisation of novamyl, a thermostable alpha-amylase. Starch-Stärke. 1998;50(1):39–45.
38. Bijttebier A, Goesaert H, Delcour JA. Hydrolysis of amylopectin by amylolytic enzymes: structural analysis of the residual amylopectin population. Carbohydr Res. 2010;345(2):235–42.
39. Le QT, Lee CK, Kim YW, Lee SJ, Zhagn R, Withers S, Kim YR, Auh JH, Paek KH. Amylolytically-resistant tapioca starch modified by combined treatment of branching enzyme and maltogenic amylase. Carbohydr Polym. 2009;75(1):9–14.
40. Borovsky D, Smith EE, Whelan WJ. On the mechanism of amylose branching by potato Q-enzyme. Eur J Biochem. 1976;62(2):307–12.
41. Takata H, Takaha T, Takagi M, Imanaka T. Cyclization reaction catalyzed by branching enzyme. J Bacteriol. 1996;178(6):1600–6.
42. Hizukuri S. Polymodal distribution of the chain lengths of amylopectins, and its significance. Carbohydr Res. 1986;147(2):342–7.
43. Shin HJ, Choi SJ, Park CS, Moon TW. Preparation of starches with low glycaemic response using amylosucrase and their physicochemical properties. Carbohydr Polym. 2010;82(2):489–97.
44. Miao M, Xiong S, Ye F. Development of maize starch with a slow digestion property using maltogenic -amylase. Carbohydr Polym. 2014;103(1):164–9.
45. Zhang G, Ao Z, Hamaker BR. Nutritional property of endosperm starches from corn mutants: a parabolic relationship between slowly digestible starch and amylopectin fine structure. J Agric Food Chem. 2008;56(12):4686–94.
46. Miao M, Zhang T, Jiang B. Preparation of slowly digestible/resistant starch in debranched, retrograded waxy corn starch. J Biotechnol. 2008;136(4):740.
47. Zhang B, Huang Q, Luo FX, FU X. Structural characterizations and digestibility of debranched high-amylose corn starch complexed with lauric acid. Food Hydrocoll. 2012;28(1):174–81.
48. Sha CX, Tian YQ, Jin ZY. Preparation and identification of V_1-type slowly digestible starch. Food Mach. 2013;29(3):37–40.

49. Wang Y. Study on the preparation and properties of cross-linked and esterification waxy rice starch. Sichuan: Sichuan Agriculture University; 2008. (In Chinese)
50. Zheng BL. Study on composite modified propreation of slowly digestible starch. Henan: Henan University of Technology; 2012. (In Chinese)
51. Arijaje EO, Wang Y. Effects of enzymatic modifications and botanical source on starch-stearic acid complex formation. Starch-Stärke. 2016;68(7–8):700–8.
52. Jiang S, Dai L, Qin Y, XIong L, Sun Q. Preparation and characterization of octenyl succinic anhydride modified taro starch nanoparticles. PLoS One. 2016;11(2):e0150043.
53. Klaochanpong N, Puncha-Arnon S, Uttapap D, Puttanlek C, Rungsardthong V. Octenyl succinylation of granular and debranched waxy starches and their application in low-fat salad dressing. Food Hydrocoll. 2017;66:296–306.
54. Bordenave N, Janaswamy S, Yao Y. Influence of glucan structure on the swelling and leaching properties of starch microparticles. Carbohydr Polym. 2014;103(1):234–43.
55. Gong M, Li X, Xiong L, Sun Q. Retrogradation property of starch nanoparticles prepared by pullulanase and recrystallization. Starch-Starke. 2016;68(3–4):230–8.
56. Li X, Qin Y, Liu C, Jiang S, Xiong L, Sun Q. Size-controlled starch nanoparticles prepared by self-assembly with different green surfactant: the effect of electrostatic repulsion or steric hindrance. Food Chem. 2016;199:356–63.
57. Qiu C, Yang J, Ge S, Chang R, Xiong L. Preparation and characterization of size-controlled starch nanoparticles based on short linear chains from debranched waxy corn starch. LWT-Food Sci Technol. 2016;74:303–10.
58. Franco CML, Preto SJDR, Ciacco CF. Factors that affect the enzymatic degradation of natural starch granules-effect of the size of the granules. Starch-Stärke. 1992;44(11):422–6.
59. Lindeboom N, Chang PR, Tyler RT. Analytical, biochemical and physicochemical aspects of starch granule size, with emphasis on small granule starches: a review. Starch-Stärke. 2004;56(3–4):89–99.
60. Tester RF, Qi X, Karkalas J. Hydrolysis of native starches with amylases. Anim Feed Sci Technol. 2006;130(2):39–54.
61. Zhang G, Hamaker BR. Slowly digestible starch: concept, mechanism, and proposed extended glycemic index. Crit Rev Food Sci Nutr. 2009;49(10):852–67.
62. Colonna P, Leloup V, Buléon A. Limiting factors of starch hydrolysis. Eur J Clin Nutr. 1992;46(Suppl 2):S17–32.
63. Zhang G, Sofyan M, Hamaker BR. Slowly digestible state of starch: mechanism of slow digestion property of gelatinized corn starch. J Agric Food Chem. 2008;56(12):4695–702.
64. Imberty A, Buléon A, Tran V, Péerez S. Recent advances in knowledge of starch structure. Starch-Stärke. 2010;43(10):375–84.
65. Jane JL, Wong KS, Mcpherson AE. Branch-structure difference in starches of A- and B-type X-ray patterns revealed by their Naegeli dextrins. Carbohydr Res. 1997;300(3):219–27.
66. Dreher ML, Dreher CJ, Berry JW. Starch digestibility of foods: a nutritional perspective. Crit Rev Food Sci Nutr. 1984;20(1):47–71.
67. Rathod RP, Annapure US. Physicochemical properties, protein and starch digestibility of lentil based noodle prepared by using extrusion processing. LWT-Food Sci Technol. 2017;80:121–30.
68. Singh J, Dartois A, Kaur L. Starch digestibility in food matrix: a review. Trends Food Sci Technol. 2010;21(4):168–80.
69. Zhang G, Ao Z, Hamaker BR. Slow digestion property of native cereal starches. Biomacromolecules. 2006;7:3252–8.
70. Huber KC, Bemiller JN. Visualization of channels and cavities of corn and sorghum starch granules. Cereal Chem. 1997;74(5):537–41.
71. Englyst KN, Vinoy S, Englyst HN, Lang V. Glycaemic index of cereal products explained by their content of rapidly and slowly available glucose. Br J Nutr. 2003;89(3):329–40.
72. Tester RF, Qi JKX. Starch structure and digestibility enzyme-substrate relationship. Worlds Poult Sci J. 2004;60(6):186–95.

73. Bauer LL, Murphy MR, Wolf BW, Jr FG. Estimates of starch digestion in the rat small intestine differ from those obtained using in vitro time-sensitive starch fractionation assays. J Nutr. 2003;133(7):2256–61.
74. Benmoussa M, Suhendra B, Aboubacar A, Hamaker BR. Distinctive Sorghum starch granule morphologies appear to improve raw starch digestibility. Starch-Stärke. 2006;58(2):92–9.
75. Fannon JE, Hauber RJ, Bemiller JN. Surface pores of starch granules. Cereal Chem. 1992;69(3):284–8.
76. Weurding RE, Veldman A, Veen WAG, Van PJ, Verstegen MW. In vitro starch digestion correlates well with rate and extent of starch digestion in broiler chickens. J Nutr. 2001;131(8):2336–42.
77. Axelsen M, Arvidsson LR, Lönnroth P, Smith U. Breakfast glycaemic response in patients with type 2 diabetes: effects of bedtime dietary carbohydrates. Eur J Clin Nutr. 1999;53(9):706–10.
78. Weurding RE, Veldman A, Veen WA, Van PJ, Verstegen MW. Starch digestion rate in the small intestine of broiler chickens differs among feedstuffs. J Nutr. 2001;131(9):2329–35.
79. Hoover R, Manuel H. Effect of heat-moisture treatment on the structure and physicochemical properties of legume starches. Food Res Int. 1996;29(8):731–50.
80. Zhang GY, Wang MZ, Peng SL. Controlled glucose delivery in food for optimal health. J Food Sci Biotechnol. 2010;29(4):481–7.
81. Srichuwong S, Sunarti TC, Mishima T, Isono N, Hisamatsu M. Starches from different botanical sources. I. Contribution of amylopectin fine structure to thermal properties and enzyme digestibility. Carbohydr Polym. 2005;60(4):529–38.
82. Björck I, Granfeldt Y, Liljeberg H, Tovar J, Asp NG. Food properties affecting the digestion and absorption of carbohydrates. Am J Clin Nutr. 1994;59(3 Suppl):699S–705S.
83. BeMiller JN, Whistler RL. Starch: chemistry and technology. 3rd ed. New York: Academic; 2009. Chapter 7
84. Hamaker BR, Zhang G. Starch fine structure and form related to nutritional effect, vol. 234. Boston: American Chemical Society; 2007.
85. Leloup VM, Colonna P, Ring SC, Roberts K, Wells B. Microstructure of amylose gels. Carbohydr Polym. 1992;18(3):189–97.
86. Xu H, Zhang G. Slow digestion property of microencapsulated normal corn starch. J Cereal Sci. 2014;60(1):99–104.
87. Katan MB, Grundy SM. Beyond low-fat diets. Vegetarian Nutr. 1997;337:563–7.
88. Rivellese AA, Giacco R, Genovese S, Patti L, Marotta G. Effects of changing amount of carbohydrate in diet on plasma lipoproteins and apolipoproteins in type II diabetic patients. Diabetes Care. 1990;13(4):446–8.
89. Giacco R, Costabile G, Riccardi G. Metabolic effects of dietary carbohydrates: the importance of food digestion. Food Res Int. 2016;88:336–41.
90. Kayode J, Sola A, Adelani A, Kolawole O, Bashiru O. The role of carbohydrate in diabetic nutrition: a review. Internet J Lab Med. 2008;3:1–9.
91. Xing JJ, Li D, Wang LJ, Adhikari B. Relationship between biphasic endotherms and multistage gelatinization of corn starch in excess water. LWT-Food Sci Technol. 2017;81:335–42.
92. Wang S, Li C, Yu J, Copeland L, Wang S. Phase transition and swelling behaviour of different starch granules over a wide range of water content. LWT-Food Sci Technol. 2014;59(2):597–604.
93. Walker CE, Ross AS, Wrigley CW, Mcmaster GJ. Accelerated starch-paste characterization with the rapid visco-analyzer. Cereal Foods World. 1988;33(6):491–4.
94. Batey IL, Crosbie GB, Ross AS. Interpretation of RVA curves. Am Assoc Clin Chem Int. 2007:19–31.
95. Meadows F. Pasting process in rice flour using rapid visco analyser curves and first derivatives. Cereal Chem. 2002;79(4):559–62.

96. Fox G, Visser J, Skov T, Meijerng I, Manley M. Effect of different analysis conditions on Rapid Visco Analyser malt viscograms in relation to malt of varying fermentability. J Inst Brew. 2014;120(3):183–92.
97. Jenkins DJ, Kendall CW, Augustin LS, Franceschi S, Hamidi M, Marchie A, Jenkins AL, Axelsen M. Glycemic index: overview of implications in health and disease. Am J Clin Nutr. 2002;76(1):266S–73S.
98. Thomas DE, Brotherhood JR, Miller JB. Plasma glucose levels after prolonged strenuous exercise correlate inversely with glycemic response to food consumed before exercise. Int J Sport Nutr. 1995;4(4):361–73.
99. Zhang GY, Venkatachalam M, Hamaker BR. Structural basis for the slow digestion property of native cereal starches. Biomacromolecules. 2006;7(11):3259–66.
100. Wachtershagedoorn RE, Priebe MG, Heimweg JA, Heiner AM, Englyst KN, Holst JJ, Stellaard F, Vonk RJ. The rate of intestinal glucose absorption is correlated with plasma glucose-dependent insulinotropic polypeptide concentrations in healthy men. J Nutr. 2006;136(6):1511–6.
101. Sands AL, Leidy HJ, Hamaker BR, Maguire P, Campbell WW. Consumption of the slow-digesting waxy corn starch leads to blunted plasma glucose and insulin response but does not influence energy expenditure or appetite in humans. Nutr Res. 2009;29(6):383–90.
102. Rose DJ, Venkatachalam M, Patterson J, Keshavarzian A. In vitro fecal fermentation of alginate-starch microspheres shows slow fermentation rate and increased production of butyrate. Fed Am Soc Exp Biol. 2007;21:6A1101.
103. Harbis A, Perdreau S, Vincentbaudry S. Glycemic and insulinemia meal responses modulate postprandial hepatic and intestinal lipoprotein accumulation in obese, insulin-resistant subjects. Am J Clin Nutr. 2004;80(4):896–2.
104. Reddy CK, Suriya M, Vidya PV, Haripriya S. Synthesis and physico-chemical characterization of modified starches from banana (Musa, AAB) and its biological activities in diabetic rats. Int J Biol Macromol. 2017;94(Pt A):500–7.
105. Shaw JE, Sicree RA, Zimmet PZ. Global estimates of the prevalence of diabetes for 2010 and 2030. Diabetes Res Clin Pract. 2010;87(1):4–14.
106. Huang TH, Peng G, Kota BP, Li GQ, Yamahara J, Roufogalis BD, Li Y. Anti-diabetic action of punica granatum, flower extract: activation of PPAR-γ and identification of an active component. Toxicol Appl Pharmacol. 2005;207(2):160–9.
107. Sharma B, Balomajumder C, Roy P. Hypoglycemic and hypolipidemic effects of flavonoid rich extract from Eugenia jambolana seeds on streptozotocin induced diabetic rats. Food Chem Toxicol. 2008;46(7):2376–83.
108. Cornier MA, Dabelea D, Hernandez TL, Lindstrom RC, Steig AJ. Endocrine reviews. Endocr Rev. 2008;29(7):777–822.
109. Niu CS, Chen W, Wu HT, Chegn KC, Wen YJ, Lin KC, Cheng JT. Decrease of plasma glucose by allantoin, an active principle of yam (dioscorea spp.), in streptozotocin-induced diabetic rats. J Agric Food Chem. 2013;58(22):12031–5.
110. Seal CJ, Daly ME, Thomas LC, Bal W, Birkett AM, Jeffcoat R, Mathers JC. Postprandial carbohydrate metabolism in healthy subjects and those with type 2 diabetes fed starches with slow and rapid hydrolysis rates determined in vitro. Br J Nutr. 2003;90(5):853–64.
111. Golay A, Koellreutter B, Bloise D, Assal JP, Würsch P. The effect of muesli or cornflakes at breakfast on carbohydrate metabolism in type 2 diabetic patients. Diabetes Res Clin Pract. 1992;15(2):135–41.
112. Olszewski PK, Shaw TJ, Grace MK, Grace MK, Höglund CE, Fredriksson R, Schiöth HB, Levine AS. Complexity of neural mechanisms underlying overconsumption of sugar in scheduled feeding: involvement of opioids, orexin, oxytocin and NPY. Peptides. 2009;30(2):226–33.
113. Benelam B. Satiation, satiety and their effects on eating behavior. Nutr Bull. 2010;34(2):126–73.

114. Jern S. Effects of acute carbohydrate administration on central and peripheral hemodynamic responses to mental stress. Hypertension. 1991;18(6):790–7.
115. Synowski SJ, Kop WJ, Warwick ZS, Waldstein SR. Effects of glucose ingestion on autonomic and cardiovascular measures during rest and mental challenge. J Psychosom Res. 2013;74(2):149–54.
116. Gonzalez-Bono E, Rohleder N, Hellhammer DH, Salvador A, Kirschbaum C. Glucose but not protein or fat load amplifies the cortisol response to psychosocial stress. Horm Behav. 2002;41(3):328–33.
117. Kirschbaum C, Gonzalez BE, Rohleder N, Gessner C, Pirke KM, Salvador A, Hellhammer DH. Effects of fasting and glucose load on free cortisol responses to stress and nicotine. J Clin Endocrinol Metab. 1997;82(4):1101–5.
118. Uijtdehaage SH, Shapiro D, Jaquet F. Effects of carbohydrate and protein meals on cardiovascular levels and reactivity. Biol Psychol. 1994;38(1):53–72.
119. Treiber F, Kamarck TN, Sheffield D, Kapuku G, Taylor T. Cardiovascular reactivity and development of preclinical and clinical disease states. Psychosom Med. 2003;65(1):46–62.
120. Fairclough SH, Houston K. A metabolic measure of mental effort. Biol Psychol. 2004;66(2):177–90.
121. Benton D, Nabb S. Carbohydrate, memory, and mood. Nutr Rev. 2003;61(5 Pt 2):S61.
122. Korol DL, Gold PE. Glucose, memory, and aging. Am J Clin Nutr. 1998;67(4):764S–71S.
123. Kaplan RJ, Greenwood CE, Winocur G, Woleve TM. Cognitive performance is associated with glucose regulation in healthy elderly persons and can be enhanced with glucose and dietary carbohydrates. Am J Clin Nutr. 2000;72(3):825–36.
124. Benton D. Carbohydrate ingestion, blood glucose and mood. Neurosci Biobehav Rev. 2002;26(3):293–308.
125. Malik VS, Schulze MB, Hu FB. Intake of sugar-sweetened beverages and weight gain: a systematic review. Am J Clin Nutr. 2006;84(2):274–88.
126. Mitra A, Gosnell BA, Schiöth HB, Grace MK, Klockars A. Chronic sugar intake dampens feeding-related activity of neurons synthesizing a satiety mediator, oxytocin. Peptides. 2010;31(7):1346–52.
127. Clegg ME, Thondre PS. Molecular weight of barley β-glucan does not influence satiety or energy intake in healthy male subjects. Appetite. 2014;83:167–72.
128. Mayer J. Glucostatic mechanism of regulation of food intake. N Engl J Med. 1953;4(5):493–6.
129. Campfield LA, Smith FJ. Blood glucose dynamics and control of meal initiation: a pattern detection and recognition theory. Physiol Rev. 2003;83(1):25–58.
130. Granfeldt Y, Liljeberg H, Drews A, Newman R, Björck I. Glucose and insulin responses to barley products: influence of food structure and amylose-amylopectin ratio. Am J Clin Nutr. 1994;59(5):1075–82.
131. Shi YC, Cui XY, Birkett AM, Thaher MG. Slowly digestible starch product: US Patent 6890571. 2005.
132. Mueller R, Innerebner F. Slowly digestible starch product: CA Patent 2551046 A1. 2005.
133. Zhang T, Jiang B. Method for producing high temperature stable slow-slaking amidon and uses thereof: CN Patent 101117352 B. 2010.
134. Hamaker BR, Han XZ. Slowly digestible starch: EP Patent 1596843. 2005.
135. Chiu CW, Mason WR. Method of replacing fats with short chain amylose: US Patent 5711986. 1998.
136. Park I, Kim YK, Bo HK, Moon TW. Encapsulated amylosucrase-treated starch with enhanced thermal stability: preparation and susceptibility to digestion. Starch-Stärke. 2014;66(1–2):216–24.
137. Rolls BJ, Drewnowski A, Ledikwe JH. Changing the energy density of the diet as a strategy for weight management. J Am Diet Assoc. 2005;105(5 Suppl 1):S98–S103.
138. Yates AA. Dietary reference intakes for energy, carbohydrate, fiber, fat, fatty acids, cholesterol, protein and amino acids. J Am Diet Assoc. 2002;102(11):1621–30.

139. Howarth NC, Saltzman E, Roberts SB. Dietary fiber and weight regulation. Nutr Rev. 2001;59(5):129–39.
140. Monsivais P, Carter BE, Christiansen M, Perrigue MM, Drewnowski A. Soluble fiber dextrin enhances the satiating power of beverages. Appetite. 2011;56(1):9–14.
141. Jolly-Zarrouk MTB, Fischer AM, Merinat SJ, Robin F, Lehmann U. Extended energy beverages: WO, EP Patent 1716768. 2006.
142. Kong L, Ziegler GR. Patents on fiber spinning from starches. Recent Pat Food Nutr Agric. 2012;4(3):210–9.
143. Kong L, Ziegler GR. Formation of starch-guest inclusion complexes in electrospun starch fibers. Food Hydrocoll. 2014;38(3):211–9.
144. Fathi M, Mozafari MR, Mohebbi M. Nanoencapsulation of food ingredients using lipid based delivery systems. Trends Food Sci Technol. 2012;23(1):13–27.
145. Santander-Ortega MJ, Stauner T. Nanoparticles made from novel starch derivatives for transdermal drug delivery. J Control Release Off J Control Release Soc. 2010;141(1):85–92.
146. Wolf BW, Bauer LL. Effects of chemical modification on in vitro rate and extent of food starch digestion: an attempt to discover a slowly digested starch. J Agric Food Chem. 1999;47(10):4178–83.
147. Svihus B. Limitations to wheat starch digestion in growing broiler chickens: a brief review. Anim Prod Sci. 2011;51(51):583–9.
148. Moran ET. Digestion and absorption of carbohydrates in fowl and events through perinatal development. J Nutr. 1985;115(5):665–74.
149. Zaefarian F, Abdollahi MR, Ravindran V. Starch digestion in broiler chickens fed cereal diets. Anim Feed Sci Technol. 2015;209:16–29.
150. Winowiski TS. Ruminant feed method of making and method of using: US Patent 5023091. 1991.
151. Weurding RE, Enting H, Verstegen MWA. The effect of site of starch digestion on performance of broiler chickens. Anim Feed Sci Technol. 2003;110(1):175–84.

Chapter 3
Resistant Starch and Its Applications

Xuehong Li

3.1 Introduction

Cereals are a major energy-providing food for the global population, and starch is the major energy component in cereals. Tubers and legumes are also important sources of starch in the diet. Starch is the main contributor to sufficient caloric intake in the global population, probably contributing to close to 40% of the global energy intake [1].

Starch is a polymer of glucose molecules. Normal starch consists of two polysaccharides, amylopectin and amylose. Amylose is essentially a linear polysaccharide with α-(1→4) linkages of D-glucopyranose units and a few branched α-(1→6) linkages. Amylopectin is a highly branched polysaccharide consisting of short linear chains connected by approximately 5% α-(1→6) branched linkages [2, 3]. The digestion of starch occurs partially in the mouth and predominantly in the small intestine, where pancreatic α-amylase is released and dextrinase, amyloglucosidase, α-glucosidase, and maltase are found in the brush border cells of the intestinal wall [4]. Starch is eventually hydrolyzed to glucose, and the glucose is rapidly absorbed in the small intestine to be used for cellular energy production [5].

However, highly digestible starch may contribute to nutrition-related health problems through several mechanisms. First, the abundance of inexpensive starchy foods has resulted in an oversupply of calories, causing a shift from providing essential nutrients to overconsumption of energy providing nutrients, which results in obesity and related health problems [6]. It was reported that more than 50% of the adult population in the developed world is now overweight or obese. Second, common starch-rich foods generally produce a large glycemic response, which increases the risks of type 2 diabetes and cardiovascular disease. Type 2 diabetes involves an

X. Li (✉)
Department of Food and Bioengineering, Zhengzhou University of Light Industry, Zhengzhou, Henan Province, China
e-mail: lixh@zzuli.edu.cn

Z. Jin (ed.), *Functional Starch and Applications in Food*,
https://doi.org/10.1007/978-981-13-1077-5_3

abnormal rise in levels of blood glucose following a starch-rich meal and a delayed reduction in postprandial blood glucose levels [7]. According to the World Health Organization, chronic high blood glucose is the third largest cause of premature mortality. Maintaining glycemic control has been established as the primary treatment goal for diabetic and prediabetic patients [8]. Cardiovascular disease is mainly caused by atherosclerosis, which is an accumulation of cholesterol-rich necrotic tissue in the intima of blood vessels that may cause blockages of arteries through thrombosis. The cholesterol-rich necrotic tissue originates from lipoproteins that transport triglycerides in the blood. Thus, cardiovascular disease is strongly correlated with obesity. Lifestyle interventions, including dietary changes, have therefore been suggested as primary treatments to enable patients to manage their body weights and blood glucose levels [9].

Because blood glucose levels are directly affected by the intake of readily digestible carbohydrates, especially starch, there is an increased interest in improving the safety and health enrichment of products with low carbohydrate digestibility. Starch has different physiological effects on human health, depending on its digestion rate. According to its digestibility, starch is generally classified as being a rapidly digestible starch (RDS), slowly digestible starch (SDS), or a resistant starch (RS), depending on its physiological effects after consumption. RDS induces a fast increase in blood glucose and insulin levels, whereas SDS is slowly digested throughout the small intestine, producing a low glycemic response. RS is that portion of starch which escapes digestion in the small intestine and can only be fermented in the colon [10].

Public health authorities and nutritionists agree that the intake of foods rich in dietary fiber provides health benefits. RS is recognized as a type of dietary fiber that can be used in foods as a functional ingredient [11]. Studies have found that RS, which is fermented by microbes in the large intestine, can provide many health benefits, including a laxative effect, lowering the risk of developing digestive tract cancer, a reduction of glucose postprandial responses, a reduction in blood lipids levels, and changing the prebiotic capacity to allow it to function as a substrate for colon flora [12].

3.2 Structure and Thermal Properties of Starch Granules

3.2.1 The Structure of Starch Granules

Native starch is a semicrystalline granule, with different shapes and sizes, depending on its botanical source. Within the granule, starch molecules are tightly packed in a radial pattern. Starch has characteristic features that vary in molecular structure, polymorph type, morphological properties of the starch granule, gelatinization and pasting properties, and enzyme digestibility [13].

Normal starch contains around 70–80% amylopectin and 20–30% amylose. Waxy starch consists mostly of amylopectin with less than 8% amylose, and high-amylose starch contains more than 40% amylose [14]. The average molecular sizes of the amylose molecules vary between an average degree of polymerization

(DP) of 324–4920 with around 9–20 branch point equivalents, to 3–11 chains per molecule. The amylose content has a significant impact on the thermal, pasting, gelling, and digestive properties of starch. Amylopectin is a much larger molecule than amylose, with a molecular weight of 1×10^7–1×10^9 and a highly branched structure with approximately 95% α-(1→4) and 5% α-(1→6) linkages. The DP of amylopectin is usually 9600–15,900. Part of the amylose in lipid-containing granules exists as an amylose inclusion complex, where the lipid chains occupy a hydrophobic core located within a single amylose helix. The amount of lipid complexed with amylose ranges from 15% to 55% of the amylose fraction in cereal starches [2]. Two forms of amylose/lipid complexes, the amorphous and crystalline amylose/lipid complexes, have been reported. Amorphous amylose/lipid complexes have lower dissociation temperatures (<100 °C) than the crystalline amylose/lipid complexes (>100 °C) [15].

In normal starch granules, branched chains of amylopectin form double helices and contribute to the crystalline structures, which are packed in three different patterns to form the X-ray diffraction patterns of the A-, B-, and C-types [16]. The A-type crystalline structure polymorph has a monoclinic unit cell, the B-type polymorph has a hexagonal unit cell, and the C-type polymorph has a combination of the A- and B-type starches. The amylopectin of A-type starch has a larger proportion of short branched chains (DP, 6–12) but a smaller percentage of longer branched chains (DP > 12) than that of B-type starch. The starch branched chain length of amylopectin has been found to be a key factor in determining the crystalline polymorph types. In addition, amylopectin of A-type starch has some branched linkages located in the crystalline region, but B-type starch has almost all the branched linkages located in the amorphous region, which explains the less porous structure and digestibility of the B-type starch granules when compared to that of A-type starch [17].

3.2.2 Starch Gelatinization and Retrogradation

Starch granules are disrupted by heating in excess water in a process commonly known as gelatinization, rendering the molecules fully accessible to digestive enzymes. Some types of hydrated cooking operations are typical examples of the preparation of starchy foods for consumption, which facilitate more rapid digestion. Starch gelatinization is an endothermic transition commonly analyzed using differential scanning calorimetry (DSC). The gelatinization properties are affected by the structure of amylopectin, the amylose content, and the minor components present in the starch granules, which depend on the botanical origin of the starch. In general, starch consisting of amylopectin with longer branched chains needs a higher gelatinization temperature and enthalpy change because longer branched chains favor the formation of stable, double-helical crystalline structures [18].

When the gelatinized starch is cooled, starch molecules reassociate and can form tightly packed structures stabilized by hydrogen bonds. These structures are thermally very stable and can only be rehydrated at 80–150°°C, depending upon the

extent and nature of the retrogradation. Both amylopectin and amylose molecules can retrograde, but retrogradation of amylopectin requires several days or even longer to form crystallites with a low dissociation temperature (40–60 °C), due to its branched structure and short branch chains. The linear amylose molecules retrograde faster and form crystallites with a higher dissociation temperature (130–170 °C) [19].

3.2.3 Starch Digestibility

Starch is digested by α-amylase in the mouth, by pancreatic amylase and glucoamylase, and by sucrose and isomaltase in the membranes of microvilli within the small intestine. The total digestive tract digestibility is almost complete for typical human diets. Measurements on human subjects with ileostomy have shown that the percentage of starch being digested in the small intestine is normally higher than 95% in common starch-rich foods, such as white bread, freshly cooked potatoes, breakfast cereals, and rice [20].

However, there still are some starches that are less easily digested in the small intestine because of specific reasons. The main reasons for indigestibility involve the large and compact particle size of cereal seeds, ungelatinized starch granules, or retrograded starch. In addition, chemical modification of starch, lipid-complexed starch, and some heat or acid treatments all increase the enzyme resistance of starches [21]. When starch-rich foods are not finely ground, such as in breakfast cereals, the digestibility of the starch decreases. The RS fraction is therefore a relevant component when considering the nutritional content.

3.3 Types of RS

RS is defined as being not hydrolyzed to D-glucose in the small intestine within 120 min of being consumed but is instead fermented in the colon. According to its structure or its routes of escaping digestion, RS is classified into five types [22].

1. RS1: Physically inaccessible starch

RS1 is physically inaccessible to digestive enzymes because it is trapped within the food matrix in proteins, cell wall materials, and other physical barriers in whole or partly milled grains, tubes, and seeds. A good example of RS1 is the RS in pasta. The compact protein matrix of pasta has been reported to be responsible for its higher RS content than other wheat products [23]. Grinding and protease hydrolysis that can destroy the physical barriers in foods reduce the RS1 content.

2. RS2: Raw granular starch with a B- or C-type polymorph

RS2 is comprised of native, uncooked granules with B- or C-type polymorphs, such as those found in raw potatoes, unripe banana starches, and high-amylose maize starches, whose granule crystallinity makes them resistant to enzymatic

hydrolysis. A disadvantage of RS2 for food applications is that its RS content decreases substantially after thermal processing. A particular type of RS2 called HAM (high-amylose maize starch) is uniquely stable to most cooking operations because of the presence of long-chain double-helical crystallites [24].

3. RS3: Retrograded starch

This starch is first gelatinized in hot water and then cooled for retrogradation. During retrogradation, the two polymer chains reassociate to form double helices stabilized by hydrogen bonds, making the structure more resistant to enzymatic hydrolysis. Linear amylose molecules are preferred for the formation of RS3 because they retrograde at a faster rate and form more resistant crystallites than amylopectin [25].

Food processing, which involves heat and moisture, generally destroys RS1 and RS2 but may form RS3. RS3 is a potential new food ingredient, because it is generally stable to heat treatments and continues to exist after most types of food processing [26].

4. RS4: Chemically modified starch

RS4 is a chemically modified starch that includes the modifications of esterification, etherification, or cross-linking. RS4 is further grouped into subcategories based on its solubility in water and the experimental protocols used for analyses. Chemical modifications reduce digestion of starch by the formation of steric hindrances at the sites of enzymatic action. For example, octenyl succinic anhydride modification of starch introduces hydrophobic octenyl succinate (OS) groups into starch molecules, which interfere with binding of starch by amylolytic enzymes [27]. Cross-linking of starch is another effective approach to prepare RS4 [28].

5. RS5: Amylose-lipid complex and resistant maltodextrin

RS5 has been proposed as two different components. The first component involves amylose-lipid complexes, which is a single helical structure formed between amylose and lipids [29]. The second component is resistant maltodextrin, which is obtained by subjecting native starch to sequential applications of pyroconversion and enzymatic hydrolysis. Resistant maltodextrins are non-sweet and low molecular weight compounds containing the native α-(1→4) and α-(1→6) bonds as well as β-(1→2) and β-(1→3) bonds and levoglucosans and have properties similar to those of dietary fiber [30]. The majority of reports describe RS5 as amylose-lipid complexes.

3.4 Factors Affecting the Digestion of Starch

There are many factors that affect the digestibility of starch, including the physical form of grains and seeds, plant genotype, associations between starch and other food components, and food processing methods (milling, cooking, annealing, high-pressure processing, autoclaving, irradiation, and extrusion and storage times).

3.4.1 The Inaccessibility of Starch

When starch-rich foods are not finely ground, the digestibility of starch may be significantly reduced. The amount of indigestibility depends on the varieties of food, structural tightness, and other matrices around the starch granule. For example, food made from barley flakes has a starch digestibility of 83.5%, while food made from the same barley in a milled form has a digestibility of 99.1%. The starch digestibility of whole canned beans is also unusually low at approximately 64.1% because of incomplete chewing, resulting in large particle sizes [31]. This form of RS (RS1) is used in a variety of conventional foods because it is relatively stable to most cooking operations. However, treatments including fine milling, which can damage the integrity of the plant cell or tissue structure, will decrease the content of RS1.

3.4.2 Starch Granules and Their Crystallinity

The botanical origin, which determines the morphology and crystalline organization, is the most important factor that determines the rate and extent of amylolytic hydrolysis of granular starches. X-ray diffraction has been used to identify distinct crystalline forms of amylose and amylopectin in starch granules. Type A is characteristic of cereals, type B is more commonly present in potatoes and bananas, and type C is an intermediate form found in legumes [32].

In A-type polymorph starch, amylopectin has a larger percentage of branch chains of DP 6–12 than that of B-type polymorph starch, and the branching linkages of the amylopectin are scattered in both the amorphous and crystalline regions. This packing of the double helices in the A-type polymorph results in starch granules containing peripheral pores with weak points in the crystalline region. However, B-type polymorph starch possesses longer branch chains to form longer and more stable double helices, and the branching linkages of amylopectin are mostly in the amorphous region, which results in a compact structure of starch granules [33]. The A-type polymorph starch granules are digested from the surface to the hilum because of their porous structure, which facilitates enzymatic hydrolysis. B-type polymorph starch granules are digested by erosion of starch granules starting from the surface, which is unfavorable to enzymatic hydrolysis of the starch molecules.

X-ray diffraction of starch granules showed that the chain fragments packed in a B-type crystalline structure with enlarged crystal lattices affect the formation of RS2. Gelatinization treatment, which eliminates starch crystallinity or damages the integrity of starch granules, reduces the RS2 content.

3.4.3 The Amylose/Amylopectin Ratio

The high amylose content of starch decreases its digestibility [34]. Amylose molecules interact with amylopectin, which restricts starch swelling and reduces the accessibility of enzymes to hydrolyze starch molecules. Also, high-amylose maize starches with very long chains can be perfectly ordered into double helices to form B-type crystallinity.

A higher content of resistant starch was found in Hylon VII than in Hylon V (high-amylose genetically modified cornstarches), which might result from the higher-amylose content in Hylon VII. Some studies with high-amylose maize starches have reported that the RS content is negatively correlated with amylopectin content of the maize ae-mutant starch, indicating that amylopectin makes little or no contribution to the RS formation in the maize ae-mutant starches [35].

3.4.4 Retrogradation of Amylose

Starch granules are disrupted by heating in an excess of water in a process commonly known as gelatinization. Upon cooling, starch molecules reassociate and form tightly packed structures stabilized by hydrogen bonding, which is commonly termed retrogradation. Retrograded amylose, which is known as RS3, is highly resistant to digestion [36].

High-amylose starch is a rich source of RS2, which produces retrograded starch or RS3 in high yields after heating and cooling treatments. Amylopectin interferes with amylose retrogradation. The yield of retrograded amylose may increase if amylopectin is debranched by a debranching enzyme such as pullulanase. The degree of polymerization of amylose also affects the yield of RS3 [37]. It is generally accepted that glucose unit ranges of 10–100 favor the formation of a double helix. This observation explains why amylopectin is so unfavorable to the formation of thermally stable resistant starch. Not only are the branches hindered in movement, but the typical lengths of 20–40 glucose units are far from the optimum number of 100.

3.4.5 The Effect of Lipids on the Digestibility of Starch

Amylose has been reported to form a single helical complex with lipids such as free fatty acids, monoglycerides, phospholipids, and long-chain alcohols [38]. The amylose-lipid complex (ALC) is classified as type I or type II depending on the

dissociation temperature of the crystalline components. Type I generally has dissociation temperatures between 90 and 105 °C, whereas type II dissociates between 105 and 125 °C. Type I complexes consist of a partially ordered structure with no distinct crystalline regions, whereas type II complexes are composed of distinct crystalline or semicrystalline structures. Type II can be further subdivided into types IIa and IIb. They differ slightly in the degree of crystallinity or the perfection of the ordered domains, in which type IIb is the most stable form of the ALC [39].

In general, the dissociation temperature of the ALC increases with increasing chain length of the fatty acids and decreases with the increasing number of double bonds. Among the unsaturated fatty acids, the fatty acids with trans double bonds form ALC with a higher dissociation temperature than those with cis double bonds. After heating at a temperature above the dissociation temperature, amorphous Type I ALC rearranges into lamellar crystallites (Type II), which display a V-type X-ray diffraction pattern and show a higher dissociation temperature (>100 °C) [40].

Single helix complex formation with lipids and the further development of lamellar crystallites protect amylose from enzymatic hydrolysis. The ALC also restricts the swelling of starch granules, to further reduce the susceptibility of starch molecules to amylolysis. Thus, the ALC has been called RS5. A study involving the effect of endogenous lipids on wheat starch showed that defatting of the starch samples resulted in a decrease of the RS content. When SDS was added to defatted wheat or amylomaize starch, the resistant starch yield decreased significantly [41]. However, regarding the preparation of RS by adding lipids to starch, the yields of RS5 from complexed lipids are lower compared to that of retrograded RS3, and the complex formation of amylose with lipids has an adverse effect on amylose recrystallization, which is important in RS formation.

3.4.6 The Interaction of Starch with Other Components in Foods

Proteins, sugars, lipids, and polyphenols, when mixed with starch in foods, significantly affect starch retrogradation by preventing hydrogen bond formation between amylopectin and amylose chains and thereby reducing the content of resistant starch.

When a mixture of potato starch and albumin was autoclaved and then cooled to −20 °C, the added albumin reduced the content of RS. The addition of soluble sugars such as glucose, maltose, and sucrose reduced the level of crystallization and subsequently reduced the yields of RS. The mechanism of retrogradation inhibition involved the interaction between sugar molecules and the starch molecular chains, which changed the matrix of gelatinized starch. The yields of RS in potato starch gels decreased in the presence of calcium and potassium ions compared with those with no added constituents, presumably because of the prevention of retrogradation [42].

Enzyme inhibitors such as phytic acid, polyphenols, and lectins, which are present in leguminous seeds, have been found to inhibit in vitro digestion and the glycemic index of starch. Both amylase and intestinal maltase activities were inhibited by tannic acid. Because phytic acid inhibits amylolysis, an increase in phytate content decreased the digestibility of starch [43].

3.4.7 Processing Conditions

In whole grains, starch is encapsulated in plant structures and therefore contains more RS (RS1) than flour. Milling is a high-shear process. When starch granules are milled, their crystalline regions are damaged, and the susceptibility to enzyme degradation increases. The extent of milling therefore affects starch digestion in cereals and legumes [44].

Starchy foods are usually subjected to heat treatments in the presence of water before consumption. The heating and cooling increases the nutritional value and generates desirable flavors and textures and can also affect both the gelatinization and retrogradation processes and thus destroy RS1 and RS2 but form RS3. The two types of starch granules involve those with either nonelevated or high-amylose starches. The former lose their RS on cooking, whereas the latter retain some granular integrity after heat processing [45].

Different types of thermal processing affect the degrees of gelatinization and retrogradation, depending on the moisture, temperature, and duration of heating and subsequent cooling. Numerous studies have reported that thermal treatments such as steam cooking, autoclaving, and baking increase the production of RS [46]. Starches isolated from several steam-heated legumes were rich in indigestible RS (19–31%), which was not observed in raw beans, suggesting that retrogradation was mainly responsible for the reduction in digestibility. White flour subjected to repeated autoclaving and cooling cycles showed a threefold increase in total RS in bread flours and a fourfold increase in pastry flours. During the tempering (holding) process, cooked grains undergo time-dependent changes involving the equilibration of either the temperature or the grain moisture. This process may further result in an improvement in the textural properties of grains and a decrease in starch digestibility. Retrogradation of starch is greatly affected by storage temperature, and the storage of starch gels at lower temperatures generally increases retrogradation [47].

Extrusion is a thermal process involving the application of high heat, high pressure, and shear forces to cooked substances such as cereal foods. Extrusion of cereals is performed using both single and twin screw extruders. The distinguishing characteristic of these cooker units is the high temperature and short time of cooking (i.e., 0.5–5 min). Mechanical energy input is the primary mechanism of cooking, although intensive thermal input via barrel heating and steam injection is also used. The results of extrusion on the RS contents of starches are controversial. Numerous studies have reported a decrease in the RS content after extrusion and attributed this

decrease to the destruction of granular structure resulting from thermal treatment, high pressure, and shear forces, but there are some studies that reported a significant increase of RS3 content in high-amylose starches after extrusion cooking [48].

3.5 RS Preparation

Many approaches can be used to increase the content of RS, including acid hydrolysis, debranching, autoclaving/cooling cycles, heat moisture treatment (HMT), chemical modification, and starch-lipid complexation.

There has been great interest in increasing the RS content in food. The content of RS formed during the processing of starchy foods is controlled by a number of factors such as water content, pH, heating temperature and time, the number of heating and cooling cycles, and freezing and drying.

3.5.1 RSs from Natural Sources

Natural cereals, seeds, and heated starch foods contain high amounts of RS (RS1 and RS2). Among nonprocessed foods, unripe bananas are the richest source of RS (47–57%), and unripe banana flour is rich in RS. Tuber starches such as potato starch contain B-type crystallinity that is highly resistant to enzymatic digestion (RS2). Whole grains are rich sources of RS1, dietary fiber, and oligosaccharides. The amylomaize VII (ae-VII) hybrid of corn contains approximately 70% amylose. The transition associated with gelatinization of ae-VII occurs between 65 and 120 °C. This is because of native RS2, which is thermally more stable than raw common cornstarch [35]. The level of resistance in a RS2 product can be increased by using hybrids, which have amylose levels >70%. Starch granules may also be fractionated by size to obtain higher-amylose levels and higher levels of RS2 resistance.

3.5.2 RS3 from the Heating and Cooling Treatment of Starch

Heating and cooling are involved in the preparation of RS3. During gelatinized starch retrogradation, starch molecules reassociate and form tightly packed structures stabilized by hydrogen bonding. These structures are thermally very stable, with the melting of amylose double helices at 80–150 °C, depending upon the extent and nature of the retrogradation. The application of repeated heating and cooling cycles of starch in the presence of moisture has been reported to increase RS3 levels. The temperatures commonly used for heat moisture treatments are usually in the range of 100–150 °C for periods ranging from 30 min to 1 h. Heat treatment in the presence of sufficient water facilitates increased starch chain mobility and

molecular rearrangement, which results in the retrogradation of gelatinized starch and increased levels of RS3 [49]. Higher temperatures are optimal. Thermal cycling may not be necessary at the extremely low temperature of 4 °C, but cycling to 140 °C is still advantageous for the formation of extremely stable RS3.

Retrogradation occurs very fast for the amylose moiety, because the linear structure facilitates cross-linkages via the formation of hydrogen bonds. The branched nature of amylopectin inhibits its recrystallization, which occurs over several days. The final level of RS is strongly dependent on the amylose content, and the retrogradation of amylose has been identified as the main mechanism for the formation of RS3 that can be generated in larger amounts by repeated autoclaving [50]. It is therefore advantageous to start with native starch high in amylose. The naturally high level of amylose in the ae-VII hybrid of corn makes it particularly suitable for the production of RS3.

CrystaLean is a commercial, highly retrograded RS3 product based on the ae-VII hybrid. It is produced by first fully hydrating and disrupting the starch granules, followed by enzymatic debranching [51]. The mixture is then treated by thermal cycling to produce a high level of retrogradation prior to drying. DSC analysis shows that the endothermic peak is located in the range of 105–145 °C, which enables it to withstand most normal cooking procedures.

3.5.3 RS from the HMT of Starch

HMT is a physical modification of starch that uses controlled heat and moisture. The treatment does not involve gelatinization and thus does not cause any damage to the granular structure. The method involves treatment of starch granules at limited moisture levels [<35% (w/w/) moisture] for 15 min to 16 h at temperatures above the gelatinization temperature (84–120 °C). This treatment promotes retrogradation and formation of RS3. The mechanism involves initial disruption of the crystalline structure and dissociation of double-helix structures, followed by reassociation of the disrupted crystals. HMT also results in the formation of starch crystallites. It initially leads to incipient swelling and the resulting mobility of amorphous regions, which then favor ordering of the double helix [52].

However, a study showed that HMT led to a decrease of RS and RDS, with an increase of SDS. The effects of HMT on enzyme digestibility usually depend on the species of starch, moisture content during the HMT, temperature and duration of the HMT, amylose-lipid interactions, and starch chain-chain interactions [53].

3.5.4 RS from Enzyme Treatment of Starch

Enzymatic debranching is a common method to produce linear chains, which results in a high content of RS. Pullulanase (EC 3.2.1.41) is one of the notable debranching enzymes that cleaves the α-1→6 linkages in pullulan, amylopectin, and other

polysaccharides. Debranching of amylopectin generates more short linear molecules to further realign a new crystalline structure that can undergo retrograde processing. Debranching is therefore commonly combined with autoclaving and cooling or HMT, which facilitate retrogradation of short linear molecules, to increase the yield of RS molecules [54].

3.5.5 RS from Chemically Modified Starches

Chemical modifications have long been used to reduce the in vitro digestibility of starch. Cross-linked starches are obtained by the reaction of starch with bi- or polyfunctional reagents such as phosphorus oxychloride, sodium trimetaphosphate (STMP), or mixed anhydrides of acetic acid and dicarboxylic acids like adipic acid [55]. Cross-linking of starches from rice, wheat, corn, potato, tapioca, oat, and mung bean using STMP, sodium tripolyphosphate (STPP), epichlorohydrin, or phosphoryl chloride (POCl3) produces RS (RS4). The levels of RS in wheat starch cross-linked with 2% POCl3, 12% STMP/STPP, and 2% epichlorohydrin were 85.6, 75.6, and 75.8 g/100 g starch, respectively. A previous study prepared acetylated bean starch with high levels of RS (44%). Acetylation of starch increased the RS content because of acetyl groups that blocked the action of digestive enzymes. Modification of starch with octenyl succinic anhydride is known to increase levels of SDS and RS more than other modifications such as acetylation, hydroxypropylation, or cross-linking [56].

3.5.6 The RS5 Starch-Lipid Complex

The ALC can be produced by classical, enzymatic, and thermomechanical methods. The classical method involves solubilizing amylose in solvents such as dimethylsulfoxide or KOH (followed by neutralizing with HCl) by heating to 121 °C, and then dissolved lipids in absolute ethanol are added to the cooled starch solution and centrifuged. The precipitates are successively washed with hot water to remove free starch and fatty acids. This method yielded type I and type II ALCs at manufacturing temperatures of 60 °C and 90 °C, respectively [57]. In the enzymatic method, glucose-1-phosphate is usually used as a primer, with a polymerization enzyme (i.e., phosphorylase) added to promote glycosidic bonds. During this process, the primer is first polymerized to produce amylose chains of sufficient length to accommodate the first lipid, with further chain extension occurring to form insoluble ALCs. ALCs formed by this method were short chain ALCs and mostly type I.

Alternative methods to produce ALCs use thermal processing technologies including steam jet cooking, homogenization, pasting, and extrusion. These thermal processing methods are more “greener” than the classical and enzymatic methods, which are suitable for the laboratory scale production of pure ALC [58].

During steam-jet cooking, water dispersions of granular starch are continuously pumped through a hydroheater, where they are instantly heated with steam under high-temperature and high-shear conditions. Mm-sized spherulites of helical inclusion complexes of amylose and the native lipid material are formed during the steam-jet cooking of high-amylose maize starch with palmitic acid. The steam-jet cooking conditions that influence the formation of spherulites involved the starch concentration, presence of lipid, and cooling conditions. Particles <1 μm were obtained with rapid cooling on ice to 25 °C.

High-pressure homogenization during heating enhanced the formation of ALC between cornstarch and fatty acids. Homogenization disintegrates starch granules to release amylose and improves the fatty acid dispersion in the starch, increasing its contact with amylose in the starch granules [30]. ALC formation increased with homogenization, and the enthalpy of the unhomogenized starch-fatty acid complex was lower than that of the homogenized complex.

Wet heat processing is continuous heating of the starch-lipid mixture in water. A biphasic pasting phenomena is often observed during the heating process. This biphasic pasting was characterized by a commonly observed paste peak viscosity after pasting for a short time (<15 min of heating) and a second, higher peak paste viscosity after pasting for a longer time (> 30 min of heating). The observed biphasic phenomenon was due to the occurrence of ALCs. Using DSC, Type I ALCs were observed after short pasting times, and type II ALCs were observed after long pasting times.

Extrusion cooking is a high temperature and short time process, which can result in the formation of ALCs due to the high temperature and high moisture combined with pressure and mechanical shear. High-amylose (45%) corn extrudates higher ALCs compared to the corresponding native cornstarch extrudates during extrusion cooking with a twin screw extruder. Taken together, the results show that the actual degree of lipid binding depends on the amylose content.

3.5.7 Resistant Dextrins from Partial Acid Hydrolysis or Pyroconversion

When starch granules are exposed to mineral acids, the hydroxonium ion attacks the oxygen in the glycosidic bond and later hydrolyzes the linkage. At temperatures below the gelatinization temperature, the acid works on the starch granule surface prior to entering the inner region of starch and alters physicochemical properties but maintains the granule structure intact. Acid hydrolysis is a common method to generate linear chains with desirable lengths for optimal formation of resistant starch [59]. For example, consecutive treatments of mild acid hydrolysis and freeze thawing enabled more amylose to aggregate and thus enhanced the possibility of retrogradation. It was reported that a combination of acid hydrolysis and three cycles of autoclaving and cooling in arrowroot starch resulted in a fourfold increase in resistant starches.

When starches are heated with partial acid hydrolysis, resistant maltodextrin is produced. The complex process, called pyroconversion of starch, includes depolymerization, transglucosidation, and repolymerization reactions. The formation of new 1→2- and 1→3-glucosidic bonds makes dextrins less susceptible to the activity of digestive enzymes [60]. Pyrodextrins are commercially produced by heating dry acidified starch in a reactor with agitation.

Some resistant dextrins are produced by microwave heating of potato starch acidified with hydrochloric and citric acids. The water solubility of samples increased with an increase in microwave power and heat exposure time. The selected dextrins with the largest low molecular weight fraction and the highest water solubility were characterized by increased (up to 25%) dietary fiber (DF) content. These enzyme-resistant dextrins did not paste, even at 20% concentration, and were characterized by a low retrogradation tendency [61]. These features make the tested enzyme-resistant potato starch dextrins suitable for use in the soft drink industry.

3.6 RS Detection

Various methods have been developed for the determination of RS involving significant differences in sample preparation, enzymes used, and the establishment of experimental conditions that mimic the gastrointestinal environment [62]. Most methods have focused on the determination of total RS, but specific methods have been developed to quantify RS1, RS2, and RS3.

A basic method for the determination of RS was proposed by Englyst et al. in 1982 [60]. Briefly, the homogenized or ground sample is heated for gelatinization, and then hydrolysis is performed with an amylase mixture at 40 °C for 16 h. The residue obtained by centrifugation is further solubilized and treated with amyloglucosidase at 65 °C. Then the amount of glucose in the supernatant is determined using gas-liquid chromatography. This protocol includes homogenization and boiling steps, which eliminate the contribution of RS1 and RS2 to the final RS; therefore the result represents only the amount of RS3 in the sample.

The above procedure was later modified by Englyst [20] to measure total glucose (TG), free glucose (FG), total RS, and RS1, RS2, and RS3 as separate fractions, and the total starch (TS) was calculated as $TS = (TG - FG) \times 0.9$. In the revised protocol for TS determination, RS1 and RS2 were eliminated by mincing or milling the food sample and subsequently heating the sample at 100 °C for 30 min. Any retrograded starch (RS3) was eliminated by treating the sample with 7 M potassium hydroxide at 0 °C. The rapidly digestible starch (RDS) and SDS of the sample were determined separately, and the RS was calculated as $RS = TS - (RDS + SDS)$. In this method, 0.8–4.0 g of sample was minced only to minimize structural changes. The

low viscosity of the samples resulted in a higher release of glucose during enzyme hydrolysis than during in vivo digestion of starch. Guar gum was therefore added to increase the viscosity, and glass beads were added to ensure the breakage of cell walls during enzyme hydrolysis. The enzyme hydrolysis was performed at 37 °C, with sequential sampling aliquots of the enzyme digest at 20 and 120 min. The release of glucose reached a plateau at 120 min. The glucose content of the 20 min enzyme digest (G_{20} fraction) represented RDS and was calculated as RDS = (G_{20} – FG)×0.9. The released glucose between 20 and 20 min represented SDS and was calculated as SDS = (G_{120} – G_{20} – FG)×0.9. RS was calculated as RS = TS – (RDS +SDS). Using this protocol, 37 °C was the highest temperature at which the sample was treated. Any RS2 in the food sample was hydrolyzed by α-amylase, and RS1 was preserved in the enzyme digest because only minced pretreatment and no milling or homogenization was used. As a result, this indirect measurement of RS included any RS1, RS2, and RS3 in the sample [20] (Figs. 3.1 and 3.2).

When considering the possible effects of sample preparation such as drying, cooling, and the storage conditions on the level of RS in RS protocols, Goni et al. further modified the method of Englyst et al. [20] by milling or homogenizing the samples before hydrolysis and decreasing the sample pH to 1.5 with HCl-KCl buffer to simulate the gastric pH. Hydrolysis with pepsin at 40 °C for 1 h was then performed. To simulate conditions in the small intestine, the sample pH was adjusted to 6.9 with Tris-maleate buffer. Instead of using a mixture of enzymes, hydrolysis was performed with α-amylase for only 16 h at 37 °C [63].

The Megazyme assay kit (Irishtown, Ireland) is widely used in analytical laboratories for the determination of RS and is the basis of both the AACC Method 32–40 and AOAC Method 2002.02. In the Megazyme protocol, the samples are ground to pass through a 1 mm sieve, and a mixture of α-amylase and amyloglucosidase is used at 37 °C for 16 h to hydrolyze starch in raw or processed food samples [62]. Because there is no boiling treatment, RS2 in raw foods is not hydrolyzed during this procedure. After inactivation of enzymes with 99% ethanol, the pellet collected from the digestion is washed with 50% ethanol and treated with 2 M potassium hydroxide to extract RS3 from the fiber-rich matrix. The resulting dextrins are hydrolyzed to glucose with amyloglucosidase at 50 °C for 30 min. Finally, the oxidase-peroxidase colorimetric assay is used to determine the glucose concentration in the final hydrolysate. The Megazyme protocol for the determination of RS cannot be used for the determination of SDS and RDS.

Other modifications have been made in the procedure to determine the RS, especially in the sample preparation step with the intent of simulating in vivo digestion [22]. However, significantly different levels of RS are detected in similar foods because of wide variations in analytical protocols, including differences in the enzymes used and in their activities, concentrations, sequences of applications, and dissimilarities in the conditions of the experimental protocols.

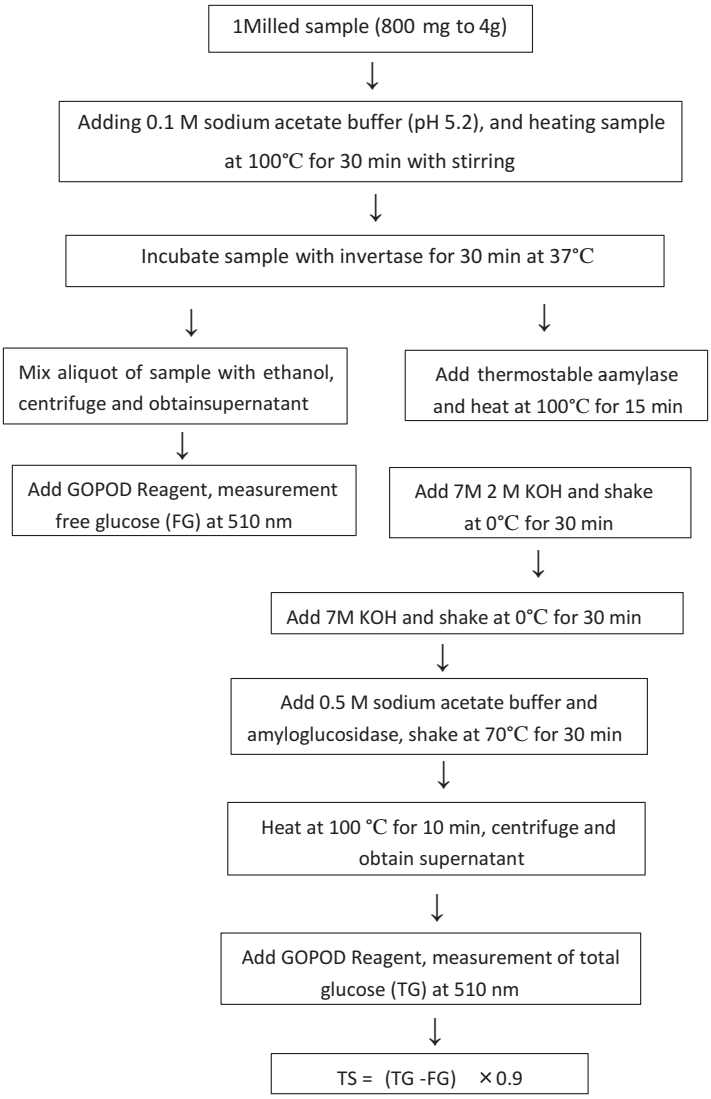

Fig. 3.1 The protocol for the determination of total starch according to Englyst et al. [20]

3.7 The Health Effects of RS

3.7.1 RS and Metabolic Responses Starch and Nutrition-Related Health Problems

Glucose produced from the digestion of starch is absorbed into the small intestine mainly by active Na^+-dependent transport in apical membranes and enters the

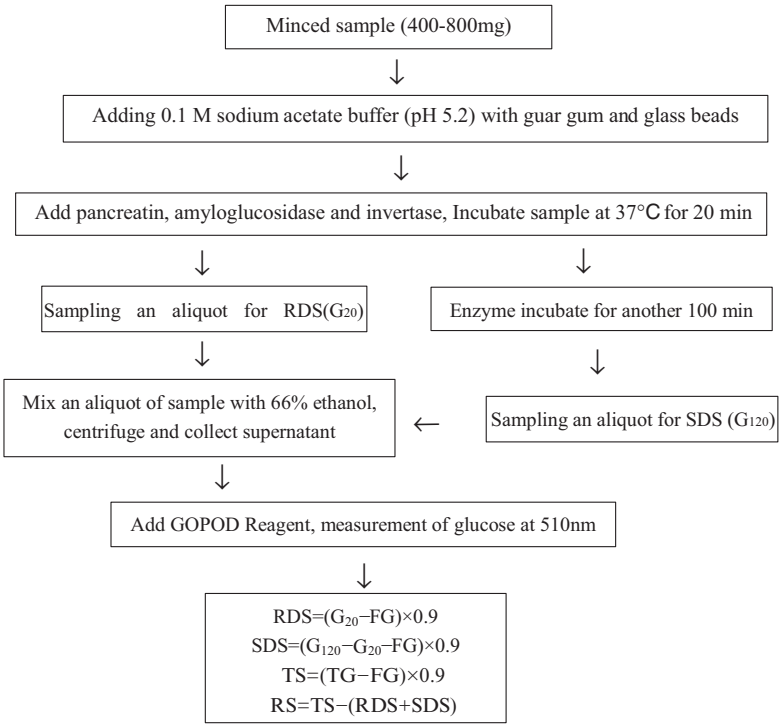

Fig. 3.2 The protocol for the determination of rapidly digestible starch (RDS) and slowly digestible starch (SDS) according to Englyst et al. [20]

bloodstream via glucose transporters in the basolateral membrane. An increase in blood glucose levels will trigger insulin secretion from the pancreatic beta cells, which will stimulate glucose uptake by cells in the body. The amount of glucose entering de novo lipogenesis (DNL) is important in the health effects of glucose. DNL activity is dependent on nutrient composition and will especially increase with an increasing proportion of carbohydrates in the diet, particularly when combined with a total energy intake exceeding the energy requirements [4].

Obesity is a major nutrition-related health problem caused by an excess intake of energy for basal metabolism and physical activity. Starch is the most important source of energy intake and is therefore a major cause of obesity. If the intake of starch matches the energy requirement of the body, the control of glucose metabolism will quickly normalize the blood glucose levels by complete oxidation of glucose. If glucose from food exceeds this oxidative need, an alternative is to store the glucose as glycogen. The maximum storage capacity for glucose is approximately 700 g, with a majority of this capacity in muscle, and only a maximum of approximately 150 g in the liver of a normal 70 kg person. If the glucose intake exceeds both the oxidative and glycogen storage capacities, the conversion of glucose to fat is the only remaining alternative. This de novo lipogenesis occurs mainly in the

liver. In the human body, the capacity for storing glucose as glycogen is limited, but the capacity to convert digestible carbohydrate to fat is much larger. Furthermore, the insulin-induced priority of the cells to use glucose as an energy source will result in body- and/or food-derived fat being saved from oxidation and used instead to increase body fat stores.

Type 2 diabetes is caused by a lack of sensitivity of cells to insulin and a reduced capacity of the pancreatic beta cells to produce sufficient amounts of insulin. The result is abnormally high blood glucose levels after ingestion of starch and other digestible carbohydrates [64]. Starch therefore can contribute to both the increasing prevalence of type 2 diabetes and the associated health problems of this disease. However, the risk of type 2 diabetes is not only linked to the intake of glucose but also to how fast the starch is digested and how fast the blood glucose enters the circulation, which can be measured using the glycemic index.

Excessive intakes of starch and/or other digestible carbohydrates result in fat formation through DNL in the liver. Increased DNL can increase the level of very low-density lipoproteins (VLDL) in the blood, which may lead to a lipid profile in blood that is associated with an increased risk of cardiovascular disease. The cholesterol-rich necrotic tissue consists of low-density lipoproteins (LDL) originating from lipoproteins such as VLDL that transport triglycerides in the blood. The main product of DNL is the saturated fatty acid, palmitic acid, which is one of the fatty acids specifically shown to increase the risk of cardiovascular disease [4].

3.7.2 RS and Metabolic Health

As previously mentioned, as the most important source of energy in the diet, starch may be a major contributor to obesity, type 2 diabetes, and cardiovascular disease. RS possesses a very low digestion rate in the small intestine and consequently leads to a sustained and lower level of glucose release, which can result in improved glycemic and insulinemic responses [65]. However, RS reduces the glycemic response simply as a result of a lack of digestible starch, rather than as a result of other physiological effects.

A series of studies on the effects of RS on metabolic health have been reported. The majority of these studies focused on the commercial ingredient, HAMS-RS2, while other studies focused on the RS from bananas, brown beans, barley, wheat breads, porridges or rice, or novel RS4 or RS3 ingredients. Most studies involved healthy individuals without insulin resistance/type 2 diabetes. Overall, supplementation with RS improved glycemic control. In addition, there was a reduced fasting blood glucose concentration, reduced postprandial response, and enhanced skeletal muscle uptake of glucose. Improvements in insulin secretion and sensitivity were also reported [12].

Metabolic health is influenced not only by glucose metabolism but also by circulating lipids, hormones, and immune mediators. Previous studies reported a significant reduction in total cholesterol and non-HDL cholesterol after the consumption

of a diet rich in RS during a period of 12 months. Other studies reported that RS had the potential to modify lipid oxidation. One study found that RS significantly increased postprandial lipid oxidation, which was consistent with the role of RS in the reduction of fat accumulation. HAM-RS2 has been reported to reduce body fat levels and increase lean body mass. Marked changes in body fat distribution occurred with reduced epididymal and retroperitoneal fat with a diet rich in RS. SCFAs like butyric acid, acetic acid, and propionic acid have been reported to inhibit adipose tissue lipolysis, and in the liver, acetate was thought to inhibit glycogenolysis, which decreased carbohydrate levels and increased fat oxidation [12].

3.7.3 RS and Colonic Health

As a type of fiber, RS would be expected to confer benefits to gut health, particularly in the large intestine where RS is fermented and results in the release of gases (methane, hydrogen, and carbon dioxide), SCFAs (formate, acetate, propionate, butyrate, and valerate), smaller amounts of organic acids (lactate and succinate), and alcohols (methanol and ethanol). This process involves several key bacterial groups, such as amylolytic gut bacteria (including *Firmicutes*, *Bacteroidetes*, and *Actinobacteria*) which mediate amylose breakdown and butyrogenic archaea (including *Eubacterium rectale*), which is involved in butyrate production, and methanogenic archaea which are necessary for the production of methane [11]. In general, the influence of RS on gut health has focused on endpoints such as gas production, SCFAs, and bacterial composition.

3.7.4 SCFA Production

SCFAs are the preferred fuel for colonocytes, increasing colonic blood flow, lowering luminal pH, and helping prevent the development of abnormal colonic cell populations. Increases in the amounts of SCFAs, particularly butyrate in the colon, are thought to be beneficial to gut health, with SCFA levels commonly used as a marker of fermentation and colonic health [66].

A number of human studies reported that RS increased fecal excretion of SCFAs, specifically butyrate. Esterified or acylated forms of RS such as acetylated, butyrated, or propionylated RS4 confer specificity in the delivery of SCFAs, because specific SCFAs are esterified to a carrier starch and released only in the large intestine, leaving the residual starch available for fermentation. Some studies took measurements in the morning following an evening meal of barley kernel bread, which is naturally rich in RS, or a white wheat flour bread control. This study design allowed adequate time for fermentation and a study of the "second meal effects." Significant increases in fasting breath hydrogen (140–160%), increased total serum SCFAs and acetate (both by 18%), and increased total plasma acetate and butyrate SCFAs (10–30%) were reported.

Other studies involving a novel high-amylose barley variety (Himalaya 292) rich in RS were performed in middle-aged, overweight volunteers who consumed 103 g of foods rich in the Himalaya 292 grain, a whole grain wheat cereal, or refined cereal for 4 weeks. The studies reported a 91% higher fecal excretion of butyrate and a 57% higher total fecal SCFA excretion compared with the refined cereal controls. In a further study using Himalaya 292, the influence of RS from a combination of sources on fecal butyrate concentrations and excretion was examined. Forty-six healthy adults for 4 weeks consumed either 25 g of non-starch polysaccharide (NSP) or 25 g of NSP plus 22 g of RS from a mix of sources (Himalaya 292, canned legumes, and HAMS) [67]. Overall, acetate, butyrate, and total SCFA concentrations were significantly higher in the RS group compared with baseline levels and the controls (NSP only group).

3.7.5 The Influence of RS on Gut Bacteria and the Microbiome

The influence of gut bacteria and microbiota on human health is well-known. Gut bacteria may influence the immune function, nutritional acquisition, appetite control mechanisms, disease states such as mental health disorders, and obesity and its associated metabolic imbalances [68]. Because RS almost entirely passes through the small intestine, it has the potential to act as a fermentable substrate for the growth of probiotic microorganisms. The effect of RS on gut microbiota was inferred through its effects on colonic pH, SCFA composition, reductions in harmful metabolites such as bile acids, phenols and ammonia, as well as enzymatic activities associated with bacterial degradative pathways.

Human intervention trials reported reduced fecal ammonia, phenols, and secondary bile acid concentrations in fecal water after intake of RS. Advances in sequencing platforms and culture-independent molecular methods, based on the analysis of 16S ribosomal RNA, have facilitated more detailed studies into how bacterial communities interact with different forms of starch. In a double-blind crossover trial, ten healthy young adults consumed crackers containing approximately 30 g of RS2, RS4, or control (4 g of fiber) for 3 weeks with a 2-week wash-out period. During this short intervention, both forms of RS increased populations of the *Actinobacteria* and *Bacteroidetes* phyla and decreased populations of *Firmicutes*. Although RS2 increased the abundance of *Ruminococcus bromii* (*Firmicutes*) and *E. rectale* (*Firmicutes*), RS4 was associated with increased *Bifidobacterium adolescentis* (*Actinobacteria*) and *Parabacteroides distasonis* (*Bacteroidetes*), with the differential activities thought to reflect differences in substrate binding [69]. *Ruminococcus bromii* has also been found to be abundant in humans and significantly involved in the fermentation of complex carbohydrates, including RS2, while *P. distasonis* has been reported to facilitate the release of esterified butyrate from butyrated HAMS. In

a follow-up in vitro study, *R. bromii* was identified as a key species for RS breakdown in the colon, facilitating RS fermentation by other species, even bacteria that were weak RS2 and RS3 fermenters when isolated.

A recent study comparing gut microbiota metabolites and the host metabolome in urban vegans and omnivores in the USA suggested that diet as a substrate affected bacterial metabolome rather than regulating gut bacteria community membership [70]. Future studies investigating the influence of RS on gut bacteria should consider the inclusion of tools such as metabolomics, to characterize the complexities of how this fermentable starch may influence the bacterial metabolome and biomarkers of bacterial activity, as well as focusing on bacterial community populations.

3.7.6 The Prevention of Colonic Cancer

RS escapes digestion in the small intestine and enters the bowel where it is fermented by probiotic bacteria to produce SCFAs. Among the SCFAs, butyrate is specifically used to reduce the risk of colon cancer, and butyrate treatment of cultured colon cancer cells can inhibit the proliferation of cancer cells and stimulate apoptosis. The proposed mechanisms explaining the function of butyrate include G-protein activity (GPR 43) and genetic and epigenetic modulation of the Wnt signaling pathway such as inhibition of histone deacetylation, reduced DNA methylation, and altered expression of miRNA [71].

A randomized, placebo-controlled 4-week crossover trial of 20 healthy volunteers showed no change in cell proliferation or DNA methylation following consumption of 25 g of HAMS. However, reduced cell proliferation in the upper colonic crypt and differential expression of key cell cycle regulatory genes in 65 adult patients with colorectal cancer have been reported following consumption of a 30 g/day blend of RS2 and RS3 for 4 weeks. Such differences in response may relate to the health status of the tissue where butyrate may increase proliferation in healthy colonic cells but suppress proliferation in cancer cells.

Diets rich in red meat have been linked to an increased risk of colon cancer, particularly in the distal region. It is thought that in the absence of fermentable carbohydrates, red meat may undergo fermentation in the colon. Thus a high protein and reduced carbohydrate diet may alter the colonic microbiota, to favor a more proinflammatory microbiota profile and decreased SCFA production. It has been reported that RS may offset this risk, by allowing greater fiber fermentation in the distal colon and attenuating red meat-induced colorectal DNA lesions [72]. RS in the high meat diet facilitated a switch from the fermentation of protein substrates to carbohydrate substrates (SCFAs), leading to a decrease in the production of promutagenic adducts that arise during protein fermentation. A second proposed mechanism involved increased telomere length, which could protect against DNA damage.

3.8 The Use of RS Starch in Foods

RS possesses unique functional properties and physiological benefits as a food ingredient. It has a lower caloric value (8 kJ/g) and is beneficial to the production of high-quality foods. Unique functional properties of RS involve a fine particle size, bland flavor, and whitish color. In addition, it possesses desirable physicochemical properties such as an increase in viscosity, gel formation, swelling index, and water-holding capacity [73]. RS therefore can be widely utilized in a large variety of food products.

However, each type of RS has a single profile of physiological and technological functionalities. For example, because of the different stabilities of different sources of RS, the appropriate selection should be considered. In most cases involving high temperature and moisture (e.g., frying and high temperature drying), RS1 and RS2 may be destroyed, but RS3 is resistant or can be formed after processing [70, 71]. In addition, cooling of baked foods at ambient temperatures enhanced RS3 formation.

Cross-linked starches prepared from maize, tapioca, and potato are used for formulations that need a pulpy texture, smoothness, flow ability, low pH storage, and high temperature storage. Commercial sources of RS2 and RS3, which are natural sources that have a high pasting temperature, excellent extrusion, film forming qualities, and lower water retaining properties than traditional fibers like bran, can form low-bulk, fiber-rich, high-quality products with good appearance and improved texture and mouth feel. Consistent with this possibility, numerous food products have been produced that were enriched in RS, including bread, cakes, muffins, pasta, cheese, battered foods, milk desserts, and even beverages.

3.8.1 RS in Bread Making

Bread has been fortified with conventional DFs such as wheat bran and barley flour, which usually have certain negative attributes like reduced volume, dark color, and poor flavor. These negative attributes prompted the use of RS.

One study evaluated the effect of oat fiber, wheat fiber, cellulose, and two commercially available RSs with 23% (Hylon™ VII) and 40% TDF (Novelose 260) characteristics of bread. The results showed that the water absorption capacity of flour added with two kinds of RSs was similar to that of the control, while flours fortified with oat fiber, wheat fiber, and cellulose showed a significantly higher water absorption capacity. The low water absorption capacity of RS consequently had less negative impact on dough rheology and was closest to the control dough. Furthermore, bread fortified with 40% RS showed greater loaf volume and better cell structure when compared with traditional fibers.

In another study, the effect of type 4 resistant wheat starch (RS4) on wheat flour dough and breads was evaluated [73]. Wheat flour was substituted by RS4 at 10%,

20%, and 30% w/w (RS10, RS20, and RS30, respectively). Rheological and thermal behaviors of dough, bread quality, starch digestibility, and bread staling were analyzed. The results showed that all substituted doughs exhibited viscoelastic behavior but lower elastic and viscous moduli. Regarding bread quality, the specific volume and crumb texture were negatively affected in breads made with RS4. However, all samples were technologically acceptable. During storage, crumb hardening was observed in breads without and with RS4, but amylopectin retrogradation was not affected. The in vitro digestibility of bread with RS showed a lower estimated glycemic index, suggesting a healthier profile [73].

The effects of wheat flour replacement by modified pea starch (PeaP) containing high levels of RS1 on dough rheological properties, bread storage, and bread performance were analyzed. The water absorption of flour significantly increased with increasing PeaP content from 54.6% to 74.6%, which was due to the high water-holding capacity (WHC) of RS. A significant increase of adhesiveness, gumminess, and hardness was also observed in dough samples with 20% and 30% of PeaP added, and addition of 30% PeaP significantly and negatively affected the ability to handle the dough. Furthermore, the hardness and chewiness of the crumb were significantly increased when the PeaP concentration was elevated, while cohesiveness and springiness were only slightly affected with the inclusion of 30% PeaP addition in the formulation. Overall, breads with 20% flour replacement with PeaP were acceptable to consumers [74].

3.8.2 RS in Baked Foods

RS is incorporated in a wide variety of baked foods, including batter systems, such as cakes, muffins, and brownies.

Firmness and adhesiveness are textural properties that are the most important parameters for cooking quality of baked cereal products. Some application tests of RS showed that it acts as a texture modifier, to impart favorable crispness or tenderness to the crumb.

It is well-known that the quality of cakes and cookies is highly affected by the quality and level of the ingredients. The textural characteristics of these products are mostly imparted by their high fat content. Fat is the principle ingredient that gives flavor, tenderness, palatability, lubricity, and mouthfeel to cookies. There has therefore been great interest in using RS as a fat replacer in bakery products. There have been many studies in this area. A type III enzyme-RS with a melting point of at least 140 °C, which could be used as a low-calorie flour replacement in bakery products, exhibited baking characteristics (cookie spread, golden brown color, pleasant aroma, and surface cracking) comparable to those achieved using conventional wheat flour. Excellent quality sponge cakes were prepared by replacing 30% of the flour with four cycled autoclaved-cooled RS3 cornstarch, cross-linked maize starch (RS4), and annealed and cross-linked RS4 maize starch (ARS4), while for the yellow layer cake, the replacement level was found to be 12.5% [75].

3.8.3 RS in Cheese

Extensive studies have investigated the feasibility of manufacturing a low fat cheese containing RS. RS has been incorporated into cheese, not as an attempt to replace the more expensive casein but rather to increase the health benefits.

Mozzarella cheese normally contains approximately 20–27% fat and is popular as an ingredient in pizza. A study showed that the addition of Novelose240 (RS2) or Novelose330 (RS3) in this cheese reduced up to 50% of the fat content, with accepted functional properties. Hardness linearly increased with increasing RS content, with RS3 being more effective than RS2. Cohesiveness was increased linearly with increasing RS2, but RS3 had no effects on the cohesiveness [76].

The effects of RS2 content on moisture absorption isotherms, and functional properties of imitation cheese, were studied. Cheese moisture remained constant (58%) when the RS2 content was increased from 8.9% to 18.2%. With increasing RS2 content, the hardness and cohesiveness showed no significant increase except at 12.9%. Moreover, the absorption behavior of the cheese was not affected by increasing the RS2 content. Overall, 18% RS2 had no effect on the cheese texture and overall acceptability [77].

3.8.4 RS as a Functional Ingredient in Other Foods

The stability of RS3 at high temperatures is greater than the other types of RSs, making RS3 acceptable in fried battered foods. Color is one of the main properties of fried battered foods, and the most desirable color is light golden brown. Replacement of wheat flour by 20% RS3 (Novelose330) caused a significant increase in the golden brown color. The main explanation for the intensified color was Maillard and caramelizing reactions. The hardness and crispness of battered fried product also were significantly increased with a 20% level of replacement. The sensory scores including color, flavor, oiliness, crispness, and overall acceptability scores were higher than five, demonstrating that all batter formulas (10% RS3, 20% RS3, and no-RS3 added) were acceptable to customers [78].

Dried pasta products fortified with 15% RS were prepared with little or no effect on dough handling and rheology during extrusion cooking. In opaque health beverages, RS may also be substituted for insoluble fibers because they involved a suspension, added opacity, imparted a gritty mouth feel, and masked flavors. In another study, fish oil was microencapsulated in a mixture of sodium caseinate and RS. The study showed that modified resistance with low molecular weight and reduced crystallinity improved the encapsulation efficiency, but not the oxidative stability of the fish oil [79].

3.8.5 Resistant Maltodextrin in Beverages

Resistant dextrins are produced by heating starch acidified with hydrochloric and citric acids. The formation of new 1→2- and 1→3-glucosidic bonds makes dextrins less susceptible to the activity of digestive enzymes. Resistant dextrins have properties such as high water solubility, low viscosity, transparent solutions, and stability, which make them suitable for use in soft drinks [80].

It is hoped that resistant dextrins may replace some of the sugars in beverages. This would reduce the caloric content of these beverages and provide a beneficial effect on the intestinal microflora of people consuming beverages enriched with enzyme-resistant dextrins, although sensory analysis should be performed prior to the industrial application of such dextrins.

References

1. Slavin J. Whole grains and human health. Nutr Res Rev. 2004;17:99.
2. Tester RF, Karkalas J, Qi X. Starch-composition, fine structure and architecture. J Cereal Sci. 2004;39(2):151–65.
3. Hizukuri, S., Takeda, J., Abe, I., et al. 1997. Starch: structure and functionality, The Royal Society of Chemistry, London,. 121–128.
4. Svihus B, Hervik AK. Digestion and metabolic fates of starch, and its relation to major nutrition-related health problems: a review. Starch/Stärke. 2016;68:302–13.
5. Robyt JF. Enzymes and their action on starch. In: BeMiller J, Whistler R, editors. Starch: chemistry and technology. New York: Elsevier; 2009. p. 237–92.
6. Robertson MD. Dietary-resistant starch and glucose metabolism. Curr Opin Clin Nutr Metab Care. 2012;15:362–7.
7. Ting Wong TH, Yu Louie JC. The relationship between resistant starch and glycemic control: a review on current evidence and possible mechanisms. Starch/Stärke. 2016;68:1–9.
8. Higgins J. Resistant starch: metabolic effects and potential health benefits. J AOAC Int. 2004;87(3):761–8.
9. IDF Clinical Guidelines Task Force. Global guideline for type 2 diabetes. Brussels: International Diabetes Federation; 2012.
10. Sajilata MG, Singhal RS, Kulkarni PR. Resistant starch-a review. Compr Rev Food Sci Food Saf. 2006;5:1–17.
11. Birt DF, Boylston T, Hendrich S, et al. Resistant starch: promise for improving human health. Adv Nutr. 2013;4:587–601.
12. Lockyer S, Nugen AP. Health effects of resistant starch. Br Nutr Found Nutr Bull. 2017;42:10–41.
13. Ratnayake WS, Hoover R, Shahidi F, et al. Composition, molecular structure, and physicochemical properties of starches from four field pea (*Pisum sativum* L.) cultivars. Food Chem. 2001;74(2):189–202.
14. Perez S, Bertoft E. The molecular structures of starch components and their contribution to the architecture of starch granules: a comprehensive review. Starch/Stärke. 2010;62:389–420.
15. Zabar S, Lesmes U, Katz I. Studying different dimensions of amylose–long chain fatty acid complexes: molecular, nano and micro level characteristics. Food Hydrocoll. 2009;23(7)
16. Contreras-Gallegos E, Domínguez FA, Hernández-Aguilar C, et al. Study of thermal and structural properties of starch granules from different maize genotypes. Food Biophysics. 2015;10(1):19–24.

17. Jayakody L, Lan H, Hoover R, et al. Composition, molecular structure, and physicochemical properties of starches from two grass pea (*Lathyrus sativus* L.) cultivars grown in Canada. Food Chem. 2007;105(1):116–25.
18. Jane J, Chen YY, Lee LF, et al. Effects of amylopectin branch chain length and amylose content on the gelatinisation and pasting properties of starch. Cereal Chem. 1999;76:629–37.
19. Zhou Z, Topping DL, Morell MK, et al. Changes in starch physical characteristics following digestion of foods in the human small intestine. Br J Nutr. 2010;104:573–81.
20. Englyst HN, Kingman SM, Cummings JH. Classification and measurement of nutritionally important starch fractions. Eur J Clin Nutr. 1992;46:S33–50.
21. Brouns F, Arrigoni E, Langkilde AM, et al. Physiological and metabolic properties of a digestion resistant maltodextrin, classified as type 3 retrograded resistant starch. J Agric Food Chem. 2007;55:1574–81.
22. Ashwar BA, Gani A, Shah A. Preparation, health benefits and applications of resistant starch—a review. Starch/Stärke. 2016;68:287–301.
23. Gelencser T, Gal V, Hodsagi M. Evaluation of quality and digestibility characteristics of resistant starch-enriched pasta. Food Bioprocess Technol. 2008;1(1):171–9.
24. Chiu YT, Stewart ML. Effect of variety and cooking method on resistant starch content of white rice and subsequent postprandial glucose response and appetite in humans. Asia Pac J Clin Nutr. 2013;22:372–9.
25. Eerlingen RC, Delcour JA. Formation, analysis, structure and properties of type III enzyme resistant starch. J Cereal Sci. 1995;22:129–38.
26. Dupuis JH, Liu Q, Yada RY. Methodologies for increasing the resistant starch content of food starches: a review. Compr Rev Food Sci Food Saf. 2014;13:1219–34.
27. Remya R, Jyothi AN, Sreekumar J. Comparative study of RS4 type resistant starches derived from cassava and potato starches via octenyl succinylation. Starch-Stärke. 2017;69:1600264.
28. Yousefi AR, Razavi SMA, Norouzyc A. In vitro gastrointestinal digestibility of native, hydroxypropylated and cross-linked wheat starches. Food Funct. 2015;6(9):3126–34.
29. Godet M, Buleon A, Tran V, Colonna P. Structural features of fatty acid-amylose complexes. Carbohydr Polym. 1993;21:91–5.
30. Ohkuma K, Wakabayashi S. Fibersol-2: a soluble, non-digestible, starch-derived dietary fibre. In: Advanced dietary fibre technology. Hoboken: Barry McCleary and Leon Prosky/Wiley-blackwell; 2008. p. 509–24
31. Svihus B, Uhlen AK, Harstad OM. Effect of starch granule structure, associated components and processing on nutritive value of cereal starch: a review. Anim Feed Sci Technol. 2005;122:303–20.
32. Shi YC, Jeffcoat R. Structural features of resistant starch. In: McCleary B, Prosky L, editors. Advanced dietary fibre technology. Oxford: Wiley Blackwell; 2001. p. 430–9.
33. Vamadevan V, Bertoft E. Structure-function relationships of starch components. Starch-Stärke. 2015;67(1, 2):55–68.
34. Jiang H, Campbell M, Blanco M, et al. Characterization of maize amylose-extender (ae) mutant starches. Part II: structures and properties of starch residues remaining after enzymatic hydrolysis at boiling-water temperature. Carbohydr Polym. 2010b;80(1):1–12.
35. Li L, Jiang H, Campbell M, et al. Characterization of maize amylose-extender (ae) mutant starches. Part I: relationship between resistant starch contents and molecular structures. Carbohydr Polym. 2008;74:396–404.
36. Haralampu SG. Resistant starch-a review of the physical properties and biological impact of RS3. Carbohydr Polym. 2000;41:285–92.
37. Patel H, Williams G, Gaisford S. Preparation and characterisation of retrograded resistant starch. Proc Nutr Soc. 2015;74:E48.
38. Putseys J, Lamberts L, Delcour J. Amylose-inclusion complexes: formation, identity and physicochemical properties. J Cereal Sci. 2010;51:238–47.
39. Rappenecker G, Zugenmaier P. Detailed refinement of the crystal structure of V-amylose. Carbohydr Res. 1981;1981(89):11–9.

40. Biliaderis CG, Galloway G. Crystallization behavior of amylose-V complexes: structure-property relationships. Carbohydr Res. 1989;189:31–48.
41. Obiro WC, Sinha Ray S, Emmambux MN. V-amylose structural characteristics, methods of preparation, significance, and potential applications. Food Rev Int. 2012;28:412–38.
42. Raigond P, Ezekiel R, Raigond B. Resistant starch in food: a review. J Sci Food Agric. 2015;95:1968–78.
43. Quek R, Henry CJ. Influence of polyphenols from lingonberry, cranberry, and red grape on in vitro digestibility of rice. Int J Food Sci Nutr. 2015;66(4):378–82.
44. Noda T, Takigawa S, Matsuura-Endo C, et al. Factors affecting the digestibility of raw and gelatinized potato starches. Food Chem. 2008;110:465–70.
45. Leeman AM, Karlsson ME, Eliasson AC, et al. Resistant starch formation in temperature treated potato starches with varying in amylose and amylopectin ratio. Carbohydr Polym. 2006;65:306–13.
46. Alsaffar AA. Effect of food processing on the resistant starch content of cereals and cereal products – a review. Int J Food Sci Technol. 2011;46(3):455–62.
47. Wolf B. Polysaccharide functionality through extrusion cooking. Curr Opin Colloid Interface Sci. 2010;15:50–4.
48. Masatcioglu TM, Sumer Z, Koksel H. An innovative approach for significantly increasing enzyme resistant starch type 3 content in high amylose starches by using extrusion cooking. J Cereal Sci. 2017;74(2017):95–102.
49. Pratiwi M, Faridah DN, Lioe HN. Structural changes to starch after acid hydrolysis, debranching, autoclaving-cooling cycles, and heat moisture treatment (HMT): a review. Starch/Stärke. 2017;68:1700028.
50. Jane JL, Hasjim J, Birt D. Resistant food starches and methods related thereto. 29pp, Application: WO. Ames: Iowa State University Research Foundation; 2009.
51. Haralampu SG. In-vivo and in-vitro digestion of resistant starch. In: Advanced dietary fibre technology. Hoboken: Barry McCleary and Leon Prosky/Wiley-blackwell; 2008. p. 413–23.
52. Sang Y, Seib PA. Resistant starches from amylose mutants of corn by simultaneous heat-moisture treatment and phosphorylation. Carbohydr Polym. 2006;63:167–75.
53. Zavareze ED, El Halal SLM, de los Santos DG. Resistant starch and thermal, morphological and textural properties of heat-moisture treated rice starches with high-, medium- and low-amylose content. Starch-Starke. 2012;64(1):45–54.
54. Reddy CK, Pramila S, Haripriya S. Pasting, textural and thermal properties of resistant starch prepared from potato (*Solanum tuberosum*) starch using pullulanase enzyme. J Food Sci Technol. 2015;52:1594.
55. Remya R, Jyothi AN, Sreekumar J. Comparative study of RS4 type resistant starches derived from cassava and potato starches via octenyl succinylation. Starch-Stärke. 2017;69(7–8):1600264.
56. Ai Y, Nelson B, Birt DF. In vitro and in vivo digestion of octenyl succinic starch. Carbohydr Polym. 2013;98(2):1266–71.
57. Genkina NK, Kiseleva VI, Martirosyan VV. Different types of V amylose-lipid inclusion complexes in maize extrudates revealed by DSC analysis. Starch-Stärke. 2015;67(9,10):752–5.
58. Meng S, Ma Y, Cui J. Preparation of corn starch-fatty acid complexes by high-pressure homogenization. Starch-Stärke. 2014;66(9,10):809–17.
59. Toraya-Avilés R, Segura-Campos M, Chel-Guerrero L, et al. Some nutritional characteristics of enzymatically resistant maltodextrin from cassava (*Manihot esculenta* Crantz) starch. Plant Foods Hum Nutr. 2017;72(2):149–55.
60. Rocío TA, Maira SC, Luis CG. Effects of pyroconversion and enzymatic hydrolysis on indigestible starch content and physicochemical properties of cassava (Manihot esculenta) starch. Starch/Stärke. 2017;69:1600267.
61. Rocío TA, Maira SC, Luis CG. Some nutritional characteristics of enzymatically resistant maltodextrin from cassava (*Manihot esculenta* Crantz) starch. Plant Foods Hum Nutr. 2017;72(2):149–55.

62. Perera A, Meda V, Tyler RT. Resistant starch: a review of analytical protocols for determining resistant starch and of factors affecting the resistant starch content of foods. Food Res Int. 2010;43:1959–74.
63. Goñi I, García-Diza L, Mańasb E, Saura-Calixto F. Analysis of resistant starch: a method for foods and food product. Food Chem. 1996;56(4):445–59.
64. Hussain A, Claussen B, Ramachandran A, et al. Prevention of type 2 diabetes: a review. Diabetes Res Clin Pract. 2007;76:317–26.
65. Stanner S. Cardiovascular disease: diet, nutrition and emerging risk factors (The report of the British Nutrition Foundation Task Force). Oxford: Wiley; 2005.
66. Zhou Z, Cao X, Zhou JYH. Effect of resistant starch structure on short-chain fatty acids production by human gut microbiota fermentation in vitro. Starc/Stärke. 2013;65:509–16.
67. Bird AR, Vuaran MS, King RA, et al. Wholegrain foods made from a novel high-amylose barley variety (Himalaya 292) improve indices of bowel health in human subjects. Br J Nutr. 2008;99:1032–40.
68. Arora T, Backhed F. The gut microbiota and metabolic disease: current understanding and future perspectives. J Intern Med. 2016;280:339–49.
69. Martinez RC, Bedani R, Saad SM. Scientific evidence for health effects attributed to the consumption of probiotics and prebiotics: an update for current perspectives and future challenges. Br J Nutr. 2015;114:1993–2015.
70. Wu GD, Compher C, Chen EZ, et al. Comparative metabolomics in vegans and omnivores reveal constraints on diet-dependent gut microbiota metabolite production. Gut. 2016;65:63.
71. Diane FB, Gregory JP. Diet, genes, and microbes: complexities of colon cancer prevention. Toxicol Pathol. 2014;42(1):182–8.
72. Le Leu RK, Winter JM, Christophersen CT, et al. Butyrylated starch intake can prevent red meat-induced O6-methyl-2deoxyguanosine adducts in human rectal tissue: a randomised clinical trial. Br J Nutr. 2015;114:220–30.
73. Gabriel Arp C, Correa MJ, Zuleta Á. Techno-functional properties of wheat flour-resistant starch mixtures applied to breadmaking. Int J Food Sci Technol. 2017;52(2):550–8.
74. Sanz-Penella JM, Wronkowska M, Soral-Smietana M, et al. Impact of the addition of resistant starch from modified pea starch on dough and bread performance. Eur Food Res Technol. 2010;231:499–508.
75. Haynes L, Gimmler N, Locke JP, et al. Process for making enzyme-resistant starch for reduced-calorie flour replacer. U.S. patent 6,013,299. Jan 11, 2000. Wilmington: Nabisco Technology Co; 2000.
76. Montesinos-Herrero C, Cottell DC, Dolores O'Riordan E, et al. Partial replacement of fat by functional fibre in imitation cheese: effects on rheology and microstructure. Int Dairy J. 2006;16:910–91983.
77. Noronha N, O'Riordan ED, O'Sullivan M. Replacement of fat with functional fibre in imitation cheese. Int Dairy J. 2007;17:1073–82.
78. Sanz T, Salvador A, Fiszman SM. Resistant starch (RS) in battered fried products: functionality and high-fibre benefit. Food Hydrocoll. 2008;22:543–9.
79. Homayouni A, Amini A, Keshtiban AK. Resistant starch in food industry: a changing outlook for consumer and producer. Starch/Stärke. 2014;66:102–14.
80. Kapusniak K, Nebesny E. Enzyme-resistant dextrins from potato starch for potential application in the beverage industry. Carbohydr Polym. 2017;172:152–8.

Chapter 4
Porous Starch and Its Applications

Lingyi Liu, Wangyang Shen, Wei Zhang, Fang Li, and Zhenzhou Zhu

4.1 Introduction

Few pores have been reported in native starch. Artificial pores can be created using many approaches. For example, a portion of the macromolecules within a granule can be hydrolyzed by enzymes or acids to low molecular fragments, and pores are formed when these hydrolyzed products dissolve. Another approach involves starch chains in a microemulsion which are cross-linked to form microspheres, and pores are present in some of the resulting products. In addition, starch gels can exhibit a porous structure when treated with freeze-thaw processes. In recent years, a solvent exchange method and other methods have been used to produce porous starch (PS) or to enhance the pore-forming efficiency.

PS contains abundant pores from the surface to the center of the granules, which increase the specific surface area, and PS acts as an excellent natural absorbent and has been widely used in food, pharmaceuticals, agriculture, cosmetics, pulp and paper, and other industries [1]. There is a growing interest in exploiting the properties of PS in various food and non-food areas. In the food industry, PSs are used as colorants, spices, flavorings, sweeteners, and carriers and to protect sensitive elements such as oils, minerals, vitamins, bioactive lipids, and food pigments such as β-carotene and lycopene which are sensitive to light, oxidation, or high temperature [2, 3].

The structure and properties of PS have been determined by Fourier-transform infrared (FTIR) spectroscopy, scanning electron microscopy (SEM), X-ray diffraction (XRD), differential scanning calorimetry (DSC), and rheometry.

Starch is a natural polysaccharide and is an important energy source for humans, and native and unmodified starch has little industrial applicability [4]. The interesting morphology of PS has attracted considerable attention in industrial applications, such

L. Liu · W. Shen (✉) · W. Zhang · F. Li · Z. Zhu
College of Food Science and Engineering, Wuhan Polytechnic University, Wuhan, China
e-mail: liulingyi607@zju.edu.cn; shenwangyang888@whpu.edu.cn; zhangwei@whpu.edu.cn; lifang@whpu.edu.cn; zhuzhenzhou@whpu.edu.cn

Z. Jin (ed.), *Functional Starch and Applications in Food*,
https://doi.org/10.1007/978-981-13-1077-5_4

as in food, pharmaceuticals, agriculture, cosmetics, pulp and paper, and other industries [1]. PS can be obtained by physical, chemical, and biological methods, of which ultrasonic and enzyme treatments have mainly been used to produce PS [1, 5, 16].

Nowadays, starch is widely used as an abundant, renewable, inexpensive, biodegradable, and environmentally friendly biopolymer [6]. However, the application of starch is limited by its naturally low surface area and pore volume. Thus, after physical, chemical, or biological modification, PS, with unique structures such as abundant micro-sized pores which extend from the surface of starch granules to the center, can be obtained and is widely used in the food, pharmaceuticals, agriculture, cosmetics, pulp and paper, and other industries [1]. This chapter reviews the recent applications of PS and its functional properties in these applications.

4.2 Porous Starch Preparation

4.2.1 Hydrolysis by Enzyme or Acid

Enzymatic hydrolysis is one of the most commonly used methods for preparing PS. When hydrolysis is conducted below the gelatinization temperature of starch, enzymes can act on the granules without damaging the granule integrity.

[7] compared the granular change of different starches during enzymolysis at sub-gelatinization temperature. The research group dispersed starch slurry in sodium acetate buffer and hydrolyzed the starch using a mixture of the enzymes alpha-amylase (from *Aspergillus kawachi*) and glucoamylase (from *Aspergillus niger*). The temperature of hydrolysis was set at 35 °C, and pH was controlled at 1.5–1.6. After 24 h reaction, the pH of the starch dispersion was adjusted to 5–6 to stop further enzymolysis. PS was collected by filtering the hydrolyzed starch with distilled water and then dried at 40 °C for 2 days. When compared with hydrolyzed mung bean, cassava, and sago starches, more porous granules were observed in hydrolyzed corn starch. After hydrolysis, corn and mung bean starch had deeper holes and a more porous structure compared with hydrolyzed cassava and sago starch. In addition, hydrolyzed cassava and sago starch had a rough surface, and some of the granules remained intact.

[8] prepared PS granules with a pore diameter ranging from 620 to 1150 nm. For this reaction, the starch was dispersed in sodium acetate buffer (pH 4.6), and glucoamylase was added to hydrolyze the starch at 50 °C. Most starch granules were first hydrolyzed superficially, and then the pores on the surface enlarged, and subsequently enzymes penetrated the granules. The distribution of pores on the surface and pore size were controlled by the enzyme/granule ratio and hydrolysis time.

[9] compared the granular structure of PS prepared from native and cross-linked starches. Corn, tapioca, and sweet potato starches were cross-linked with epichlorohydrin, and STARGENTM 001 (a blend of α-amylase and glucoamylase) was used to hydrolyze these starches at 35 °C for 24 h. Compared with native starches, all

cross-linked starches had fewer porous granules after hydrolyzation. Enzymatic erosion occurred mainly on the surface of starch granules, with deep pores in the interior part of the granules.

[10] compared the hydrolysis process of different enzymes in preparing porous waxy maize starch. They found that α-amylase was highly effective in hydrolyzing waxy maize starch, but produced fewer porous granules than β- and γ-amylases. β-Amylase and glucoamylase seemed to produce equally porous granules.

[11] studied the different effects of fungal α-amylase and amyloglucosidase on corn starch at sub-gelatinization temperature to obtain PS. Corn starch was suspended in NaH_2PO_4 buffer (pH 6.0) or sodium acetate buffer (pH 4.0), and the two enzymes were added to each suspension, respectively. The reaction mixtures were placed in a shaking water bath at 50 °C for 24 h. The results showed that at sub-gelatinization temperatures, hydrolysis led to the porous structure of starch, but the microstructure surface and internal morphology differed in the α-amylase and amyloglucosidase suspensions. Enzymatic modification of the starch resulted in porous structures with more agglomerates in the amyloglucosidase suspension.

Cross-linked PS samples were produced by partially hydrolyzing cross-linked corn starch with a mixture of α-amylase and glucoamylase [12]. The cross-linking agent sodium trimetaphosphate was added to corn starch slurry containing Na_2CO_3 and NaCl. The mixture was stirred at 50 °C for the cross-linking reaction. After this reaction, the pH of the slurry was adjusted to 6.5, and the cross-linked starch product was washed with deionized water. The cross-linked starch was then dispersed in sodium acetate buffer (pH 4.6), and the slurry was preheated at 40 °C for 20 min. A mixture of α-amylase and glucoamylase at a ratio of 1:4 was added for hydrolysis. The starch product in the slurry was then separated by centrifugation, washed, and lyophilized. The hydrolysis caused an obvious increase in pore area, pore diameter, and porosity. The magnitude of the total pore area of cross-linked PS was increased 10–20 times compared with that of the native starch.

[13] investigated the impact of combined α-amylase and hydrochloric acid hydrolysis on the structure of starch granules. The α-amylase was dissolved in sodium phosphate buffer (pH 6.9) containing $CaCl_2$. Waxy rice starch was dispersed in the enzyme solution and incubated at 37 °C. After hydrolysis, absolute ethanol was added to stop the reaction, and the solution was then centrifuged. The precipitates were dried overnight at 35 °C. The hydrolyzed starch was treated with 2.2 mol/L HCl at 35 °C. After this reaction, the resulting mixture was neutralized, and ethanol was added to precipitate starch. The final solution was centrifuged and the residues were dried at 35 °C. Numerous pinholes appeared on the enzyme-treated waxy rice starch granules, which were openings to channels that provided access to the granule interior. As the hydrolysis time increased, the holes became larger. The surface pores showed no visible change with increased hydrolysis time. Furthermore, the granular size sharply decreased, and many fragments were formed when the enzyme-pretreated starch sample was exposed to the mild acid for 24 h during combined hydrolysis.

[14] used mild heat to treat starch before enzymolysis to prepare PS. The pretreated starch was obtained by incubating the starch slurry (sodium acetate buffer)

in a water bath at 60 °C for 30 min. The temperature of the slurry was then decreased to 35 °C for hydrolysis. The mild heat treatment caused the starch to swell, resulting in enlargement of the pinholes on the surface of the starch granules. This permitted the enzyme to penetrate the granules more extensively and form pores and channels in the starch granules during hydrolysis.

Microporous wheat starch was prepared using different levels of α-amylase, different sonication treatments, and a combination of both methods [15]. A starch suspension was left at ambient temperature overnight to fully hydrate before ultrasonic treatment. The suspension was then poured into an ultrasound bath and sonicated at a frequency of 35 kHz. During sonication, the temperature was maintained at 40 °C. α-Amylase was added to the starch suspension, and the hydrolysis temperature was set at 45 °C. The resulting product was centrifuged, and the pellet was recovered and washed three times with distilled water and then dried at 80 °C. The PS product was ground and sieved to obtain an average particle size of 100 μm. The combination of α-amylase and ultrasound treatment increased the quantity and size of the micropores. However, sonication of the enzyme-treated samples destroyed some of the starch granules. This effect was more pronounced when samples were sonicated for 40 and 60 min.

PS granules were formed by partial hydrolysis of starch using amylase. An ultrasonic technique to assist enzymatic hydrolysis was used to pretreat raw starch [1]. The starch was suspended in pH 4.6 buffer solution and then treated with ultrasonic waves at temperatures below the gelatinization point. Following pretreatment, fungal amylase (or beta-amylase) was added to treat the starch at 55 °C. The solution was then centrifuged, washed with distilled water, dried in a vacuum dryer at 60 °C and then comminuted. PS prepared by fungal amylase had better pores than that prepared with beta-amylase. Compared with raw starch, ultrasonic pretreatment facilitated the attack by fungal amylase on starch and increased the size and depth of pores. The optimal ultrasonic power and time of ultrasonic action was 400 W and 15 min, respectively.

Microporous starch was prepared from corn starch by glucoamylase catalysis combined with ultrasonic treatment [16]. Three different ultrasonic treatments were performed; sequential sonication was performed before, simultaneously, or after hydrolysis. Corn starch was dispersed in Na_2HPO_4–citric acid buffer (pH 4.0), and glucoamylase was added for the reaction at 40 °C. After the reaction, the dispersion was centrifuged to isolate hydrolyzed starch, which was then washed with deionized water and dried at 55 °C. A combination of glucoamylase and ultrasound treatment accelerated the formation of holes and increased the specific surface area in microporous starch granules. Of the three different ultrasound treatments, simultaneous ultrasound treatment during glucoamylase digestion efficiently facilitated the micropore formation process, followed by ultrasound treatment before digestion, while the efficacy of ultrasound treatment after digestion was unremarkable.

The susceptibility of cereal starches (normal maize, waxy maize, amylomaize V and VII, rice, and oat) to hydrolysis with high concentrations of acid was examined [17]. Starches were hydrolyzed with 2.2 mol/L HCl at 35 °C. The granular residue was separated by centrifugation and washed three times with deionized water. The

products were resuspended in a small amount of water and lyophilized. In hydrolyzed oat starch, many of the granules were deformed, and their surfaces were completely covered with small pores. In contrast, hydrolyzed waxy maize starch exhibited a total loss of granular shape, and the whole mass was covered with pores and cracks. Granule shape was clearly discernible in both amylomaize V and amylomaize VII starches, but their external appearances were different. The surface of some amylomaize V granules was extensively corroded with numerous pores and cracks. In contrast, the surface of amylomaize VII granules was wrinkled and devoid of cracks. Very few pores were present on the granule surface of amylomaize VII starch.

4.2.2 Freeze-Thaw Method

After freeze-drying, PS xerogels can be formed by inserting mercaptosuccinic acid molecules into the starch chains [18]. Mercaptosuccinic acid was dissolved in water, and potato starch was added to the solution. The mixtures were heated to 90 °C to form gelatinized composites of starch and mercaptosuccinic acid. The composites were first frozen at −4 °C and then freeze-dried at −52 °C under pressure of 20 Pa. The porous structure was observed, and the number of pores (6–7 μm in diameter) increased with increasing mercaptosuccinic acid content. The researchers indicated that the introduction of mercaptosuccinic acid broke the intrinsic hydrogen bonds within starch chains and intermolecular hydrogen bonds were formed between mercaptosuccinic acid and starch, which resulted in the formation of the pore structure.

Magnetic PS was prepared using a freeze-thaw process [19]. An aqueous suspension of native corn starch was heated with a magnetic iron oxide suspension or magnetic fluid. The resulting magnetic gel was frozen at −18 °C and thawed at room temperature. After three freeze-thaw cycles, the insoluble magnetic starch gel formed was disintegrated and sieved to obtain particles with a diameter of less than 0.5 mm. The size of porous magnetic starch particles was 300–500 μm.

4.2.3 Cross-Linking Method

Calcein-containing starch acetate microparticles were prepared by a modified water-in-oil-in-water (W/O/W) double-emulsion technique [20]. Potato starch acetate was dissolved in chloroform, and the solution was cooled in an ice bath. The aqueous calcein solution was emulsified in the organic polymer solution using an Ultra Turrax Homogenizer. The primary W/O emulsion was poured into aqueous PVA solution as homogenization was carried out using Ultra Turrax. The W/O/W emulsion was stirred to allow evaporation of chloroform. After this, the microparticles were sieved (Ø 15 μm). The microparticles were isolated by centrifugation,

washed, and dried under vacuum at room temperature. The mean diameter of starch acetate microparticles was 11 μm, with small pores distributed in the microparticles.

Starch/cyclodextrin bioadhesive porous microspheres were prepared as a platform for nasal administration of drugs [21]. Starch and cyclodextrin were dissolved in NaOH solution in the presence of $NaBH_4$. After complete removal of air bubbles under vacuum, the solution was added to 1,2-dichloroethane-containing cellulose acetate butyrate CAB. Epichlorohydrin (ECH) was added to the obtained W/O emulsion, and the cross-linking reaction was carried out at 50 °C. The cross-linked microspheres were recovered by filtration, which were then washed with 1,2-dichloroethane, acetone, water/acetic acid solution (30%, v/v), water, and methanol. The microspheres were then completely dried at 60 °C under vacuum. These microspheres were characterized by a narrow size distribution with 70% of microparticles between 50 and 160 μm. The microspheres displayed a homogeneous and dense internal structure with small pores.

Soluble starch-based biodegradable and microporous microspheres were prepared by an emulsion chemical cross-linking technique using trisodium trimetaphosphate as cross-linker [22]. Starch and trisodium trimetaphosphate were mixed in sodium hydroxide aqueous solution, which was used as the water phase. Liquid paraffin-containing emulsifier (Span 80 and Tween 80 at a volume ratio of 1:1) was used as the oil phase. The water phase was then added dropwise into the oil phase, and the cross-linking reaction took place at 45 °C. The obtained microspheres were collected and washed three times with petroleum ether, acetone ethanol, and deionized water, respectively. Finally, the products were dried in a vacuum. The surfaces and the internal structure of the microspheres had a compacted and continuous network with certain microporosities. The research group indicated that the formation of microporosities may be related to the mechanisms of air bubbles or entrapped organic solvent evaporating during the cross-linking and drying processes.

4.2.4 Solvent Exchange Method

The exchange solvent is an important factor in displacing water from the hydrogel to maintain the porous structure of the gel. Alcohol as the exchange solvent can avoid contraction and collapse of the aquagel due to direct air drying. A biodegradable PS foam (BPSF) was prepared by the solvent exchange method [5, 16]. A suspension of soluble amylum was heated to 100 °C for 0.5 h, and the melt was lowered to 85 °C and then poured into a Petri dish. The resulting slurry was chilled to 5 °C overnight to facilitate gelation. The gel was then transferred to four volumes of 40%, 60%, 90%, and 100% ethanol/water solution, respectively, and equilibrated for 24 h in order to maintain the porous structure of the gel, whereby ethanol displaced the water in the aquagel to form an alcogel. The resulting foam was obtained by rotary evaporation drying at 30 °C. The dry PS foam was milled in a mortar and passed through an 80 mesh sieve, and the BPSF particles were stored in a vacuum

dryer. The pore size distribution of the PS foam was narrow (lower than 200 nm), and 60% of the pores had a diameter of 20–80 nm. The pore size distribution of PS foam was between that of mesopores and large pores.

PS microspheres were prepared by the W/O emulsion-freeze-thawing method/m [12]. The water phase was a soluble starch aqueous suspension, which was boiled to 100 °C for 0.5 h and then lowered to 85 °C for use. The water phase was then added to the oil phase which was formulated with a methylbenzene and chloroform solution (2:1) and Span 80 as the emulsifier. The mixed liquid was homogenized to form a stable W/O emulsion. The emulsion was stored at −20 °C for the emulsion drops to gelatinize. Using the solvent exchange technique, the products were equilibrated with four concentrations of ethanol (40%, 60%, 90%, and 100%), which displaced the water in the aquagel to form an alcogel. The products were filtered and dried under a vacuum at room temperature. Particle size distribution of the PS microspheres was 20–100 μm. The PS microspheres possessed a nanometer porous-connected structure (500 nm).

[23] treated gel microspheres prepared by emulsion cross-linking with the solvent exchange method to obtain a porous structure. Oil/starch emulsions were prepared by mixing corn starch aqueous dispersion with vegetable oil. The resulting emulsion was then heated and pressurized at 0.1–0.2 MPa in an autoclave. The pressure in the autoclave was then released and the temperature of the emulsion lowered using an ice bath. After centrifugation, particles were separated from the oil phase, soaked in ethanol, and placed in the refrigerator for retrogradation. After retrogradation, starch particles were transferred to fresh ethanol solution. The resulting starch alcogels were dried by extraction of the solvent using supercritical carbon dioxide. The starch alcogel was then loaded into the autoclave and immersed in ethanol to prevent shrinkage. The autoclave was heated to 40 °C, and pressure was set at 11.0–12.0 MPa. After treatment, the starch microspherical alcogel was dried to remove the solvent. The spherical particles of starch in the range of 200–400 μm with a nanoporous texture characterized by a high specific surface area and total mesopore volume were obtained.

[24] prepared wheat starch foam using the solvent exchange method. Wheat starch gel was obtained by adding starch to water in a rapid viscoamylograph specimen vial. The instrument was programmed to ramp from 25 °C at a rate of 10 °C/min to 95 °C and then hold at that temperature for 5 min. Following the temperature treatment, the starch melt was immediately transferred to cylindrical molds and stored at 5 °C overnight. The gelled starch was removed from the molds and equilibrated in a graded ethanol series (40%, 70%, 90%, and three changes of 100% ethanol) to displace the water. Wheat starch microcellular foam was produced by simply evaporating the ethanol from the samples under a stream of dry nitrogen gas. Starch foam panels made from wheat starch consisted of a porous matrix of starch interspersed with granule remnants which appeared relatively nonporous.

PS can be prepared by replacing ice crystals in frozen starch gel with ethanol using the solvent exchange technique [25]. Potato starch was added to distilled water, and the mixture was heated at 90 °C for complete gelatinization. It was then cooled to 5 °C to obtain the starch gel. The gel was cut into cubes and frozen at

−10 °C. The frozen cubes were immersed in ethanol three times. The cubes were dried at 50 °C to remove the ethanol, and white solid PS cubes were obtained. With increasing starch paste concentration, the pore size of PS gradually decreased.

4.2.5 Other Methods

Porous carboxymethyl sago starch-acid hydrogel was prepared by an irradiation technique [26]. Sago starch powder was added to isopropanol and sodium hydroxide to form a slurry, and sodium monochloroacetic acid was added for the etherification process at 55 °C. After the reaction mixture was cooled to room temperature, the produced carboxymethyl sago starch was washed with methanol three times, neutralized with glacial acetic acid followed by absolute ethanol, and then dried in an oven at 60 °C. Carboxymethyl sago starch-acid hydrogel was prepared by dissolving the carboxymethyl sago starch in lactic acid. This composite mixture was then transferred into a plastic mold. Irradiation was conducted using electron beam radiation. A typical hydrogel structure was obtained, which had three-dimensional networks with empty pores.

A new simple processing route to produce starch-based porous materials was developed based on a microwave baking methodology [27]. The bowing powder was mixed with the corn starch/ethylene vinyl alcohol blend powders. H_2O_2, acting as a bowing agent, was then added until a consistent slurry dispersion was obtained. The mixture was then heated in a microwave oven. The oven power and treatment time were optimized to range between 250 and 400 W and 1 and 5 min, respectively. The samples were then dried at 50 °C. The samples were prepared in a cylindrical shape, which were then cut into rectangles. The microwave blowing method leads to porous materials, and the porosity increases with the amount of bowing agent.

Glenn et al. [24] prepared porous high-amylose corn starch microspheres by spraying dissolved starch with ethanol. The starch was heated to 140 °C using a pressure reactor. The temperature was held for 10 min before cooling the starch melt to 85 °C. The starch melt was pumped through an atomizing nozzle at a rate of 100 mL/min. The air pressure supplied to the nozzle was maintained at 0.55 MPa. The atomized starch was air classified into two fractions that were collected in two separate ethanol (95%) baths. The first fraction was collected directly from the spray stream and contained the largest particle size range. The second fraction was collected from droplets suspended by air turbulence and drawn by vacuum into a second ethanol bath. Both baths were stirred constantly to provide agitation and help minimize particle-to-particle interaction. The samples collected were stored in ethanol. The porous microspheres from the first collector consisted of spheres ranging in size from approximately 10 μm to greater than 300 μm with a mean size of more than 100 μm. The sample consisted of very fine microspheres ranging in size from approximately 2 to 15 μm with a mean size of 5 μm.

4.3 Porous Starch Structure and Properties

4.3.1 Porous Starch Structure

4.3.1.1 Characterization by FTIR

The FTIR spectra of native corn starch and corn porous starch were studied by [24], who found that the positions of the characteristic absorption peaks did not change markedly after enzymatic reaction. The reason for this is that the enzymatic reaction did not lead to a change in the molecular structure of starch. Therefore, the functional groups of corn PS were similar to native corn starch. However, the intensity of the characteristic absorption peaks decreased after the reaction, which was due to pore formation resulting in the reduction of starch granular density.

[28] studied the FTIR spectra of PS. In the case of PS, the intensity of peaks decreased, and smoothening of the peaks was observed, when compared with the neat starch. This may be due to the fact that pore formation in PS may have resulted in decreased starch granular density [29]. Important peaks [30] characterizing starch were 764 cm^{-1} (C–C stretch), 1067 cm-1 (C–H bending), 1344 cm-1 (C–O–H bending and –CH2 twisting), and 3165 cm-1 (-CH2 deformation) [31].

4.3.1.2 Granule Morphology Analysis by SEM

[29] investigated the micrographs of native corn starch and corn PS by SEM. It was found that native corn starch had a round and polygonal granular shape, and the surface was relatively smooth. The granular shape of corn PS was also round and polygonal, but the surface was rough. Many pores were formed on the starch granules. It is interesting that some of the pores even extended from the surface of the starch granules to the interior, and large internal cavities were present in the starch granules. These structural properties provide a large specific surface area. Therefore, it could be inferred that PS has excellent adsorption capacity and can be widely used as an adsorbent in various applications.

[32] reported that porous structures with a diverse pore size distribution and pore area depend on the enzyme type and its level. The effect of two different enzymes, fungal amylase and amyloglucosidase, on corn starch at sub-gelatinization temperature was studied as an alternative to obtaining PS [11]. Microscopic analysis of the granules confirmed that enzymatic modification of the starches resulted in porous structures with more agglomerates in amyloglucosidase-treated starches. α-Amylase produced some holes in the starch granules, and its action was not dependent on granule size. Amyloglucosidase was markedly active on the starch granules, and perforated granules were obtained. [33] demonstrated that in corn and sorghum starch granules, amyloglucosidase produced openings to channels providing access to the granule interior, and the surface pores enlarged through the channels from the hilum region to the outside. In the present study, both enzymes attacked the starch

granules on the fingerprint of protein bodies, which seem to be the weaker points and are more susceptible to enzymatic hydrolysis. In addition, amyloglucosidase-treated starches displayed a more stacked structure, with a type of gel joining the granules. It is likely that the polymer chains leached out more easily during amyloglucosidase enzymatic incubation and resulted in more gel in the treated starch granules. Alternatively, it could be that the hydrolyzed amylose chains that leached out to the periphery of the granules were readily crystallized after cooling yielding the jelly structure.

Analysis of the size of the holes revealed that α-amylase treatment led to small holes of 0.15 ± 0.04 μm, whereas amyloglucosidase resulted in larger holes (1.72 ± 0.18 μm), and the eccentricity ranged from 0.10 to 0.13, indicating very rounded pores in both cases [11].

It is generally accepted that granules contain amorphous and crystalline domains arranged in alternating concentric rings that create a semicrystalline environment within the granule [34], which were only evident on the amyloglucosidase-treated starch granules. Considering that the crystalline domains are mainly composed of amylopectin, while bulk amorphous domains are made up of amylose traversed by noncrystalline regions of amylopectin, it might be expected that treatment at 50 °C promoted changes in the amorphous areas of granules [35], leading to a more structured internal structure.

4.3.1.3 X-Ray Diffraction (XRD)

The crystalline and amorphous regions of starch, native corn starch, and corn PS were examined by XRD [29]. It was shown that native corn starch exhibited an A-type crystalline pattern, characteristic of cereal starch, with strong reflections at 2θ of 13°, 15°, 17°, and 23°. Corn PS also showed the same basic A-type pattern. However, a little increase in crystallinity was observed. The peaks appeared higher and sharper, indicating that hydrolysis preferentially occurred in the amorphous region during the enzymatic reaction. Therefore, the enzymatic reaction resulted in a decrease in the amorphous region and an increase in the crystalline region, that is, the crystallinity of corn PS was higher than native corn starch. According to these results, it can be inferred that corn PS is more difficult to dissolve than the native starch and should be a focus in their applications.

4.3.2 Porous Starch Properties

Compared with native starch or other modified starch, PS has excellent adsorption properties due to its large specific surface area [35]. For example, in the food industry, PS is an ideal sustained-release material adsorbing spices, sweeteners, acid condiments, enzymes, and flavorings [36]. In addition, some materials, such as

docosahexaenoic acid (DHA), eicosapentaenoic acid (EPA), vitamin E, vitamin A, carotene, and lycopene, which are easily oxidized or decomposed in the atmosphere or under light, can be effectively protected after adsorption by PS [24].

4.3.2.1 Adsorption Capacity

One of the most important parameters of PS is its adsorption capacity, which significantly affects its application. [29] reported that PS had a greater adsorption capacity than the native starch, and the adsorption capacity was optimized by investigating the reaction factors, including the mass ratio of α-amylase to glucoamylase ($m_{\alpha\text{-amylase}}/m_{glucoamylase}$), the mass ratio of total amount of enzymes to starch (m_{enzyme}/m_{St}), the ratio of liquid volume to starch mass (V_{H2O}/m_{St}), pH value of the reaction solution, enzymatic reaction temperature, and enzymatic reaction time.

[32] summarized the adsorptive capacity of PSs for water and sunflower oil. The hydrophilic nature was significantly dependent on both enzyme type and concentration, while the hydrophobic nature depended only on the enzyme type. In general, all enzymatic treatments increased the water adsorption capacity of the starches; while the adsorptive oil capacity of starch was only significantly modified when treated with α-amylase.

[37] reported that enzymatically treated corn starches showed significantly lower swelling capacity (SC); thus, less water was absorbed by these starches. It seems that either some physical impediment related to binding water molecules or the hydrophobic nature of the internal wall of the pinholes was responsible of that behavior. Therefore, the enzymatic treatment modified the granular integrity of the starch affecting its SC.

Swelling power and solubility provide evidence of the magnitude of the interaction between starch chains within both the amorphous and crystalline domains. The extent of interaction is influenced by the ratio and characteristics of amylose and amylopectin in terms of molecular weight distribution, degree of branching, length of branches, and conformation of molecules [34]. Swelling power decreased, and solubility increased with increasing duration of acid treatment. The swelling power of native starch was 14 g/g, which decreased to 0.78 g/g after 72 h of acid treatment; however, it improved with 0 h acid treatment [38]; [17] also observed an increase in the swelling factor of cereal starches at the first stage of acid hydrolysis and suggested that this change was due to the interaction between hydrolyzed amylose and water. The decrease in swelling power with increased duration of acid hydrolysis was consistent with the increase in crystallinity indicated in X-ray diffractograms. [39] associated the decrease in swelling power with acid treatment to the stiffness of the entangled amylopectin network in the crystalline region of the starch. The effect of disruption of hydrogen bonding between adjacent starch polymers and erosion of the amorphous regions during limited and prolonged acid treatment, respectively, on swelling power cannot be ruled out [17].

4.3.2.2 Thermal Properties

Thermal properties of the enzymatically modified corn starches were determined by differential scanning calorimetry (DSC) to detect possible changes in physical states of the starch structures. The transition temperatures (To, Tp, and Tc), gelatinization temperature range (Tc – To), enthalpies of gelatinization (H), and peak height index (PHI) significantly ($P < 0.05$) differed between native corn starch and corn PS. Gelatinization temperature (Tp) of the corn starch was 71.4 °C, which was higher than the previously described value of 64–69 °C [31, 40]. However, this increase may be ascribed to the annealing process which took place during incubation at 50 °C and produced an increase in the peak temperature [40]. Differences were observed in the thermal parameters derived from the pH effect; gelatinization temperatures were shifted to higher values, with the exception of T_p, when the reaction pH was increased. The effect was even more accentuated when the gelatinization temperature range was compared at both pH 4.0 and pH 6.0; pH 6.0 led to a narrow gelatinization range, which was related to a major proportion of the crystalline region [29]. It is well known that during the endothermic transition, namely, gelatinization, primarily water molecules freely diffuse into the amorphous region of starch and then penetrate the crystalline region [41]. As differences were mainly observed in the T_o, this may indicate that the amorphous region was more affected at higher pH during incubation.

4.3.2.3 Pasting Properties

Starch pasting occurs due to gelatinization and includes granule swelling, lower-weight polymer leaching, and, eventually, full degradation of the granules [42].

Typical pasting curves were observed when starch suspensions were subjected to a heating and cooling cycle. [32] reported that lower cooking temperature was required for the gelatinization of PSs, likely due to faster water absorption on the starch granules, as a negative correlation was observed between onset temperature and pore size ($r = -0.4581$, $P < 0.001$). PSs had a significantly lower peak viscosity, through final viscosity and setback compared to native starch, which was in agreement with previous results [11]. In this regard, pore size, ratio of pore area to granule area, and water adsorptive capacity were negatively correlated with peak viscosity.

[43] studied the steady shear viscosity versus temperature of the native corn starch and porous corn starch samples using a rheometer at a shear rate of 200 1/s. The viscosity versus temperature plots showed the characteristic variation in viscosity with temperature in the starch-water slurry commonly observed in the starch gelatinization process. The pasting onset temperatures of the native starch and PS samples were not significantly different ($P > 0.05$). The peak gelatinization temperatures of the PS samples were also similar, but higher than those of the native corn starch, and the difference in the shear viscosity data between the native and PS

samples can be attributed to the difference in granule structure of native and PS samples [16].

The shear viscosity of PS samples decreased significantly ($P < 0.05$) after enzymatic hydrolysis [43]. The decrease in peak viscosity may have been due to an increase in the porous structure at the surface of the starch granules. These pores are capable of increasing the ability of the granules to hold water and therefore decrease the peak viscosity [7]. The length of starch chains was shorter after hydrolysis. As a consequence, the stability against shearing and mixing was markedly weakened, which was reflected by lower viscosity [44]. One interesting observation in the peak viscosity versus time plot was that the peak viscosity values in porous corn starch samples were obtained at slightly longer times than that of the native corn starch. This may be due to the fact that it takes longer for the denser crystalline structure in PS to gelatinize than the native starch, which has lower crystallinity.

4.4 Mechanism of the Formation of Pores in Starch

4.4.1 Starch Granules Are Not Destroyed

4.4.1.1 Hydrolysis

PS can be produced by reacting various raw starches with starch-hydrolyzing enzymes under the gelatinization temperature of starch [45]. Using this method, the starch granules are not destroyed, although pits/craters on their surface and/or extensive interior erosion develop due to hydrolysis of the amorphous regions of starch.

PS can be generated based on α-amylase and glucoamylase used as hydrolysis enzymes. The microstructure of the starch granules was greatly dependent on the enzymatic treatment, but in both cases PS granules were obtained. α-Amylase produced some holes in the starch granules, and its action was not dependent on granule size. Glucosidase was considerably active on starch granules resulting in perforated granules. α-Amylase is an incision enzyme, which can randomly hydrolyze α-1,4 glycosidic bonds of starch, and glucoamylase is an excision enzyme, which can not only hydrolyze α-1,4 glycosidic bonds but also α-1,6 glycosidic bonds [46]. The pores are formed when α-amylase and glucoamylase degrade the amorphous regions of the starch granule. However, as the hydrolysis rate of the glucoamylase is low, a single enzyme type cannot hydrolyze starch efficiently. With an increasing amount of enzyme, the hydrolysis ratio increases continuously, as more enzyme molecules combine with starch molecules [29]. When a small quantity of enzyme was added, small and shallow pores were formed in the starch, and more pores were formed only when the enzyme ratio increased. These changes were more obvious on the A-type (large) granules, and the equatorial zone of the granules (the middle section) was much more susceptible to the enzyme than other parts of the granule due to the weaker structure [11, 15].

As starch is a solid granular powder and insoluble in water, a certain volume of solvent is required to ensure that starch granules are uniformly dispersed in the reaction system and efficiently contact with the enzyme. Only when V_{H2o}/m_{starch} increased to the extent that the enzymatic reaction was carried out efficiently, numerous pores were formed, and a larger specific surface area was generated [29].

Temperature is another important restrictive factor which affects pore formation. α-Amylase and glucoamylase have less activity when the environmental temperature is low. When the temperature reaches a suitable range for the enzyme (about 50 °C), the reaction efficiency increases. When the temperature is increased to 55 °C, an increase in the hydrolysis ratio and a decrease in the adsorption ratio are observed. The reason for this is that the reaction temperature is required to reach the gelatinization temperature of starch, and gelatinization then occurs. The hydrogen bonds between starch chains are broken, and the crystalline region is damaged. Therefore, the hydrolysis ratio significantly increases. However, when the degree of hydrolysis is high, the pores in the starch granules become larger and eventually collapse and break.

However, native starch is often poorly and slowly hydrolyzed in its granular form. Enzymatic treatment is usually combined with other treatments such as sonication [5]. The native starch granules have a smooth surface. However, after sonication, the surface of the granules was uneven, and some grooves and fissures appeared on the exterior of the granules which increased with increased sonication time. High-power ultrasound has an obvious impact on starch granules due to the collapse of cavitation bubbles and high-pressure gradients which mainly affect the amorphous regions of the granules and induce pores and fissures on the granules and change some physicochemical properties of the starch [47].

4.4.1.2 Acting as Pore-Forming Agents

Starch can be used as a pore-forming agent, e.g., as an additive in traditional slip casting, or it may be used as a combined pore-forming and body-forming agent (consolidating agent) in so-called starch consolidation or starch consolidation casting. It was proved that the starch powder starts to burn to release CO_2 at ~350 °C and is complete at ~550 °C; thus, pores with a pore size as large as the particle size of used starch (~10 μm) are then expected to form.

In a study of porous Si_3N_4 ceramics produced by the addition of potato starch, bulk density and porosity changed gradually as the starch content increased, while increased porosity did not fit the volume of the starch added [48]. The collapse of starch-originated pores during starch removal may be the reason for these inconsistencies. Porosity was affected by starch content, while the changes were not consistent which may have been caused by different sources of starch. More large pores approximately 10–15 mm in size were formed in the specimen when the corn starch content was increased [49]. During the production of hierarchically porous silica ceramics, a change in concentration of soluble starch hydrosol can affect the final microstructure of the template, such as macropore size and wall thickness, in the

unidirectional solidification process [50]. For hydrosol containing 10 wt.% soluble starch, the pore size was in the range of 3.5–12 μm. Different to the 10 wt.% starch monolith, the 15 wt.% starch material had reduced macropore size and dendritic-like features, with a pore size in the range of 4–9.5 μm. This may have been due to the tip splitting of the local ice dendrite and subsequent entrapment of a small fraction of starch species created by tip healing. Calcination temperature also affected the apparent porosity and flexural strength of porous starch ceramics [49].

However, starch granules generally change their size as well as their shape due to swelling in the aqueous suspension; therefore, it is difficult to determine the characteristics of the pores of the final porous ceramics. To solve this problem, porous alumina ceramics with ultrahigh porosity were prepared by combining the gel-casting process with the pore-forming agent technique [51]. When dissolved in water, starch will absorb water and generate a fibrous structure. This phenomenon has been applied in starch consolidation, in which starch works as a body-forming agent, to connect the ceramic powders together.

4.4.2 Starch Granules Are Destroyed

PS can also be prepared when starch granules have been partly or completely destroyed. Guan and Hanna prepared starch foam by extruding a native corn starch/starch acetate blend in a twin screw extruder, and EI-Tahlawy et al. prepared microcellular foams by reacting starch with alkyl ketene dimer in an alkaline medium, followed by precipitation by solvent exchange [52, 53].

4.4.2.1 Physical Activation

A freezing-solvent exchange has been used to prepare PS by replacing ice crystals in frozen starch gel with a mixed solvent of ethanol and water. In this method, porous structures were created following replacement of ice crystals in the frozen gel with various ethanol/water solutions [54]. Different porous structures were obtained when ice crystals were replaced with different ethanol/water solutions. Water was immobilized in the gel when the paste was cooled to room temperature and then frozen. Porous structures were created after replacement of ice crystals in the frozen gel with various ethanol/water solutions. The size of the holes in PS varied with different ethanol/water ratios [54]. The products from this method usually exhibit a low degree of crystallinity, which impairs their scope of applications [55]. Microwave vacuum drying is an alternative method to achieve good porosity and other properties. With this method, pores are formed by a pressure difference established between the inside and outside of the tissue due to steam generation [56]. Microwave energy is absorbed directly by physical movement of the material, and rapid drying occurs in a vacuum, along with material generating pores [57].

PS can be prepared via gelatinization by breaking the intrinsic hydrogen bonds within the macromolecular chain of starch, followed by freeze-drying and carbonization. [18] tried to modify starch with mercaptosuccinic acid during the gelatinization of potato starch and after freeze-drying and prepared PS xerogel by inserting mercaptosuccinic acid molecules into the starch chains [18]. The water molecules within the gelatinized starch evaporated gradually during the process of freeze-drying, resulting in self-aggregation of the macromolecular chains of starch. Due to the insertion (during gelatinization) and evaporation (during freeze-drying) of water molecules within the starch chains, starch xerogels exhibited a wrinkle-shaped morphology. The appearance of the porous structure was attributed to the fact that mercaptosuccinic acid molecules were introduced into starch to break the intrinsic hydrogen bonds within the starch chains [58]. The entrapped mercaptosuccinic acid molecules were retained in the starch xerogel during the freeze-drying process due to the formation of intermolecular hydrogen bonds between mercaptosuccinic acid and starch. As a result, the self-aggregation of starch chains was hindered due to the existence of mercaptosuccinic acid molecules, leading to the formation of macropores within the obtained xerogels, and the presence of abundant macropores. The aerogel template was removed by thermal treatment to decompose the starch.

Supercritical CO_2 technology was also introduced and promoted as an innovative technique for the production of PS. Soluble starch was dissolved in water. The water in the gel was then replaced with ethanol, resulting in monolithic starch aerogels after drying using a supercritical CO_2 technique [59]. Reactive supercritical fluid extrusion was also investigated in the cross-linking of starch blends by phosphorylation. A starch blend was mixed with sodium trimetaphosphate and extruded at 60–70 °C with NaOH solution and supercritical CO_2 as a blowing agent to generate starch foams [60]. It is worth mentioning that this process greatly influenced the structure and controllability of the resultant holes in the starch foams.

4.4.2.2 Chemical Activation

Compared with physical activation, chemical activation is the preferred method to obtain high-performance porous carbon from different materials. The most commonly used chemical activation agents are KOH, NaOH, H_3PO_4, $ZnCl_2$, K_2CO_3, and Na_2CO_3 [44, 61–64]. During the preparation of supercapacitors from cationic starch using KOH, $ZnCl_2$, and $ZnCl_2/CO_2$ activation, hysteresis is mainly due to factors such as the asymmetric slit-shape pores and the presence of ink bottle-type pores [65]. In addition, KOH-activated starch is quite different to the others in terms of its surface morphology characteristics, as it has a number of shallow concave round pores on the surface, which may be suitable for ion mobility and storage. H_3PO_4 is the preferred chemical activator as the activation conditions are milder. H_3PO_4 can be recovered, and the corresponding porous carbon has a high yield and well-developed pore structure. When starch was directly impregnated with H_3PO_4, starch particles assembled together, and H_3PO_4 interacted with them to form phosphate and polyphosphate bridges. The pores were generated through dehydration

reactions between acid molecules upon heating. The pore structures were created by the insertion of phosphate groups during the dilation processes [66].

High concentrations of acid and base are usually used to destroy the intermolecular hydrogen bond interactions and crystallization regions, which then facilitates the chemical reaction between the starch and modifiers [67]. A base can weaken the intermolecular interactions of the starch molecules and facilitate the reaction between starch and modifiers. When the modifier/starch mole ratio was increased, the porous structure was maintained, and when the NaOH concentration was increased to a high level, the porous structure was destroyed and disappeared [68].

4.4.2.3 Direct Carbonization

To circumvent the disadvantages of an inert atmosphere to eliminate non-carbon elements, high-energy consumption and corrosion-resistant equipment have been used. In the study by [8], a series of porous carbons were prepared by two distinct synthesis methods, including a direct solid-state method plus hydrothermal treatment and the post-annealing method. The outcomes of these two methods were compared. The charge storage mechanism for the porous carbon can be described as a double-layer model, which is a reversible ion adsorption process on the carbon surface. The charge is reserved in the interface between the carbon electrode and the electrolyte, thus leading to the so-called double-layer capacitance. Porous carbons are produced by carbonization of the precursor in an inert atmosphere to eliminate non-carbon elements, followed by activation of the char with an activation agent to create the porous structure [69].

4.5 Application of Porous Starch

4.5.1 Food Application

4.5.1.1 Flavor Delivery

Raw materials can easily lose their original flavor during production processes. To improve the sensory attributes of food products, flavors are widely added. However, flavors, which are generally liquid blends of molecules in solvents, are often liable to damage when exposed to heat, air, humidity, and other factors [2]. To achieve longer stability, flavors are generally converted into a powder form. Usually, a liquid flavor is dispersed into a bulk powder carrier, such as salt or maltodextrin. After spray drying, microencapsulation is performed to protect the liquid flavor from the outside environment, thus prolonging its shelf life, whereas a simple blended flavor is not protected from oxygen, air, moisture, or heat [70]. However, recently, the application of PS for flavor delivery has received considerable attention in the food industry, due to its advantages such as lower production costs (simple plating rather

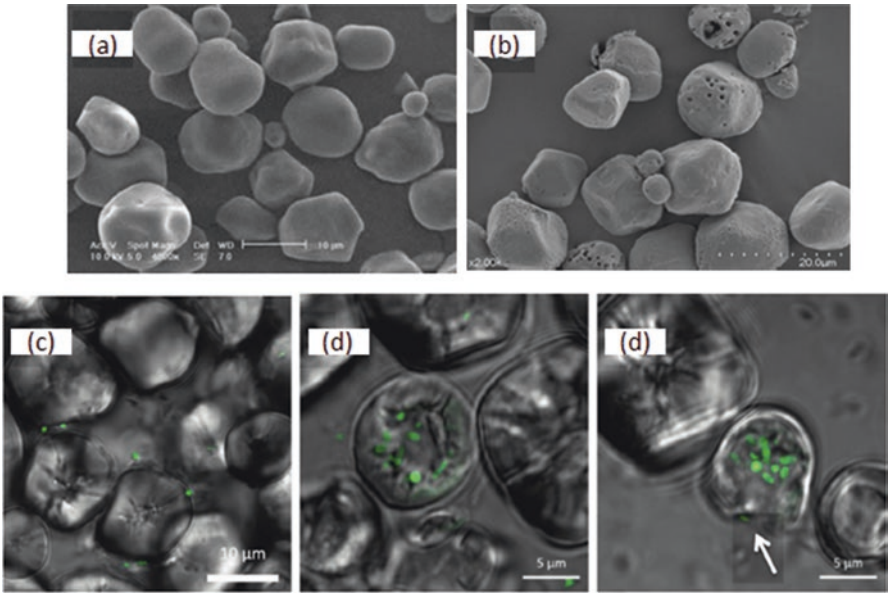

Fig. 4.1 Scanning electron micrographs of starch granules before (**a**) and after enzymatic digestion (**b**) and confocal laser scanning microscope images of (**c**) unmodified starch with cells attached to the granule surface, (**d**) 30-min hydrolyzed microcapsule, and (**e**) 120-min hydrolyzed microcapsule with cells trapped inside (arrow shows large pore opening) [73]

than spray drying) and the high liquid-to-powder ratio achieved (even higher than with spray drying) [2]; [24] compared the tomato flavor carrying performance between plating flavor onto PS, encapsulating flavor by spray drying and blending flavor onto a nonporous conventional carrier (maltodextrin). Although, these three flavor systems showed similar flavor content after sterilization and similar behavior during their shelf life, flavor delivery with PS was preferred due to easy processing and low cost. Moreover, the flavor delivery capacity of PS was confirmed to be related to the polarity of the solvent used for plating; thus, a better flavor delivery system with PS may be expected following appropriate solvent selection.

4.5.1.2 Probiotic Encapsulation

Nowadays, the incorporation of probiotics into functional foods is encouraged as they play an important role in health promotion. For example, *Lactobacillus plantarum* 299v has health properties including the improvement of irritable bowel syndrome [71] and vascular endothelial function [72]. Thus, it is widely added to many food products, especially fermented milks. However, its applications are limited by the viability of probiotic cells, which is affected by processing and storage conditions and the environment in the gastrointestinal tract. [73] proposed the encapsulation of *L. plantarum* 299v with PS to facilitate its functional effect in the body

(Fig. 4.1). With encapsulation, the effects of probiotic bacteria and enzyme-resistant starch could be combined in one product. Compared to free bacteria (*L. plantarum* 299v), PS-encapsulated bacteria showed greater acid and bile salt tolerance, with a significantly lower reduction in viability over the entire test period. Moreover, encapsulation with maize starch granules combined with a gelatinized starch coating significantly improved the heat tolerance of *L. plantarum* 299v.

4.5.1.3 Food Preservation

Allicin is the main compound derived from garlic and possesses various biological functions such as antiparasitic, antihypertensive, cardioprotective, anti-inflammatory, and anticancer properties [74]. Allicin, due to its broad-spectrum of antibacterial activity against Gram-negative and Gram-positive bacteria, is regarded as a potential food preservative, which may be used in the food industry. However, it has low stability and water solubility. Wang et al., investigated encapsulation of allicin using β-cyclodextrin with PS via spray drying to increase its solubility which limits its use as food preservatives [74]. The solubility of microencapsulated allicin was significantly improved, leading to direct dissolution in water. By retaining the desired antimicrobial activity of allicin, encapsulation also improved the stability of allicin microcapsules against heat, pH, light, and oxygen during allicin loading from approximately 20% to 40%.

4.5.2 Drug Delivery

As the most acceptable route for the treatment of chronic diseases, oral delivery has limitations in that the therapeutic efficacy of active ingredients significantly depends on their systemic exposure after oral administration [75]. The application of many commercial drugs or potential drug candidates is restricted due to the fact that they are poorly soluble in water and exhibit low bioavailability following oral delivery [75, 76]. Several approaches have been developed to improve the oral absorption of lipophilic drugs [77, 78]. Of these approaches, PS is considered a promising candidate due to its stable pore structure, high pore volume, and good biocompatibility. With its high specific surface area, PS can be applied in the adsorption of liquid flavors and plant oils, tissue engineering scaffolds, and controlled drug delivery [5, 16, 76, 79, 80].

[5, 16] prepared a biodegradable porous starch foam (BPSF) as a carrier to improve the dissolution and enhance the oral bioavailability of lovastatin, a statin drug, naturally found in foods such as oyster mushrooms and red yeast rice, which is used to lower cholesterol (hypolipidemic agent) in those with hypercholesterolemia to reduce the risk of cardiovascular disease. The Brumauer–Emmet–Teller specific surface area (BET-SSA) and total pore volume of BPSF were estimated to be 127.75 m^2/g and 0.38 mL/g. The rod-shaped lovastatin was observed to disperse

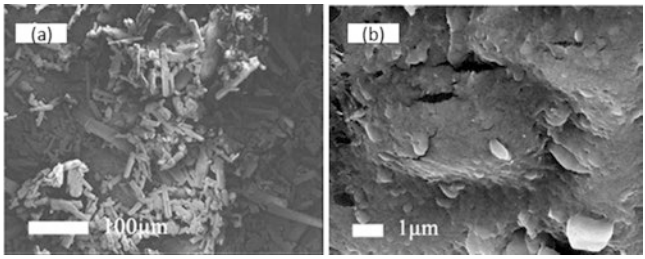

Fig. 4.2 SEM images of crude lovastatin (**a**) and lovastatin-loaded BPSF particles (**b**) [5]

in the pores and surface of BPSF (Fig. 4.2). The in vitro drug release studies revealed that the use of hydrophilic BPSF as a carrier for poor water-soluble drugs resulted in the fast release of lovastatin. The release of 80% lovastatin required 15 min using the BPSF system, while 45 min was required for the current commercial product. In addition, enhanced oral bioavailability of lovastatin loaded in BPSF, in comparison with crude lovastatin and commercial capsules, was also observed [5, 16].

[76] prepared a PS-based self-assembled nano-delivery (PSN) for loading lipophilic probucol. The probucol-loaded nanocarrier (PLN) was used to investigate the biodistribution of PSN in rat intestine, cellular uptake of PSN in Caco-2 cell monolayers, and the pharmacokinetic behavior of PSN in rats. The results showed that PLN, formed by self-assembly when PSN was dispersed in gastrointestinal (GI) fluids, were nanometer-sized particles with a narrow size distribution and exhibited good stability in GI fluids. Using the PSN delivery system, the aqueous solubility of probucol was increased over 50,000-fold, and the cumulative release of probucol was increased by more than 80% in GI fluids. The distribution of probucol in the duodenum, jejunum, and ileum was also improved 7.17-, 15.99-, and 33.61-fold by PSN. With PSN, the oral bioavailability of probucol was greatly improved by approximately 9.96-fold, compared to that of the free drug suspension, confirming that the PS-based system enhanced the oral absorption of lipophilic drugs.

4.5.3 Wastewater Treatment

4.5.3.1 Decolorization

Due to economic development, the application of natural and synthetic dyes has expanded in food and non-food industrial fields. However, approximately 10% of the dyes used are wasted and discharged into aquatic systems, leading to serious threats to the environment and public health [81]. Thus, the removal of dyes from wastewater is of great importance for environmental protection. A decolorization process is widely used in either wastewater treatment or the manufacture of

industrial products. Compared with other decolorization technologies, such as biological treatments, advanced oxidation processes, and photocatalytic degradation, adsorption is considered a safe technology without causing secondary pollution [82–84]. The preparation of safer, more stable, and efficient absorbents is essential to improve the application of adsorption technology. In recent years, starch-based adsorbents, which are safer for dye removal, have been a focus of attention in the development of biodegradable and safe adsorbents.

[85] prepared cross-linked porous starch (CPS) by hydrolyzing cross-linked starch (native starch cross-linked with epichlorohydrin) with α-amylase and applied this CPS, as a biodegradable and safe adsorbent, for the removal of methylene blue (MB) from aqueous solution. CPS showed higher adsorption capacity than native starch. In addition, investigations showed that the adsorption of MB on CPS was endothermic and spontaneous in nature. The equilibrium adsorption data were well described by the Langmuir isotherm model with a maximum adsorption capacity of 9.46 mg/g under the conditions of a MB initial concentration of 10 mg/L at 20 °C. [6] compared MB adsorption capacity between PS and SA-modified PSs (SAPSs) obtained by modification of PSs with succinic anhydride (SA) in a solvent-/catalyst-free medium. The results showed that the capacity of MB adsorption by SAPSs increased gradually with increasing degree of substitution. In a system containing 10 g/L of SAPS and 0.0854 mmol/L (31.93 mg/L) MB dye, SAPs showed better adsorption than PS without substitution, 2.6 mg/g and 1.6 mg/g for SAPs with a degree of substitution of 1.9 and PS, respectively.

In order to remove hazardous gardenia yellow (GY), a natural colorant which is genotoxic, [18] modified potato starch with mercaptosuccinic acid (MSA) during its gelatinization by breaking the intrinsic hydrogen bonds within the macromolecular chains of starch. Porous starch xerogels (PSX) were obtained after freeze-drying, by inserting MSA molecules into the starch chains (Fig. 4.3a). The obtained PSX/MSA exhibited a porous structure due to the existence of MSA molecules within the macromolecular chains of starch (Fig. 4.3b). The results showed that the number of macropores within the PSX/MSA samples increased when the MSA content in the composites increased and improved the adsorption of GY. Adsorption of GY by PSX/MSA adsorbents was markedly higher, with a capacity of 72 mg/g, compared with natural potato starch and starch xerogels alone, with a capacity of less than 10 mg/g. These results were due to the different structures of these adsorbents. In the case of potato starch, the movement of GY molecules was categorized into surface diffusion over the solid surface of potato starch; however, in the case of PSX/MSA adsorbents, both pore and surface diffusion occurred due to the presence of macropores. According to [85], as the activation energy for diffusion was lower than the energy of adsorption, the contribution of surface diffusion was negligible when pore diffusion occurred. Thus, pore diffusion made a significant contribution to the adsorption of GY by these PSX/MSA adsorbents.

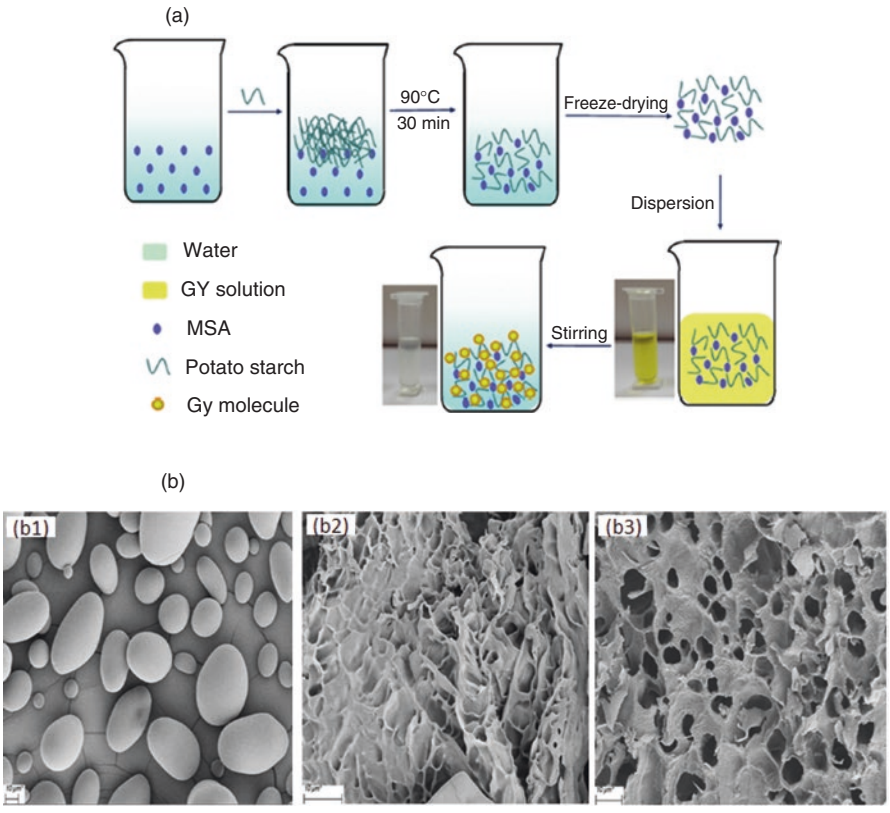

Fig. 4.3 Schematic illustration showing the process of PSX/MSA preparation and GY adsorption by the adsorbents (**a**) and field emission scanning electron microscopy of pure potato starch (**b1**), SX (**b2**) and PSX/MSA (**b3**) [18]

4.5.3.2 Heavy Metal Ion Removal

Heavy metal ions, such as Cu^{2+}, Cd^{2+}, and Pb^{2+}, pose a threat to public health and environmental safety. Recently, various adsorbents, including oxidized carbon nanotubes, graphene oxide, clay, and biomass sources [86, 87], have been used to remove heavy metals from aqueous solutions. Considering their low cost, availability, and biodegradability, biomass-based adsorbents are preferred. Natural polysaccharide-based adsorbents have been shown to efficiently remove heavy metal ions. However, adsorbents prepared from polysaccharides are usually soluble or in powder form, leading to the difficulty of separation after the adsorption process. PS, which has the advantages of being biodegradable with easy and economical solid–liquid separation, is now attracting the interest of researchers [29, 72, 86, 88].

By reacting PS with carbon disulfide, and PS with citric acid, Ma et al. (2015) prepared porous starch xanthate (PSX) and porous starch citrate (PSC), respectively. The attached xanthate and carboxylate groups formed chelation and electrostatic

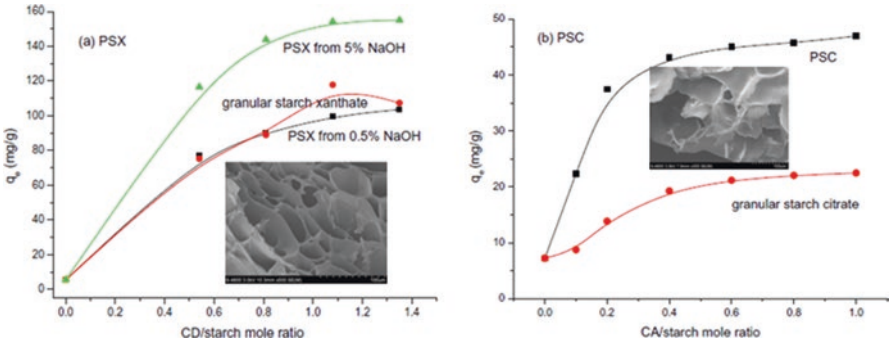

Fig. 4.4 Effect of mole ratio of (**a**) CD/starch and (**b**) CA/starch on equilibrium adsorption capacity of Pb^{2+} by PSX and PSC. Initial concentrations: $Pb2^{+}$ 0.5 g/L; adsorbent 2 g/L. The insets are SEM images of PSX and PSC, respectively [88]

interactions, respectively, with heavy metal ions during the adsorption process. The adsorption capacity of PSX and PSC for lead(II) ions was evaluated in a system containing 2 g/L of the adsorbents and PbNO3 solution (0.5 g/L Pb^{2+}). The adsorption capacity was found to be highly dependent on the carbon disulfide/starch and citric acid/starch mole ratios used during preparation. The maximum adsorption capacity for PSX and PSC was 109.1 mg/g and 57.6 mg/g, respectively, and showed promising efficiency for the removal of heavy metals from contaminated liquids (Fig. 4.4). [89] prepared a starch-based nanocomposite (starch/SnO_2) as an effective adsorbent to remove Hg^{2+} from aqueous medium. The adsorption performance was demonstrated by an increase in temperature, indicating an endothermic adsorption. At room temperature (25 °C), the maximum adsorption capacity was 192 mg/g.

References

1. Qian J, Chen X, Ying X, LV B. Optimisation of porous star preparation by ultrasonic pretreatment followed by enzymatic hydrolysis. Int J Food Sci Technol. 2011b;46:179–85.
2. Belingheri C, Giussani B, Rodriguez-Estrada MT, Ferrillo A, Vittadini E. Oxidative stability of high-oleic sunflower oil in a porous starch carrier. Food Chem. 2015;166:346–51.
3. Luo Z, Cheng W, Chen H, Fu X, Peng X, Luo F, et al. Preparation and properties of enzyme-modified cassava starch/zinc complexes. J Agric Food Chem. 2013;61(19):4631–8.
4. Kapelko-Żeberska M, Zieba T, Spychaj R, Gryszkin A. Acetylated adipate of retrograded starch as RS 3/4 type resistant starch. Food Chem. 2015;188:365–9.
5. Wu C, Wang Z, Zhi Z, Jiang T, Zhang J, Wang S. Development of biodegradable porous starch foam for improving oral delivery of poorly water soluble drugs. Int J Pharm. 2011;403(1–2):162–9.
6. Chang PR, Qian D, Aanerson DP, MA X. Preparation and properties of the succinic ester of porous starch. Carbohydr Polym. 2012;88:604–8.
7. Uthumporn U, Zaidul IS, Karim AA. Hydrolysis of granular starch at sub-gelatinization temperature using a mixture of amylolytic enzymes. Food Bioprod Process. 2010;88(1):47–54.

8. Chen XY, Chen C, Zhang ZJ, Xie DH. Synthesis and capacitive performance of nitrogen doped porous carbons derived from sodium carboxymethyl starch. Powder Technol. 2013;246:201–9.
9. Yussof NS, Utra U, Alias AK. Hydrolysis of native and cross-linked corn, tapioca, and sweet potato starches at sub-gelatinization temperature using a mixture of amylolytic enzymes. Starch-Starke. 2013;65(3–4):285–95.
10. Lecorre D, Vahanian E, Dufresne A, Bras J. Enzymatic pretreatment for preparing starch nanocrystals. Biomacromolecules. 2012;13(1):132–7.
11. Dura A, Błaszczak W, Rosell CM. Functionality of porous starch obtained by amylase or amyloglucosidase treatments. Carbohydr Polym. 2014;101:837–45.
12. Gao F, Li D, Bi CH, Mao ZH, Adhikari B. Preparation and characterization of starch cross-linked with sodium trimetaphosphate and hydrolyzed by enzymes. Carbohydr Polym. 2014;103:310–8.
13. Jiao A, Wei B, Wu C, Jin Z, Tian Y, Li H, et al. Impact of α-amylase combined with hydrochloric acid hydrolysis on structure and digestion of waxy rice starch. Int J Biol Macromol. 2013;55:276–81.
14. Shariffa YN, Karim AA, Fazilah A, Zaidul ISM. Enzymatic hydrolysis of granular native and mildly heat-treated tapioca and sweet potato starches at sub-gelatinization temperature. Food Hydrocoll. 2009;23(2):434–40.
15. Majzoobi M, Hedayati S, Farahnaky A. Functional properties of microporous wheat starch produced by -amylase and sonication. Food Bioscience. 2015;11:79–84.
16. Wu Y, Du X, Ge H, Lv Z. Preparation of microporous starch by glucoamylase and ultrasound. Starch-Stärke. 2011;63(4):217–25.
17. Jayakody L, Hoover R. The effect of lintnerization on cereal starch granules. Food Res Int. 2002;35(7):665–80.
18. Bao L, Zhu X, Dai H, Tao Y, Zhou X, Liu W, Kong Y. Synthesis of porous starch xerogels modified with mercaptosuccinic acid to remove hazardous gardenia yellow. Int J Biol Macromol. 2016;89:389–95.
19. Mirka S, Katerina H, Zdenka M, Alexandra T, Viara IP, Ivo S. Magnetic porous corn starch for the affinity purification of cyclodextrin glucanotransferase produced by Bacillus circulans. Biocatal Biotransformation. 2012;30(1):96–101.
20. Tuovinen L, Ruhanen E, Kinnarinen T, Rönkkö S, Pelkonen J, Urtti A, …, Järvinen K. Starch acetate microparticles for drug delivery into retinal pigment epithelium—in vitro study. J Control Release. 2004; 98(3), 407–13.
21. Fundueanu G, Constantin M, Dalpiaz A, Bortolotti F, Cortesi R, Ascenzi P, Menegatti E. Preparation and characterization of starch/cyclodextrin bioadhesive microspheres as platform for nasal administration of Gabexate Mesylate (Foy®) in allergic rhinitis treatment. Biomaterials. 2004;25(1):159–70.
22. Peng H, Xiong H, Wang S, Li J, Chen L, Zhao Q. Soluble starch–based biodegradable and microporous microspheres as potential adsorbent for stabilization and controlled release of coix seed oil. Eur Food Res Technol. 2011;232(4):693–702.
23. García-González CA, Uy JJ, Alnaief M, Smirnova I. Preparation of tailor-made starch-based aerogel microspheres by the emulsion-gelation method. Carbohydr Polym. 2012;88(4):1378–86.
24. Glenn GM, Klamczynski AP, Woods DF, Chiou B, Orts WJ, Imam SH. Encapsulation of plant oils in porous starch microspheres. J Agric Food Chem. 2010;58(7):4180–4.
25. Qian D, Chang PR, Ma X. Preparation of controllable porous starch with different starch concentrations by the single or dual freezing process. Carbohydr Polym. 2011;86(3):1181–6.
26. Basri SN, Zainuddin N, Hashim K, Yusof NA. Preparation and characterization of irradiated carboxymethyl sago starch-acid hydrogel and its application as metal scavenger in aqueous solution. Carbohydr Polym. 2016;138:34–40.
27. Malafaya PB, Elvira C, Gallardo A, Román JS, Reis RL. Porous starch-based drug delivery systems processed by a microwave route. J Biomater Sci Polym Ed. 2001;12(11):1227–41.

28. Ali MT, Fule R, Sav A, Amin P. Porous starch: a novel carrier for solubility enhancement of carbamazepine. AAPS PharmSciTech. 2013;14(3):919–26.
29. Zhang B, Cui D, Liu M, Gong H, Huang Y, Han F. Corn porous starch: preparation, characterization and adsorption property. Int J Biol Macromol. 2012;50(1):250–6.
30. Vasko PD, Blackwell J, KoenigInfrared JL. Raman spectroscopy of carbohydrates: part II: normal coordinate analysis of α-Dglucose. Carbohydr Res. 1972;23(3):407–16.
31. Cael SJ, Koenig JL, Blackwell J. Infrared and Raman spectroscopy of carbohydrates: part III: Raman spectra of the polymorphic forms of amylose. Carbohydr Res. 1973;29(1):123–34.
32. Benavent-Gil Y, Rosell CM. Comparison of porous starches obtained from different enzyme types and levels. Carbohydr Polym. 2017;157:533–40.
33. Huber KC, BeMiller JN. Channels of maize and Sorghum starch granules. Carbohydr Polym. 2000;41:269–76.
34. Ratnayake WS, Hoover R, Warkentin T. Pea starch: composition, structure and properties – a review. Starch. 2002;54:217–34.
35. Zhao J, Madson MA, Whistler RL. Cavities in porous corn starch provide a large storage space. Cereal Chem. 1996;73(3):379–80.
36. WR Y, HY Y. Adsorbent characteristics of porous starch. Starch/Stärke. 2002;54(6):260–3.
37. Dura A, Rosell CM. Physico-chemical properties of corn starch modified with cyclodextrin glycosyltransferase. Int J Biol Macromol. 2016;87:466–72.
38. Singh H, Sodhi NS, Singh N. Structure and functional properties of acid thinned sorghum starch. Int J Food Prop. 2009;12:713–25.
39. Kainuma K, French DN. Amylodextrin and its relationship to starch granule structure. I. Preparation and properties of amylodextrins from various starch types. Biopolymers. 1971;10:1673–8.
40. Rocha TS, Felizardo SG, Jane J, Franco CML. Effect of annealing on the semicrystalline structure of normal and waxy corn starches. Food Hydrocoll. 2012;29(1):93–9.
41. Biliaderis CG. The structure and interactions of starch with food constituents. Can J Physiol Pharmacol. 1991;69(15):60–78.
42. Singh N, Singh J, Kaur L, Singh-Sodhi N, Singh-Gill B. Morphological, thermal and rheological properties of starches from different botanical sources. Food Chem. 2003;81:219–31.
43. Gao F, Li D, Chong-hao B, Mao Z-h, Adhikari B. Application of various drying methods to produce enzymatically hydrolyzed porous starch granules. Dry Technol. 2013;31:1627–34.
44. Xu Z, Miao M. Functional modified starch. Beijing: China Light Industry Press; 2010. p. 12–38. (in Chinese)
45. Wang X, Wang H, Dai Q, Li Q, Yang J. Preparation of novel porous carbon spheres from corn starch. Colloids Surf A Physicochem Eng Asp. 2009;346:213–5.
46. Tester RF, Qi X, Karkalas J. Hydrolysis of native starches with amylases ☆. Anim Feed Sci Technol. 2006;130:39–54.
47. Anetrezek J, Zoran H, Drago S, Jurislav B, Mladen B, Suzanarimac B, Tomislav B, Domagoj C, Branko T, Jurica G. Ultrasound effect on physical properties of corn starch. Carbohydr Polym. 2010;79:91–100.
48. Topates G, Petasch U, Adler J, Kara F, Mandal H. Production and permeability of porous Si3N4 ceramics produced by starch addition. J Asian Ceramic Soc. 2013;1:257–61.
49. Xu G, Chen Z, Zhang X, Cui H, Zhang Z, Zhan X. Preparation of porous Al2TiO5-Mullite ceramic by starch consolidation casting and its corrosion resistance characterization. Ceram Int. 2016;42:14107–12.
50. Zhang Y, Hu L, Han J, Jiang Z, Zhou Y. Soluble starch scaffolds with uniaxial aligned channel structure for in situ synthesis of hierarchically porous silica ceramics. Microporous Mesoporous Mater. 2010;130:327–32.
51. Li S, Wang C-A, Zhou J. Effect of starch addition on microstructure and properties of highly porous alumina ceramics. Ceram Int. 2013;39:8833–9.
52. Guan J, Hanna MA. Extruding foams from corn starch acetate and native corn starch. Biomacromolecules. 2004;5:2329–39.

53. El-Tahlawy K, Venditti R, Pawlak J. Effect of alkyl ketene dimer reacted starch on the properties of starch microcellular foam using a solvent exchange technique. Carbohydr Polym. 2008;73:133–42.
54. Chang PR, Yu JG, Ma XF. Preparation of porous starch and its use as a structure-directing agent for production of porous zinc oxide. 2011. Chen G, Zhang B. Hydrolysis of granular corn starch with controlled pore size. J Cereal Sci. 2012;56(2), 316–320.
55. Patel VR, Amiji MM. Preparation and characterization of freeze-dried chitosan-poly(ethylene oxide) hydrogels for site-specific antibiotic delivery in the stomach. Pharm Res. 1996;13:588–93.
56. Scaman CH, Durance TD, Drummond L, Sun DW. Combined Microwave Vacuum Drying[M]. Emerg Technol Food Process. 2005:427–45.
57. Cui ZW, Xu SY, Sun DW. Microwave-vacuum drying kinetics of carrot slices. J Food Eng. 2004;65:157–64.
58. Qiao X, Tang Z, Sun K. Plasticization of corn starch by polyol mixtures. Carbohydr Polym. 2011;83:659–64.
59. Miao Z, Ding K, Wu T, Liu Z, Han B, An G, Miao S, Yang G. Fabrication of 3D-networks of native starch and their application to produce porous inorganic oxide networks through a supercritical route. Microporous Mesoporous Mater. 2008;111:104–9.
60. Manoi K, Rizvi SSH. Physicochemical characteristics of phosphorylated cross-linked starch produced by reactive supercritical fluid extrusion. Carbohydr Polym. 2010;81:687–94.
61. Guo Y, Rochstraw DA. Activated carbons prepared from rice hull by one-step phosphoric acid activation. Microporous Mesoporous Mater. 2007;100:12–9.
62. Jiang J, Bao L, Qiang Y, Xiong Y, Chen J, Guan S, Chen J. Sol-gel process-derived rich nitrogen-doped porous carbon through KOH activation for supercapacitors. Electrochim Acta. 2015;158:229–36.
63. He X, Ling P, Yu M, Wang X, Zhang X, Zheng M, He X, Ling P, Yu M, Wang X. Rice husk-derived porous carbons with high capacitance by ZnCl2 activation for supercapacitors. Electrochim Acta. 2013;105:635–41.
64. Ilnicha A, Lukaszewicz JP. Synthesis of N-rich microporous carbon materials from chitosan by alkali activation using Na 2 CO 3. Mater Sci Eng B. 2015;201:66–71.
65. Wang H, Zhong Y, Li Q, Yang J, Dai Q. Cationic starch as a precursor to prepare porous activated carbon for application in supercapacitor electrodes. J Phys Chem Solids. 2008;69:2420–5.
66. Ding L, Zou B, Li Y, Liu H, Wang Z, Zhao C, Su Y, Guo Y. The production of hydrochar-based hierarchical porous carbons for use as electrochemical supercapacitor electrode materials. Colloids Surf A Physicochem Eng Asp. 2013;423:104–11.
67. Xiaofei M, Xueyuan L, Anderson DP, Chang PR. Modification of porous starch for the adsorption of heavy metal ions from aqueous solution. Food Chem. 2015;181:133–9.
68. Ma XF, Chang PR, Yu JG, Stumborg M. Properties of biodegradable citric acid-modified granular starch/thermoplastic pea starch composites. Carbohydr Polym. 2009;75:1–8.
69. Xiang YC, Zhou QQ. The production of porous carbon from calcium lignosulfonate without activation process and the capacitive performance. Electrochim Acta. 2012;71:92–9.
70. Nielsen A, Getler J. Spray drying and other methods for encapsulation of flavourings. In: Ziegler H, editor. Flavourings. Weinheim: Wiley-VCH; 2007. p. 97–108.
71. Niedzielin K, Kordechi H, Enabirkenfeld B. A controlled, double-blind, randomized study on the efficacy of Lactobacillus plantarum 299V in patients with irritable bowel syndrome. Eur J Gastroenterol Hepatol. 2001;13:1143–7.
72. Malik M, Widlansky ME, Suboc T, Coulliard A, Su J, Salzman NH, Baker JE. The probiotic bacterium lactobacillus Plantarum 299v improves vascular endothelial function and decreases inflammatory biomarkers in men with established cardiovascular disease. Circulation. 2015;132:A10898.
73. Li H, Thuyho VT, Turner MS, Dhital S. Encapsulation of Lactobacillus plantarum in porous maize starch. LWT Food Sci Technol. 2016;74:542–9.

74. Wang Y-F, Shao J-J, Wang Z-L, Lu Z-X. Study of allicin microcapsules in β-cyclodextrin and porous starch mixture. Food Res Int. 2012;49:641–7.
75. Porter CJ, Trevaskis NL, Charman WN. Lipids and lipid-based formulations: optimizing the oral delivery of lipophilic drugs. Nat Rev Drug Discov. 2007;6:231–48.
76. Zhang Z, Huang J, Jiang S, Liu Z, Gu W, Yu H, Li Y. Porous starch based self-assembled nano-delivery system improves the oral absorption of lipophilic drug. Int J Pharm. 2013;444:162–8.
77. Brewster ME, Loftsson T. Cyclodextrins as pharmaceutical solubilizers. Adv Drug Deliv Rev. 2007;59:645–66.
78. Florence AT. Nanoparticle uptake by the oral route: fulfilling its potential? Drug Discov Today Technol. 2005;2:75–81.
79. Balmayor ER, Tuzlakoglu K, Marques AP, Azevedo HS, Reis RL. A novel enzymatically-mediated drug delivery carrier for bone tissue engineering applications: combining bio-degradable starch-based microparticles and differentiation agents. J Mater Sci Mater Med. 2008;19:1617–23.
80. Lee SY, Eskridge KM, Koh WY, Hanna MA. Evaluation of ingredient effects on extruded starch-based foams using a supersaturated split-plot design. Ind Crop Prod. 2009;29:427–36.
81. Liu J, Liu G, Liu W. Preparation of water-soluble β-cyclodextrin/poly(acrylic acid)/graphene oxide nanocomposites as new adsorbents to remove cationic dyes from aqueous solutions[J]. Chem Eng J. 2014;257:299–308.
82. Galindo C, Jacques P, Kalt A. Photodegradation of the aminoazobenzene acid orange 52 by three advanced oxidation processes: UV/H 2 O 2, UV/TiO 2 and VIS/TiO 2: comparative mechanistic and kinetic investigations. J Photochem Photobiol A Chem. 2000;130:35–47.
83. Sanghi R, Bhattacharya B. Review on decolorisation of aqueous dye solutions by low cost adsorbents. Color Technol. 2002;118:256–69.
84. Guo L, Li G, Liu J, Meng Y, Tang Y. Adsorptive decolorization of methylene blue by cross-linked porous starch. Carbohydr Polym. 2013;93:374–9.
85. Schneider P, Smith J. Chromatographic study of surface diffusion. AICHE J. 1968;14:886–95.
86. Tofighy MA, Mohammadi T. Adsorption of divalent heavy metal ions from water using carbon nanotube sheets. J Hazard Mater. 2011;185:140–7.
87. Jain M, Garg V, Kadirvelu K. Chromium (VI) removal from aqueous system using *Helianthus annuus* (sunflower) stem waste. J Hazard Mater. 2009;162:365–72.
88. Ma X, Liu X, Anderson DP, Chang PR. Modification of porous starch for the adsorption of heavy metal ions from aqueous solution. Food Chem. 2015;181:133–9.
89. Naushad M, Ahamad T, Sharma G, Ala'a H, Albadarin AB, Alam MM, Alothman ZA, Alahehri SM, Ghfar AA. Synthesis and characterization of a new starch/SnO 2 nanocomposite for efficient adsorption of toxic Hg^{2+} metal ion. Chem Eng J. 2016;300:306–16.

Chapter 5
Starch Microemulsions and Its Applications

Haoran Fan, Xiuting Hu, Jianwei Zhao, and Jinpeng Wang

5.1 Introduction

Microemulsions are isotropic, clear or translucent, thermodynamically stable dispersions containing water, oil, surfactant, and a cosurfactant, usually alcohol [1, 2]. Because of their unique properties, including an ultralow interfacial tension, large interface, and the ability to solubilize otherwise immiscible liquids, microemulsions are widely used in various fields, including tertiary oil recovery, separation [3], pharmaceuticals [4], nanoparticle synthesis [5–7], and chemical engineering [8]. They are either "water in oil" (W/O) or "oil in water" (O/W) dispersions, stabilized with pure or mixed amphiphiles. Amphiphiles are required to significantly reduce the oil–water interfacial tension by their adsorption to the interface, which minimizes the positive free energy change of dispersion associated with surface formation [9, 10]. Microemulsions differ physicochemically from macroemulsions, which are normally called "emulsions." In macroemulsions, the particle size is much larger; they are nontransparent, have only short-term stability, and allow only restricted handling. Occasional homogenization with agitation is required to prevent macroemulsions from breaking or phase separation. Therefore, they are kinetically stable, whereas microemulsions can form with the expenditure of very little energy (which can be provided by the thermal energy of the system) and are thus thermodynamically stable. A mixture with the right composition of water, amphiphile, and oil may spontaneously homogenize, forming a microemulsion. A water–oil microemulsion is topologically similar to reverse micelles (in which the polar heads of the amphiphile molecules are oriented inward and the nonpolar tails are

H. Fan · J. Zhao · J. Wang (✉)
School of Food Science and Technology, Jiangnan University, Wuxi, China
e-mail: h.fan@ufl.edu; zhaojw@jiangnan.edu.cn; jpwang1984@jiangnan.edu.cn

X. Hu
School of Food Science and Technology, Nanchang University, Nanchang, China
e-mail: xthu@ncu.edu.cn

Z. Jin (ed.), *Functional Starch and Applications in Food*,
https://doi.org/10.1007/978-981-13-1077-5_5

oriented toward the oil continuum), and their distinction rests on the availability of free water in the core, called the "micro-pool." Compositions yielding a rigid interior or core are called "reverse micelles," in which the water present is immobilized by the hydration of the polar or ionic heads of the amphiphile and the counterions (when present). Compositions with mobile or free water in the core after the hydration requirements of the amphiphile head groups and counterions are satisfied are called "microemulsions." The size of the reverse micelles is normally restricted to 5 nm, because a grown size <5 nm changes the status of the mixture to a microemulsion. This dimension-dependent change in status may not apply to oil–water dispersions where the solvent-dependent bound and free oil in the pool is less physicochemically significant, as in reverse micelles. Of course, normal micelles can consume oil and grow in size, forming a microemulsion.

Starch, an inexpensive, renewable, biodegradable natural polymer, is widely used in food and industrial fields as a thickener, gelling agent, bulking agent, and water-retention agent [11, 12]. However, native starch has several limitations, including its poor processability and solubility, which limit its industrial applications. However, starch can be modified with physical, chemical, or enzymatic treatments to improve its properties [13, 14].

5.2 Starch Microemulsion Preparation

Microemulsions have received much attention as media for polymerization reactions, which are analogous to emulsion polymerization. These complex fluids are composed of water, a hydrophobic oil, and a surfactant and may contain cosurfactants and other additives [15]. A starch microemulsion is a biodegradable microemulsion that can be used either as a controlled-release system or a "traditional" drug delivery system.

5.2.1 Mechanism of Microemulsion Preparation

Most starch microemulsions are prepared as a reversed-phase (inverse-phase) microemulsion system or W/O microemulsions. First, the starch is treated so that it disperses homogeneously in the water to produce an aqueous starch solution. Second, the oil phase is prepared with an organic solvent, such as soybean oil, methylbenzene, or chloroform, and the surfactant, such as Span 60 (Sinopharm Chemical Reagent Co., Ltd., China), is added and mixed with mechanical stirring until the surfactant is completely dissolved. The low-concentration starch solution is gradually dropped into the oil phase with stirring to generate a homogeneous stable W/O starch microemulsion. The starch molecules are restricted to the aqueous microdroplets and dispersed in the oil phase, which is conducive to the later formation of

small starch nanoparticles. A cross-linking agent is then added dropwise to the microemulsion with fast mechanical stirring, and the cross-linking reaction occurs in the microdroplets. Because the cross-linking reaction is restricted to microdroplets ranging in size from 10 to 100 nm, the interactant exchange between different microdroplets is hindered, and the size of the final cross-linked starch particles can be limited to the nanometer level. Nanoparticles and particles have diameters of 1–100 nm, and microemulsions have micellar droplets with diameters of 5–140 nm [16].

In the starch microemulsion system, the starch is dissolved in the aqueous-phase microdroplets. The amount of surfactant required is greater than the critical micelle concentration, resulting in the formation of greater amounts of reverse-phase micelle in the nanometer size range. Before cross-linking, the microemulsion consists only of swelling micelles in which all the starch monomers are distributed. During the polymerization reaction, a large quantity of micelles is present in the microemulsion system. Until the end of the polymerization reaction, only a small fraction of surfactant molecules is distributed at the interface of the polymers, and most surfactant molecules are present as micelles. Even at a high conversion ratio, new polymer particles will be present, showing continuous particle nucleation. Particle nucleation continues until all the monomers are absorbed by the polymer particles.

5.2.2 Common Steps in the Preparation of Starch Microemulsions

Starch microemulsion is prepared by adding the starch solution dropwise into the oil phase with mechanical stirring. When researchers prepare starch microemulsions to generate starch microspheres or nanoparticles [17–19], the main steps used [18] are the preparation of the starch solution, the preparation of the oil phase, emulsification, the cross-linking reaction, and posttreatment.

5.2.3 Factors That Influence Starch Microemulsions

Because a reaction occurs between the starch aqueous phase and the oil phase and the microparticles grow in the fine inner water droplets, the microparticle size and size distribution are controlled by adjusting the formation parameters of W/O microemulsions. The formulation parameters, such as the type of reaction medium, the type of surfactant, the surfactant concentration, the oil/ethanol ratio, the loading time, and the initial concentration of the object to be loaded into the nanoparticles, affect the particle size and the loading efficiency of the object in the starch nanoparticles [17].

1. Starch

Raw starch granules are insoluble in cold water, with a particle size of about 1–100 μm, which varies according to the botanical source. To form an aqueous starch solution, an aqueous starch suspension (15%) is heated in a boiling water bath until transparent [20]. The starch solution can then be used to prepare a starch microemulsion.

A low concentration (1% w/w) of starch will result in a small particle size and a narrow size distribution of cross-linked starch nanoparticles, whereas a high concentration of starch will generate a wide size distribution of cross-linked starch microspheres with high granularity. A low concentration of starch (1% w/v) was used in the preparation of curcumin starch nanoparticles [17].

The complete swelling and dissolution of starch reduce the intertwisting of the starch chains and the possibility of multiple starch chains within one micelle, which will generate small cross-linked starch particles. Fewer large starch molecules distributed in the micelle will produce smaller cross-linked starch nanoparticles.

The addition of an electrolyte, such as sodium hydroxide (NaOH 2 mol/L), can facilitate the homogeneous distribution of the starch chains in aqueous solution because it breaks the hydrogen bond between the chains and disrupts the movement of water molecules among them. This will induce the formation of the microemulsion interface between the starch molecules and the surfactant, which is conducive to the preparation of small size nanoparticles. Sodium chloride (NaCl 2 mol/L) can also be used as the electrolyte in the preparation of starch solutions.

A precooled (−8 to −10 °C) aqueous solution containing 6% NaOH and 4% urea can be used to dissolve the starch to prepare small (30–100 nm) starch nanoparticles.

2. Oil phase

The oil phase is prepared by mixing the oil, the organic liquid, and a surfactant. Methylbenzene and chloroform have been used to prepare the oil phase of a polyoxometalate starch nanomaterial [20]. Four different reaction media, including ethanolic solution, cyclohexane/ethanol microemulsion solution, sunflower oil/ethanol microemulsion solution, and oleic acid/ethanol microemulsion solution, have been used to prepare curcumin starch nanoparticles. Higher curcumin-loading efficiencies of 78% and 48% were achieved with the oleic acid/ethanol microemulsion and the sunflower oil/ethanol microemulsion than with the other two reaction systems. The smallest mean particle size of curcumin in the loaded starch nanoparticles was achieved with the oleic acid/ethanol microemulsion [17].

Increasing the volumetric oil phase/water phase ratio can reduce the particle size of starch microspheres.

The effects of n-alkyl alcohols, alkanes, water content, and temperature on the properties of a microemulsion have been studied in dilution experiments. The main effect of n-alkyl alcohol molecules is to change the hydrophilicity of the amphiphilic mixture, and n-alkyl alcohols with longer chains achieve this more readily. Alkane molecules with short carbon chains are most appropriate for the formation of microemulsions [21].

3. Surfactant and cosurfactant

A low-hydrophilicity (hydrophilic–lipophilic balance [HLB], low HLB value) surfactant in a microemulsion will reduce the sensitivity of the electrolyte, so less electrolyte is required. A high level of electrolyte will cause a phase change in the microemulsion. Span-60 (HLB 4.7) instead of Tween 20 (HLB 16.7) has been used in the preparation of microemulsions, and Span-80 was used as the surfactant in the preparation of an oil phase [20, 22].

4. Emulsification

The volume of the oil phase is greater than that of the aqueous phase, and the volumetric ratio of the oil phase to the aqueous phase generally ranges from 15/1 to 20/1 [23].

The aqueous starch phase is added dropwise to the oil phase with mechanical stirring until the microemulsion forms, and microemulsions containing smaller starch nanoparticles are also sonicated [20].

In a starch emulsion that was prepared with cyclohexane as the oil phase, amylose as the aqueous phase, and Span-60 or Tween 60 as the emulsifier, the influence of various factors on the conformation of the starch emulsion was investigated with dissipative particle dynamic (DPD) simulations. The size of the microparticles first decreased and then increased as the content of either emulsifier increased, increased as the starch content increased, and increased as the cyclohexane content decreased. The parameters of the stable starch emulsion system included an oil-to-water ratio of 7–20 and an emulsifier content of 9–18%. When the emulsifier content ranged from 11% to 15%, the size of the microspheres decreased as the emulsifier content increased. The size of the microspheres increased when the content of emulsifier exceeded 15%.

5. Cross-linking reaction

Chloromethoxy propane (0.3 mL/g starch) has been used as the cross-linker in the preparation of starch nanoparticles. Other cross-linkers, such as phosphorus oxychloride ($POCl_3$, 0.05%), have been used for dialdehyde starch nanoparticles [23] and polyoxometalate starch nanomaterials [20]. The cross-linking agent was added to the microemulsion and stirred for 1 h or more [20], and the stirring speed significantly affected the particle size of the prepared starch microspheres.

5.2.4 Methods for the Preparation of Starch Microemulsions

There are several approaches to the preparation of starch microemulsions, including the solvent evaporation, precipitation, and emulsion cross-linking techniques [24–26].

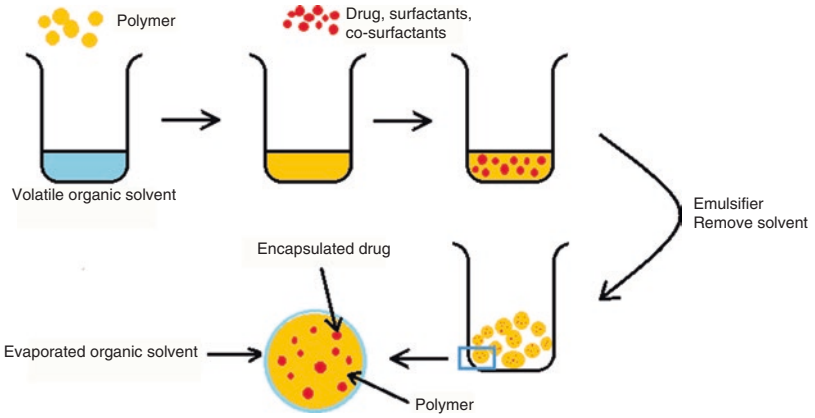

Fig. 5.1 Microemulsion formation by solvent evaporation. The drug-containing polymer droplets are dispersed within the continuous aqueous phase, forming a solvent–polymer emulsion. The emulsion hardens as the organic solvent evaporates

5.2.4.1 Solvent Evaporation

The solvent evaporation method is one of the earliest and most commonly used microemulsion preparation methods [27–29]. Typically, a polymer is dissolved in a volatile organic solvent, such as methylene chloride [30, 31], and this mixture is emulsified in an aqueous solution containing an emulsifying agent, such as poly(vinyl alcohol) (PVA). The resulting emulsion is stirred for hours until most of the organic solvent is removed. The hardened microemulsion is collected by filtration and washed with water and then either vacuum-dried or freeze-dried. Figure 5.1 is a schematic depiction of the generation of a microemulsion by solvent evaporation. To facilitate solvent evaporation, the system is often maintained under vacuum during the solidification process.

5.2.4.2 Coacervation

Coacervation, also known as phase separation, is a process in which a polymer solution is separated into two immiscible liquid phases: a dense coacervate phase concentrated in the polymer and a dilute polymer phase. These two phases are in equilibrium [32]. When only one polymer is present in the system, this phenomenon is called "simple coacervation" [33, 34], but when more than one polymer is present, it is referred to as "complex coacervation." Simple coacervation can be initiated by a change in temperature or ionic strength or by the addition of a nonsolvent [34–36]. All these changes promote polymer–polymer interactions over polymer–solvent interactions, resulting in the dehydration of the polymer. In complex coacervation, the electrostatic interactions between the two or more polymers are the driving force of this phenomenon [37].

Although coacervation has been successfully used to prepare many microemulsions, a number of drawbacks are associated with this method. Phase separation can only occur at specific pHs. Furthermore, heat or chemical cross-linking agents are required to stabilize the coacervate droplets, which may be harmful to the entrapped drugs. The retention of the encapsulants relies on the extent of cross-linking, which may cause batch-to-batch variance. Burgess and Singh developed a stable coacervate system requiring no chemical cross-linker or the application of heat. This system is potentially useful for the delivery of sensitive drugs, such as proteins and peptides [37].

5.2.4.3 Emulsion Cross-Linking Technique

The W/O emulsion technique is most commonly used and is based on water (dispersed phase), oil (continuous phase), and a surfactant. The surfactant reduces the interfacial tension between the water and oil phases, which makes the system a very stable microemulsion, in which the water phase is surrounded by the oil phase as W/O droplets. The size of starch microemulsion can be controlled in this minireactor by adjusting the relevant parameters. However, most starch microemulsions synthesized with the conventional W/O emulsion cross-linking technique have large particles (micrometer level) [38, 39] and therefore have limited applications as microemulsions in drug-loaded systems and other contexts. A further concern is that the conventional W/O emulsion cross-linking method involves large amounts of organic solvents, which can seriously damage the environment. Therefore, novel strategies to synthesize starch nanoparticles have drawn increasing attention in recent years.

5.2.4.4 Solvent Extraction

The solvent extraction method is very similar to the solvent evaporation method, differing only in the properties of the solvents used [27]. The solvent extraction method does not require solvents with high vapor pressures. Nonvolatile solvents can be removed by increasing the difference in the solvent concentrations in the dispersed and continuous phases or by adding a third solvent to the continuous phase to facilitate polymer precipitation.

5.2.4.5 Ionic Gelation

Ionic gelation refers to the cross-linking of polyelectrolytes in the presence of multivalent counter ions. For instance, spraying a sodium alginate solution into a calcium chloride solution generates rigid gel particles. The complexation of oppositely charged polyelectrolytes is often used after ionic gelation to form a membrane on the surface of the gelled particles to enhance their mechanical strength. In calcium

alginate gelling, polylysine is usually used for this purpose. This method was first developed by Lim and Sun for the encapsulation of live cells [40], and it has since been widely applied to drugs and other bioactive agents. Various polymer systems, such as chitosan/alginate chitosan/triphosphate, pectin/calcium, and polyphosphazene/polylysine, have been utilized.

5.2.4.6 Interfacial Polymerization

Microemulsions can be formed by interfacial polymerization [41]. This involves dispersing a monomer solution into a nonsolvent, for example, dispersing an oil solution of organic monomers into an aqueous medium or dispersing an aqueous solution of water-soluble monomers into an organic medium. Polymerization occurs at the interface of the two immiscible liquids. Many methods, including emulsion, suspension dispersion, and sedimentation, can be used in this process. Different techniques produce different final products, with particle sizes ranging from 0.01 to 500 mm.

5.2.4.7 Supercritical-Assisted Atomization

Supercritical-assisted atomization (SAA) is an alternative to the conventional jet-milling process. During the process, supercritical CO_2 is dissolved in a liquid drug-loaded solution. The mixture is sprayed through a nozzle [42], and the microemulsion forms as a result of atomization. Figure 5.2 shows a schematic representation of the SAA apparatus. SAA is more suitable for thermolabile compounds than conventional jet-milling or spray-drying technologies because the operation temperature is very close to room temperature. SAA also allows better control of the particle size.

5.2.4.8 Starch Nanoparticle Preparation in an Ionic Liquid-in-Oil (IL/O) Microemulsion System

Another new method of preparing starch nanoparticles is in an IL/O microemulsion system. Dried cornstarch (0.5 g) was added to 1-octyl-3-methylimidazolium acetate ([Omim]Ac, 9.5 g) in a three-neck round flask, mixed, and heated in an oil bath at 135 °C for 2.5 h. The [Omim]Ac starch (10 g) and cyclohexane (68.6 g) were then added to a small beaker. After thermal equilibrium (25 °C) was reached, the solution was titrated with a mixture of the surfactant Triton X-100 (TX-100; 35.1 g) and 1-butanol (mass ratio 3:1), until the stratified and hazy liquid solution became transparent, forming an IL/O microemulsion system. The cross-linker epichlorohydrin was added to the IL/O microemulsion and stirred at a speed of 1200 rpm at 50 °C for 3 h. The starch nanoparticles were then precipitated with anhydrous ethanol, centrifuged, and washed. The prepared starch nanoparticles were spherical granules with smooth surfaces, and the size distribution of the nanoparticles was relatively concentrated, with a mean diameter of 96.9 nm [43].

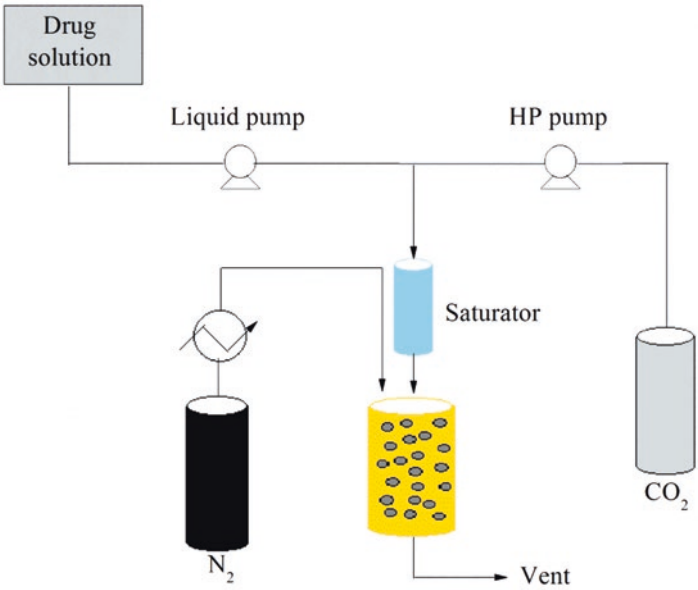

Fig. 5.2 Schematic representation of the SAA apparatus

5.2.4.9 Starch Nanoparticles Prepared in a Water-in-Ionic Liquid (W/IL) Microemulsion System

The preparation of starch microspheres in a W/O microemulsion using a cross-linking technique requires toxic organic reagents, which influence the quality and size of the starch microspheres produced and cause pollution. Therefore, starch nanoparticles were prepared in a W/IL starch microemulsion. Acid-treated granular starch (0.5 g) was dissolved in 9.5 g of NaOH solution ($NaOH:H_2O$ = 1:50, w/w) to form the water phase. The starch solution was then poured into 1-butyl-3-methylimidazolium hexafluorophosphate ($[Bmim]PF_6$, 40 g, as the oil phase) to form the W/IL microemulsion, with the addition of 40 g of a mixture of the surfactant TX-100 and cosurfactant 1-butanol (TX-100:1-butanol = 3:1, w/w). After magnetic stirring for several minutes, the cross-linker epichlorohydrin (1.84 g) was added to the microemulsion with stirring at 1200 rpm for 4 h at 50 °C. The reaction solution was then cooled to room temperature, and the starch nanoparticles were precipitated with methanol with vigorous stirring, followed by centrifugation. The precipitate was washed with methanol and ethanol, centrifuged, and vacuum-dried at 45 °C for 24 h.

The phase behavior of the water/TX-100 + 1-butanol/$[Bmim]PF_6$ system is considered to be similar to that of traditional W/O microemulsions. The size distribution of the microemulsion particles increased from 12.99 to 27.13 nm, measured with dynamic light scattering (DLS), with the mass ratio of $[Bmim]PF_6$ to water ranging from 4:1 to 20:1. The size distribution of the starch nanoparticles was relatively concentrated, with a mean diameter of 91.4 nm [19].

In another similar method, a 1-hexadecyl-3-methylimidazolium bromide (C_{16}mimBr)/butan-1-ol/cyclohexane/water ionic liquid microemulsion was prepared. The effects of the n-alkyl alcohols, alkanes, water content, and temperature on the properties of microemulsion were studied in a dilution experiment. Starch nanoparticles were prepared with the microemulsion cross-linking method, using C_{16}mimBr as the surfactant. The prepared starch nanoparticles had a mean diameter of 94.3 nm and a narrow size distribution [21].

Two ionic liquids, 1-hexadecyl-3-methylimidazolium bromide ([C_{16}mim]Br) and 1-octyl-3-methylimidazolium acetate ([C_8mim]Ac), were simultaneously used as substitutes for the surfactant and the polar phase, respectively, in the preparation of an ionic liquid starch microemulsion, which was used to prepare starch nanoparticles with a mean diameter of 80.5 nm [44].

5.3 Starch Microemulsion Properties

5.3.1 Characterization Methods for Starch Microemulsions

5.3.1.1 Droplet Size and Size Distribution

The microsphere particle size plays a very important role in the drug-release profile and varies with different microsphere preparation methods. The smaller the particle, the higher the surface area exposed to the release medium. The erosion rates of water-insoluble polymers are also greater for smaller microspheres. The particle size distribution is more meaningful than the average particle size when comparing different microsphere preparation methods because microspheres with the same average particle size but different size distributions may have very different drug-release profiles.

Particle size can be measured with various methods, including optical microscopy, resistance and light-blocking methods, light scattering, laser diffraction analysis, scanning electron microscopy [45], and photon-correlation spectroscopy. For example, light-scattering methods are widely used to measure particles and require highly diluted emulsions when droplet sizes are measured. However, in most cases, the addition of water to a microemulsion causes phase separation, and an O/W emulsion is formed. To overcome this limitation, a model has been proposed to correct the scattering data for undiluted microemulsions. With this numerical approach, it is possible to estimate particle sizes in undiluted microemulsions.

As well as size determination, DLS is a good method for measuring the translational diffusion coefficients of starch microemulsion droplets (i.e., colloidal particles) and is useful in the investigation of concentrated dispersions. When a coherent beam of light (such as a laser) interacts with colloidal particles in Brownian motion, the intensity correlation function provides information on the translational diffusion

coefficient of the scattering particles and therefore the hydrodynamic radius, according to the Stokes–Einstein equation. The diffusion coefficient can be related to a parameter called the "correlation length" in a more general way than the diffusion coefficient, because it conveniently characterizes both discrete droplets and clusters, providing scope for estimating interparticle interactions. Therefore, the DLS method is potentially important in the analysis of the particle sizes and related physical characteristics of starch microemulsions.

5.3.1.2 Morphology

Freeze-fracture electron microscopy (FFEM) delivers images of starch microemulsion structures. The starch microemulsion is rapidly frozen and ruptured, and the fracture face is replicated. Depending on the composition, both droplet-like structures and bicontinuous structures can be identified in a simple three-component system [46].

5.3.1.3 Other Methods

In addition to the methods described above, several other methods are used to study starch microemulsions.

1. Small-angle X-ray scattering (SAXS)

   SAXS can be used to measure structures with sizes in the nanometer range and provides information on ordered systems, such as liquid crystalline phases. It has been used to measure the structures of starch microemulsions.

2. Small-angle neutron scattering (SANS)

   SANS uses elastic neutron scattering to investigate the structures of liquid systems in the range of 1–1000 nm. It is used to study the particle sizes, polydispersity, and fluctuations in starch microemulsions. It covers a larger range of wave vectors than SAXS and is therefore suited to the investigation of short- and long-range structures in liquid systems. The scattering data are fitted to models of the starch microemulsion structures [47].

3. Nuclear magnetic resonance (NMR)

   When characterizing starch microemulsions, NMR spectroscopy is used to measure the self-diffusion coefficients of surfactants, cosurfactants, oils, and water. The results give a clear indication of the structure of the starch microemulsion. O/W, W/O, and bicontinuous-type microemulsions can be distinguished by the self-diffusion coefficients of the oil- and water-phase molecules [48].

5.3.2 Characteristics of Starch Microemulsions

5.3.2.1 Stability

Many factors must be considered when producing microspheres with a desirable particle size or size distribution. These factors include, but are not limited to, the polymer type and concentration in the organic phase, the volume fraction of the dispersed phase, the identities and amounts of excipients, the rate of stirring during hardening, the temperature during preparation, the speed of homogenization, and the identity and amount of surfactant. Whether the droplets have approximately the same density and continuous phase must be evaluated to predict their stability. Emulsions that are initially homogeneous, without creaming or sedimentation on visual inspection, are thought to be stable. Microscopic images and droplet size distributions are also used to analyze stability.

1. Temperature and stability

Starch microemulsions are thermodynamically stable and form spontaneously (or with very low-energy input) under the right conditions [49]. However, thermodynamic stability comes at a price: starch microemulsions require a greater amount of surfactant than emulsions, which may increase their potential irritability.

Because colloidal dispersions are thermodynamically stable systems, their free energy is lower than the free energy of the separate phases (oil and water) [49, 50]. Therefore, in principle, starch microemulsions form spontaneously, without energy input. In practice, some energy input (in the form of gentle mixing, stirring, or heating) facilitates their formation because there are kinetic energy barriers that must be overcome or mass transport limitations that retard their formation [50].

2. Particle size and stability

The emulsifying ability of starch granules seems inversely proportional to their size. When the diameters of starch nanoparticles (SNPs) were 150–700 nm, the mean droplet size of an emulsion stabilized by the SNPs increased from 29.33 to 48.76 μm [51].

3. Ions and stability

Generally, as the salt concentration increases, there is a greater tendency for the particles of a microemulsion to aggregate because the stabilizing repulsive forces are weakened by the increase in the electrolyte concentration. However, NaCl concentrations of 0–90 mM had no obvious effect on the stability of a Pickering emulsion stabilized with cornstarch-based nanoparticles [51].

4. Oil concentration and stability

After an emulsion is prepared, the freshly established oil droplets probably undergo limited coalescence during the first hour, until the SNP coverage is sufficient to stabilize the droplets. A marked increase in the oil fractions of corn, tapioca, sweet potato, and waxy cornstarch nanoparticles was observed after 1 month in

storage [51]. When the oil fractions were 0.6 and 0.75, the internal oil phase accounted for a great proportion of the emulsified phase, which approached or even exceeded the critical oil fraction for closely packed emulsion systems, and thus easily underwent phase inversion; oiling off occurred after 1 day in storage. A progressive increase in the volume of the emulsified phase was observed after 3 h in storage when the oil fraction was increased from 0.25 to 0.5 [51].

5. Kinetic instability

The internal contents of starch microemulsion droplets are known to be exchanged between droplets, typically on a millisecond time scale [52, 53]. They diffuse and collide, and if the collisions are sufficiently violent, then the surfactant film may rupture, facilitating droplet exchange. Therefore, the droplets are kinetically unstable. However, if the emulsions are dispersed to sufficiently small droplets (<500 Å), the tendency to coalesce is counteracted by an energy barrier. The system will then remain dispersed and transparent for long periods (months).

5.3.2.2 Interfacial Tension

The drops of the dispersed phase are generally large (>0.1 μm), so they often take on a milky, rather than a translucent, appearance. Once the conditions are right, starch microemulsions will form spontaneously. In simple aqueous systems, the formation of starch microemulsions is dependent on the surfactant type and structure. If the surfactant is ionic and contains a single hydrocarbon chain (e.g., sodium dodecyl sulfate), microemulsions only form if a cosurfactant (e.g., a medium-sized aliphatic alcohol) and/or electrolyte (e.g., 0.2 M NaCl) is also present. With double-chain ionic surfactants (e.g., Aerosol-OT (Sinopharm Chemical Reagent Co., Ltd., China)) and some nonionic surfactants, a cosurfactant is unnecessary. This results from one of the most fundamental properties of microemulsions, the ultralow interfacial tension between the oil and water phases.

5.3.2.3 Percolation Phenomena

Starch microemulsions can display percolation phenomena at specific volumetric fractions of water [54]. According to the percolation theory, phase transformation from reverse structures (W/O) to normal-type systems (O/W) through the emergence of bicontinuous systems and other aggregates may occur as the aqueous content of the system increases [55, 56]. This is generally accompanied by an increase in the system's electrical conductivity, which has often been used as a method of characterizing the internal structure of emulsions. Below a critical water volumetric fraction (Φ_c), water droplets are embedded in a low-conductivity oil medium and isolated from each other. As the volumetric fraction of water reaches Φ_c (the percolation threshold), an increase in the interlinking of the aqueous droplets occurs, and other structures form [52, 53]. This is usually apparent as a sharp increase in

conductivity [55]. Transition to a water-continuous system then follows as the water fraction continues to increase.

5.3.2.4 Rheological Behavior

The flow behavior of starch microemulsions is an important factor for their technical applications. Processes such as pumping, spraying, or spreading each require a different flow behavior. One example is the use of gels for skin treatments. On the one hand, they must spread easily but, on the other hand, must not run off the skin. For this application, a microemulsion requires low viscosity at high shear rates and a significantly higher viscosity at low shear rates. The flow behavior can be optimized by varying the composition of the microemulsion.

5.4 Applications of Starch Microemulsions

The advantages of starch microemulsions, such as their thermodynamic stability, spontaneous formation, easy scale-up, large interfacial area, nanosized droplets, isotropy, and low viscosity, make them applicable to many fields of science and technology. Furthermore, the high solubilization capacities of microemulsions for both organic and inorganic compounds make them useful in extraction processes [57]. With these characteristics, starch microemulsions can be used to coat volatile or nonpolar compounds to increase their stability or solubility in food systems or during storage and processing [58]. Starch microemulsions have potential utility in a wide range of systems, including in pharmaceuticals, edible oil recovery, targeted delivery systems for bioactive compounds, and the protection of nutrients and nutraceuticals.

5.4.1 Drug Delivery

Starch microemulsions can be used as a type of controlled drug delivery system. Considerable research into starch microemulsions has been conducted in the past four decades: (1) to establish the basic principles of drug release from solid matrices, (2) to develop mathematical models of controlled drug release, (3) to synthesize new biocompatible polymers for the preparation of these controlled delivery systems, (4) to identify the parameters that affect the physical and chemical properties of microemulsions, and (5) to determine the release profiles of the incorporated drugs. Many excellent reviews have been published describing the progress that has been made and the challenges that remain in microemulsion technology [59].

Starch microemulsions have several specific advantages over other controlled drug delivery systems, including (1) that the rate of drug release and its duration can be tailored by altering the materials and fabrication techniques used [59]; (2) that starch microemulsion are more stable than other controlled drug delivery systems, such as liposomes; and (3) that patient compliance is greater because the dosing frequency is lower.

"Drug targeting" refers to the oriented delivery of drugs to diseased tissues by exploiting the pH sensitivity, thermal sensitivity, or magnetism of the drug carrier. The methods of targeted drug delivery can be divided into the passive delivery and active methods. The passive delivery of a drug mainly depends on changes in the hydrophilic/hydrophobic character of the carrier surface and the size of the carrier. Active delivery systems can also transfer drugs to the necessary pathological sites in the human body under the guidance of an external magnetic field or the specific affinity of coupled ligands. This method not only reduces the possible toxic side effects but also reduces the quantity of drug required. Magnetic drug microemulsions contain drugs, magnetic particles, and framework materials. Fe_3O_4 and γ-Fe_2O_3 are the main magnetic particles used in targeted drugs. Generally, the framework is made of a polymer, such as albumin, chitosan, starch, glucosan, polyethylene glycol, or PVA. These materials have high biocompatibility and biodegradation. Drugs that have already been prepared as magnetic microemulsions include hydrochloric doxorubicin, mitomycin C, actinomycin D, etc. Currently, many commercial magnetic microemulsions or nanoemulsions are used as carriers for target drugs. A magnetic nanoemulsion, with starch-coated particles of 100 nm diameter, was developed and produced by Chemicell GmbH (Berlin, Germany), and a similar material has been made by another German company, Nano-Technologies GBR. However, most studies of targeted drugs that use magnetic carriers are still in the research stage.

5.4.2 Metal Ion Adsorbents

Heavy metal contamination of natural waters is both an environmental hazard and a threat to human health, especially through the food chain. Therefore, it is very important to develop effective ways to remediate heavy metal contamination [60]. Starch, an agricultural biopolymer, is highly attractive for industrial use because it is renewable, biodegradable, and inexpensive. However, starch by itself cannot be used satisfactorily to chelate or adsorb heavy metal ions, because it has no inherent chelating or metal-interacting capacity. Therefore, several approaches have been developed to utilize starch as a metal scavenger. Many studies have shown that modified starch has potential utility in adsorbing heavy metal ions from aqueous solutions [61–63]. Among the various modified starches tested, starch microemulsions, with their microporous structures, are potentially very useful for wastewater treatment [64].

5.4.3 Topical Hemostasis

Starch microemulsions have been approved and used as topical hemostasis agents, absorbing excess fluid from the blood and concentrating endogenous coagulation factors to maintain hemostasis. Topical hemostatic agents are a heterogeneous group of products developed to complement traditional surgical techniques and to ensure hemostasis during surgery. They are applied to bleeding tissues and maintain hemostasis through different modes of action. They can be classified according to their working mechanisms as either passive or active agents or combinations of the two [65]. Starch microemulsions have been used for many years to induce temporary vascular occlusion during the coadministration of cytotoxic drugs in the treatment of malignancies. Since 2002, starch microemulsions have also been approved for intraoperative applications and used clinically as topical hemostatic agents.

5.4.4 Embolization Agents

The treatment of nonresectable primary and secondary liver tumors is still problematic. Liver metastasis is the most frequent cause of death in patients with colorectal carcinoma after curative resection. Chemoembolization combines two palliative approaches, arterial chemotherapy and local tumor ischemia, providing both local advantages and longer cytostatic retention. Starch microemulsions, such as absorbable gelatin powder and prolamine, have been used as embolizing agents.

5.5 Application of Starch Microemulsions to Foods

Foods are usually very complex systems, in which oil and water are the most common ingredients. Therefore, emulsions play very important roles in the formulation of foods, including beverages, sausages, sauces, ice creams, milk, salads, and so on. Commonly used food emulsifiers include egg yolks, whey protein, and soy protein, and starch-based emulsifiers are increasingly used, including starch octenyl succinic anhydride, so-called OSA starch. The macromolecular structure of OSA starch allows it to modify aqueous viscosity and to stabilize O/W emulsions. OSA starches are currently approved for use in food products in many countries, and the maximum permitted level of OSA is 3%, based on the dry starch weight (a degree of substitution [DS] <0.03). OSA starches are cheap and almost colorless and tasteless in solution [66]. Furthermore, unlike proteins, their use as emulsifiers is essentially independent of the pH and ionic strength of the medium [67].

As stated above, various kinds of foods contain emulsions, and many types of emulsions are suitable for different uses [68]. Some emulsions are end products in themselves. Products such as coffee creamers and cream liqueurs are relatively simple emulsions, which must only remain stable to creaming and coalescence during

their production and shelf life. In contrast, emulsions can be used as ingredients that contribute to the structures of more complex products. These include yoghurts and other gelled systems, which contain emulsion droplets that must interact with other food ingredients but cannot be destabilized in the process. The droplets of an emulsion may also create new structures, such as in ice creams or whipped products, where the emulsion itself is required to destabilize the matrix to create the structure of the product. It is clear that the required compositions and properties of emulsion droplets differ in these three different cases. However, except in the simplest products, the emulsion droplets must interact with themselves or with the other food components to generate the required structures and thus the desired textures. The application of OSA-starch-stabilized emulsions to foods is discussed in detail below.

5.5.1 Improving the Quality of Beverage Products

Beverage emulsions are O/W emulsions and can generally be categorized as either cloud emulsions (imparting opacity) or flavor emulsions (providing flavor in addition to cloudiness). A finished beverage typically consists of a small percentage of beverage emulsion dispersed in water, together with a number of other ingredients, including caloric and/or high-intensity sweeteners, acidulants (to add taste and lower the pH), dyes (for color), and preservatives (to prevent microbial spoilage) [69]. Phase separation of the emulsions in beverage products can definitely influence the flavor and color profiles and limit the shelf lives of these products. Strategies to increase the stability of beverage emulsions generally involve homogenization and emulsifiers. Because the macromolecular structures of OSA starches can improve aqueous viscosity and stabilize O/W emulsions, emulsions stabilized with OSA starches are commonly used in beverage products to maintain the appearance, flavor, and color of the products. Other components also significantly affect the stability of beverage emulsions stabilized with OSA starch. For example, maltose increased the viscosity of an orange beverage emulsion formed with OSA starch and enhanced the elastic structure of the emulsion through its interaction with the OSA starch and water [70]. Increasing the viscoelasticity of this emulsion system retarded the free motion of the oil droplets and strengthened the mutual interaction forces between the droplets, thus delaying creaming, flocculation, and the coalescence of the oil droplets. Reiner et al. (2010) reported that all gum acacia and modified gum acacia emulsifiers were superior in stability to those based on OSA starches, at all temperatures, in orange-terpene-based beverages. However, the commercial use of gum acacia as a stabilizer in beverage emulsions is associated with many issues, including quality, availability, and cost [69].

Oil-containing solid beverages are usually prepared with spray-drying O/W emulsions, in a process also called “microencapsulation,” with emulsifying agents that are often called “wall materials.” The emulsions form again when reconstituted in water. These solid beverages are usually quite stable, which allows the retention of nutraceuticals and aromas. For example, passionfruit juice was encapsulated with

OSA starch using a spray dryer and stored at two different temperatures [71]. The samples stored at 7 °C and 25 °C retained 77.1% and 71.5% of their vitamin C, respectively, after 77 days in storage. OSA starch is an interesting material with which to encapsulate passionfruit juice, and spray drying was an inexpensive alternative to freeze drying, allowing the retention of vitamin C during a long storage period. The passionfruit juice was also easily diluted to reconstitute it for human consumption. Lee et al. (2017) evaluated the effects of sucrose monopalmitate, OSA starch, and Tween 80 on the retention and release of coffee aroma from O/W emulsion matrices (coffee oil was the flavor matrix) and when instant coffee was spiked to enrich its aroma [72]. Controlled aroma release was achieved with coffee emulsions stabilized with sucrose monopalmitate and OSA starch, and these also enriched the aroma of the spiked instant coffee.

5.5.2 Protecting Oil from Oxidation

The essential fatty acids α-linolenic acid and linoleic acid have many health benefits for humans. α-Linolenic acid can be converted into eicosapentaenoic acid (EPA) and docosahexaenoic acid (DHA) during its metabolism. However, the oxidation products of polyunsaturated fatty acids not only reduce the nutritional quality and sensorial properties of a food but may also have health implications. Therefore, the utilization of oils that are rich in essential fatty acids is limited by their strong susceptibility to oxidation. OSA-starch-stabilized O/W emulsions cause the oil to be entrapped by water, protecting it from the ambient environment, including the effects of air, oxygen, light, heat, and other components. For instance, flax seed oil is rich in α-linolenic acid, but its use as a functional ingredient in O/W systems is limited by its vulnerability to oxidation. To overcome this, emulsions were formulated with eugenol, a natural antioxidant, and two OSA starches (Purity Gum Ultra and Purity Gum 2000) (National starch, USA) [73]. Emulsions containing eugenol and stabilized with Purity Gum Ultra showed better physical and oxidative stability during storage than emulsions stabilized with Purity Gum 2000. More α-linolenic acid (66.34%) and eugenol (63.20%) were retained in the Purity Gum Ultra-stabilized emulsions stored for 4 weeks at 40 °C than in the Purity Gum 2000-stabilized emulsions. This was attributed to the antioxidative function of eugenol and the formation of a thick protective layer at the oil–water interface by Purity Gum Ultra, because its molecular weight and density are higher than those of Purity Gum 2000.

Microencapsulation by OSA starch in a spray-dried OSA-starch-stabilized O/W emulsion has also been used to protect oil. Drusch and Schwarz (2006) evaluated the suitability of two different types of OSA starch, which differed significantly in their viscosity but had the same DS, for the microencapsulation of a fish oil rich in long-chain polyunsaturated fatty acids. They found that stable feed emulsions for microencapsulation could be prepared with both types of OSA starch. However, at a high oil load (50%), the emulsion crucially required a low pH (pH 4.5) to maintain

its stability. At 50% oil content, a smaller oil droplet size in the reconstituted spray-dried emulsion and a lower content of unencapsulated oil were produced with low-viscosity starch than with medium-viscosity starch. As well as OSA starches, syrups, maltodextrin, and plant proteins are often used as wall materials. For example, fish oil with 33% long-chain polyunsaturated fatty acids was microencapsulated in a matrix of OSA starch and glucose syrup and stored at different temperatures (5, 20 or 40 °C) and relative humidities (11%, 33%, 48–59%, or 75%) [74]. The changes in the lipid oxidation parameters during storage depended to a certain extent on the temperature but to a much greater extent on the relative humidity. Temperature had no significant effect on the changes in the lipid oxidation parameters when the samples were stored at 11% or 33% relative humidity. An increase in the hydroperoxide concentration with increasing storage temperature was observed at 48–59% relative humidity. In all the samples, the changes in the lipid oxidation parameters were not linear or exponential and differed significantly from those described in the literature for bulk oils and emulsions. The use of silica derivatives and tricalcium phosphate also efficiently improved the flow properties of the microencapsulated fish oil without affecting the oxidative stability of the product. Serfert et al. (2009) investigated the effects of the emulsifying carrier matrix constituents, OSA starch, and the processing conditions, including the drying medium, on the physical characteristics and oxidative stability of fish oil microencapsulated within OSA starch [75]. The particle characteristics and lipid oxidation of the microencapsulated fish oil were both influenced by the type of OSA starch and the drying conditions used. The highest oxidative stability was observed for fish oil microencapsulated in an OSA starch with the lowest average molecular weight and glucose syrup and spray-dried at a moderate temperature. The particle characteristics of the microcapsules were not responsible for the differences in lipid oxidation during storage. The size of the spray-dried carrier matrix particles increased as the average molecular weight of the OSA starch increased, and this increase was considered to increase the air inclusion. Therefore, differences in the lipid oxidation of the microencapsulated fish oil were attributed to the differences in air inclusion, which were attributed to the type of OSA starch used. When spray drying was performed under inert conditions in the presence of air, the lipid oxidation of the microencapsulated fish oil was attributed to the oxygen available in the feed emulsion rather than to that in the drying gas. Maltodextrin improved the encapsulation efficiency of flaxseed oil by two kinds of OSA starch (Hi-Cap 100™ and Capsul TA® (Ingredion, China)) in a mass ratio of 25:75, although maltodextrin had a greater effect on Hi-Cap 100™ than on Capsul TA® [76].

5.5.3 Carriers for Bioactive Food Components

The incorporation of functional ingredients, such as vitamins, polyunsaturated fatty acids, carotenoids, and flavor compounds, into food systems provides a simple way to develop novel functional foods with desirable health benefits and organoleptic

properties. However, a large number of functional ingredients are water-insoluble and sensitive to heat, light, oxygen, etc., which limits their wide application in the food industry. O/W emulsions stabilized with OSA starches can act as carriers for these functional ingredients, because the ingredients can be incorporated into oil droplets where they are isolated from the external environment by the interface and the water phase. This improves their physicochemical stability, water-dispersing capacities, and bioaccessibility. Studies of various functional ingredients have provided evidence that emulsions are potential delivery systems in the design of novel functional foods [77]. β-Carotene, a common carotenoid, is a well-known active phytochemical with many health-promoting properties, including the greatest "provitamin A" activity known and strong antioxidant activity. However, its insolubility, low stability, and low oral bioaccessibility restrict its applications in foods. Therefore, the use of β-carotene as a natural colorant in food and nutraceutical products requires an appropriate formulation to protect it from degradation and overcome its low bioaccessibility, which results from its low solubility in aqueous media. To overcome those shortcomings, O/W emulsions stabilized with food-grade OSA starches have been used as carriers of β-carotene [78]. After 30 days in storage, the retention of β-carotene in O/W emulsions stabilized with food-grade OSA starches was significantly higher than that of β-carotene dispersed in bulk oil. After its digestion in vitro, the bioaccessibility of β-carotene increased from 3.1% to 35.6% with emulsification. Similar results were obtained for coenzyme Q_{10} [79]. OSA starch with rice bran oil used to entrap coenzyme Q_{10} within nanoscale particles, and the freeze-dried form maintained a constant absorbance at 281 nm over a period of 3 months. Over the study period, temperature (4 or 25 °C) had no effect on the stability of the coenzyme Q_{10} emulsion formed with OSA starch or on the coenzyme Q_{10}. When reconstituted in deionized water, the coenzyme Q_{10} emulsion formed with OSA starch was visibly stable at temperatures over 90 °C overnight and in a low-pH (3 or 7) environment over a period of 20 days. An OSA-starch-stabilized emulsion was also used as a carrier for vitamin E. When an emulsion containing 4% vitamin E was stored for 4 weeks at 25 ± 2 °C, there was a gradual increase in the size of the emulsion particles as the storage time increased, but the increase was quite small, and the emulsion showed no physical instability. Consequently, an emulsion containing 4% vitamin E stabilized with OSA starch can be used for the development of functional foods.

An O/W emulsion formed with OSA starch has also been used as a delivery system for natural antimicrobial compounds, to prolong their efficacy. Natural antimicrobials have strong antibacterial abilities and are also generally considered safe for inclusion in foods. Therefore, the use of antimicrobial compounds to prevent the contamination of fresh-cut produce by foodborne pathogens has received much attention. However, the use of these compounds is hindered by their rapid depletion in foods. These compounds include nisin, ε-poly-L-lysine, and thymol. Nisin, an antimicrobial peptide, exerts strong inhibitory activity against *Listeria monocytogenes*. However, various factors, such as the pH of the food system, the storage temperature, and the food components (enzymes, glutathione, sodium metabisulfite, and titanium dioxide), can readily deplete nisin activity. To prolong its efficacy,

Sarkar et al. (2016) evaluated the protective effects of OSA-starch-stabilized emulsions on nisin in a cantaloupe juice model [80]. Their results showed that the proteolytic enzyme in cantaloupe juice depleted nisin, whereas the adsorption of nisin within an emulsion considerably protected its antimicrobial activity. After nisin was incorporated with cantaloupe juice for 1, 3, or 6 days, the sizes of the *L. monocytogenes* inhibitory rings produced by the emulsion formulations in a bacterial growth inhibition assay were 7.64, 7.60, and 2.97 mm, respectively, whereas the rings decreased from 3.60 mm to a negligible level when the bacteria were treated with nisin alone. Sarkar et al. (2017) also used OSA-starch-based O/W emulsions to stabilize nisin and thymol in cantaloupe juice-containing fluid [81]. *Listeria monocytogenes* V7 and *Salmonella enterica* serovar *Typhimurium* were used as the model pathogens to evaluate the antimicrobial activities of the nisin and thymol formulations in cantaloupe juice. The emulsions retained much greater nisin and thymol activity during storage and inhibited *Listeria* and *Salmonella* much more strongly than the non-emulsion, aqueous formulations. The OSA-starch-based emulsions not only retained the individual nisin and thymol activities but also their cooperative antibacterial effects. Similar results were obtained for ε-poly-L-lysine, a model antimicrobial peptide [82]. An emulsion stabilized with OSA starch retained appreciable ε-poly-L-lysine activity. After 5 days in deep-well storage, both ε-poly-L-lysine alone and ε-poly-L-lysine stabilized with a Tween 20 emulsion partially inhibited bacterial growth (2 log CFU/mL *Escherichia coli*). However, after 5 days, the OSA-starch-emulsion-stabilized ε-poly-L-lysine fully inhibited the bacterial growth (no detectable *E. coli* colonies). This difference in antibacterial efficacy correlated with the retention of ε-poly-L-lysine in the system, with greater retention leading to higher efficacy.

These studies demonstrate that OSA starch emulsions are excellent carriers of bioactive components. OSA starch emulsions can also improve the stability and retention of bioactive components after storage. Therefore, the use of OSA starch emulsions as carriers can add nutritional value to common beverages and fruit juices and may also have utility in the development of functional foods. OSA emulsions can also prolong antimicrobial efficacy and improve the shelf lives of foods.

5.5.4 Fat Replacers

Fat plays a critical and direct role in the flavor, texture, and appearance of foods and increases the consumer's feeling of satiety during their ingestion. However, the clear relationship between dietary fat and the development of cardiovascular diseases, hypertension, and obesity has prompted consumers to be more aware of and concerned about the amount of fat in their diet. Therefore, low-fat foods have gained popularity in recent years with the increasing demand for low-calorie products [12]. However, as a major of food component, fat contributes to several of the sensory and physiological properties of these products. These properties are related to the flavor, mouth feel, texture, and stability of fat-based products, such as emulsions

(Table 5.1) [83]. The modification of these products by directly reducing their fat content clearly does not work, and a fat replacer is often viewed as an effective way to overcome these problems [84]. Emulsions formed with OSA starches are widely used as fat replacer in otherwise high-fat foods.

Muffins are often eaten as a breakfast food. One muffin formula included 100 g of wheat flour, 50 g of butter, 50 g of sugar, 50 g of egg, 50 g of milk, 3.33 g of baking powder, and 0.4 g of salt [85], which suggests that muffins contain high fat. OSA starches and maltodextrin were evaluated as partial fat substitutes in muffins by Chung et al. [85]. The muffins containing OSA starches had higher specific volumes and a softer texture than the muffin containing maltodextrin. Among the OSA starches tested, the starch prepared under acidic conditions produced muffins with a greater volume, which was attributed to the low molecular weight of the starch. The muffin that contained an emulsion stabilized with OSA starch (DS = 0.0057) had the softest texture and characteristics relatively close to those of the full-fat muffin.

Mayonnaise is a semisolid O/W emulsion, typically containing a high oil content (70–80%), egg yolk, vinegar, and additives. To produce a fat-reduced mayonnaise, it is necessary to reduce the dispersed phase and increase the water content. OSA starch was used as a fat replacer in 25%, 50%, and 75% fat-reduced mayonnaise (Table 5.1). The stability and rheological behavior of mayonnaises were examined and compared with those of full-fat mayonnaise. OSA starch was successfully used to replace 50% of the fat, reducing the fat content of the mayonnaise while retaining its rheological properties, stability, and especially its color during storage. Chivero et al. (2016) also successfully produced an O/W mayonnaise-like emulsion using OSA starch instead of egg yolk, and the emulsion displayed pseudoplastic behavior similar to that of typical mayonnaise [86]. However, its long-term stability remained a problem.

Shortenings, which contain high amounts of saturated fatty acids (SFA), are traditionally used in the production of cookies. To reduce the SFA content in cookies, Hadnađev et al. (2015) investigated the effects of incorporating structured oil (in the form of 50% and 70% O/W emulsions) and unstructured oil (50% and 70%) or traditional shortening (100% vegetable fat) in cookie formulations. They measured the rheological properties of the cookie dough, the textural properties of the cookies (break strength), and their spread, color, moisture, and sensory attributes [87]. Replacing vegetable fats with emulsions or unstructured oils reduced the elastic modulus of the dough and increased the cookie firmness. Cookies containing oil in the form of an emulsion showed higher dough strength and lower cookie spread than those containing an unstructured oil. However, although all the cookies were sensorily acceptable, those containing traditional shortening had superior sensory characteristics.

An OSA-starch-stabilized emulsion was also used to replace the fat in salad dressing [88]. Ninety percent replacement of soybean oil with debranched OSA starch produced dressings of similar quality to commercial dressing. When the egg yolk was reduced to half the amount in the reference formula, the texture remained unchanged. No phase separation was observed, although the color was slightly paler.

Table 5.1 Attributes associated with fat for several categories of food [20]

Baked goods	Dairy products	Salad dressings	Frozen desserts	Creamed soup, sauces, and gravies	Fried foods	Meats	Frosting and fillings
Flavor	Flavor	Flavor	Flavor	Mouthfeel	Flavor	Flavor	Viscosity/body
Viscosity/body	Creaminess	Viscosity/body	Viscosity/body	Opacity	Heat transfer	Mouthfeel	Mouthfeel
Richness	Saltiness	Yield stress	Creaminess	Flavor	Crispness	Juiciness	Creaminess
Texture	Acidity	Saltiness	Mouthfeel	Saltiness	Aroma	Tenderness	Aeration
Aeration	Viscosity/ body	Acidity	Melt	Satiety	Color	Texture	Spread
Shortness	Yield stress	Smoothness	Heat-shock stability			Bite	Emulsion
Tenderness	Smoothness	Smoothness	Overrun			Handling	Smoothness
Elasticity	Mouthfeel	Aeration	Opacity			Heat transfer	Melt
Flakiness	Melt	Mouthfeel				Satiety	
Leavening	Emulsion	Shear sensitivity					
Lubricity	Aeration	Color					
Dough handling	Color	Opacity					
Moisture retention	Sheen	Cold storage stability					
	Opacity						
	Satiety						

These studies suggest that OSA-starch-stabilized emulsions have potential utility as fat replacer, allowing the fat contents of foods to be reduced. However, fats play important roles in the quality of foods, and emulsion droplets interact with themselves or with other food components [83]. Therefore, considering the functions played by fat in foodstuffs, it is still challenging to develop commercial low-fat foods based on OSA-starch-stabilized emulsions.

References

1. Acosta E, Szekeres E, Sabatini DA, Harwell JH. Net-average curvature model for solubilization and supersolubilization in surfactant microemulsions. Langmuir. 2003;19(1):186–95.
2. Moulik SP, Digout LG, Aylward WM, Palepu R. Studies on the interfacial composition and thermodynamic properties of W/O microemulsions. Langmuir. 2000;16(7):3101–6.
3. Firman P, Kahlweit M. Quaternary liquid mixtures separating into four liquid phases. J Phys Chem. 1996;100(4):1216–9.
4. Acosta EJ, Nguyen T, Witthayapanyanon A, Harwell JH, Sabatini DA. Linker-based biocompatible microemulsions. Environ Sci Technol. 2005;39(5):1275–82.
5. Ethayaraja M, Bandyopadhyaya R. Population balance models and Monte Carlo simulation for nanoparticle formation in water-in-oil microemulsions: implications for CdS synthesis. J Am Chem Soc. 2006;128(51):17102–13.
6. Khomane RB, Manna A, Mandale AB, Kulkarni BD. Synthesis and characterization of dodecanethiol-capped cadmium sulfide nanoparticles in a Winsor II microemulsion of diethyl ether/AOT/water. Langmuir. 2002;18(21):8237–40.
7. Xing Y, Li M, Davis SA, Mann S. Synthesis and characterization of cerium phosphate nanowires in microemulsion reaction media. J Phys Chem B. 2006;110(3):1111–3.
8. Candau F, Zekhnini Z, Heatley F. Carbon-13 NMR study of the sequence distribution of poly(acrylamide-co-sodium acrylates) prepared in inverse microemulsions. Macromolecules. 1986;19(7):1895–902.
9. Edser C. Microemulsions: putting theory into practice. Focus on Surfactants. 2011;2011(11):1–2.
10. Vold RD. Microemulsions, theory and practice. J Colloid Interface Sci. 1978;65(3):595.
11. Che L, Li D, Wang L, Necati Ö, Chen X, Mao Z. Effect of high-pressure homogenization on the structure of cassava starch. Int J Food Prop. 2007;10(4):911–22.
12. Luo Z, Xu Z. Characteristics and application of enzyme-modified carboxymethyl starch in sausages. LWT Food Sci Technol. 2011;44(10):1993–8.
13. Jobling S. Improving starch for food and industrial applications. Curr Opin Plant Biol. 2004;7(2):210–8.
14. Lu X, Luo Z, Yu S, Fu X. Lipase-catalyzed synthesis of starch palmitate in mixed ionic liquids. J Agric Food Chem. 2012;60(36):9273–9.
15. Morgan JD, Lusvardi KM, Kaler EW. Kinetics and mechanism of microemulsion polymerization of hexyl methacrylate. Macromolecules. 1997;30(7):1897–905.
16. Messner M, Kurkov SV, Jansook P, Loftsson T. Self-assembled cyclodextrin aggregates and nanoparticles. Int J Pharm. 2010;387(1):199–208.
17. Chin SF, Mohd Yazid SNA, Pang SC. Preparation and characterization of starch nanoparticles for controlled release of curcumin. Int J Polym Sci. 2014;2014:1–8.
18. Xiao S, Tong C, Liu X, Yu D, Liu Q, Xue C, Tang D, Zhao L. Preparation of folate-conjugated starch nanoparticles and its application to tumor-targeted drug delivery vector. Chin Sci Bull. 2006;51(14):1693–7.

19. Zhou G, Luo Z, Fu X. Preparation of starch nanoparticles in a water-in-ionic liquid microemulsion system and their drug loading and releasing properties. J Agric Food Chem. 2014;62(32):8214–20.
20. Wang X, Liu J, Pope MT. New polyoxometalate/starch nanomaterial: synthesis, characterization and antitumoral activity. Dalton Trans. 2003. (5):957–60.
21. Wang X, Chen H, Luo Z, Fu X. Preparation of starch nanoparticles in water in oil microemulsion system and their drug delivery properties. Carbohydr Polym. 2016;138(Supplement C):192–200.
22. Zhai F, Li D, Zhang C, Wang X, Li R. Synthesis and characterization of polyoxometalates loaded starch nanocomplex and its antitumoral activity. Eur J Med Chem. 2008;43(9):1911–7.
23. Yu D, Xiao S, Tong C, Chen L, Liu X. Dialdehyde starch nanoparticles: preparation and application in drug carrier. Chin Sci Bull. 2007;52(21):2913–8.
24. Bezemer JM, Radersma R, Grijpma DW, Dijkstra PJ, van Blitterswijk CA, Feijen J. Microspheres for protein delivery prepared from amphiphilic multiblock copolymers: 2. Modulation of release rate. J Control Release. 2000;67(2):249–60.
25. Kawashita M, Tanaka M, Kokubo T, Inoue Y, Yao T, Hamada S, Shinjo T. Preparation of ferrimagnetic magnetite microspheres for in situ hyperthermic treatment of cancer. Biomaterials. 2005;26(15):2231–8.
26. Sturesson C, Carlfors J. Incorporation of protein in PLG-microspheres with retention of bioactivity. J Control Release. 2000;67(2):171–8.
27. Freitas S, Merkle HP, Gander B. Microencapsulation by solvent extraction/evaporation: reviewing the state of the art of microsphere preparation process technology. J Control Release. 2005;102(2):313–32.
28. Li M, Rouaud O, Poncelet D. Microencapsulation by solvent evaporation: state of the art for process engineering approaches. Int J Pharm. 2008;363(1):26–39.
29. Li W-I, Anderson KW, Deluca PP. Kinetic and thermodynamic modeling of the formation of polymeric microspheres using solvent extraction/evaporation method. J Control Release. 1995;37(3):187–98.
30. Rawat A, Burgess DJ. Effect of ethanol as a processing co-solvent on the PLGA microsphere characteristics. Int J Pharm. 2010;394(1):99–105.
31. Zolnik BS, Leary PE, Burgess DJ. Elevated temperature accelerated release testing of PLGA microspheres. J Control Release. 2006;112(3):293–300.
32. Lim LY, Wan LSC. Effect of magnesium stearate on chitosan microspheres prepared by an emulsification-coacervation technique. J Microencapsul. 1998;15(3):319–33.
33. Lazko J, Popineau Y, Legrand J. Soy glycinin microcapsules by simple coacervation method. Colloids Surf B: Biointerfaces. 2004;37(1):1–8.
34. Weiβ G, Knoch A, Laicher A, Stanislaus F, Daniels R. Simple coacervation of hydroxypropyl methylcellulose phthalate (HPMCP) II. Microencapsulation of ibuprofen. Int J Pharm. 1995;124(1):97–105.
35. Bachtsi AR, Kiparissides C. Synthesis and release studies of oil-containing poly(vinyl alcohol) microcapsules prepared by coacervation. J Control Release. 1996;38(1):49–58.
36. Nihant N, Grandfils C, Jérôme R, Teyssié P. Microencapsulation by coacervation of poly(lactide-co-glycolide) IV. Effect of the processing parameters on coacervation and encapsulation. J Control Release. 1995;35(2):117–25.
37. Singh ON, Burgess DJ. Characterization of albumin-alginic acid complex coacervation. J Pharm Pharmacol. 1989;41(10):670–3.
38. Franssen O, Hennink WE. A novel preparation method for polymeric microparticles without the use of organic solvents. Int J Pharm. 1998;168(1):1–7.
39. Mao S, Chen J, Wei Z, Liu H, Bi D. Intranasal administration of melatonin starch microspheres. Int J Pharm. 2004;272(1):37–43.
40. Lim F, Sun A. Microencapsulated islets as bioartificial endocrine pancreas. Science. 1980;210(4472):908–10.

41. Alexandridou S, Kiparissides C, Mange F, Foissy A. Surface characterization of oil-containing polyterephthalamide microcapsules prepared by interfacial polymerization. J Microencapsul. 2001;18(6):767–81.
42. Porta GD, Adami R, Gaudio PD, Prota L, Aquino R, Reverchon E. Albumin/gentamicin microspheres produced by supercritical assisted atomization: optimization of size, drug loading and release. J Pharm Sci. 2010;99(11):4720–9.
43. Zhou G, Luo Z, Fu X. Preparation and characterization of starch nanoparticles in ionic liquid-in-oil microemulsions system. Ind Crop Prod. 2014;52:105–10.
44. Wang X, Cheng J, Ji G, Peng X, Luo Z. Starch nanoparticles prepared in a two ionic liquid based microemulsion system and their drug loading and release properties. RSC Adv. 2016;6(6):4751–7.
45. Kiskan B, Dogan F, Durmaz YY, Yagci Y. Synthesis, characterization and thermally-activated curing of azobenzene-containing benzoxazines. Designed Monomers Polym. 2008;11(5):473–82.
46. Strey R. Microemulsion microstructure and interfacial curvature. Colloid Polym Sci. 1994;272(8):1005–19.
47. Shelton DP. Raman overtone intensities measured for H_2. J Chem Phys. 1990;93(3):1491–5.
48. Stilbs P, Rapacki K, Lindman B. Effect of alcohol cosurfactant length on microemulsion structure. J Colloid Interface Sci. 1983;95(2):583–5.
49. Lawrence MJ, Rees GD. Microemulsion-based media as novel drug delivery systems. Adv Drug Deliv Rev. 2012;64(Supplement):175–93.
50. McClements DJ. Nanoemulsions versus microemulsions: terminology, differences, and similarities. Soft Matter. 2012;8(6):1719–29.
51. Ge S, Xiong L, Li M, Liu J, Yang J, Chang R, Liang C, Sun Q. Characterizations of Pickering emulsions stabilized by starch nanoparticles: influence of starch variety and particle size. Food Chem. 2017;234:339–47.
52. Cabaleiro-Lago C, García-Río L, Hervella P. The effect of changing the microstructure of a microemulsion on chemical reactivity. Langmuir. 2007;23(19):9586–95.
53. Malheiro AR, Varanda LC, Perez J, Villullas HM. The aerosol OT + n-butanol + n-heptane + water system: phase behavior, structure characterization, and application to $Pt_{70}Fe_{30}$ nanoparticle synthesis. Langmuir. 2007;23(22):11015–20.
54. Kogan A, Garti N. Microemulsions as transdermal drug delivery vehicles. Adv Colloid Interf Sci. 2006;123–126:369–85.
55. Hathout RM, Woodman TJ, Mansour S, Mortada ND, Geneidi AS, Guy RH. Microemulsion formulations for the transdermal delivery of testosterone. Eur J Pharm Sci. 2010;40(3):188–96.
56. Kogan A, Aserin A, Garti N. Improved solubilization of carbamazepine and structural transitions in nonionic microemulsions upon aqueous phase dilution. J Colloid Interface Sci. 2007;315(2):637–47.
57. Walsh D. Microemulsions. Background, new concepts, applications, perspectives. Edited by Cosima Stubenrauch. Angew Chem Int Ed. 2009;48(25):4474.
58. Zhong F, Yu M, Luo C, Shoemaker CF, Li Y, Xia S, Ma J. Formation and characterisation of mint oil/S and CS/water microemulsions. Food Chem. 2009;115(2):539–44.
59. Jain R, Shah NH, Malick AW, Rhodes CT. Controlled drug delivery by biodegradable poly(ester) devices: different preparative approaches. Drug Dev Ind Pharm. 1998;24(8):703–27.
60. Chen Y, Li F. Kinetic study on removal of copper(II) using goethite and hematite nano-photocatalysts. J Colloid Interface Sci. 2010;347(2):277–81.
61. Kim BS, Lim ST. Removal of heavy metal ions from water by cross-linked carboxymethyl corn starch. Carbohydr Polym. 1999;39(3):217–23.
62. Kweon DK, Choi JK, Kim EK, Lim ST. Adsorption of divalent metal ions by succinylated and oxidized corn starches. Carbohydr Polym. 2001;46(2):171–7.
63. Xu S, Feng S, Yue F, Wang J. Adsorption of Cu(II) ions from an aqueous solution by cross-linked amphoteric starch. J Appl Polym Sci. 2004;92(2):728–32.

64. Fang Y, Wang L, Li D, Li B, Bhandari B, Chen XD, Mao Z-h. Preparation of crosslinked starch microspheres and their drug loading and releasing properties. Carbohydr Polym. 2008;74(3):379–84.
65. Samudrala S. Topical hemostatic agents in surgery: a surgeon's perspective. AORN J. 2008;88(3):S2–S11.
66. Tesch S, Gerhards C, Schubert H. Stabilization of emulsions by OSA starches. J Food Eng. 2002;54(2):167–74.
67. Charoen R, Jangchud A, Jangchud K, Harnsilawat T, Naivikul O, McClements DJ. Influence of biopolymer emulsifier type on formation and stability of rice bran oil-in-water emulsions: whey protein, gum arabic, and modified starch. J Food Sci. 2011;76(1):E165–72.
68. Dalgleish DG. Food emulsions-their structures and structure-forming properties. Food Hydrocoll. 2006;20(4):415–22.
69. Reiner SJ, Reineccius GA, Peppard TL. A comparison of the stability of beverage cloud emulsions formulated with different gum acacia- and starch-based emulsifiers. J Food Sci. 2010;75(5):E236–46.
70. Li C, Fu X, Luo F, Huang Q. Effects of maltose on stability and rheological properties of orange oil-in-water emulsion formed by OSA modified starch. Food Hydrocoll. 2013;32(1):79–86.
71. Borrmann D, Pierucci APTR, Leite SGF, Leão MHM d R. Microencapsulation of passion fruit (Passiflora) juice with n-octenylsuccinate-derivatised starch using spray-drying. Food Bioprod Process. 2013;91(1):23–7.
72. Lee LW, Liu X, Wong WSE, Liu SQ. Effects of sucrose monopalmitate (P90), Tween 80 and modified starch on coffee aroma retention and release in coffee oil-based emulsions. Food Hydrocoll. 2017;66:128–35.
73. Zhu F, Yan X, Liu S. Preparation and recognition characteristics of alanine surface molecularly imprinted polymers. Anal Methods. 2015;7(20):8740–9.
74. Drusch S, Serfert Y, Schwarz K. Microencapsulation of fish oil with n-octenylsuccinate-derivatised starch: flow properties and oxidative stability. Eur J Lipid Sci Technol. 2006;108(6):501–12.
75. Serfert Y, Drusch S, Schmidt-Hansberg B, Kind M, Schwarz K. Process engineering parameters and type of n-octenylsuccinate-derivatised starch affect oxidative stability of microencapsulated long chain polyunsaturated fatty acids. J Food Eng. 2009;95(3):386–92.
76. Deng H, Wei Z, Wang X. Enhanced adsorption of active brilliant red X-3B dye on chitosan molecularly imprinted polymer functionalized with Ti(IV) as Lewis acid. Carbohydr Polym. 2017;157:1190–7.
77. Mao L, Miao S. Structuring food emulsions to improve nutrient delivery during digestion. Food Eng Rev. 2015;7(4):439–51.
78. Liang R, Shoemaker CF, Yang X, Zhong F, Huang Q. Stability and bioaccessibility of β-carotene in nanoemulsions stabilized by modified starches. J Agric Food Chem. 2013;61(6):1249–57.
79. Cheuk SY, Shih FF, Champagne ET, Daigle KW, Patindol JA, Mattison CP, Boue SM. Nano-encapsulation of coenzyme Q_{10} using octenyl succinic anhydride modified starch. Food Chem. 2015;174:585–90.
80. Sarkar P, Bhunia AK, Yao Y. Emulsion stabilized with starch octenyl succinate prolongs nisin activity against *Listeria monocytogenes* in a cantaloupe juice model. J Food Sci. 2016;81(12):M2982–7.
81. Sarkar P, Bhunia AK, Yao Y. Impact of starch-based emulsions on the antibacterial efficacies of nisin and thymol in cantaloupe juice. Food Chem. 2017;217:155–62.
82. Bi L, Yang L, Bhunia AK, Yao Y. Emulsion stabilized with phytoglycogen octenyl succinate prolongs the antimicrobial efficacy of ε-poly-l-lysine against *Escherichia coli* O157:H7. LWT Food Sci Technol. 2016;70:245–51.
83. Lucca PA, Tepper BJ. Fat replacers and the functionality of fat in foods. Trends Food Sci Technol. 1994;5(1):12–9.
84. Thaiudom S, Khantarat K. Stability and rheological properties of fat-reduced mayonnaises by using sodium octenyl succinate starch as fat replacer. Procedia Food Sci. 2011;1:315–21.

85. Chung H, Lee S, Han J-A, Lim S-T. Physical properties of dry-heated octenyl succinylated waxy corn starches and its application in fat-reduced muffin. J Cereal Sci. 2010;52(3):496–501.
86. Chivero P, Gohtani S, Yoshii H, Nakamura A. Assessment of soy soluble polysaccharide, gum arabic and OSA-starch as emulsifiers for mayonnaise-like emulsions. LWT Food Sci Technol. 2016;69:59–66.
87. Dapčević Hadnađev T, Hadnađev M, Pojić M, Rakita S, Krstonošić V. Functionality of OSA starch stabilized emulsions as fat replacers in cookies. J Food Eng. 2015;167:133–8.
88. Klaochanpong N, Puncha-arnon S, Uttapap D, Puttanlek C, Rungsardthong V. Octenyl succinylation of granular and debranched waxy starches and their application in low-fat salad dressing. Food Hydrocoll. 2017;66:296–306.

Chapter 6
Nano-sized Starch: Preparations and Applications

Benxi Wei, Canxin Cai, and Yaoqi Tian

6.1 Introduction

Nano-sized starch is a type of organic starch nanoparticles (SNs) with a size of 50−200 nm that are prepared from starch through either physical or chemical methods. SNs are of great economic importance due to their abundance and functional performance, particularly their renewability, biocompatibility, low density, and high biodegradability [1]. Compared with inorganic nanoparticles, SNs also exhibit a modulus >100 GPa (i.e., high rigidity), a high specific surface area (usually several hundred square meters per gram) [2], a diverse morphology, and a high specific strength. Another advantage is the abundance of hydroxyl groups on their surface, equating to 0.0025 mol hydroxyl groups per g of freeze-dried starch nanocrystals (SNCs) [3] that contribute to the positive surface and associated chemical properties and make them ready for derivatization and incorporation of functional properties. Due to these advantages, SNs have great potential for applications in preparing nanocomposites, and this aspect has attracted much attention. Moreover, the novel properties of SNs also make them suitable for applications, serving as templates and smart materials, and use in biomedical devices, pollution decontamination, emulsions, biosensors, and biomarkers.

B. Wei
School of Food and Biological Engineering, Jiangsu University, Zhenjiang, China
e-mail: bxwei@ujs.edu.cn

C. Cai · Y. Tian (✉)
State Key Laboratory of Food Science and Technology, Jiangnan University, Wuxi, China
e-mail: 7160112001@vip.jiangnan.edu.cn; yqtian@jiangnan.edu.cn

Z. Jin (ed.), *Functional Starch and Applications in Food*,
https://doi.org/10.1007/978-981-13-1077-5_6

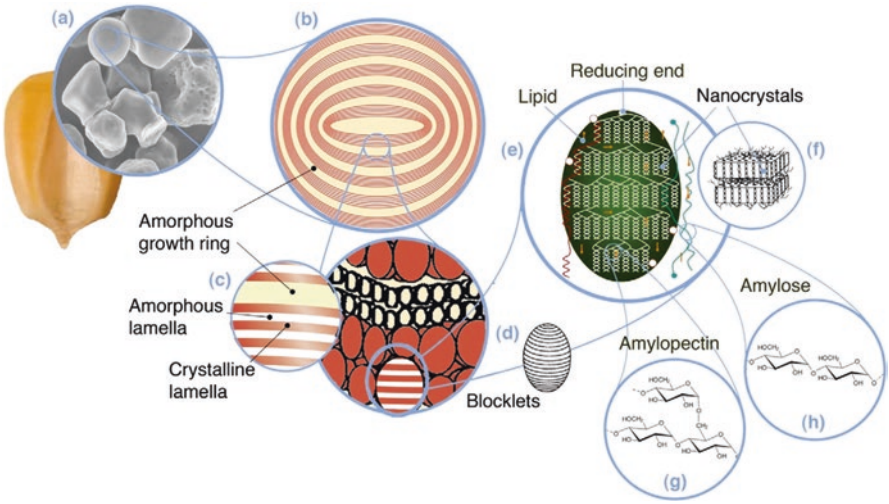

Fig. 6.1 Multiscale structures of starch. (**a**) Starch granules from normal maize (30 μm). (**b**) Amorphous and semicrystalline growth rings (120−500 nm). (**c**) Amorphous and crystalline lamellae (9 nm), magnified to show semicrystalline growth rings. (**d**) Blocklets (20−50 nm) constituting a unit within growth rings. (**e**) Amylopectin double helices forming the crystalline lamellae of the blocklets. (**f**) Starch nanocrystals (SNCs) formed when crystalline lamellae are separated by acid hydrolysis. (**g**) Molecular structure of amylopectin. (**h**) Molecular structure of amylose (0.1−1 nm) [8]. (Reproduced with permission from [8])

6.2 Classification of Nano-sized Starch

Nano-sized starch can be roughly divided into two categories based on its preparation methods and properties: SNs and SNCs. Strictly speaking, SNCs are a particular type of SNs. In this chapter, we emphasize the distinction between them in order to better understand nano-sized starch.

Over the last decade, SNCs have attracted growing interest due not only to their nanoscale size but also their renewable and biodegradable nature. SNCs are crystalline platelets resulting from the disruption of the semicrystalline structure of starch granules by hydrolysis of amorphous regions and vary in size from 5 to 7 nm thick, 20−40 nm in length, and 15−30 nm in width (Fig. 6.1) [4]. In comparison to native starches, the relative crystallinity (RC) of SNCs is increased by ~10% owing to the preferential hydrolysis of the amorphous regions [5, 6]. Thus, SNCs possess excellent ability for reinforcing nanocomposites. In general, the yield of SNCs (~15%) is below the theoretical crystallinity of starch (~40%) [7]. This is due to the fact that hydrolysis occurs simultaneously in both amorphous and crystalline regions. However, the side chains of amylopectin is arranged in an orderly fashion in crystalline parts, resulting in a much lower rate of hydrolysis than occurs in amorphous regions (Fig. 6.1).

SNCs have attracted much interest from the research community, but studies in this field are now slowly declining. By contrast, SNs are attracting increasing attention. SNs are usually prepared by the regeneration method as spherical or oval

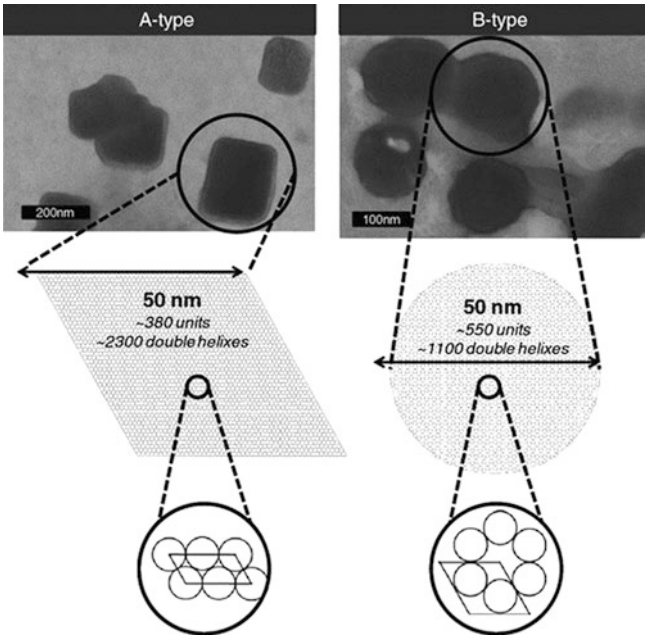

Fig. 6.2 Morphological differences of SNCs prepared from waxy maize starch (A-type) and high-amylose starch (B-type) [9]. (Reproduced with permission from [9])

structures with a diameter of 10−100 nm. The main differences between SNs and SNCs are the appearance and the preparation protocol. Regarding appearance, SNCs present a platelet shape with an angular (A-type) or rounded (B-type) edge depending on the crystalline type of the native starch (Fig. 6.2) [9]. Regarding the preparation protocol, SNCs are usually obtained by hydrolysis (acid or enzymolysis) of the amorphous regions of native starches, and any protocol that accelerates the hydrolysis process can shorten the preparation time. By contrast, SNs are often prepared through the recrystallization or cross-linking of starch molecules [8]. Thus, native starches must be gelatinized then subjected to other pretreatments (such as debranching) to facilitate the formation of SNs [10]. Due to the different preparation mechanisms of nano-sized starch, the yield of SNs is generally much higher than that of SNCs. As a result, more and more researchers are paying attention to SNs.

6.3 Preparation of Nano-sized Starch

Existing preparation approaches for nano-sized starch can be divided into top-down and bottom-up methodologies (Fig. 6.3). Top-down technologies are essentially disintegration methods involving physical or chemical treatments of native starch granules. By contrast, bottom-up approaches start from starch molecules, which are

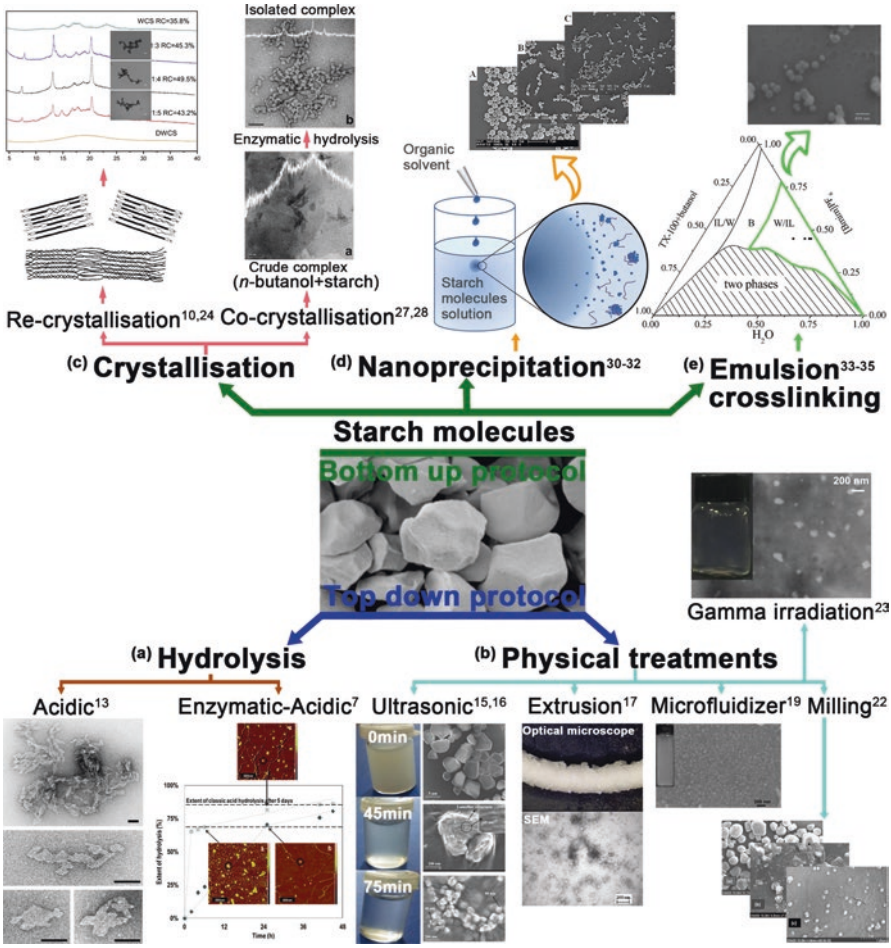

Fig. 6.3 Different methods of producing nano-sized starch: (**a**) Angellier et al. optimized the preparation parameters of SNCs (3.16 M H_2SO_4 hydrolysis at 40 °C for 5 days) and achieved a yield of 15.7% [13]. LeCorre et al. introduced an enzymatic pretreatment of starches before acid hydrolysis and found that only 45 h was needed to achieve the same yield as was achieved with the method of Angellier [7]; (**b**) Bel Haaj prepared SNs with a yield of ~100% via high-power ultrasonication (80% power, 8 °C, 75 min), but their crystallinity was lost [15]. Sun et al. proposed an ultrasonic-assisted oxidation method for the preparation of SNs with a size of 20−60 nm, but the crystallinity of resultant SNs was significantly decreased or lost, depending on the ultrasonic-oxidation treatment [16]. Starch mixtures (starch, water, glycerol) were extruded in a reactive extruder (55–110 °C), and SNs with a size of ~160 nm were obtained, but the crystallinity was significantly decreased [17]. A microfluidizer was employed to prepare SNs under a pressure of 207 MPa over 20 cycles, resulting in particles of 10−20 nm and a yield of ~100%, but the crystallinity was completely lost [19]. Patel et al. prepared SNs with a size of ~245 nm using stirred media milling over 90 min, but crystallinity was lost [22]. Gamma radiation at a dose of 20 kGy (14 kG/h) was employed to prepare SNs of 20−30 nm, but a decrease in crystallinity was detected [23]; (**c**) Sun et al. proposed a green preparation of SNs (60−120 nm) through enzymolysis and recrystallization in a process taking ~2 days, which produces SNs with a crystallinity of 55.4% and

dissolved and precipitated by adding solvent to a non-solvent or by using other chemical treatments. Basically, one can differentiate between top-down and bottom-up technologies as explained briefly below.

6.3.1 Top-Down Protocols

6.3.1.1 Hydrolysis

Top-down protocols can be classified into hydrolysis (Fig. 6.3a) and physical treatments (Fig. 6.3b). Regarding hydrolysis, acid hydrolysis and/or enzymatic hydrolysis can be employed. The preparation of SNCs through acid hydrolysis is the most common approach and can be dated back to the preparation of amylodextrin by Nägeli in 1874 [11]. A small amount of acid-resistant low-molecular-weight dextrin was obtained after hydrolysis of potato starch at room temperature for 30 days in a 15% H_2SO_4 suspension. Thereafter, in 1886, Lintner processed potato starch using a suspension of 7.5% (w/v) HCl at 30−40 °C to produce a high-molecular-weight starch suspension referred to as lintnerized starch [12]. The starch fraction remaining after acid hydrolysis comprises SNCs. In recent decades, numerous researchers have improved methods for the preparation of SNCs. For example, Angellier et al. optimized acid hydrolysis conditions using a response surface methodology and produced aqueous suspensions of SNCs after 5 days using 3.16 M H_2SO_4 hydrolysis at 40 °C and stirring at 100 rpm, achieving a yield of 15.7 wt% (starch concentration = 14.69 wt%) [13]. These hydrolysis conditions have been widely adopted by researchers due to easy handling and high repeatability. However, some obvious disadvantages are apparent, including the low SNC yield and the long duration of the acid hydrolysis process. In order to improve the acid hydrolysis protocol, LeCorre et al. developed an enzymatic pretreatment of starch to reduce the duration of acid hydrolysis [7]. Compared with the previous method for preparing SNCs, hydrolysis of pretreated starch was much faster, it takes only 6 h to reach the same hydrolysis effect compared with 24 h for the previous method, and the final yield of the regular method was reached after 45 h (15% after 5 days for acid hydrolysis). Application of enzymatic hydrolysis independent for preparing SNCs was reported

Fig. 6.3 (continued) a yield of 85% [10]. Kim et al. reported the preparation of nanocrystals by complex formation between amylose and n-butanol, and enzymatic hydrolysis yields crystalline particles (10−20 nm) with a yield of 10−15% [28]; (**d**) Particle size can be controlled by regulation of the polymer concentration in acetone, the proportions of water to organic phases, and the molecular weight and degree of substitution of the starch esters to produce starch-based nanospheres (121−490 nm) by nanoprecipitation [30]. Qin et al. further investigated the influence of amylose content and starch type on the formation of SNs by nanoprecipitation. A positive relationship between the relative crystallinity (RC) and the amylose content was detected, and the smaller the starch granules, the smaller the resulting SNs [31]; (**e**) Zhou et al. prepared SNs with a mean diameter of 96.9 nm and a narrow size distribution by cross-linking starch molecules in ionic liquid-in-oil microemulsion systems (cross-linked at 50 °C for 3 h) [34]. (Reproduced with permission from [7, 13, 15, 17, 19, 22, 23, 27, 30, 32, 35–38])

by Kim et al. [14], but it is believed to lead to the formation of blocklets rather than nanoparticles.

6.3.1.2 Physical Treatments

SNs and SNCs have been prepared using physical treatments such as ultrasound, extrusion, microfluidizer, milling, and gamma radiation (Fig. 6.3b). In comparison to other physical treatments, ultrasound is the most frequently adopted method for preparing SNs because it is environmentally friendly and allows easy processing. Belhaaj et al. found that ultrasound treatment of a starch suspension in water at low temperatures for 75 min resulted in the formation of starch nanoparticles between 30 and 100 nm in size [15]. However, a high ultrasonication energy resulted in serious disruption of the crystalline structure of clustered amylopectin, apparently leading to nanoparticles with low crystallinity or amorphous character. Sun et al. proposed an ultrasound-assisted oxidation method for the preparation of SNs, resulting in SNs of 30−50 nm, 20−50 nm, and 20−60 nm after a single oxidation followed by ultrasonic treatment, a double oxidation and two ultrasonic treatments, and TEMPO-mediated oxidation with ultrasonic treatment, respectively [16]. However, the RC of samples decreased from 36.32% (native starch) to 11.35%, 1.64%, and 1.72%, respectively.

By manipulating the shear force and extrusion temperature, SNs can also be prepared via reactive extrusion. Song et al. found that the addition of appropriate cross-linkers yielded SNs with an average size of ~160 nm, whereas the diffraction peaks diminish or even disappear after extrusion treatments [17].

Another physical treatment frequently used to prepare SNs involves the use of a microfluidizer, which is characterized by simultaneous high pressure, shear, turbulence, cavitation, and velocity gradients [18]. Liu et al. successfully transferred the method for producing microfibrillated cellulose to the production of SNs [19]. A 5% slurry of high-amylose cornstarch was passed through a microfluidizer several times (up to 30), and the obtained particle size after more than ten passes was below 100 nm, with an almost 100% yield. However, the resultant SN suspension was the result of the breakdown of both amorphous and crystalline domains, rendering an amorphous diffraction pattern after ten passes. It could be concluded that high-amylose cornstarches are partially gelatinized when passed through the interaction chambers. As the temperatures of liquid processing is increased by increasing the homogenizing pressure at a rate of ~0.2 °C/MPa [20], the final temperature of the starch slurry in the interaction chambers increases sufficiently to gelatinize the starches.

Stirred ball mill is an efficient process for the preparation of ultrafine materials due to its simple construction, ease of operation, high size reduction rate, and low wear contamination [21]. Patel et al. proposed a fast and scalable preparation method for SNs by stirred media milling [22] in which the particle size of native starch was reduced from 3 to 20 μm to around 245 nm within 90 min, although the crystallinity was significantly reduced. Stirred media milling can produce SNs

effectively without the use of any surfactants or additives; hence it is considered a green method for the preparation of various types of nanoparticles.

Gamma irradiation has also been employed for the preparation of SNs because it generates free radicals that hydrolyze glycosidic linkages, thereby producing smaller fragments of starch called dextrins [23]. Lamanna et al. obtained SNs with a size of 20 and 30 nm from cassava and waxy maize starches, respectively, using a dose of 20 kGy gamma radiation. The thermal degradation behavior and the maximum mass loss zone of SNs prepared using gamma irradiation are similar to those of nanoparticles obtained from acid hydrolysis [23]. Therefore, this physical treatment method is considered a low-cost, simple, and scalable way of preparing SNs.

It should be clarified that different preparation methods result in different final products (SNC or SNs) with different properties. Generally speaking, products prepared by hydrolysis exhibit the same or even higher RC in comparison with native starches and can be referred to as SNCs. Consequently, SNCs produced in this way possess excellent mechanical strength and are widely used as fillers to enhance the strength of nanocomposites. However, the yield is often low because amorphous and crystalline regions of starches are simultaneously hydrolyzed in the preparation process. By contrast, the final products prepared by physical treatments usually have lower RC values (as low as 0%) than native starches. Thus, products prepared by physical methods are referred to as SNs or nano-colloids and are produced in much higher yields (up to ~100%), facilitating their application to many other areas.

6.3.2 Bottom-Up Protocols

6.3.2.1 Crystallization

Bottom-up protocols for the preparation of nano-sized starch include crystallization (Fig. 6.3c), nanoprecipitation (Fig. 6.3d), and emulsion cross-linking (Fig. 6.3e). Crystallization results in SNs with an ordered arrangement of starch molecules or complex formation between starch molecules and other components, and methods can be roughly divided into recrystallization and co-crystallization.

In this chapter, recrystallization refers to amylose or the linear parts of amylopectin molecules of gelatinized starch systems rearranging hydrogen bridges to form a more crystalline structure (Fig. 6.3c). This can also be considered retrogradation of liner molecules of gelatinized starch. Sun et al. prepared SNs through a green method based on the combined enzymolysis and recrystallization of waxy maize starch [10]. After pullulanase treatment of gelatinized native starches, suspensions were air-dried or freeze-dried, resulting in a decrease in particle diameter from several μm (native starches) to ~60−120 nm, with a maximum degree of crystallinity of 55.41% and a yield up to 85%. Thereafter, the effect of the duration (0.5, 4, 12, and 24 h) of the retrogradation process on the formation of proso-millet SNs was studied by the same group [24]. The results showed that the size of SNs varied between 20 and 100 nm, and the crystal pattern changed from A-type (native starch)

to B-type, with an obvious increase in RC. A duration of 12 h produced SNs with the highest degree of crystallinity (47.04%). Furthermore, the effects of sodium dodecyl sulfate (SDS), polysorbate 80 (Tween 80), and sorbitan monooleate (Span 80) on the recrystallization of starch molecules were investigated [25]. It was found that surfactants significantly increased the dispersion and thermal stability of SNs. Short-chain amylose debranched from waxy cornstarch had a lower degree of polymerization than that debranched from potato starch and was easier to retrograde, resulting in SNs with a higher gelatinization enthalpy. However, SNs prepared from potato were smaller in size and achieved better stability than SNs from waxy cornstarch due to stronger electrostatic repulsion caused by a higher absolute zeta potential. It should be noted that SNs prepared by recrystallization usually exhibit serious aggregation behavior, which restricts their applications in different areas, since a homogenous dispersion of SNs is fundamental for capitalizing on the advantages of the nano-sized properties.

Unlike recrystallization, co-crystallization refers to the formation of complexes of starch molecules and guest compounds known as V crystals, and only single helices are presented. Depending on the guest compounds, different types of V-amylose complexes can be produced and are classified into V6 and V8 categories according to the structure of the helix [26]. Based on this theory, Kim prepared nano-sized starch particles by complex formation with n-butanol [27]. Firstly, crude complexes were formed as platelets with an average length less than 100 nm. Then, enzymatic hydrolysis was used to selectively retain crystalline particles, while amorphous matrices were removed by hydrolysis using α-amylase, resulting in starch crystallites of 10−20 nm with a V6I X-ray diffraction pattern. The same group subsequently studied the effect of chain length on the formation of nanocrystal complexes between dextrins and n-butanol [28]. The results revealed the formation of platelets with an average length of less than 100 nm, interspersed in amorphous matrices, in complexes of DP_n 311 and 142, but complexes of DP_n 39 showed a different morphology and were limited in number. After hydrolysis by α-amylase, crystallites in complexes of DP_n 142 and 39 were eroded, forming large aggregates. It can be concluded that only dextrins of a certain length can complex with *n*-butanol to form perfect crystals.

6.3.2.2 Nanoprecipitation

The process of nanoprecipitation as a procedure for the regeneration of nanoparticles was first described by Fessi et al. [29]. This process involves the addition of a dilute solution of polymer to a non-solvent, which leads to polymer precipitation at the nanoscale (Fig. 6.3d). The method is essentially based on the interfacial deposition of polymers following displacement of a semipolar solvent that is miscible with water from a lipophilic solution [30]. With nanoprecipitation, external energy sources or toxic solvents are not needed, and a narrow size distribution of submicron particle sizes can be obtained. Tan et al. demonstrated that the size of nanospheres obtained by nanoprecipitation can be easily controlled through regulation of

the polymer concentration in acetone, by manipulating the proportions of water and organic phases, and by altering the molecular weight and degree of substitution of the starch esters [30]. The concentration of starch acetate was positively correlated with the size of the resultant SNs. Moreover, a linear relationship between the polarity value of water-acetone mixtures and particle size was observed. Thereafter, Sun et al. studied the influence of amylose content, starch type, and short linear chains from debranched waxy cornstarch on the fabrication of SNs by nanoprecipitation [31, 32]. Their results demonstrated that the smaller the particle size of starch granules, the smaller the obtained SNs. All SN samples displayed a typical V-type crystalline structure. Moreover, a high positive correlation ($R^2 = 0.95$) between the amylose content and the RC of SNs was observed. Compared with the influence of amylose content, SNs prepared by nanoprecipitation of short linear chains generally have higher RC values (43.2−49.5%). Consequently, it can be concluded that recrystallization of liner starch molecules is simultaneously involved in the nanoprecipitation process.

6.3.2.3 Emulsion Cross-Linking

Emulsion cross-linking refers to the synthesis of SNs by cross-linking starch molecules in droplets of water/oil (w/o) or oil/water (o/w) emulsions or miniemulsion reaction systems, especially in water-in-ionic liquid microemulsion systems (Fig. 6.3e). This approach for the preparation of SNs is efficient and environmentally friendly. Shi et al. explored the effects of process parameters (surfactant content, w/o ratio, starch concentration, homogenization pressure, and number of cycles) on the preparation of SNs through high-pressure homogenization and miniemulsion cross-linking [33]. The final products displayed a narrow size distribution, good dispersibility, and a spherical shape. Thereafter, Zhou et al. prepared SNs by cross-linking starch molecules in ionic liquid-in-oil microemulsions and water-in-ionic liquid microemulsion systems, and the mean diameters of the resultant SNs were 96.9 nm and 91.4 nm [34, 35]. SNs prepared in ionic liquid-in-oil microemulsions display a narrow size distribution, whereas aggregation behavior was detected for SNs prepared in water-in-ionic liquid microemulsion systems, presumably due to strong van der Waals forces and electrostatic attractions among particles [35].

Generally speaking, SNCs and SNs prepared by hydrolysis and recrystallization methods exhibit much higher RC than SNs prepared by physical treatments, co-crystallization, and nanoprecipitation, making them more suitable for the preparation of nanocomposites. Ultrasonic and microfluidizer methods can reach SN yields up to 100%, and the yield of methods is roughly ordered crystallization >nanoprecipitation >hydrolysis. However, the duration of the preparation process is roughly ordered hydrolysis >recrystallization, co-crystallization >nanoprecipitation >physical treatments. Thus, the hydrolysis method has disadvantages such as long duration and low yield, but it is the most widely adopted by researchers due to its easy operability. However, attention is gradually transferring from top-down to bottom-up approaches, mainly due to advantages including high yield, short duration time, and

high conversion ratio of native starches. Recrystallization and nanoprecipitation show the greatest potential and are generally easy to control.

6.3.3 Multi-Treatment Protocol

In order to shorten the acid hydrolysis processing of starch, ultrasonic treatments can be employed to pretreat native starches. Kim et al. investigated the effects of ultrasonic treatments on nanoparticle preparation using acid hydrolysis of waxy maize starch. They found that the amount of SNs in the hydrolysates increased from 20% to 70% following ultrasonic treatment (20% amplitude, 30 min), and aggregation of the resultant nanoparticles was effectively prevented [39]. A method of cold acid hydrolysis and ultrasonication was later proposed by the same research group to prepare crystalline starch nanoparticles [40]. The final products obtained in the above two studies are reportedly a mixture of SNCs and SNs. These methods are yet to be widely practiced, possibly due to the complexity of the preparation procedures. Consequently, the sulfuric acid hydrolysis method for preparing SNCs remains dominant.

6.4 Improving the Functionality of Nano-sized Starch Particles

6.4.1 Surface Chemistry of SNs

Starch is the main energy store in plants, and it can be chemically fractionated into two types of glucan polymer: amylose and amylopectin. Glucose residues linked by either α(1–4) or α(1–6) glucosidic bonds form amylose and amylopectin, respectively. Consequently, starch granules possess a reactive surface covered with numerous hydroxyl groups, which provide the possibility for chemical modification. As the size of starch granules is decreased down to the nanometer scale, important changes occur; both the specific surface area and total surface energy increase. Thus, SNs display a highly reactive surface with a greater number of hydroxyl groups than native starches. Based on the Connolly surface methodology, Angellier et al. estimated the hydroxyl group content presented at the surface of SNCs to be ~14% of the total amount available (i.e., in 1 g of freeze-dried SNCs, 0.0025 mol of hydroxyl groups are reactive) [3]. Meanwhile, Siqueira assumed that a third of hydroxyl groups on the surface of cellulose nanocrystals are available for chemical modification [41], which corresponds to ~0.0038 mol g^{-1} [42]. The differences in the number of reactive surface hydroxyl groups between SNCs and cellulose nanowhiskers may result from their distinct morphologies. Platelet-like SNCs are ~5−7 nm thick, 20−40 nm long, and 15−30 nm wide [4], while cellulose nanowhiskers have a larger specific surface area (average length and diameter of 250 nm and

Table 6.1 Methods for improving the functionality of nano-sized starch

Functionality	Method	References
Aqueous dispersity	Oxidation, adjusting the pH of the dispersion, cross-linking by sodium hexametaphosphate	[5, 44, 45]
Hydrophobicity, dispersion in organic solvents, or compatibilities with matrix		
Chemical derivatization	Esterification, acetylation, silylation, cross-linking and esterification	[3, 6, 46–50]
Grafting onto	Poly(ethylene glycol) methyl ether (PEGME), poly(tetrahydrofuran) (PTHF), poly(ethylene glycol) monobutyl ether (PPGBE), poly(caprolactone) (PCL), poly(styrene) (PS), and isocynate	[48, 51–55]
Grafting from	Poly(caprolactone) (PCL)	[56, 57]
Enzyme-catalyzed modification	Regioselective esterification	[58]
Increase of crystallinity	Heat-moisture treatment	[59]

4 nm, respectively). However, it should be noted that not all surface hydroxyl groups are accessible, due to the fact that some are oriented toward the inside of SNCs.

All available hydroxyl groups of SNs are potentially active, can in principle be oxidized or reduced, and may participate in the formation of hydrogen bonds. By contrast, for each anhydroglucose unit in starch, the reactivity of the hydroxyl groups varies for different sites in the molecules. The hydroxyl group at the C6 position is reportedly ten times more reactive than the other OH groups, while the reactivity of the hydroxyl group in the C2 position was found to be twice that of the hydroxyl group at the C3 position [43]. The different methods used to improve the functionality of SNs are summarized in Table 6.1.

6.4.2 Improving the Dispersity of Nano-sized Starch in Aqueous Media

SNs are easily self-aggregated either in aqueous media or in organic media due to hydrogen bonding and van der Waals forces between particles and then settle in water to form agglomerates at the micrometer scale. This aggregation tendency greatly limits their applications, since a homogeneous dispersion of SNCs is required for the high mechanical performance of rubber and other materials [60]. Thus, for the processing of composite materials, SNCs are generally used in the form of aqueous suspensions, matrices, and latexes [3, 47]. However, SNCs in the form of aqueous suspensions also suffer from numerous disadvantages, such as high cost for transportation, easy proliferation of bacteria, and difficulty in determination the concentration [5]. These disadvantages are the same for SNs. Thus, preparation of SN powders that can be re-dispersed in aqueous or organic solvents to form a homogenous dispersion is of great importance for their applications.

The use of H_2SO_4 for the preparation of SNCs leads to more stable aqueous suspensions than those prepared using HCl [61]. It was deduced that the formation of sulfate-ester groups and the introduction of carboxyl groups on the surface of SNCs during H_2SO_4 hydrolysis limit flocculation and produce more stable suspensions. Thereafter, Wei et al. verified the above results by studying the surface chemical composition of SNCs prepared by H_2SO_4 and HCl hydrolysis [62], and Araki et al. also drew the same conclusion for cellulose nanocrystals [63].

The stability of SNC suspensions is, to a large extent, dependent on the surface charge distribution, and the mechanism can be interpreted by DLVO theory (named after Derjaguin, Landau, Verwey, and Overbeek). Electrostatic repulsive forces (expressed as zeta potential) among particles can be illustrated by electrical double layer theory. Briefly, the electrical double layer consists of a layer of electrons (if the nonelectrolytic phase is a metal or electronic conductor), a layer of adsorbed ions or ionizable groups on solid particles, and a diffuse double layer consisting of an ionic atmosphere, in which ions of one charge are in excess of their normal concentration, whereas those of the opposite charge are in deficit [64]. In general, the stability of a disperse system depends on the balance of electrostatic repulsive energy and the van der Waal's attraction energy [65]. Consequently, any strategy that can increase the electrostatic repulsive energy or decrease the van der Waal's attraction energy or hydrogen bonding will improve the dispersity of SNs.

Improved dispersibility of SNCs in water was observed after cross-linking with sodium hexametaphosphate (SHMP) [45]. This result demonstrated that cross-linking reactions did not disrupt the crystalline structure of SNCs, and a uniform suspension was obtained. The effect of the pH of the dispersion on the zeta potential, size distribution, and aggregation behavior of H_2SO_4-prepared SNCs was also investigated [44]. It was shown that zeta potential decreased with increasing pH of the dispersion, and aggregated platelet-like nanocrystals (1.5 μm) became monodispersed spherical-like nanoparticles (50 nm). It was concluded that stable SNC suspensions could be obtained by adjusting the pH of the aqueous phase in the range of 7.44−9.45. Subsequently, the aqueous re-dispersibility of SNC powders was improved by sodium hypochlorite oxidation (NaClO) with >2% (w/w) active chlorine [5]. NaClO oxidation (2% active chlorine) induced minor destruction (reduced from 45.6% to 42.8%.) to SNCs. The introduction of carboxyl groups led to highly individualized SNCs with a particle size of 20 nm, and the suspension maintained stability for at least 20 days.

6.4.3 Improving the Hydrophobicity (Dispersity in Organic Media) of Nano-sized Starch

The abundance of hydroxyl groups on the surface of nano-sized starch results in a high hydrophilicity, which restricts applications. To broaden the number of possible applications, the hydrophobicity of the surface of SNs can be improved. Over recent decades, much effort has been conducted to improve the hydrophobicity of SNs.

Hydrophobic modification methods can be categorized into three distinct groups: (1) chemical derivatization of surface hydroxyl groups with modifying agents, (2) surface modification by "grafting onto" using a coupling agent, and (3) surface modification by "grafting from" radical polymerization.

6.4.3.1 Chemical Derivatization

Chemical derivatization of SNs can be classified into three routes: esterification, acetylation, and silylation. Surface esterification is the most common method, during which hydroxyl groups of SNs are condensed with carboxylic acid groups, forming ester functional groups on the surface. However, direct esterification between hydroxyl groups of SNs and carboxylic acid groups is difficult due to their relatively low activity. Consequently, acetylation, a simple method of esterification that introduces an acetyl group on the surface of SNs, has received much attention. Organic acid chloride and alkenyl succinic anhydride are the main acetylating agents used for hydrophobic modification of SNs. Thielemans et al. successfully modified SNCs using stearic acid chloride and poly(ethylene glycol) methyl ether [48]. Furthermore, the crystalline structure of SNCs was not altered after surface modification, and individualization of nanoparticles resulted from a reduction of polar and hydrogen bonding forces. SNCs modified in this way can be used as compatible polymer additives, surface-active particles, and co-continuous nanocomposite precursors. Namazi et al. modified SNCs using octanoyl, nonanoyl, and decanoyl chloride in aqueous media under mild condition [49]. They concluded that the onset temperature of the modified SNCs was increased, and the starch nanoparticles showed greater thermal stability after introduction of the fatty acids. Wettability tests showed that the surface properties of SNCs changed during modification, and modified SNCs have a higher affinity toward organic solvents than aqueous solutions.

Anhydride is another frequently used hydrophobic modifying agent that has been widely studied. Angellier et al. modified SNCs using two different reagents, alkenyl succinic anhydride and phenyl isocyanate, and found that chemical modification led to more hydrophobic SNCs with retained morphology and crystallinity [3]. Wettability tests showed that the high polar nature of the SNC surface was significantly reduced. Xu et al. prepared acetylated SNCs that can be solubilized in organic solvents such as N,N-dimethylformamide, acetone, carbon tetrachloride, and toluene [47]. However, the crystalline structure of the acetylated SNCs changed from A-type to V-type, and the platelet-like morphology became sphere-shaped after modification, while the size increased from 20−40 to 63−271 nm. Ren et al. successfully modified SNCs through esterification using dodecenyl succinic anhydride, 2-octen-1-ylsuccinic anhydride, and acetic anhydride in green media (water, ethanol, or a water/ethanol mixture) [50]. Their results showed that modified SNCs could be dispersed in nonpolar solvents such as chloroform, dichloromethane, and toluene, and the dispersibility increased with increasing degree of substitution (DS). X-ray diffraction (XRD) results showed that the crystalline structure of SNCs was preserved after modification. Thereafter, the hydrophobicity of SNCs was enhanced

through a dual modification via cross-linking and esterification [6]. The results showed that dual modification resulted in a higher DS than single esterification modification. SNCs with dual modifications are less polar and more hydrophobic than SNCs with single cross-linking or esterification modifications and can therefore be dispersed in nonpolar solvents such as chloroform, dichloromethane, and toluene. The authors concluded that cross-linking protected the crystalline structure of SNCs from disruption in subsequent esterification reactions. Modified SNCs can not only be used as reinforcements in hydrophobic polymer matrices but also as emulsion stabilizers and rheology modifiers.

In order to overcome the disadvantages of esterifying and acetylating SNCs, such as the presence of unstable ester groups, low efficiency, and complex preparation processes, Wei et al. proposed a silylation strategy using hexadecyltrimethoxysilane (HDS) to improve the hydrophobicity [46]. The long, hydrophobic hydrocarbon chain was covalently linked to the surface of SNCs through Si-O-C bonds via a condensation reaction between hydroxyl and silanol groups. Due to the multilayer coverage of the long hydrocarbon chains, they crystallized on the surface of SNCs. The hydrophobicity and hydrophobic stability were increased with increasing application of HDS. The contact angle of modified SNCs increased from 43 to 119° as the applied HDS was increased from 0% to 0.3% (v/v). The modification significantly improved the dispersibility of SNCs in nonpolar solvents, and a homogenous suspension could be obtained in acetone or n-hexane.

6.4.3.2 The "Grafting Onto" Strategy

The "grafting onto" strategy involves the attachment of presynthesized polymer chains to the surface of SNs through their reactive end groups. Commonly used grafting polymers include poly(ethylene glycol) methyl ether (PEGME) [48], poly(tetrahydrofuran) (PTHF) [51], poly(ethylene glycol) monobutyl ether (PPGBE) [51], poly(caprolactone) (PCL) [51–53], poly(styrene) (PS) [54], and isocynate [55]. Among them, PCL is the most commonly employed polymer for improving the hydrophobicity of SNs due to its high biodegradability, PPGBE is used based on good compatibility of starch with poly(propylene glycol) and its applicability to drug and other medical products, and the benefits of PTHF lie somewhere between these two polymers. These studies expanded on the work of Thielemans from the same team at the Grenoble Institute of Technology. The length of the grafted chains was not sufficient to allow the formation of a continuous film by hot-pressing the modified nanoparticles [48]. Song et al. subsequently prepared amphiphilic SNCs through graft copolymerization of SNCs with PS in an aqueous emulsion system. After hydrophobic modification, the size of SNCs increased from ~50 to 80−100 nm, and they could be uniformly dispersed both in the water and oil phase, demonstrating excellent amphiphilicity [54]. Valodkar et al. prepared nanosized starch derivatives by isocyanate modification, and the resultant SNCs are excellent reinforcing agents for bionanocomposites [55]. In general, the crystalline structure of SNs is not changed after polymer grafting, and modification only occurs on the surface. The surface coating of SNs has a large effect on their

individualization because it reduces hydrogen bonding and polar interactions between the individual particles. The grafting efficiency of polymer chains onto the surface of SNs decreases with increasing polymeric chain length, as demonstrated for PCL by Labet et al. [51]. Consequently, a high grafting density cannot be achieved using the "grafting onto" strategy due to steric hindrance and blocking of reactive sites of the already grafted polymer chains.

6.4.3.3 The "Grafting from" Strategy

The "grafting from" strategy involves mixing SNs with a monomer and an initiator agent to induce polymerization of the monomer, and the resulting polymers cover the surface of SNs. Compared with the "grafting onto" strategy, the "grafting from" strategy is more effective for achieving a higher grafting density and well-controlled polymer structure on different kinds of surfaces [66]. Surface-initiated ring-opening polymerization (ROP) is the main method used for the "grafting from" strategy for SNs. In this process, hydroxyl groups on the surface of SNs serve as initiators, and the ratio of monomer (such as ε-caprolactone, CL) to initiating groups determines the density of the grafted polymer chains. Namazi et al. synthesized SNs-g-PCL through ROP of CL in the presence of $Sn(Oct)_2$ as initiator, and their results indicated no alteration of the crystalline structure or morphology of SNs [56]. Yu et al. prepared SNC-g-PCL via microwave-assisted ROP of PCL and found that the modified SNCs exhibited superior reinforcing activity when incorporated into a poly(lactic acid) matrix to produce fully biodegradable nanocomposites [57]. The same results were obtained when SNC-g-PCL was incorporated into a PCL-based waterborne polyurethane matrix [53]. Due to the low viscosity of the reaction medium and limitations of steric hindrance, the "grafting from" strategy is considered an efficient way of achieving the hydrophobic modification of SNs. However, the strategy also has drawbacks, including difficulties in determining and characterizing the resulting grafted polymers.

6.4.3.4 Enzyme Modification

The chemical modification of SNs always involves the use of polar aprotic solvents such as dimethyl sulfoxide (DMSO) and harsh conditions to facilitate the modification process, which can restrict its applications. Chakraborty et al. developed an enzyme-catalyzed regioselective modification of SNs using reverse micelles stabilized by bis(2-ethylhexyl) sodium sulfosuccinate (AOT) with the catalyst lipase B (CAL-B) from *Candida antarctica* in immobilized (Novozym 435) and free (SP-525) forms [58]. The results showed that starch esters with a DS of 0.8, 0.6, and 0.4 were obtained for reactions at 40 °C for 48 h with vinyl stearate, ε-caprolactone, and maleic anhydride, respectively. Substitution occurred regioselectively at the C-6 position of the SNs without altering the dimensions, and modified SNs could be redispersed in DMSO or water [58].

6.4.4 Improving the Compatibility of Nano-sized Starch with Different Matrices

As SNs can be readily dispersed in water due to their hydrophilic nature, they are commonly used in the form of aqueous suspensions. However, improving the compatibility of nano-sized starch with various matrices is important for novel applications and generally involves hydrophobic modification of the surface. Improving compatibility can improve interaction between the filler (SNs) and the matrix, resulting in composite materials with better mechanical properties. Thus, all the aforementioned hydrophobic modifications of SNs (section "Improving the Hydrophobicity (Dispersity in Organic Media) of Nano-sized Starch") can be considered to improve the compatibility of nano-sized starch with the matrix.

6.4.5 Improving the Crystallinity of Nano-sized Starch

The crystallinity of nano-sized starch differs depending on the preparation protocol. In general, SNs prepared by the hydrolysis method have larger RC values than SNs prepared by other methods. A lower RC value can restrict the applications of SNs, especially their use as fillers in the preparation of nanocomposites, because a high mechanical strength is fundamental for good mechanical properties of composite materials. Therefore, researchers are attempting to enhance the RC of SNs in order to extend their range of applications. Ji et al. studied the effects of heat-moisture treatment (HMT) on the physicochemical properties of starch nanoparticles and found that their crystalline structures changed from B-type to A-type, and the crystallinity increased significantly, while the size and shape were not altered [59]. As the HMT temperature and SN moisture content was increased, the hydrogen bonds between the starch molecule chains became stronger. These findings could help food processors tailor the properties of SNs modified using different moisture and temperature levels, and SNs subjected to a single HMT could be widely used in both the food and nonfood sectors.

6.5 Applications of Nano-sized Starch

SNs are rigid, biodegradable, biocompatible, renewable, eco-friendly materials. They have many advantages such as a high specific surface area (>100 $m^2\ g^{-1}$), high modulus (>100 GPa), high aspect ratio, low density, and an abundance of hydroxyl groups readily available for introducing new functionalities [67]. For these reasons, they have been used in various areas including the preparation of nanocomposites, stabilization of Pickering emulsions, drug carriers, biosensors, and biomarkers. Among these applications, their use as reinforcing fillers to prepare nanocomposites

Table 6.2 Applications of nano-sized starch

Application	Functionality	References
Fillers		
Reinforcing effects	Reinforcement of the nanocomposites	[68, 71, 80, 81, 86, 92, 95, 96]
Swelling properties	Increase or decrease water uptake	[72, 82, 85, 92]
Barrier properties	Formation of tortuous diffusion pathway	[72, 73, 75, 80–82, 85]
Emulsion stabilizer	Adsorption on water-oil interface against coalescence	[103–110]
Delivery vehicles		
Drug carrier	Drug release regulator for sustained drug delivery system	[35, 116–119]
Enhancement of bioactivity	Encapsulation of bioactive compounds	[120–122]
Decontamination of wastewater	Adsorption of organic pollutants	[126]
Binders	Decrease of paste viscosity, increase of binding capability	[127]
Thermo-responsive materials	Cross-linker and fillers exhibited thermo-responsive properties	[128]
Templates		
Hollow nanospheres	Incorporation into the nano-matrix and hydrolysis of the SNs	[129]
Fluorescent carbon nanodots	Precursor material for the carbon nanodots	[130]
Biosensors or biomarkers	Hydroxyl groups ready for fluorescent labeling	[132]
Inhibition of enzyme activity	Alteration of the enzyme conformation	[133]

is the most common and has been well-studied in recent decades. An increasing number of researchers are investigating the emulsifiability of SNs, and other applications as drug carriers, biosensors, and biomarker are also receiving increasing attention, as discussed below. The applications of SNs are summarized in Table 6.2.

6.5.1 Fillers

Polymer nanocomposites reinforced by SNs generally display improved mechanical properties, reinforcing effects, and swelling and barrier properties, as has been reviewed extensively in several publications and book chapters [8, 42, 43, 68–70]. This is discussed briefly below, with a focus on comparing these diverse studies and drawing conclusions.

Different polymeric matrices have been coupled with SNs to prepare nanocomposite materials. The first study in this field was performed by Dufresne et al. in

1996, in which a copolymer of styrene and a butyl acrylate (poly[S-co-BuA]) matrix in the latex form were used [71]. The latex was mixed with an aqueous suspension of SNCs, and the mixture was freeze-dried and hot-pressed. Subsequent work has generally involved using the casting/evaporation method due to its simplicity and good dispersion of nanoparticles in water [68]. Therefore, water-soluble polymers such as pullulan [72], gelatinized starch [73–81], carboxymethyl chitosan [82], polyvinyl alcohol [83], and soy protein isolate [84], as well as polymers in the latex form (aqueous polymer dispersions) such as natural rubber [85–90], poly(β-hydroxyoctanoate) [91], poly(S-co-BuA) [61, 71, 92], and waterborne polyurethane [53, 57, 93, 94], have been investigated.

Most such matrices have involved aqueous systems. To broaden the number of possible polymeric matrices from aqueous systems to organic solvents, SNs have been hydrophobically modified by transforming their polar hydroxyl groups as described above in section "Improving the Hydrophobicity (Dispersity in Organic Media) of Nano-sized Starch," resulting in modified SNs that are better able to interact with nonpolar polymers. However, Angellier et al. reported that the mechanical performance of ASA- and PI-modified SNC-reinforced natural rubber (NR) was lower than unmodified SNC-reinforced NR [86]. This unexpected result was ascribed to the coating of the grafting agents on SNCs, which hindered interactions between SNCs and matrices. Aqueous and toluene mixtures used for unmodified and modified SNCs, respectively, also may have affected the results of this study. By contrast, Habibi et al. found that PCL-grafted SNCs possessed lower modulus values in nanocomposite films but significantly higher strain at break, which contributed to the formation of a percolating network between SNC-g-PCL and the matrix [52]. Similar results were observed when hydrophobically modified SNs were incorporated into matrices of waterborne polyurethane [53], NR [55], and PLA [57].

It should be noted that the processing temperature of nanocomposites is generally below the gelatinization temperature of SNs in order to avoid destruction of SN crystallinity.

6.5.1.1 Improving the Mechanical Properties of Nanocomposites (Reinforcing Effects)

The mechanical reinforcement effects of SNs in nanocomposites were evaluated either in linear (dynamic mechanical analysis, DMA) or nonlinear ranges (tensile tests) [68]. SNs incorporated into nanocomposites generally show high reinforcing effects [71, 92] and induce an increase in both the tensile modulus and strength [80, 81, 95], whereas the strain at break is usually decreased. Compared with fly ash and carbon black, SNCs present superior mechanical properties [86]. Bel Haaj compared the reinforcing effects of SNCs and SNs and found that SNCs performed better in polymer films as a result of their platelet-like morphology [96]. On the other hand, SNs reduce the transparency of nanocomposite films to a lesser extent than SNCs due to their smaller size.

Similar to cellulose nanocrystals, the reinforcing mechanisms of SNs can generally be ascribed to two aspects: (1) in ternary systems, the formation of a jammed network consisting of SNs with different geometrical characteristics is believed to play an important role in the enhancement of the cross-linked network; (2) strong hydrogen bonding interactions between SNs and the matrix are believed to further improve the mechanical properties [68]. Mele et al. developed a phenomenological modelling approach in an attempt to understand the reinforcing mechanism of SNCs in a nonvulcanized natural rubber matrix [88]. Nonlinear dynamic mechanical experiments highlighted the significant reinforcing effects of SNCs and revealed Mullins and Payne effects. Two models were used to predict the Payne effect based on the domination by filler-filler (Kraus model) or matrix-filler (Maier and Göritz model) interactions.

6.5.1.2 Swelling Properties

Incorporation of SNs into nanocomposites can either increase or decrease the swelling properties due to changes in the dimensions and physical properties of the materials, depending on the nature of the matrices and the swelling solvents. For instance, incorporation of SNCs into poly(styrene-butyl acrylate-acrylic acid-acrylamide) [92] or NRs [85] induces a swelling of the nanocomposites and results in two well-defined regions, presumably due to the hydrophilic nature of starch and the hydrophobic nature of the matrix, which induces a strong adsorption of water. However, for sorbitol-plasticized pullulan, a decrease in water uptake was observed when SNCs were incorporated, especially upon high loading [72]. The result was ascribed to the formation of a three-dimensional network of nanoparticles that restricts swelling of the matrix, which contributes to the decreased water uptake. Similar results were also found when SNCs were incorporated into carboxymethyl chitosan [82].

6.5.1.3 Barrier Properties

Incorporation of SNCs into nanocomposites can dramatically reduce the water vapor permeability (WVP) value. Angelier et al. observed a continuous decrease in the WVP of NRs upon SNC addition (up to 30%) [85]. Garcia et al. reported a 40% decrease in WVP for a cassava starch plasticized matrix reinforced with only 2.5 wt% SNs [73]. A similar decreasing trend in WVP was observed when SNs were incorporated into carboxymethyl chitosan [82] and starch-based films [80, 81]. The decrease in the WVP value probably results from the difficult diffusion pathway created by the incorporated SNs, which restricts the ability of water molecules to pass through. However, Kristo et al. reported unchanged WVP values between pullulan films and those containing up to 20 wt% SNCs [72]. Moreover, increased WVP values were reported when using a glycerol-plasticized waxy maize starch matrix [75].

6.5.2 Emulsion Stabilizer

Particle-stabilized emulsions, usually referred to as Pickering emulsions, were first reported by Ramsden in 1903 [97]. It was found that the adsorption of solid particles at the air-water interface contributes to foaming and the recovery of solid particles adsorbed as a rigid layer at the surface of liquids. Later, S.U. Pickering studied o/w emulsions stabilized by solid particles adsorbed at the surface of oil droplets [98]. This study is generally considered to be the first report of Pickering emulsions, which have since attracted considerable research interest in the past decade due to their unique properties, and SNs are among the most extensively studied particle stabilizers due to their excellent properties compared with inorganic nanoparticles. Several articles have reviewed Pickering emulsions stabilized by either nanoparticles or microparticles [99–102], but SN-stabilized Pickering emulsions are summarized independently from other aspects such as preparations, modifications, and applications.

The first report of SN-stabilized Pickering emulsions was by Li et al. in which SNCs were used as emulsifiers to stabilize oil-in-water emulsions of 50 vol% paraffin liquid [103]. The size of the droplets decreased with increasing concentration of SNCs. These emulsions are highly stable against coalescence over months, and the creaming of emulsions decreases with increasing concentration of SNCs, which indicates that SNCs are surface-active particles. Tan et al. prepared starch-based nanospheres through a simple nanoprecipitation procedure using acetic anhydride and phthalic anhydride [104]. These pH-responsive amphiphilic starch-based nanospheres were then used as particle emulsifiers to stabilize Pickering emulsions, and the catastrophic inversion and transitional inversion of such emulsions could be easily achieved by varying the water:oil volume ratio and the pH of the aqueous dispersion, respectively. Thereafter, SNs were used as particle emulsifiers for triglyceride water emulsions, and catastrophic phase inversion from oil-in-water (o/w) to water-in-oil (w/o) emulsions was achieved by increasing the volume fraction of oil beyond 0.65 [105]. The stability to creaming of o/w emulsions increases as phase inversion is approached, as does the stability to sedimentation of w/o emulsions.

Ge et al. studied the influence of the starch variety and particle size of SNs on the fabrication of Pickering emulsions and found that SNs from tapioca, sweet potato, and corn were appropriate for their preparation [106]. Pickering emulsions prepared by medium-sized (100−220 nm) nanoparticles have better stability than others, and they are stable against changes of temperature and sodium chloride. Ye et al. investigated the effects of different hydrophobic modifications such as octenylsuccinylation of soluble SNs (OSA-SSNs) and insoluble SNs (ISNs) on the stabilization of oil-in-water Pickering emulsions [107]. The rheological results indicated that both Pickering emulsions displayed shear-thinning behavior as a non-Newtonian fluid. The droplet size distribution of the Pickering emulsion stabilized by OSA-SSNs exhibited a narrow peak, whereas a broader bimodal size distribution was observed for the Pickering emulsion stabilized by ISNs. When the Pickering emulsions were

stored for 30 days, no phase separation was detected, revealing high stability for both OSA-SSNs and ISNs.

The applications of SN-stabilized Pickering emulsions have not yet been extensively studied, and few reports are published. Bel Haaj et al. verified the improved performance of nanocomposites through SNC-stabilized Pickering emulsion polymerization [108]. This in situ polymerization technique not only facilitates the use of SNC nanoparticles but also provides valuable nanocomposites with enhanced mechanical properties and high transparency. Nikfarjam et al. synthesized expandable spherical polystyrene beads containing well-dispersed water microdroplets that serve as a green blowing agent through Pickering emulsion polymerization stabilized by cross-linked SNs (CSNs) forming a w/o/w system [109]. The entrapped water microdroplets have an average size of 3−4 μm and are surrounded by a dense layer of CSNs. The droplet density and water encapsulation efficiency in the polystyrene beads increase with increasing CSN concentration. Marku et al. studied starch-based Pickering emulsions and evaluated their possible use as vehicles for topical drug delivery [110]. The results showed that it is possible to produce oil in water starch-stabilized Pickering emulsions with an oil content up to 56%. The emulsions show good stability during storage over 8 weeks, even toward mild centrifugation, and the particle size of the droplets is only dependent on oil/starch ratio. Other types of liquid oil do not affect the droplet size of these emulsions, and transport over the skin is affected by the Pickering emulsion formulation, since the flux was twice that of previously reported solutions.

6.5.3 Delivery Vehicles

SNs benefit from many of the advantages of starch, since they are nontoxic, biodegradable, and biocompatible, making them excellent candidates for applications in the control, carriage, and release of active compounds and drugs. The use of SNs as delivery vehicles can generally be classified into two aspects: (1) drug carriers and (2) the protection of bioactive compounds.

It has been reported that a higher intracellular uptake of nanoparticles can be achieved compared with micron-sized particles, and they can access a wider variety of biological tissues due to their smaller size and higher mobility [111]. Starch used in either the granular or gelatinized state can serve as a drug carrier for phenethylamines [112], acetylsalicylic acid (Aspirin) [113], estrone [114], and other drugs [115]. However, herein we focus only on the use of SNs as drug carriers. SNs and modified SNs have been used as delivery carriers for tumor-targeted drugs and transdermal drugs [116–118]. Propyl-SNs loaded with flufenamic acid exhibit enhanced permeation through human skin and achieve a high encapsulation efficiency of flufenamic acid, testosterone, and caffeine [117]. Dialdehyde starch nanoparticles (DASNs) are a new type of drug carrier that can sustain the loading and release of 5-fluorouracil (5-Fu) antitumor drugs. DASNs binding 5-Fu significantly enhance breast cancer cell (MCF-7) inhibition in vitro in comparison with

free 5-Fu [118]. Lin et al. developed a SNC-reinforced pH-sensitive alginate microsphere-controlled release system for drug delivery and found a more consistent swelling pattern and a higher encapsulation efficiency of the microsphere, as well as a promising sustained release profile of the drug, following the incorporation of SNs [119].

SNs are also used as delivery vehicles to control the release of salvianolic acid B [120] and to enhance the antioxidative or antimicrobial activities of essential oils (EOs) and bioactive compounds such as menthone, oregano, cinnamon, lavender, citral [121], and polyphenols [122]. Li et al. fabricated an oral delivery system of SNs/gum nanoparticles for salvianolic acid B and found that SNs with chitosan and gum arabic exhibited an obvious core-shell structure with loading capacities of up to 8.26% and 8.08% for SNs/chitosan and SNs/gum arabic nanocomposites, respectively [120]. The in vitro release of Sal B from SNs/gum nanocomposites was sustained for over 12 h, indicating that it is a good candidate for the controlled release of Sal B. Qiu et al. found that the antioxidative and antimicrobial activities of EOs were enhanced after encapsulation in SNs prepared from short glucan chains [121]. Liu et al. studied the adsorption mechanism of the polyphenols catechin, (−)-epicatechin, (−)-epigallocatechin-3-gallate, and proanthocyanidins onto SNs and detected an enhanced antioxidant activity of polyphenols under adverse conditions [122].

It should be noted that much attention has been paid to the safety of SNs, especially those used in medicines or foods. Some studies have reported that nanoparticles used in drug delivery may cause a toxic effect in the human body [123, 124]. However, Kim et al. reported no issues with the safety of SNs, including those injected directly in veins [125]. The safety of SNs therefore requires further investigation.

6.5.4 Adsorbents

Currently, there is a growing interest in developing renewable and low-cost alternatives such as biopolymer-based materials for the adsorption of organic pollutants from wastewater. Alila et al. developed stearate-grafted SNs as adsorbent materials for the removal of aromatic organic pollutants from aqueous solutions [126]. Stearate modification of SNs significantly improved the maximum adsorption capacity of nanometric substrates compared with unmodified SNs (from 50 μmol g^{-1} and 40 μmol g^{-1} to 687 μmol g^{-1} and 559 μmol g^{-1} for 2-naphthol and nitrobenzene, respectively). The adsorption kinetics followed a two-step process: the initial pure adsorption of aromatic compounds onto the surface of the nanoparticles and diffusion of the compounds into the layer of surface chains grafted onto the nanoparticles. The driving force for the adsorption process is largely governed by van der Waals interactions between the grafted chains and the organic solute. Therefore, any factor increasing these interactions will likely contribute to an enhancement of the adsorption capacity, as concluded by the authors [126].

6.5.5 Binders

Due to the low viscosity and other derived advantages of starch, SNs can be used as binders in papermaking and papercoating. Bloembergen et al. replaced petroleum-based latex binders in papermaking with a starch-based biolatex and found that it can resolve the problems arising when using cooked starches, such as (1) the low absorption of starch on cellulose substrates, which is limited by the saturation of the absorption, and (2) the operational problems caused by the high viscosity of cooked native starches [127].

6.5.6 Thermo-responsive Materials

Valodkar et al. synthesized diisocyanates (HMDI)-cross-linked insoluble SNs which were reactive enough for use in the synthesis of nanocomposites [128]. When incorporated into polyether-polyurethane films, the high degree of cross-linking and effective filling of the modified SNs facilitates electrical conductivity, and the nanocomposite films exhibit thermo-responsive properties. These polyurethanes have potential applications as temperature sensors.

6.5.7 Templates for Preparing New Nano-materials

The carbohydrate polymers in SNs can be hydrolyzed by various amylases. Li et al. have successfully fabricated hollow short linear glucan (SLG)@gum arabic (GA) nanospheres and hollow in situ SLG/GA hybrid nanospheres by removing sacrificial SNs templates by α-amylase treatment and Ostwald ripening [129]. The two resulting types of hollow nanospheres have a huge cavity for the encapsulation of phenolic acids and can be used as nanoreactors to enhance or improve their antioxidative activity or stability, respectively, when exposed to high salt concentrations, UV light, or heat treatment.

SNs can also be used as templates for the synthesis of fluorescent carbon nanodots (CDs). Chin et al. reported a two-step synthesis routine for CDs using sago SNs [130] that are firstly carbonized and then subjected to surface oxidation in an aqueous medium. The use of SNs as the precursor material gave better control over the morphology of the final CDs products, which were highly homogenous and possessed monodispersed physiochemical properties. Due to the ease of preparation, low cost, and efficient fluorescence emission, these fluorescent CDs are promising materials for various biomedical applications [130].

6.5.8 Biosensors and Biomarkers

SNs have the potential for biobasing nanomaterials as they are easily processed, renewable, biocompatible, and nontoxic in comparison with inorganic nanoparticles [68, 131]. Cai et al. proposed a facile approach for fluorescein labeling of SNCs via polar covalent binding. The reaction was conducted through two steps: (1) introduction of reactive amino groups onto SNCs via silane coupling and (2) formation of thiourea covalent bonds between isothiocyanato groups of fluorescein isothiocyanate (FITC) and the introduced reactive amino groups [132]. In comparison with FITC, FITC-labeled SNCs (F-SNCs) display a more obvious fluorescence intensity and a higher photostability, and the particles are biocompatible with cells and easily internalized [132]. Therefore, F-SNCs hold great potential for applications as biosensors and biomarkers in the food and biomedical industries.

6.6 Conclusions

In recent decades, SNs have been successfully prepared by a wide range of methods, and much effort has been devoted to their modification and improvement to overcome disadvantages or introduce new properties. The application of SNs to various areas such as nanocomposites, emulsion stabilizers, delivery vehicles, adsorbents, binders, thermo-responsive materials, templates for preparing new nano-materials, biosensors, and biomarkers has also been explored. However, further research is needed, especially regarding industrial-scale production and the dispersibility and re-dispersibility of powdered SN products.

References

1. Dufresne A. Comparing the mechanical properties of high performances polymer nanocomposites from biological sources. J Nanosci Nanotechnol. 2006;6(2):322–30.
2. Šturcová A, Davies GR, Eichhorn SJ. Elastic modulus and stress-transfer properties of tunicate cellulose whiskers. Biomacromolecules. 2005;6(2):1055–61.
3. Angellier H, Molina-Boisseau S, Belgacem MN, et al. Surface chemical modification of waxy maize starch nanocrystals. Langmuir. 2005;21(6):2425–33.
4. Putaux JL, Molina-Boisseau S, Momaur T, et al. Platelet nanocrystals resulting from the disruption of waxy maize starch granules by acid hydrolysis. Biomacromolecules. 2003;4(5):1198–202.
5. Wei B, Zhang B, Sun B, et al. Aqueous re-dispersibility of starch nanocrystal powder improved by sodium hypochlorite oxidation. Food Hydrocoll. 2016;52:29–37.
6. Ren L, Wang Q, Yan X, et al. Dual modification of starch nanocrystals via crosslinking and esterification for enhancing their hydrophobicity. Food Res Int. 2016;87:180–8.
7. Lecorre D, Vahanian E, Dufresne A, et al. Enzymatic pretreatment for preparing starch nanocrystals. Biomacromolecules. 2012;13(1):132–7.

8. Le Corre D, Bras J, Dufresne A. Starch nanoparticles: a review. Biomacromolecules. 2010;11(5):1139–53.
9. Lecorre D, Bras J, Dufresne A. Influence of botanic origin and amylose content on the morphology of starch nanocrystals. J Nanopart Res. 2011;13(12):7193–208.
10. Sun Q, Li G, Dai L, et al. Green preparation and characterisation of waxy maize starch nanoparticles through enzymolysis and recrystallisation. Food Chem. 2014;162:223–8.
11. Nägeli W. Beiträge zur näheren Kenntniss der Stärkegruppe. Justus Liebigs Ann Chem. 1874;173(2):218–27.
12. Lintner CJ. Studien über Diastase. J Prakt Chem. 1886;34:378–94.
13. Angellier H, Choisnard L, Molina-Boisseau S, et al. Optimization of the preparation of aqueous suspensions of waxy maize starch nanocrystals using a response surface methodology. Biomacromolecules. 2004;5(4):1545–51.
14. Kim JY, Park DJ, Lim ST. Fragmentation of waxy rice starch granules by enzymatic hydrolysis. Cereal Chem. 2008;85(2):182–7.
15. Belhaaj S, Magnin A, Pétrier C, et al. Starch nanoparticles formation via high power ultrasonication. Carbohydr Polym. 2012;92(2):1625–32.
16. Sun Q, Fan H, Xiong L. Preparation and characterization of starch nanoparticles through ultrasonic-assisted oxidation methods. Carbohydr Polym. 2014;106:359–64.
17. Song D, Thio YS, Deng Y. Starch nanoparticle formation via reactive extrusion and related mechanism study. Carbohydr Polym. 2011;85(1):208–14.
18. Wei B, Cai C, Jin Z, et al. High pressure homogenization induced degradation of amylopectin in a gelatinized state. Starch-Stärke. 2016;68:734–41.
19. Liu D, Wu Q, Chen H, et al. Transitional properties of starch colloid with particle size reduction from micro-to nanometer. J Colloid Interf Sci. 2009;339(1):117–24.
20. Che L, Wang L-J, Li D, et al. Starch pastes thinning during high-pressure homogenization. Carbohydr Polym. 2009;75(1):32–8.
21. Toraman OY, Katircioglu D. A study on the effect of process parameters in stirred ball mill. Adv Powder Technol. 2011;22(1):26–30.
22. Patel CM, Chakraborty M, Murthy Z. Fast and scalable preparation of starch nanoparticles by stirred media milling. Adv Powder Technol. 2016;27(4):1287–94.
23. Lamanna M, Morales NJ, García NL, et al. Development and characterization of starch nanoparticles by gamma radiation: potential application as starch matrix filler. Carbohydr Polym. 2013;97(1):90–7.
24. Sun Q, Gong M, Li Y, et al. Effect of retrogradation time on preparation and characterization of proso millet starch nanoparticles. Carbohydr Polym. 2014;111:133–8.
25. Li X, Qin Y, Liu C, et al. Size-controlled starch nanoparticles prepared by self-assembly with different green surfactant: the effect of electrostatic repulsion or steric hindrance. Food Chem. 2016;199:356–63.
26. Bail PYL, Rondeau C, Buleon A. Structural investigation of amylose complexes with small ligands: helical conformation, crystalline structure and thermostability. Int J Biol Macromol. 2005;35(1):1–7.
27. Kim J-Y, Lim S-T. Preparation of nano-sized starch particles by complex formation with n-butanol. Carbohydr Polym. 2009;76(1):110–6.
28. Kim JY, Yoon JW, Lim ST. Formation and isolation of nanocrystal complexes between dextrins and n-butanol. Carbohydr Polym. 2009;78(3):626–32.
29. Fessi H, Puisieux F, Devissaguet JP, et al. Nanocapsule formation by interfacial polymer deposition following solvent displacement. Int J Pharm. 1989;55(1):R1–R4.
30. Tan Y, Xu K, Li L, et al. Fabrication of size-controlled starch-based nanospheres by nanoprecipitation. ACS Appl Mater Interfaces. 2009;1(4):956–9.
31. Qin Y, Liu C, Jiang S, et al. Characterization of starch nanoparticles prepared by nanoprecipitation: influence of amylose content and starch type. Ind Crop Prod. 2016;87:182–90.

32. Qiu C, Yang J, Ge S, et al. Preparation and characterization of size-controlled starch nanoparticles based on short linear chains from debranched waxy corn starch. LWT Food Sci Technol. 2016;74:303–10.
33. Shi A, Li D, Wang L, et al. Preparation of starch-based nanoparticles through high-pressure homogenization and miniemulsion cross-linking: influence of various process parameters on particle size and stability. Carbohydr Polym. 2011;83(4):1604–10.
34. Zhou G, Luo Z, Fu X. Preparation and characterization of starch nanoparticles in ionic liquid-in-oil microemulsions system. Ind Crop Prod. 2014;52:105–10.
35. Zhou G, Luo Z, Fu X. Preparation of starch nanoparticles in a water-in-ionic liquid microemulsion system and their drug loading and releasing properties. J Agric Food Chem. 2014;62(32):8214–20.
36. Jane JL, Robyt JF. Structure studies of amylose-V complexes and retrograded amylose by action of alpha amylases, and a new method for preparing amylodextrins. Carbohydr Res. 1984;132(1):105–18.
37. Leloup V, Colonna P, Ring S, et al. Microstructure of amylose gels. Carbohydr Polym. 1992;18(3):189–97.
38. Mcdonald TO, Tatham LM, Southworth FY, et al. High-throughput nanoprecipitation of the organic antimicrobial triclosan and enhancement of activity against *Escherichia coli*. J Mater Chem B. 2013;1(35):4455–65.
39. Kim H, Han J, Kweon D, et al. Effect of ultrasonic treatments on nanoparticle preparation of acid-hydrolyzed waxy maize starch. Carbohydr Polym. 2013;93(2):582–8.
40. Kim H-Y, Park DJ, Kim J-Y, et al. Preparation of crystalline starch nanoparticles using cold acid hydrolysis and ultrasonication. Carbohydr Polym. 2013;98(1):295–301.
41. Siqueira G, Bras J, Dufresne A. Cellulose whiskers versus microfibrils: influence of the nature of the nanoparticle and its surface functionalization on the thermal and mechanical properties of nanocomposites. Biomacromolecules. 2009;10(2):425–32.
42. Lin N, Huang J, Dufresne A. Preparation, properties and applications of polysaccharide nanocrystals in advanced functional nanomaterials: a review. Nanoscale. 2012;4(11):3274–94.
43. Huang J, Chang PR, Lin N, et al. Polysaccharide-based nanocrystals: chemistry and applications. Wiley: Weinheim; 2015.
44. Wei B, Hu X, Li H, et al. Effect of pHs on dispersity of maize starch nanocrystals in aqueous medium. Food Hydrocoll. 2014;36:369–73.
45. Ren L, Jiang M, Zhou J, et al. A method for improving dispersion of starch nanocrystals in water through crosslinking modification with sodium hexametaphosphate. Carbohydr Polym. 2012;87(2):1874–6.
46. Wei B, Sun B, Zhang B, et al. Synthesis, characterization and hydrophobicity of silylated starch nanocrystal. Carbohydr Polym. 2016;136:1203–8.
47. Xu Y, Ding W, Liu J, et al. Preparation and characterization of organic-soluble acetylated starch nanocrystals. Carbohydr Polym. 2010;80(4):1078–84.
48. Thielemans W, Belgacem MN, Dufresne A. Starch nanocrystals with large chain surface modifications. Langmuir. 2006;22(10):4804–10.
49. Namazi H, Dadkhah A. Convenient method for preparation of hydrophobically modified starch nanocrystals with using fatty acids. Carbohydr Polym. 2010;79(3):731–7.
50. Ren L, Dong Z, Jiang M, et al. Hydrophobization of starch nanocrystals through esterification in green media. Ind Crop Prod. 2014;59(0):115–8.
51. Labet M, Thielemans W, Dufresne A. Polymer grafting onto starch nanocrystals. Biomacromolecules. 2007;8(9):2916–27.
52. Habibi Y, Dufresne A. Highly filled bionanocomposites from functionalized polysaccharide nanocrystals. Biomacromolecules. 2008;9(7):1974–80.
53. Chang PR, Ai F, Chen Y, et al. Effects of starch nanocrystal-graft-polycaprolactone on mechanical properties of waterborne polyurethane-based nanocomposites. J Appl Polym Sci. 2009;111(2):619–27.

54. Song S, Wang C, Pan Z, et al. Preparation and characterization of amphiphilic starch nanocrystals. J Appl Polym Sci. 2008;107(1):418–22.
55. Valodkar M, Thakore S. Organically modified nanosized starch derivatives as excellent reinforcing agents for bionanocomposites. Carbohydr Polym. 2011;86(3):1244–51.
56. Namazi H, Dadkhah A. Surface modification of starch nanocrystals through ring-opening polymerization of ε-caprolactone and investigation of their microstructures. J Appl Polym Sci. 2008;110(4):2405–12.
57. Yu J, Ai F, Dufresne A, et al. Structure and mechanical properties of poly(lactic acid) filled with (starch nanocrystal)-graft-poly(ε-caprolactone). Macromol Mater Eng. 2008;293(9):763–70.
58. Chakraborty S, Sahoo B, Teraoka I, et al. Enzyme-catalyzed regioselective modification of starch nanoparticles. Macromolecules. 2005;38(1):61–8.
59. Ji N, Li X, Qiu C, et al. Effects of heat moisture treatment on the physicochemical properties of starch nanoparticles. Carbohydr Polym. 2015;117:605–9.
60. Dufresne A. Polysaccharide nano crystal reinforced nanocomposites. Can J Chem. 2008;86(6):484–94.
61. Angellier H, Putaux JL, Molina-Boisseau S, et al. Starch nanocrystal fillers in an acrylic polymer matrix. Macromol Symp. 2005;221:95–104.
62. Wei B, Xu X, Jin Z, et al. Surface chemical compositions and dispersity of starch nanocrystals formed by sulfuric and hydrochloric acid hydrolysis. PLoS One. 2014;9(2):e86024. https://doi.org/10.1371/journal.pone.0086024.
63. Araki J, Wada M, Kuga S, et al. Flow properties of microcrystalline cellulose suspension prepared by acid treatment of native cellulose. Colloids Surf A Physicochem Eng Asp. 1998;142(1):75–82.
64. Grahame DC. The electrical double layer and the theory of electrocapillarity. Chem Rev. 1947;41(3):441.
65. Adamczyk Z, Weroński P. Application of the DLVO theory for particle deposition problems. Adv Colloid Interf Sci. 1999;83(1):137–226.
66. Ranjan R, Brittain WJ. Synthesis of high density polymer brushes on nanoparticles by combined RAFT polymerization and click chemistry. Macromol Rapid Commun. 2008;29(12–13):1104–10.
67. Dufresne A. Interfacial phenomena in nanocomposites based on polysaccharide nanocrystals. Compos Interfaces. 2003;10(4–5):369–87.
68. Dufresne A. Crystalline starch based nanoparticles. Curr Opin Colloid Interf Sci. 2014;19(5):397–408.
69. Dufresne A. Starch and nanoparticle. Polysaccharides: Bioactivity Biotechnol. 2015; 417–49.
70. Dufresne A, Castaño J. Polysaccharide nanomaterial reinforced starch nanocomposites: a review. Starch-Stärke. 2016;1500307:1–19.
71. Dufresne A, Cavaillé J-Y, Helbert W. New nanocomposite materials: microcrystalline starch reinforced thermoplastic. Macromolecules. 1996;29(23):7624–6.
72. Kristo E, Biliaderis CG. Physical properties of starch nanocrystal-reinforced pullulan films. Carbohydr Polym. 2007;68(1):146–58.
73. García NL, Ribba L, Dufresne A, et al. Physico-mechanical properties of biodegradable starch nanocomposites. Macromol Mater Eng. 2009;294(3):169–77.
74. Angellier H, Molina-Boisseau S, Dole P, et al. Thermoplastic starch-waxy maize starch nanocrystals nanocomposites. Biomacromolecules. 2006;7(2):531–9.
75. García NL, Ribba L, Dufresne A, et al. Effect of glycerol on the morphology of nanocomposites made from thermoplastic starch and starch nanocrystals. Carbohydr Polym. 2011;84(1):203–10.
76. Viguié J, Molina-Boisseau S, Dufresne A. Processing and characterization of waxy maize starch films plasticized by sorbitol and reinforced with starch nanocrystals. Macromol Biosci. 2007;7(11):1206–16.

77. Fan H, Ji N, Zhao M, et al. Characterization of starch films impregnated with starch nanoparticles prepared by 2,2,6,6-tetramethylpiperidine-1-oxyl (TEMPO)-mediated oxidation. Food Chem. 2016;192:865–72.
78. Jiang S, Liu C, Wang X, et al. Physicochemical properties of starch nanocomposite films enhanced by self-assembled potato starch nanoparticles. LWT Food Sci Technol. 2016;69:251–7.
79. Liu C, Jiang S, Zhang S, et al. Characterization of edible corn starch nanocomposite films: the effect of self-assembled starch nanoparticles. Starch-Starke. 2015;68:239–48.
80. Li X, Qiu C, Ji N, et al. Mechanical, barrier and morphological properties of starch nanocrystals-reinforced pea starch films. Carbohydr Polym. 2015;121:155–62.
81. Dai L, Qiu C, Xiong L, et al. Characterisation of corn starch-based films reinforced with taro starch nanoparticles. Food Chem. 2015;174:82–8.
82. Duan B, Sun P, Wang X, et al. Preparation and properties of starch nanocrystals/carboxymethyl chitosan nanocomposite films. Starch-Stärke. 2011;63(9):528–35.
83. Chen Y, Cao X, Chang PR, et al. Comparative study on the films of poly (vinyl alcohol)/pea starch nanocrystals and poly (vinyl alcohol)/native pea starch. Carbohydr Polym. 2008;73(1):8–17.
84. Zheng H, Ai F, Chang PR, et al. Structure and properties of starch nanocrystal-reinforced soy protein plastics. Polym Compos. 2009;30(4):474–80.
85. Angellier H, Molina-Boisseau S, Lebrun L, et al. Processing and structural properties of waxy maize starch nanocrystals reinforced natural rubber. Macromolecules. 2005;38(9):3783–92.
86. Angellier H, Molina-Boisseau S, Dufresne A. Mechanical properties of waxy maize starch nanocrystal reinforced natural rubber. Macromolecules. 2005;38(22):9161–70.
87. Angellier H, Molina-Boisseau S, Dufresne A. Waxy maize starch nanocrystals as filler in natural rubber. Macromol Symp. 2006;233:132–6.
88. Mele P, Angellier-Coussy H, Molina-Boisseau S, et al. Reinforcing mechanisms of starch nanocrystals in a nonvulcanized natural rubber matrix. Biomacromolecules. 2011;12(5):1487–93.
89. Bouthegourd E, Rajisha KR, Kalarical N, et al. Natural rubber latex/potato starch nanocrystal nanocomposites: correlation morphology/electrical properties. Mater Lett. 2011;65(23–24):3615–7.
90. Lecorre DS, Bras J, Dufresne A. Influence of the botanic origin of starch nanocrystals on the morphological and mechanical properties of natural rubber nanocomposites. Macromol Mater Eng. 2012;297(10):969–78.
91. Dubief D, Samain E, Dufresne A. Polysaccharide microcrystals reinforced amorphous poly(β-hydroxyoctanoate) nanocomposite materials. Macromolecules. 1999;32(18):5765–71.
92. Dufresne A, Cavaille J. Clustering and percolation effects in microcrystalline starch-reinforced thermoplastic. J Polym Sci B Polym Phys. 1998;36(12):2211–24.
93. Chen G, Wei M, Chen J, et al. Simultaneous reinforcing and toughening: new nanocomposites of waterborne polyurethane filled with low loading level of starch nanocrystals. Polymer (Guildf). 2008;49(7):1860–70.
94. Wang Y, Tian H, Zhang L. Role of starch nanocrystals and cellulose whiskers in synergistic reinforcement of waterborne polyurethane. Carbohydr Polym. 2010;80(3):665–71.
95. Ma X, Jian R, Chang PR, et al. Fabrication and characterization of citric acid-modified starch nanoparticles/plasticized-starch composites. Biomacromolecules. 2008;9(11):3314–20.
96. Haaj SB, Thielemans W, Magnin A, et al. Starch nanocrystals and starch nanoparticles from waxy maize as nanoreinforcement: a comparative study. Carbohydr Polym. 2016;143:310–7.
97. Ramsden W. Separation of solids in the surface-layers of solutions and 'Suspensions'(observations on surface-membranes, bubbles, emulsions, and mechanical coagulation) – preliminary account. Proc R Soc Lond. 1903;72:156–64.
98. Pickering SU. Emulsions. J Chem Soc Lond. 1907;91:2001–21.
99. Dickinson E. Use of nanoparticles and microparticles in the formation and stabilization of food emulsions. Trends Food Sci Technol. 2012;24(1):4–12.

100. Xiao J, Li Y, Huang Q. Recent advances on food-grade particles stabilized Pickering emulsions: fabrication, characterization and research trends. Trends Food Sci Technol. 2016;55:48–60.
101. Dickinson E. Food emulsions and foams: stabilization by particles. Curr Opin Colloid Interf Sci. 2010;15(1–2):40–9.
102. Berton-Carabin CC, Schroën K. Pickering emulsions for food applications: background, trends, and challenges. Annu Rev Food Sci Technol. 2015;6:263–97.
103. Li C, Sun P, Yang C. Emulsion stabilized by starch nanocrystals. Starch-Stärke. 2012;64:497–502.
104. Tan Y, Xu K, Liu C, et al. Fabrication of starch-based nanospheres to stabilize pickering emulsion. Carbohydr Polym. 2012;88(4):1358–63.
105. Tan Y, Xu K, Niu C, et al. Triglyceride–water emulsions stabilised by starch-based nanoparticles. Food Hydrocoll. 2014;36:70–5.
106. Ge S, Xiong L, Li M, et al. Characterizations of Pickering emulsions stabilized by starch nanoparticles: influence of starch variety and particle size. Food Chem. 2017;234:339–47.
107. Ye F, Miao M, Jiang B, et al. Elucidation of stabilizing oil-in-water Pickering emulsion with different modified maize starch-based nanoparticles. Food Chem. 2017;229:152–8.
108. Haaj SB, Thielemans W, Magnin A, et al. Starch nanocrystal stabilized Pickering emulsion polymerization for nanocomposites with improved performance. ACS Appl Mater Interfaces. 2014;6(11):8263–73.
109. Nikfarjam N, Qazvini NT, Deng Y. Cross-linked starch nanoparticles stabilized Pickering emulsion polymerization of styrene in w/o/w system. Colloid Polym Sci. 2014;292(3):599–612.
110. Marku D, Wahlgren M, Rayner M, et al. Characterization of starch Pickering emulsions for potential applications in topical formulations. Int J Pharm. 2012;428(1–2):1–7.
111. Kreuter J. Nanoparticle-based dmg delivery systems. J Control Release. 1991;16(1–2):169–76.
112. Weiner B-Z, Tahan M, Zilkha A. Polymers containing phenethylamines. J Med Chem. 1972;15(4):410–3.
113. Stjärnkvist P, Laakso T, Sjöholm I. Biodegradable microspheres XII: properties of the cross-linking chains in polyacryl starch microparticles. J Pharm Sci. 1989;78(1):52–6.
114. Won C-Y, Chu C-C, Yu T-J. Synthesis of starch-based drug carrier for the control/release of estrone hormone. Carbohydr Polym. 1997;32(3–4):239–44.
115. Lenaerts V, Moussa I, Dumoulin Y, et al. Cross-linked high amylose starch for controlled release of drugs: recent advances. J Control Release. 1998;53(1):225–34.
116. Xiao S, Tong C, Liu X, et al. Preparation of folate-conjugated starch nanoparticles and its application to tumor-targeted drug delivery vector. Chin Sci Bull. 2006;51(14):1693–7.
117. Santander-Ortega M, Stauner T, Loretz B, et al. Nanoparticles made from novel starch derivatives for transdermal drug delivery. J Control Release. 2010;141(1):85–92.
118. Xiao S, Liu X, Tong C, et al. Dialdehyde starch nanoparticles as antitumor drug delivery system: an in vitro, in vivo, and immunohistological evaluation. Chin Sci Bull. 2012;57:1–7.
119. Lin N, Huang J, Chang PR, et al. Effect of polysaccharide nanocrystals on structure, properties, and drug release kinetics of alginate-based microspheres. Colloids Surf B: Biointerfaces. 2011;85(2):270–9.
120. Li X, Ge S, Yang J, et al. Synthesis and study the properties of StNPs/gum nanoparticles for salvianolic acid B-oral delivery system. Food Chem. 2017;229:111–9.
121. Qiu C, Chang R, Yang J, et al. Preparation and characterization of essential oil-loaded starch nanoparticles formed by short glucan chains. Food Chem. 2017;221:1426–33.
122. Liu C, Ge S, Yang J, et al. Adsorption mechanism of polyphenols onto starch nanoparticles and enhanced antioxidant activity under adverse conditions. J Funct Foods. 2016;26:632–44.
123. Hoet PH, Brüske-Hohlfeld I, Salata OV. Nanoparticles–known and unknown health risks. J Nanobiotechnol. 2004;2(1):12.
124. Nel A, Xia T, Mädler L, et al. Toxic potential of materials at the nanolevel. Science. 2006;311(5761):622–7.

125. Kim H-Y, Park SS, Lim S-T. Preparation, characterization and utilization of starch nanoparticles. Colloids Surf B: Biointerfaces. 2015;126:607–20.
126. Alila S, Aloulou F, Thielemans W, et al. Sorption potential of modified nanocrystals for the removal of aromatic organic pollutant from aqueous solution. Ind Crop Prod. 2011;33(2):350–7.
127. Bloembergen S, Mclennan I, Lee DI, et al. Paper binder performance with biobased nanoparticles. A starch-based biolatex can replace petroleum-based latex binders in papermaking. In: Paper 360 deg of angle Around the Industry, around the World, vol 3(8). 2008. p. 46–8.
128. Valodkar M, Thakore S. Isocyanate crosslinked reactive starch nanoparticles for thermoresponsive conducting applications. Carbohydr Res. 2010;345(16):2354–60.
129. Li X, Li M, Liu J, et al. Preparation of hollow biopolymer nanospheres employing starch nanoparticle templates for enhancement of phenolic acid antioxidant activities. J Agric Food Chem. 2017;65:3868–82.
130. Chin SF, Yazid SNAM, Pang SC, et al. Facile synthesis of fluorescent carbon nanodots from starch nanoparticles. Mater Lett. 2012;85:50–2.
131. Zhang X, Huang J, Chang PR, et al. Structure and properties of polysaccharide nanocrystal-doped supramolecular hydrogels based on cyclodextrin inclusion. Polymer (Guildf). 2010;51(19):4398–407.
132. Cai C, Wei B, Jin Z, et al. Facile method for fluorescent labeling of starch nanocrystal. ACS Sustain Chem Eng. 2017;5(5):3751–61.
133. Yang J, Chang R, Ge S, et al. The inhibition effect of starch nanoparticles on tyrosinase activity and its mechanism. Food Funct. 2016;7(12):4804–15.

Chapter 7
Starch-Lipid and Starch-Protein Complexes and Their Application

Tao Feng, Haining Zhuang, Feng Chen, Osvaldo Campanella, Deepak Bhopatkar, Marcelo A. Carignano, and Sung Hyun Park

7.1 Introduction to Starch-Copolymer Compounds

Amylose, the linear fraction of starch, forms crystalline complexes categorized under the general name of V amylose with a variety of small ligands, including linear alcohols and monoacyl lipids, which consist of a sixfold left-handed helix repeating at

T. Feng (✉)
School of Perfume and Aroma Technology, Shanghai Institute of Technology, Shanghai, China
e-mail: fengtao@sit.edu.cn

H. Zhuang
Institute of Edible Fungi, Shanghai Academy of Agricultural Sciences, Key Laboratory of Edible Fungi Resources and Utilization (South), Ministry of Agriculture, Shanghai, People's Republic of China

National Engineering Research Center of Edible Fungi, Shanghai, China
e-mail: zhuanghaining@saas.sh.cn

F. Chen
Texas Advanced Computing Center, Advanced Computing Building (ACB), J.J. Pickle Research Campus, Austin, TX, USA
e-mail: chenk@tacc.utexas.edu

O. Campanella · D. Bhopatkar
Whistler Center for Carbohydrate Research, Department of Food Science, Purdue University, West Lafayette, IN, USA
e-mail: campa@purdue.edu; deepak@purdue.edu

M. A. Carignano
Qatar Environment and Energy Research Institute, Doha, Qatar
e-mail: mcarignano@qf.org.qa

S. H. Park
Biomedical Engineering Department and Chemistry of Life Processes Institute, Northwestern University, Evanston, IL, USA
e-mail: shpark@purdue.edu

Z. Jin (ed.), *Functional Starch and Applications in Food*,
https://doi.org/10.1007/978-981-13-1077-5_7

0.80 nm [1–4]. Additionally, three crystalline complexes with branched alcohols have also been reported, with both V_6 and V_8 families identified, with each number representing the D-glucosyl units per turn. Three inclusion modes have been suggested for V_6 types, V_{6I}, V_{6II}, and V_{6III}, where I, II, and III represent the different spaces between helices in crystalline stacking. For V_{6I}, small molecules can be trapped only into the cavity of the helix [3], and for V_{6II} and V_{6III}, small molecules can also be incorporated between helices. Another possibility is that a larger cavity with eight D-glucose units per turn (V_8) allows the inclusion of bulky molecules [5, 6].

Amylose can form molecular inclusion compounds with various small ligands, and large ensembles of amylose-lipid inclusion complexes are found in native starch compounds. These inclusion complexes reduce starch-swelling capacity, solubility, and granule disruption [7, 8], as well as enhance gelatinization temperature [9]. In situ complexation between amylose and lipids, either at the surface or inside the granule, prevents the entry of water or leaching of soluble carbohydrates [10]. Additionally, complex formation restrains amylose solubility and mobility.

Compared with β-cyclodextrin, amylose displays a more flexible folding behavior in the presence of different flavor molecules. This might be attributable to the excellent adaptability of amylose, which is precisely distinguished from that of α,β-cyclodextrin (α,β-CD).

Furthermore, some amylose-free fatty acid (FFA) complexes might form soluble nanoparticles in aqueous solution. All of these characteristics drive research into the study of amylose inclusion complexes using different encapsulation methods [11–14].

7.1.1 Research Progress into Nanoparticles

In the early 1950s, NCR Corporation of the United States used this technology to develop carbonless copy paper and first realized industrialization. Subsequently, the medical community developed a series of medicinal slow-release capsules, from which microcapsule technology has been further developed. In the mid-1970s, microcapsule technology underwent rapid development, as during this period, multiple microencapsulated products and processes were created. Currently, microcapsule technology is widely used in the food, light, medicine, petrochemical, agriculture, and biotechnology industry among others.

Microcapsule technology involves the use of natural or synthetic polymer film-forming materials comprising solid, liquid, or even the core of the gas material and coated in a semipermeable or sealed capsule within a coating technology. The size of the microcapsules can be between 1 and 1000 μm, with its properties determined by particle size, distribution, geometrical properties, core material, sustained-release mechanism, and stability among other parameters. As the microcapsule core material, cystic wall material and microencapsulation methods differ, leading to different morphologies and structure. However, microcapsules are mainly spherical to round, although there are also more complex or irregular shapes. Following

microencapsulation, the color, shape, quality, volume, solubility, reactivity, heat resistance, and storage properties of the material change towards stability and durability.

The rapid development of science and technology has resulted in numerous innovations; however, traditional materials and preparation processes have been unable to meet the requirements for capsule use. With spray drying, in situ polymerization, freeze-drying, rotary evaporation, and other technical means of continuous optimization, acquisition of nano-microcapsules with smaller diameters and higher embedding effects has been possible. Nanoparticles, also known as microcapsules, are nano-sized microcapsules with particle sizes ranging from ~1 to 1000 nm. Nano-capsules are multiphase functional materials due to their small size and easy dispersal and suspension in water to form colloidal solutions, which appears clear and transparent.

In 1976, the concept of nanoparticles was already known. After the 1980s, nanoparticles were applied to the pharmaceutical industry, and currently, the application of nano-capsules is being rapidly expanded into fields associated with pesticides, flame retardants, petroleum products, and food spices, making them a compelling high-tech research target. Although the preparation of nano-capsules is well documented, there remain numerous obstacles worthy of studying due to the broad nature of potential applications.

7.1.2 Overview of Commonly Used Wall Materials for Microcapsules

Microcapsule granulation technology is the basic principle for the use of different core materials and the choice of one or several composite wall materials for coating. Generally, oil-soluble heartwood should consist of water-soluble wall materials, and water-soluble heartwood must consist of oil-soluble wall materials.

In the food industry, necessary ingredients in food need to be additives for use as core materials. The flexible composition of the core material allows the design and development of different uses for microcapsule products. Currently, food additives can be used as core materials, including as flavor spices, sour agents, antioxidants, preservatives, starters, pigments, sweeteners, vitamins, trace elements, amino acids, flavoring agents, and enzyme preparations.

Microcapsule wall material mainly consists of natural polymer compounds, synthetic polymer compounds, and their derivatives. For a microcapsule product, the appropriate wall material is very important, as different wall materials largely determine the physical and chemical properties of the product. Due to the wide variety of commonly used microcapsules, their advantages and disadvantages also vary. The required types of wall materials differ among applications and according to the different roles. The basic principle for choosing wall materials concerns core material compatibility, but not chemical reactions, to meet food industry safety and health

requirements. Materials should also have the appropriate permeability, hygroscopicity, solubility, and stability. In the food industry, the choice of crystalline wall materials is generally carbohydrates, including starch, β-cyclodextrin, maltodextrin, dextrin, monosaccharides, white dextrin, disaccharides, and polysaccharides, modified starches, lipids, including paraffin, monoglyceride, and stearic acid, cellulose, including ethyl cellulose, sodium carboxymethyl cellulose, and methyl cellulose, and animal and plant gum, including carrageenan, gelatin, sodium alginate, gluten, and casein.

7.1.2.1 Natural Polymer Materials

Natural polymer materials are among the most common types of microcapsule wall material and characterized by non-toxicity, good film-forming performance, and good stability. Dextrin can be divided into α, β, or γ types exhibiting different glucose molecules, of which the β-type application in the form of β-CD is the most common and harbors a D-pyran-type glucose linked to α-1,4 glycosidic linkages of the ring polysaccharide, resulting in a melting point between 300 and 350 °C and a degree of polymerization of 7. β-CD is acid resistant, heat resistant, and alkali resistant and is not easily decomposed by enzymes. β-CD has a cavity diameter of between 7.0 and 8.0 nm, is easily embedded in oily substances, and can mask grease-specific odors, as the oil plays a role in emulsification. Grease is a hydrophobic substance closely related to β-CD and can avoid light, heat, and oxygen under reaction processes, thereby improving stability and enabling an extended shelf life.

Starch has the longest history of use as a capsule wall material. There are many different types of modified starches developed and successfully applied in different fields. Starch not only has a wide range of sources, but the molecule also contains a lipophilic group that aids it as an emulsion core material and the formation of stable systems. Starch is non-emulsifying but in high-solid concentrations exhibits a lower viscosity, which can be shared with a general emulsifier to improve the production of solids. The starch structure is loose and exhibits strong adsorption characteristics, with some modified starches showing good solubility, safety, and non-toxicity, and is a low-cost option. Microporous starch, also known as “porous starch,” exhibits amylase activity in starch gelatinization at temperatures below the threshold of starch granules produced by a honeycomb porosity of the modified starch, with hole diameters of ~1 μm. Microporous starch has a large specific surface area and is widely used in microcapsule processes.

7.1.2.2 Semisynthetic Polymer Materials

Some of the commonly used fiber derivatives are characterized by increased solubility after salting, easy hydrolysis, low toxicity, high viscosity, and the need for fresh preparation. These reactions should not be undertaken at high temperatures. Common semisynthetic polymer materials include ethyl cellulose, methyl cellulose, phthalic acid acetate cellulose, and sodium carboxymethyl cellulose.

7.1.2.3 Fully Synthetic Polymer Materials

Common synthetic polymer materials include polyvinylpyrrolidone, polyamide, polyethylene ethanol, and polyethylene glycol. All synthetic polymer materials and films exhibit good chemical stability, with recent synthesis of biodegradable wall materials for in vivo use attracting high levels of attention.

7.1.3 Research into Amylose Microcapsule Wall Materials

Amylose is a linear polysaccharide derived from D-glucopyranose units from α-1,4-glycosidic linkages, which can form complexes with some inorganic or organic groups to form helical configuration. The molecular weight of amylose ranges from 5 million to 200 million daltons, with a degree of polymerization ranging from 300 to 1200. Amylose is widely found in a variety of food crops and is a natural polymer compound. Amylose content in different food crops varies, with the amylose content of natural starch between ~20% and 30%, higher in potato and corn, and that in common cornstarch at ~25%, whereas high-chain cornstarch contains ~70% amylose, and waxy cornstarch contains almost no amylose.

Amylose use uses intramolecular hydrogen bonds, with some flavor molecules, such as iodine, lipids, alcohols, and surfactants undergoing formation of single helical structures. The most common of these is amylose-lipid clathrate, which is generally present in native starch and can be formed by the addition of lipids or during starch coagulation. Similar to the structure of cyclodextrin, the hydrophobic nature of the guest molecules in amylose-flavor-molecule complexes is transferred from the water to the weakly polar environment inside the amylose spiral. This encapsulates the hydrophobic region of the complex inside the starchy spiral structure, with the hydroxyl group of the glucose unit located on the outer surface of the helix to enable formation of a more hydrophobic cavity inside. The inner diameter of the helical structure is determined by the size of the object, with each helix potentially consisting of six to eight glucose units. Each helix often contains six glucose groups, with each inclusion compound containing two or three helices. Compared with the commonly used carbohydrate dextrin, amylose is more likely to interact with more guest molecules, because dextrin is limited by the size and shape of the guest molecules. This enables amylose to have wider potential applications.

7.2 Starch-Lipid and Starch-Protein Complex Preparation and Their Properties

7.2.1 Amylose Preparation and Optimization

Starch is a mixture of amylose and amylopectin; therefore, it is not a single substance, unlike amylose, which is a linear molecule of polysaccharides. However, amylose and amylopectin in the structure exhibit very different chemical activities.

Amylose and amylopectin are not homogeneous in size, which varies greatly according to characteristics of polydispersity. In amylopectin, the crystal area is small, the molecules in the crystal structure are not packed, and the starch granules are large. Amylose particles are small, the degree of association between the molecular chain and the molecular chain is large, and the microcrystalline crystal is compact, with a large crystal area. Amylose particles are small, and the associated crystal structures show tightly packed molecules. Hydrogen bonds involved in the degree of association are such that water molecules are unable to break the bonds, indicating that amylose molecules contain multiple intramolecular bonds in the absence of water molecules. This enables amylose to be dissolved in water, whereas amylopectin exhibits low viscosity. Amylose starch exhibits a strong cohesive sedimentation performance in cold aqueous solution, and amylopectin has a large molecular weight. The force between molecules is reduced due to branching, enabling water molecules to easily incorporate into amylopectin within the microcrystalline beam, thereby hindering amylopectin agglomeration and promoting amylopectin sinking in solution. These characteristics result in the differences in industrial use between the two molecules [15].

According to these differences, amylose extraction methods involve salting out, aging, selective leaching, complete dispersion, and enzyme desorption. The select leaching method is only applicable in dilute starch suspensions but is a low-cost method resulting in decreased purification efficiency. Salting out, aging, and enzymatic desorption allow precipitant formation, which is obtained by centrifugation. The resulting purity of the amylose acquired by this method and in the presence of amylopectin is low; however, amylose samples purified by lye dispersion result in high levels of purity in the absence of amylopectin.

7.2.1.1 Amylose Separation and Purification

Cornstarch contains an amylose content of ~25%. The specific extraction method is as follows:

1. Weigh 10 g cornstarch, and add a small amount of anhydrous ethanol to evenly disperse the sample. Ethanol allows hydroxyl dispersion of starch to preclude aggregate formation. Additional starch can then be added until complete dispersal, no paste formation, and a milky white coloration forms.

2. Prepare 0.5 M sodium hydroxide in advance, and stir into the starch emulsion until the starch emulsion is viscous and transparent, without flocculation or block formation, and is evenly distributed. The mixture is then stirred in a boiling water bath for 20 min until completely dispersed, with stirring continuing while cooling to room temperature.
3. The resulting starch alkaline solution is centrifuged at 6000× g for 20 min, and the supernatant is adjusted to (pH 7) with 2 M hydrochloric acid with continuous stirring.
4. N-butanol-isoamyl alcohol (3:1, v/v) was added to 100 mL of the solution, heated in a water bath, and stirred for 20 min, followed by cooling to room temperature. The solution is covered in plastic wrap and placed in the refrigerator for 24 h.
5. Discard the upper layer of dirt, and then centrifuge 6000× g, for 20 min; after the completion of removal of supernatant, the precipitate is the initial purification of amylose.
6. The resulting precipitate was poured into a saturated aqueous solution of 120 mL of n-butanol and stirred and dispersed. The mixture was heated in a water bath and allowed to dissolve for ~15 min to remove remaining lipids and soluble impurities. The solution is cooled to room temperature and transferred to the refrigerator for 24 h.
7. The upper layer of pollutants is discarded and centrifuged at 6000× g for 20 min, and the precipitate plus 120 mL n-butanol solution is dissolved by heating, followed by repetition of the purification process in triplicate.
8. The precipitate is immersed in 100% ethanol solution for 24 h to remove the organic solvent prior to centrifugation at 6000× g for 20 min. The resulting precipitate was washed repeatedly with 100% ethanol to obtain high-purity amylose.

7.2.1.2 Amylose Drying

The resulting amylose is dried in two ways: a blast-drying method and a vacuum freeze-drying method. The blast-drying method involves drying the sample in a blast oven at 40 °C for 8 h to obtain dried pure amylose. Vacuum freeze-drying occurs after the sample is frozen for 24 h, followed by placement in a vacuum freeze dryer for 12 h to get obtain dried pure amylose.

Vacuum freeze-drying requires the wet material or solution to be frozen (~−50 to −10 °C) into a solid state, followed by drying in a vacuum (~1.3 to 13 Pa) to avoid direct sublimation of water into gas. As the material during sublimation dehydration has been frozen before the formation of a fixed solid skeleton, this remains essentially unchanged. Two kinds of amyloses obtained from two different drying methods can be compared according to molecular weight and spectral absorption characteristics.

7.2.1.3 Molecular Weight of Two Kinds of Amylose

The relative molecular mass of the prepared amylose starch is determined by high-performance gel permeation chromatography (GPC) to determine differences in amylose of maize. The extracted amount (2–6 mg) of corn amylose is dissolved in ~3 mL of the mobile phase, which can be heated to facilitate its dissolution (the mobile phase is an analytically pure solution of deuterium oxide), followed by filtration using a 0.45-μm microporous membrane into the GPC vial.

Figures 7.1 and 7.2 and Table 7.1 show that the uniformity of starch No. 2 exhibited better chromatographic peak distribution than No. 1, and the peak molecular weight of sample No. 2 was also greater than that of No. 1. Notably, the two kinds of starch were separated and purified using the same method, but different drying methods resulted in a greater impact. A previous study [16] reported the effects of extraction temperature on the amylose component distribution of maize with molecular weight of between ~8 14×10^4 and 14×10^4 Da. The molecular weight of amylose was consistent with the literature; however, the molecular weight of starch No. 1 differed from previous reports. These findings showed results of the use of starch No. 2 corn amylose for preparation of a triplex complex.

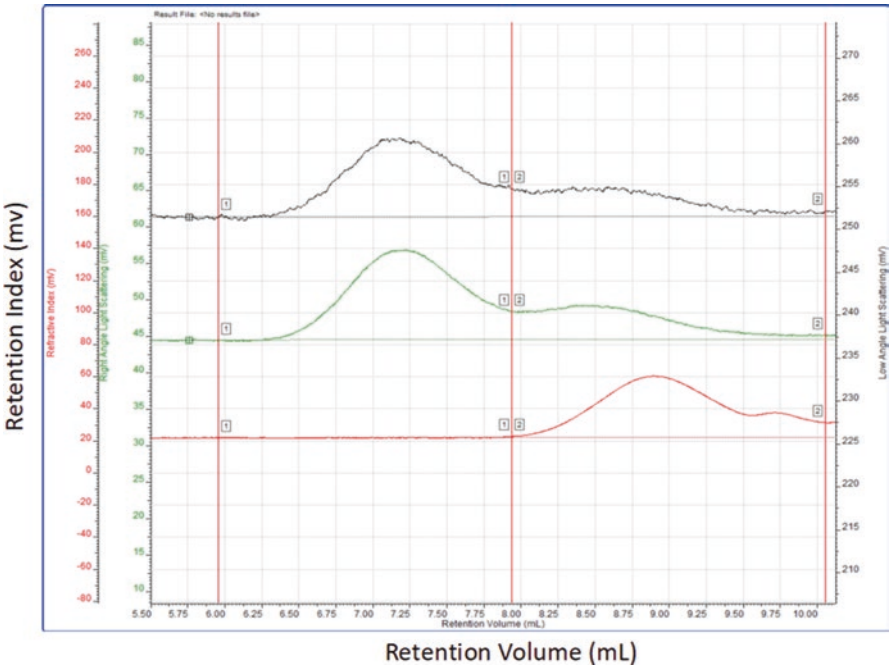

Fig. 7.1 Molecular weight distribution curve of amylose obtained from blast drying (black and green represent standard potato amylose, and red represents the sample prepared in our lab and is signified as No. 1)

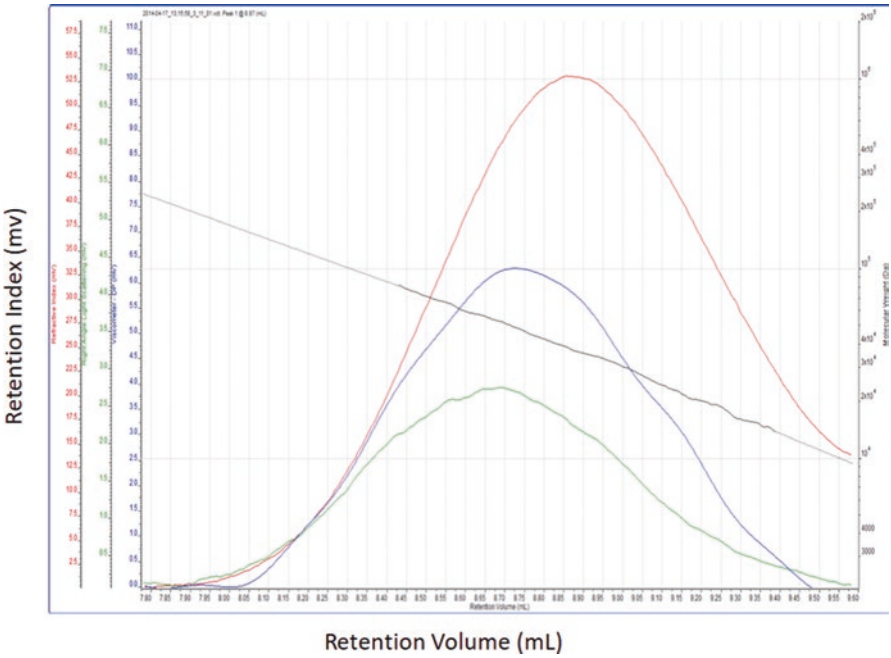

Fig. 7.2 Molecular weight distribution curve of amylose obtained from vacuum freeze-drying (black and green represent standard potato amylose, and red represents the sample prepared in our lab and is signified as No. 2)

Table 7.1 Comparison of molecular weight distribution of two kinds of amylose

	Name	M_n	M_w	M_P	M_w/M_n
1	No. 1	29,425	42,164	36,850	1.433
2	No. 2	85,525	149,822	101,911	1.752

No.1 represents amylose obtained from blast drying. No. 2 represents amylose obtained from vacuum freeze-drying. M_n, number-average molecular weight; M_w, weight-average molecular weight; M_P, peak molecular weight; M_w/M_n, ratio of M_w and M_n

7.2.1.4 UV-Vis Absorption of Two Kinds of Amylose

The lowest energy level is referred to as the ground state, and the stability of the ground state is usually the highest. Energy levels exceeding the ground state are referred to as excited states. The translational energy of a molecule is continuous, non-quantified, and independent of the absorption spectrum, and the electrons, vibrations, and rotations in the molecule belong to the motion inside the molecule, with their corresponding energy levels being discontinuous and quantized. When light at the appropriate frequency illuminates atoms or molecules at the ground state and the energy possessed by the photon is exactly equal to the energy difference between the excited state and the ground state, the energy of the photon will transfer to the atom or molecule to allow transition from the ground state to the excited state

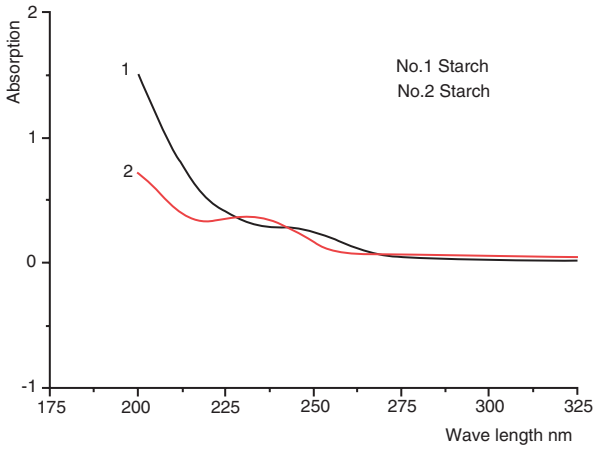

Fig. 7.3 UV absorption spectra of two kinds of amylose

while generating absorption spectra. The wavelength of the far-ultraviolet region ranges from 10 to 200 nm, and the wavelength of the near-ultraviolet region ranges from 200 to 380 nm. The far-ultraviolet region is also known as vacuum UV, and the near-ultraviolet region is also called quartz ultraviolet. Here, we used the near ultraviolet region, and data were analyzed using the Origin software (v8.0; OriginLab, Northampton, MA, USA).

As shown in Fig. 7.3, the two samples of corn amylose show strong absorption peaks in the range of 220–250 nm, indicating the presence of two conjugated unsaturated bonds (conjugated diene or α,β-unsaturated aldehydes and ketones) and the presence of carbonyl or conjugated carbonyl groups in the range of 250–350 nm. The carbonyl content of amylose No. 1 was greater than that of No. 2, indicating a higher degree of oxidation. Previous studies on banana taro starch using the lye dispersion method to extract amylose showed UV-vis absorption spectrum determination curves ranging from 200 to 400 nm at low-intensity absorption, but without an absorption peak. Compared with cornstarch, there is no carbonyl group in the amylose of banana taro, and the degree of oxidation is low, resulting in different types of extracted amylose from different plants.

7.2.1.5 Infrared Absorption of Two Kinds of Amylose

The wavelength of infrared light is in the range of 0.75–300 μm, and the infrared spectrum is further divided into three regions: near infrared (λ = ~0.75 to 3.0 μm), mid-infrared (λ = ~3.0 to 30 μm), and far infrared (λ = ~30 to 300 μm). The general infrared absorption spectrum mainly refers to the infrared range, with a wave number between ~400 and ~4000 cm^{-1}. This experiment was measured in the range of mid-infrared, and data were analyzed using Origin software (v8.0; OriginLab). The resulting graph is shown in Fig. 7.4.

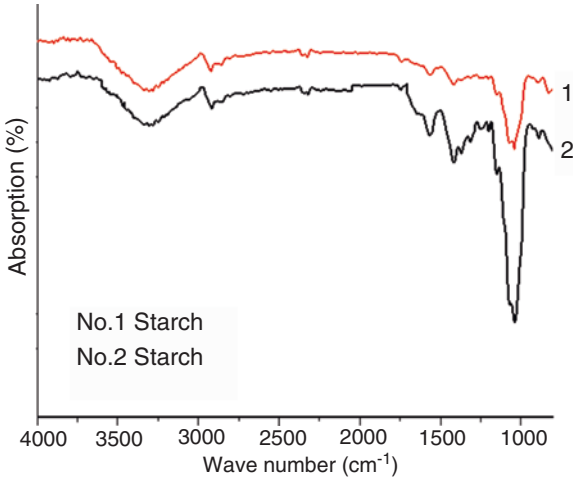

Fig. 7.4 Infrared absorption spectra of two kinds of amylose

As shown in Fig. 7.4, the two starches emitted in the ~1820 to ~1660 cm^{-1} region, indicating the presence of carbonyl groups in both starches. There were carbonyl absorption peaks in the range of ~1740 to ~1685 cm^{-1}, and there was no hydroxyl absorption in the vicinity of ~2820 cm^{-1} and 2750 cm^{-1}. The images of the two starches are similar in terms of the position and width of the absorption peak. Fertig et al.'s [17] determination of the corn amylose infrared-absorption spectrum showed a similar reading at 1700 cm^{-1} near the absorption peak, suggesting the presence of carbonyl groups.

Here, two kinds of amylose obtained by the blast-drying method and the vacuum freeze-drying method were, respectively, analyzed by UV-vis spectroscopy and infrared spectroscopy. The results showed similarities in the spectra of the two starches, whereas starch No. 2 showed a higher molecular weight starch and greater homogeneity relative to starch No. 1. The starch yield was 3.4% and 25.9%, and the dissolution rates were 40% and 36% for starches No. 1 and No. 2, respectively. Therefore, nano-capsules were prepared using the method of vacuum freeze-drying.

7.2.2 Preparation and Characterization of the Amylose/α--Linoleic Acid/β-Lactoglobulin Triplex

In a previous experiment, we found that the order of addition of starch, α-linoleic acid, and β-lactoglobulin, as well as the method used for the addition, greatly influenced the preparation of the amylose solution. Therefore, we made some adjustments and performed experiments according to these factors. By direct observation of the transparency and uniformity of the obtained liquid, we determined that the

best method involved initially heating and stirring the amylose (95 °C at 450 r/min for ~75 min; starch/α-linoleic acid/β-lactoglobulin = 20:5:1 (w/w/w)). α-Linoleic acid dissolved in absolute ethanol was added first and stirred prior to the addition of β-lactoglobulin aqueous solution. After stirring for 20 min in a water bath at 450 r/min, the mixture was cooled to room temperature for 4 h and filtered using a 0.45-μm filter (Tansoole, Shanghai, China).

7.2.2.1 The Effect of Solution pH

The gelatinization temperature was 95 °C, the pH of the solution was 6.90, and half of the starch solution pH was subsequently adjusted to 5.0 using α-linoleic acid. The other half of the solution underwent addition of α-linoleic acid and β-lactoglobulin directly instead of changing the pH (95 °C at 450 r/min for ~75 min; starch/α--linoleic acid/β-lactoglobulin = 20:5:1 (w/w/w)). The mixture was heated and stirred for 20 min at room temperature for 4 h until the filtrate was analyzed by UV-vis spectrophotometry.

As shown in Fig. 7.5, the peak positions of the UV spectra for the two curves were completely different. The isoelectric point of β-lactoglobulin is between 5.1 and 5.3, and its structure and properties vary greatly with pH. In the reaction, at a pH of <5.1, β-lactoglobulin is a dimer and positively charged. At this point, the amylose/α-linoleic acid complex can interact to form the triplex complex, exhibiting an absorption peak of ~240 nm.

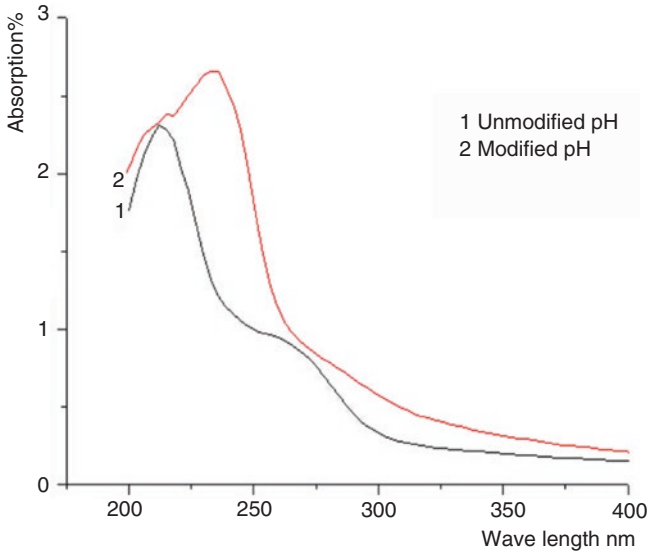

Fig. 7.5 The effect of pH on triplex complex formation

7.2.2.2 The Effect of Gelatinization Time

The gelatinization temperature was 95 °C at times for amylose of 60 min, 80 min, and 100 min, with solution pH adjusted using α-linoleic acid to 5.0 (95 °C at 450 r/min for ~75 min; starch/α-linoleic acid/β-lactoglobulin = 20:5:1 (w/w/w)). The solution was stirred for 20 min at room temperature for 4 h, and the filtrate was analyzed by UV-vis spectrophotometry.

As shown in Fig. 7.6, the UV spectra of curves 1 and 2 were similar in shape and the characteristic peaks, whereas curve 3 showed a blue shift at the position of the absorption peak. After starch gelatinization, the solution became a homogeneous paste, and light transmission decreased, while the absorbance increased on the UV spectrum. The longer gelatinization time resulted in higher degrees of amylose gelatinization via increased degrees of interaction with α-linoleic acid and β-lactoglobulin. At 230 nm, curve 2 was larger than curve 1 in absorption peak intensity, indicating a high degree of starch gelatinization.

Amylose is a wall material, and the optimal preparation conditions involve encapsulation of α-linoleic acid and β-lactoglobulin at amylose gelatinization time of 80 min at 95 °C. Ethanol solution was used for solution titration to pH 5.0 (95 °C at 450 r/min for ~75 min; starch/α-linoleic acid/β-lactoglobulin = 20:5:1 (w/w/w)). After stirring for 20 min in a water bath at 450 r/min and cooling at room temperature for 4 h, the solution was filtered with a 0.45-μm filter (Millipore) before freeze-drying.

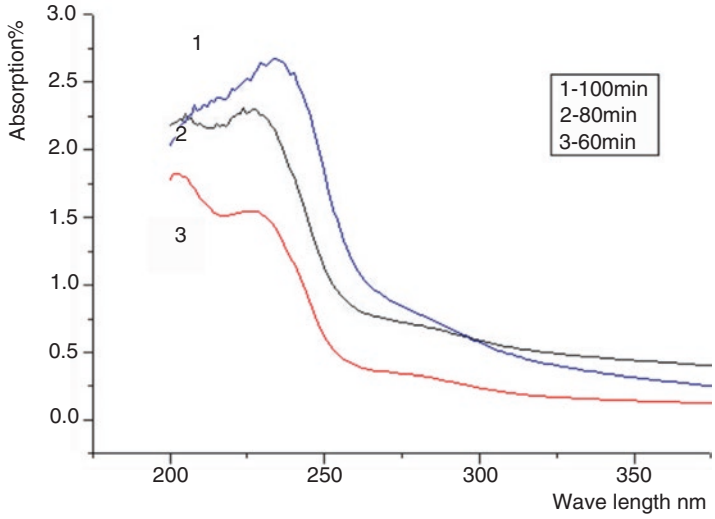

Fig. 7.6 The effect of gelatinization time on triplex complex formation

7.2.2.3 SEM Analysis of the Triplex Complex

This method requires pasting of double-sided adhesive on the sample table and placing the appropriate amount of sample powder on the double-sided adhesive prior to applying enough pressure to trap the thin layer of the inclusion powder on the conductive double-sided adhesive base. A blade is then used to scratch the surface of the excess sample powder for observation after applying gold via spraying. Because the blade can break the microcapsule structure, the number of profiles needs to be increased in the internal structure. In this study, SEM detection was used at a 5000× magnification. The amylose/α-linoleic acid/β-lactoglobulin mixture in the sample was prepared by adding the same amount of α-linoleic acid solution and β-lactic acid solution after the amylose was dissolved by heating with stirring at 25 °C for 20 min at 450 r/min. The solution was then cooled to room temperature and stirred for 4 h prior to filtration (0.45-μm filter; Millipore) and vacuum drying.

Formation of the triplex complex as visualized by SEM is shown in Fig. 7.7. The amylose surface structure was smooth and almost flat, and β-lactoglobulin was flaky, with a smooth surface. The image in Fig. 7.7c shows that the amylose/α--linoleic acid/β-lactoglobulin mixture formed a large structure that was structurally flat and solidly textured. Because the amylose/α-linoleic acid/ β-lactoglobulin mixture is only dissolved by physical heating without stirring, the molecules exist only between the simple physical plane and do not produce complex three-dimensional (3D) structures. Figure 7.7d shows that the triplex complex showed no obvious plate structure, and its 3D structure lacked a strong and solid texture. These results showed that the spatial structure of the amylose/α-linoleic acid/β-lactoglobulin mixture and the triplex complex were quite different.

7.2.2.4 TGA of the Triplex Complex

TGA is used to measure relationships between the mass and temperature or time at the programmed temperature. The main feature of thermogravimetry is its highly quantitative and accurate measurement of changes in mass and the rates of those changes. This method is useful as long as the material exhibits qualitative changes. The TGA curve is characterized by its ability to accurately reflect the initial reaction temperature, the maximum reaction rate temperature, and the reaction termination temperature for each weight-loss stage. The area of each peak on the primary derivative TG curve (DTG) corresponds to that on the TG curve, and the weight loss of the sample is proportional to the DTG curve when the TG curve is unclear for some heating processes [18].

Determination of specific methods involves initial indium calibration, followed by the transfer of the same amount of sample (3–5 mg) to a small crucible. The temperature is set to between ~30 and 160 °C at a heating rate of 10 °C/min, and nitrogen is used as the protection gas. The instrument records the sample temperature, quality, and other related data automatically. Data were analyzed using the Universal Analysis V4.5A instrument software (TA Instruments, New Castle, DE, USA).

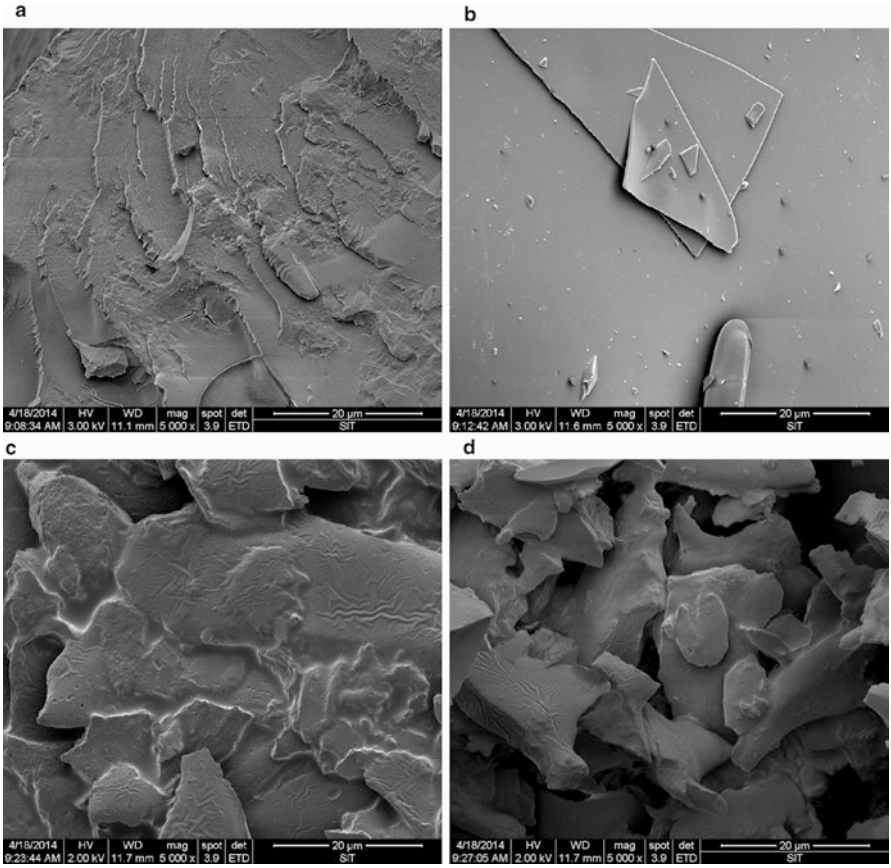

Fig. 7.7 SEM analysis of the triplex complex. (**a**) Amylose, (**b**) β-lactoglobulin, (**c**) amylose/α--linoleic acid/β-lactoglobulin mixture, and (**d**) the amylose/α-linoleic acid/β-lactoglobulin triplex complex

Figure 7.8 shows that amylose underwent two weight-loss stages during the heat-loss stage and thermal decomposition, whereas the amylose/α-linoleic acid/β--lactoglobulin mixture underwent four weight-loss stages corresponding to the processes of water loss, α-linoleic acid evaporation, amylose melting phase transition, and amylose heat decomposition. From the TGA diagram of the triplex complex, only two larger weight-loss stages were observed corresponding to the melting phase transition and the thermal cracking stage of the complex. Due to formation of the inclusion complex, the temperature of the melting phase transition was reduced, greatly increasing the stability of α-linoleic acid and β-lactoglobulin. Previous studies found that greater proportions of weight loss translated into worse stability. The amylose/α-linoleic acid/β-lactoglobulin mixture showed a greater weight-loss ratio as compared with the triplex complex, further demonstrating that the stability of the complex exceeded that of the mixture.

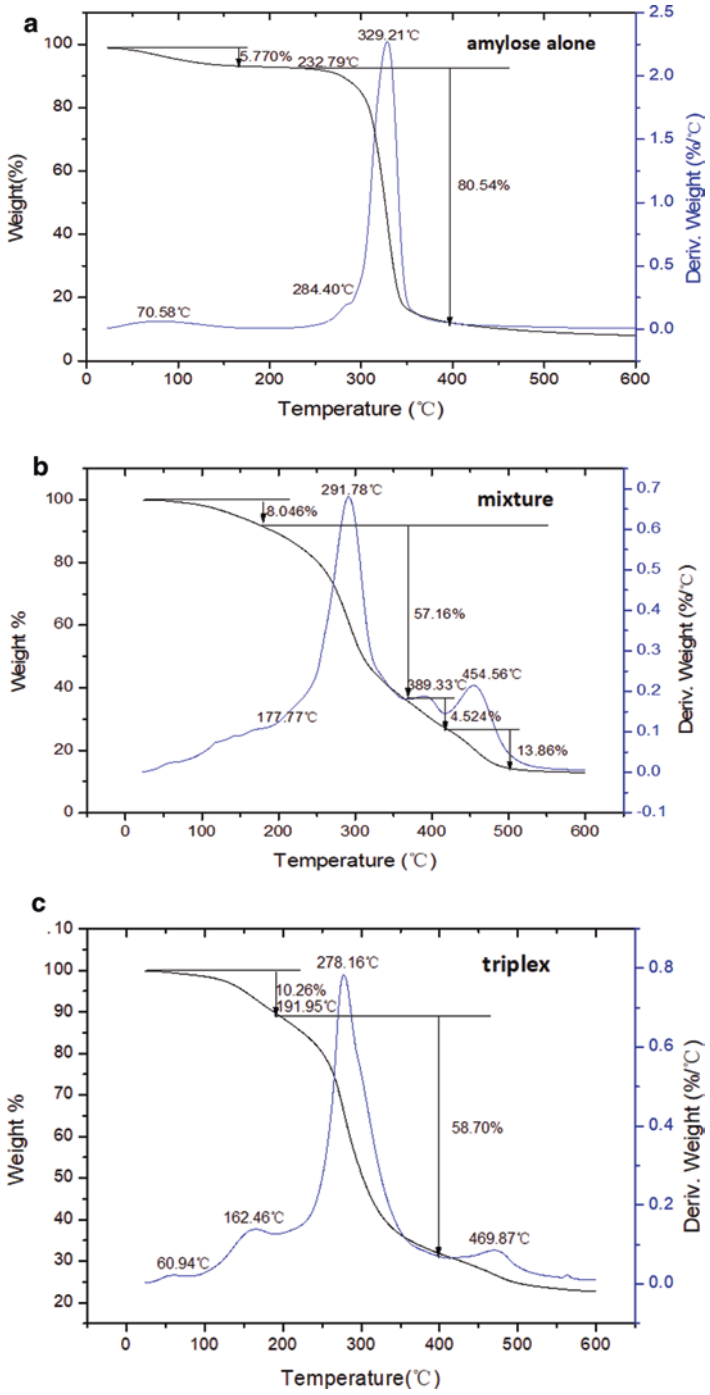

Fig. 7.8 TG curves. (**a**) Amylose alone, (**b**) the amylose/α-linoleic acid/β-lactoglobulin mixture, and the (**c**) amylose/α-linoleic acid/β-lactoglobulin triplex complex (Table 7.2)

Table 7.2 TG analysis of amylose, the amylose/α-linoleic acid/β-lactoglobulin mixture, and the amylose/α-linoleic acid/β-lactoglobulin triplex complex

Samples Results	Amylose	Amylose/α-linoleic acid/β--lactoglobulin mixture	Amylose/α-linoleic acid/β--lactoglobulin triplex complex
Total weight loss %	86%	83%	69%

7.2.2.5 DSC Analysis of the Triplex Complex

DSC allows measurement of changes in the heat flow rate with respect to the reference material under the control of temperature. DSC and DTA curve patterns show similarities based on sample temperature changes in the thermal effect generated for the detection of the foundation. DSC technology to overcome the DTA in the calculation of changes in heat is difficult in the process of obtaining thermal effects for quantitative data. This method is used to determine polymer heat thresholds, crystallinity, and isothermal crystallization kinetics. The glass transition temperature (Tg) can be measured, and reaction, polymerization, cross-linking, and decomposition can be studied. The ability to investigate reaction temperature and kinetic parameters is indispensable for conducting polymer research.

The method involves the use of the amylose/α-linoleic acid/ β-lactoglobulin mixture and the triplex samples in separate platinum crucibles along with an empty platinum crucible as a control. The temperature is changed at a rate of 10 °C/min using a scanning range of ~−60 to ~200 °C and nitrogen as a measurement gas. The DSC curve was recorded, and data were analyzed using TA-60s software (TA Instruments).

Figure 7.9 shows that amylose exhibited a characteristic absorption peak and an endothermic peak near its gelatinization temperature (98.1 °C and 87.27 °C, respectively) according to the DSC curve, which differed between the mixture and the triplex complex. The DSC curve of the mixture showed small absorption peaks at 75.5 °C and 145.9 °C and a large exothermic peak at 111.3 °C, whereas the triplex complex showed endothermic peaks at 85.3 °C and 114.9 °C and no exothermic peak. The peak temperature of the triplex complex was lower than that for amylose only, indicating that the formation of the triplex affected the peak gelatinization temperature of amylose. The most stable thermostructures were associated with changes in α-linoleic acid and β-lactoglobulin [19]. The findings suggested that DSC allowed a more complete analysis of the formation of the triplex complex.

7.2.2.6 XRD of the Triplex Complex

XRD patterns change based on different molecular constructs; therefore, the formation of an inclusion complex consisting of amylose, α-linoleic acid, and β-lactoglobulin will alter XRD patterns from those observed in the separate molecules. Multiple studies reporting several different crystal structures have been

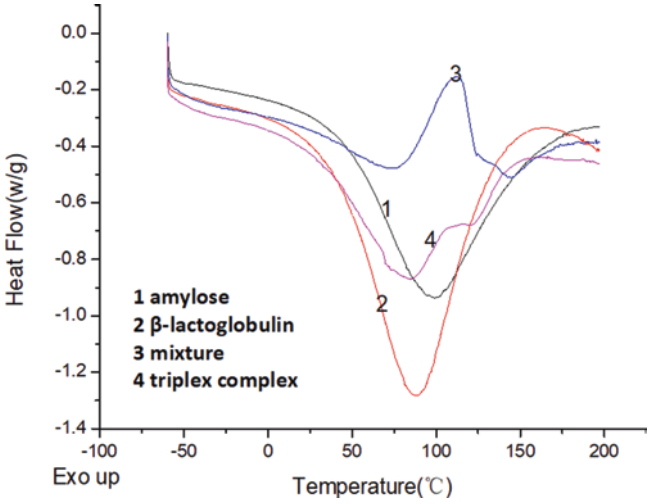

Fig. 7.9 DSC curves. *1* Amylose. *2* β-Lactoglobulin. *3* Amylose/α-linoleic acid/β-lactoglobulin mixture. *4* Amylose/α-linoleic acid/β-lactoglobulin triplex complex

obtained by X-ray crystallography involving different crystallographic solutions consisting of six or seven glucose residues. There are also other molecules consisting of eight glucose residues per starch and capable of allowing crystal formation. Additionally, studies of inclusion complex formation by highly linear cornstarch and unsaturated free fatty acids, limonenes, and thymols showed that highly linear cornstarch can form different crystals with different molecules. The inclusion complex of limonene, thymol, and highly linear amylose cornstarch was V6 (i.e., containing six droplets per helix), with characteristic peaks (2θ) at 7.1°, 12.9°, and 17.8°. Highly linear amylose corn clathrate formed by the amylose was V7 (i.e., containing seven drops per helix), with type characteristic peaks (2θ) at 13.7° and 20.6°. The experiment analyzed the complexes and mixtures of amylose and amylose/α-linoleic acid/β-lactoglobulin using a wide-angle X-ray diffractometer. The measuring current was set to 30 mA and 30 Kv, the divergence-slit width was 0.2 mm, the diffraction-slit width was 0.6 mm, and the receiving-slit width was 0.2 mm. The diffraction angle range was set to the thickness of the instrument ((2θ), 4–60°) using a scanning speed of 6°/min at a time interval of 0.4 s, with a step width of 0.02°. Data were analyzed using Origin software (v8.0; OriginLab).

Figure 7.10 shows the triplet complex, the mixture of the three molecules, and the XRD pattern of amylose. Curves 2 and 3 (the amylose solution) were similar to those for the mixture, exhibiting XRD peaks at ~8° and ~12°, respectively. The triplex complex (curve 1) differed significantly from the peak profiles of curves 2 and 3. Amylose clathrate showed a variety of diffraction peaks. The peak types for fatty acids and other molecules of the V6 type usually comprise six glucose residues and constitute a spiral, with characteristic peaks (2θ) at 12.9° and 17.8° [20]. The amylose and the other two molecules involved in formation of the triplex complex showed peaks consistent with a previous report [20]. We speculated that the inclu-

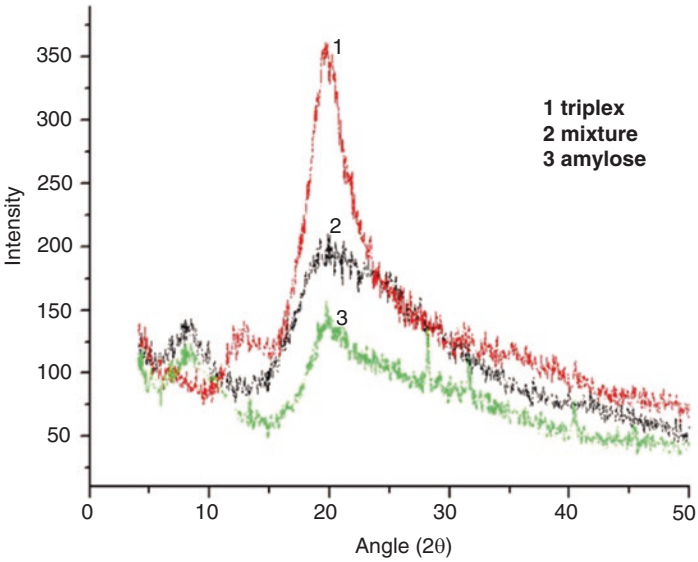

Fig. 7.10 XRD curves. *1* Amylose/α-linoleic acid/β-lactoglobulin triplex complex. *2* Amylose/α--linoleic acid/β-lactoglobulin mixture. *3* Amylose alone

sion structure (V6) consisted of a helical amylose triplex complex. These data suggested that amylose reacted with α-linoleic acid and β-lactoglobulin to produce the triplex complex.

7.2.2.7 UV-Vis Absorption of the Triplex Complex

We used a quartz cuvette to measure the UV spectra of α-linoleic acid dissolved in 100% ethanol and amylose dissolved in distilled water. Data were analyzed using Origin software (v8.0; OriginLab).

As shown in Fig. 7.11, the UV spectra of the mixture of amylose and the amylose/β-lactoglobulin/α-linoleic acid showed consistencies at the characteristic peak positions. Additionally, the use of the other two feedstocks enhanced UV absorption, with the maximum absorption peaks for the amylose/β-lactoglobulin/α-linoleic acid triplex complex undergoing a blue shift following the addition of amylose. Furthermore, reactions between the other two raw materials changed the molecule substituents, thereby causing a shift in the maximum absorption wavelength to the left.

7.2.2.8 Infrared Spectroscopy of the Triplex Complex

All samples were vacuum freeze-dried to solid form, and the triplex complex and mixture solution were ground into a powder. Data were analyzed using Origin (v8.0; OriginLab).

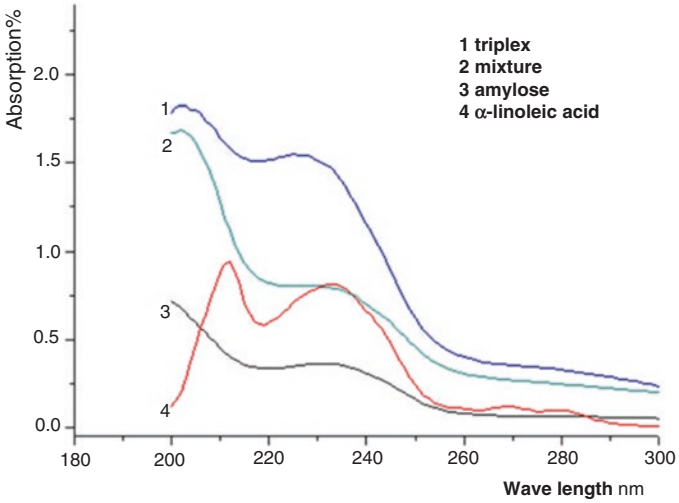

Fig. 7.11 UV absorption curves. *1* Amylose/α-linoleic acid/β-lactoglobulin triplex complex. *2* Amylose/α-linoleic acid/β-lactoglobulin mixture. *3* Amylose. *4* α-Linoleic acid

As shown in Fig. 7.12, the infrared spectra of the amylose/β-lactoglobulin/α--linoleic acid triplex complex and solution differed significantly between curves 2 and 3 (1700 cm^{-1} vs. 3400 cm^{-1}, respectively). The absorption peak width of the triplex complex was larger than that of the mixture solution, likely a result of the hydrogen bonds formed during interactions between the raw materials. These findings suggested that interactions between the three constituents resulted in complex formation.

In the preparation of amylose starch, cornstarch was washed with n-butanol and isoamyl alcohol to remove impurities, such as proteins and lipids, followed by vacuum drying to obtain highly pure amylose. The amylose was dissolved using the heat melting method and then aged at 95 °C. At pH 5.0, the amylose content of the amylose/α-linoleic acid/β-lactoglobulin (20:5:1, w/w/w) was incorporated by stirring for 20 min at 450 r/min and cooled at room temperature for 4 h, followed by filtration through a 0.45-μm filter (Millipore) and vacuum-dried to prepare the triplex complex. The resulting nanoparticles had exhibited very good stability.

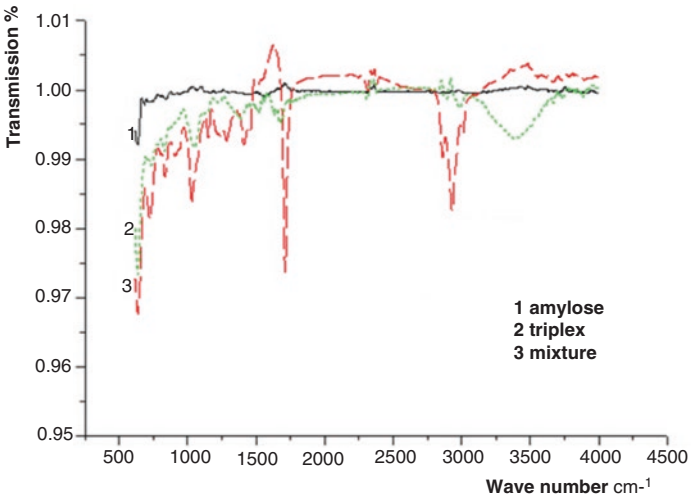

Fig. 7.12 Infrared absorption spectra. *1* Amylose. *2* Amylose/α-linoleic acid/β-lactoglobulin mixture. *3* Amylose/α-linoleic acid/β-lactoglobulin triplex complex

7.3 Complexation Behavior of Starch-Lipid and Starch-Protein Complexes

Amylose and lipids can form complexes. And the presence of ligands in complexes leads to the formation of tight helical structures with hydrophobic cavities. The nonpolar ends of lipid molecules enter these spiral cavities with the C-terminal end extending outside of the cavity [21]. Helix formation might be induced by lower free energy of the ligand in the helix cavity [22]. The driving force for the creation of these complex structures should be the tendency of amylose to minimize its interaction with water via interactions associated with van der Waals forces and hydrogen bonding, which occur between residues in the helix and add stability [23]. By contrast, these forces stabilize interactions between amylose and its ligand [8].

Amylose is a fatty acid complex that shows a V-type X-ray pattern and normally consists of six glucose residues per turn, which forms a left-handed helix [24]. The complexes formed by amylose and long-chain fatty acids have been studied by Zabar et al. [25] at the nanoscale and micrometer scales, but not at the atomic level. Although previous reports on the formation of stable complexes by amylose and α- linoleic acid are abundant, few focused on complexation behavior and mechanisms at the atomic level. MD simulations allow a method to analyze this activity, and with the rapid development of computer technology, this method has become an important tool for predicting system stability, verifying theoretical assumptions, and improving theoretical modeling. MD simulations have previously been undertaken in amylose studies [26].

Here, we used MD simulations to investigate complexation behavior between amylose and α-linoleic acid and to illustrate the mechanisms associated with FFA

stabilization of amylose conformation at the atomic level. The thermostable conformation of the amylose-α-linoleic acid complex and changes in hydrogen bonding patterns during complexation are also to be discussed.

7.3.1 Study on the Complexation Behavior of Amylose and α-Linoleic Acid

7.3.1.1 Molecular Dynamics (MD) Method

Models of Amylose and α-Linoleic Acid

The molecular model of V amylose employed in this study was kindly provided by Dr. Gregor Fels. This amylose model contains a sixfold left-handed helix with 55 glucose residues. The resulting helical structure measures ~54 nm for the inner diameter and 135 nm for the outer diameter and is ~738 nm long. Due to the differences in glycosidic linkages, "GLC," "GLM," and "GLK" were used to represent the initial, middle, and end glucose residues in the amylose structure. The file for the Protein Data Bank (PDB) for α-linoleic acid was downloaded from http://xray.bmc.uu.se/hicup/EIC/ and contains 20 atoms selected from the MSDchem database. The initial structure of α-linoleic acid was generated by the PRODRG server (http://davapc1.bioch.dundee.ac.uk/prodrg/). EIC was used to represent α-linoleic acid.

Force Field

The force field was parameterized according to previously described methods [27, 28]. All simulations were performed in a simulated water box with SPC glucose force fields aligned according to the amylose structure. The labels of the atoms are shown in Fig. 7.13, and the charges of the atoms were shown in Table 7.3.

MD Procedure

Leapfrog of motion was integrated with the Gromacs MD package (http://www.gromacs.org/) using a 2-fs time step for 2,500,000,000 simulation steps for a total simulation time of 500 ns. The LINCS algorithm was used to constrain all bonds, including heavy atom-hydrogen bonds, and lengths (lincs_iter = 1; lincs_order = 4). The temperature was maintained at 373 K by modified Berendsen thermostat coupling between different groups, with relaxation times of 0.1 ps. The pressure was

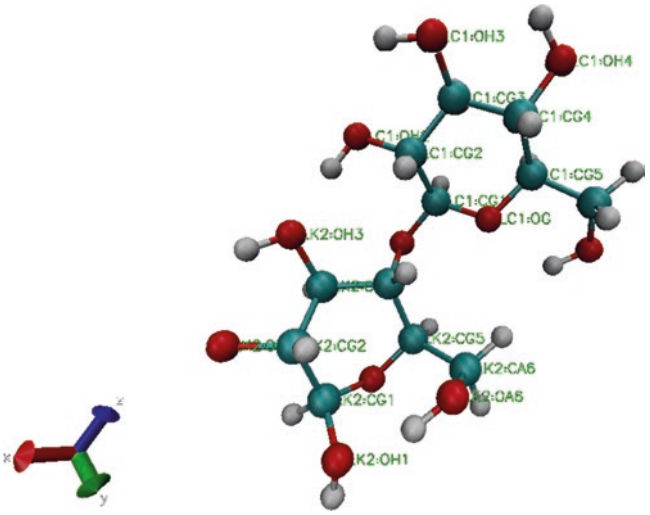

Fig. 7.13 Atomic labels used in the glucose topological structure

Table 7.3 Charge distribution of atoms in glucose topological structure

Atomic label	Atomic type	Charge	Number
OG	opls_180	−0.400	1
CG1	opls_193	0.300	1
HG1	opls_196	0.100	1
OH1	opls_186	−0.400	1
CG5	opls_183	0.170	1
HG5	opls_185	0.030	1
CA6	opls_157	0.145	2
HA1	opls_140	0.060	2
HA2	opls_140	0.060	2
OA6	opls_154	−0.683	2
HA6	opls_155	0.418	2
CG2	opls_174	0.205	3
HG2	opls_176	0.060	3
OH2	opls_169	−0.700	3
HO2	opls_170	0.435	3
CG3	opls_174	0.205	3
HG3	opls_176	0.060	3
OH3	opls_169	−0.700	3
HO3	opls_170	0.435	3
CG4	opls_174	0.205	3
HG4	opls_176	0.060	3
OH4	opls_169	−0.700	3
HO4	opls_170	0.435	3

Note: OG, CG1~CG5, and HG1~HG5 represent oxygen, carbon, and hydrogen atoms in the ring structure of glucose, respectively. OH1~OH4 represents hydroxyl oxygen atoms in the ring structure of glucose, and HO2~HO4 represents hydroxyl hydrogen atom in the ring structure of glucose. The atom labels all correspond to the atomic labels in Fig. 7.1

maintained at 1.0 bar by Parrinello-Rahman coupling to a pressure bath via an isotropic coordinate, scaling with a relaxation time of 2 ps. Nonbonded interactions were handled using a neighboring grid cell cutoff scheme. Within a short-range neighbor list based on a cutoff of 0.9 nm, interactions were evaluated at every time step based on a pair list recalculated every five time steps. The short-range electrostatic cutoff radius of 0.9 nm and a short-range van der Waals cutoff of 1.4 nm were, respectively, evaluated simultaneously with each pair-list update and assumed to be constant [1].

Simulation and Analysis of Amylose and the Amylose Complex

Two simulations were performed, both of which initiated from the cylindrical 3D structure (the columnar structure of glucose formation, consisting of six glucose residues per turn). For amylose alone in water, the 55-mer amylose chain was placed in a cubic box (10×10×10 nm) containing 12,631 water molecules. Water molecules were simulated using the TIP4P model. Before initiating the MD simulation, the interchain energy was minimized by steepest descent. Simulations were run for 500 ns to obtain a stable conformation of amylose in water.

For the complex simulations, amylose and α-linoleic acid were mixed in advance. Under experimental pH conditions, the hydrogen proton at the C-terminus of α- linoleic acid would be completely dissociated, resulting in an overall negative charge. Therefore, a sodium ion was added to the system to balance the negative charge. The amylose starting structure represented a completely folded V-type, with the polar end of α-linoleic acid placed inside its spiral cavity. The 55-mer amylose and α-linoleic acid were placed in a cubic box (10×5×5 nm) filled with 12,631 water molecules, and simulations were run for 500 ns. All simulations and analyses were performed using Gromacs 4.6.1.

Analysis of the Conformational Cluster

We used a previously described method to determine the typical conformation from trajectories [29]. The root-mean-square deviation (RMSD) value of the adjacent atomic position of amylose was lowered by 0.2 nm at the cluster center. The process was repeated until no relevant trajectory was extracted (Fig. 7.14).

7.3.1.2 Dynamic Structural Changes in Amylose and Its Complex

After a 500-ns simulation, the trajectories of amylose and the amylose-α-linoleic acid complex were determined (Fig. 7.15). Both groups of simulations showed a large number of recombinations in the overall structure. Within 100 ns, α-linoleic acid was separated from amylose but reincorporated into the middle region of the amylose molecule at 200 ns where it remained until the end of the simulation. In the complex, amylose maintained an extended left-handed helical conformation

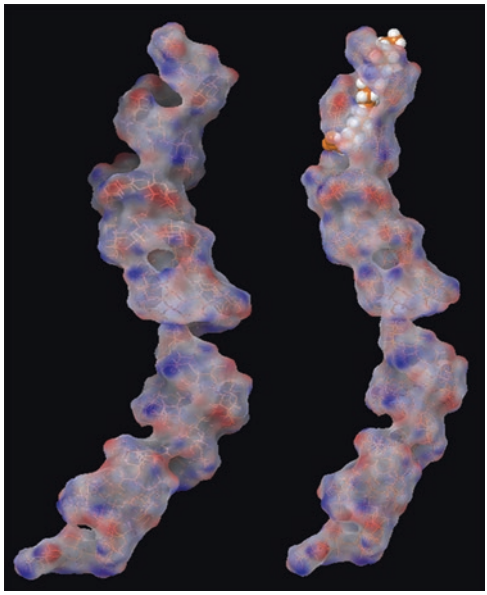

Fig. 7.14 Possible conformation of amylose during interaction with α-linoleic acid. The model was based on XRD test data. In the presence of α-linoleic acid, the amylose sample exhibited a spectrum of conformations in both single amylose (left) and α-linoleic acid (right). Amylose is colored according to its three elements: oxygen (red), carbon (white), and hydrogen (blue)

(Fig. 7.15a); however, in the absence of α-linoleic acid, amylose formed a completely folded conformation. Changes in amylose folding from the midpoint of the helix were also evident (Fig. 7.15b), suggesting higher degrees of conformational freedom in the amylose molecule relative to the amylose complex.

The displacement distance between the amylose backbone (GLK_GLM_GLC&CA6 and GLK) is shown in Fig. 7.15c. Within 500 ns, the average simulated displacement distances of the complex and amylose alone were 1.0 nm and 3.0 nm, respectively. These displacement-distance trajectories indicated that the atoms on the amylose backbone moved less in the presence of α-linoleic acid. When complexed with α-linoleic acid, amylose maintained a relatively stable conformation from 200 to 500 ns of the simulation, whereas in the absence of complex formation, amylose alone presented a twisted, unstable conformation for the duration of the simulation. A preliminary conclusion suggested that amylose conformation in aqueous solution was unstable but that its stability was greatly improved in the presence of α-linoleic acid. The consistency between the MD simulation and experimental results (amylose formed a stable complex with α-linoleic acid) confirmed that MD simulations provided a precise way to understand conformation changes in amylose in the presence of α-linoleic acid.

7.3.1.3 The Dynamic Shifts in Independent Amylose Domains During Amylose Complex Formation

The RMSD results associated with shifts in the amylose backbone relative to the GLC, GLK, and GLM domains are presented in Fig. 7.3. The RMSD values of the amylose-α-linoleic acid complex were consistently smaller than those for amylose alone, indicating that dynamic displacement changes in atomic positions were

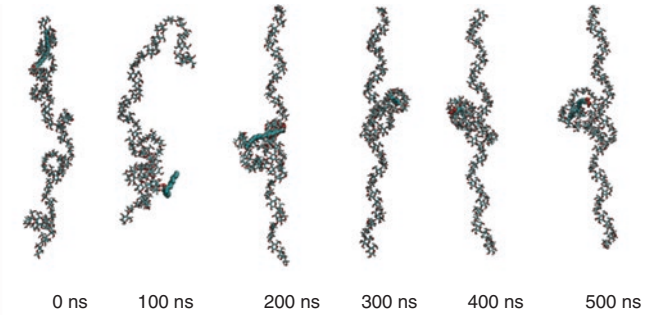

(a) The dynamic trajectories of amylose complexes from 0 ns to 500 ns.

(b) The dynamic trajectories of amylose from 0 ns to 500 ns.

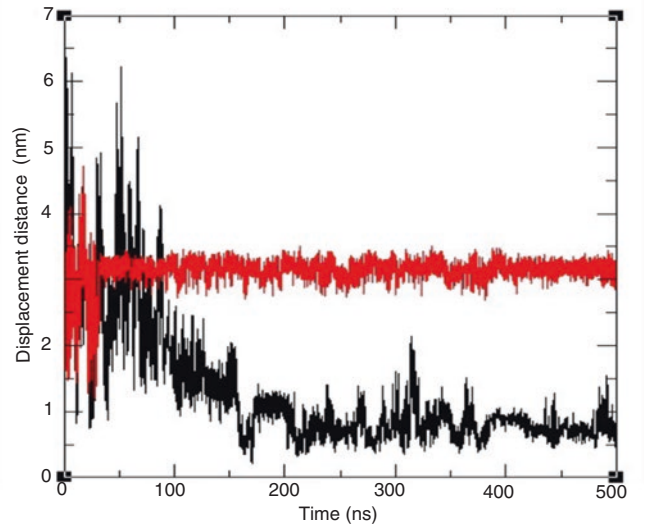

(c) The displacement distance between the amylose backbone (GLk_GLM_GLC&CA6) with GLk (red) of amylose alone and with GLK (black) of the amylose-α-linoleic acid complex.

Fig. 7.15 Conformation changes in and backbone displacement of amylose and the amylose-α-linoleic acid complex. (**a**) The dynamic trajectories of amylose complexes from 0 ns to 500 ns. (**b**) The dynamic trajectories of amylose from 0 ns to 500 ns. (**c**) The displacement distance between the amylose backbone (GLK_GLM_GLC&CA6) with GLK (red) of amylose alone and with GLK (black) of the amylose-α-linoleic acid complex

smaller in the complex. In both systems, the RMSD of the amylose backbone relative to the GLM domain were the most consistent, indicating that the GLM domain was the most stable of the three domains. RMSD changes in the amylose backbone relative to the GLC and GLK domains were more dramatic, with the GLC domain showing the largest change (7.0 nm in the complex; 6.0 nm in amylose alone). However, these changes only occurred within 100 ns of the start of the simulation, after which both systems remained in equilibrium, with the complex showing a lower RMSD value. In the two systems, the RMSD curve for the amylose backbone relative to the GLK domain followed a trend indicating atomic displacement distance between the GLK skeletons (Fig. 7.2c). In the presence of α-linoleic acid, the conformational rearrangement in the amylose molecule was less dramatic than that observed in amylose alone. These findings indicated that α-linoleic acid exerted a stabilizing effect on amylose conformation were consistent with the analysis of displacement distance and dynamic trajectories described in Fig. 7.16.

7.3.1.4 Differences in Hydrogen Bonding Between the Amylose-α-Linoleic Acid Complex and Amylose Alone

Generally, donor-acceptor distances <0.35 nm and bond angles <30° are considered geometric criteria necessary for the formation of hydrogen bonds [30]. The average numbers of hydrogen bonds formed between amylose-α-linoleic acid complex and amylose alone with water molecules were 50 and 40, respectively. These results indicated that the amylose complex attained a more compact conformation through the formation of additional hydrogen bonds, which played a major role in the polymerization and stabilization of the complex (Fig. 7.17).

7.3.1.5 Principal Component Analysis (PCA) of the Amylose-α-Linoleic Acid Complex and Amylose Alone

PCA is used to investigate the primary cumulative fluctuations in a structure. The simulated structure is projected onto a plane, which is constructed by the vector values of the two principal components of the covariance matrix. In both amylose alone and the amylose complex models, all simulation systems along the trajectory had overlapping and separated basic spaces. For amylose alone, the broader set of points were derived from the GLM domain, which showed a relatively extended and dispersed area during MD simulations. For the amylose complex, a localized and enclosed region was observed, indicating smaller conformational changes. In the two systems, the simulated structures covered wider spatial regions and were sufficient for comparison. Amylose alone showed a larger basic space, suggesting its higher range conformational changes and supporting the hypothesis that the presence of α-linoleic acid stabilized amylose conformation (Fig. 7.18).

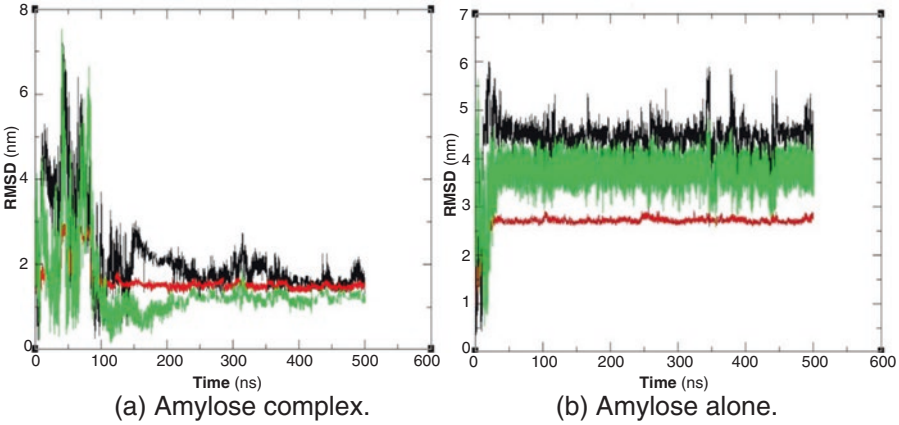

Fig. 7.16 RMSD results showing the shift in the amylose backbone relative to the GLC, GLK, and GLM domains. (**a**) Amylose complex. (**b**) Amylose alone

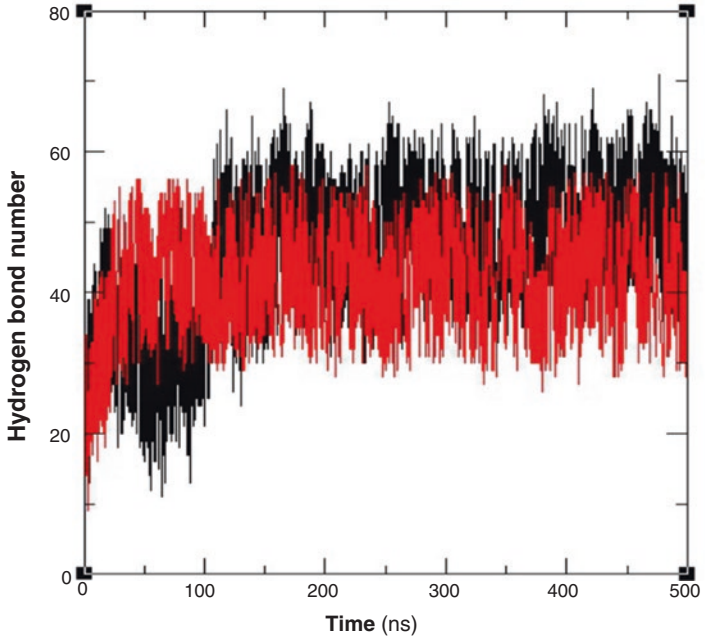

Fig. 7.17 The number of hydrogen bonds formed in amylose alone (red) and the amylose complex (black)

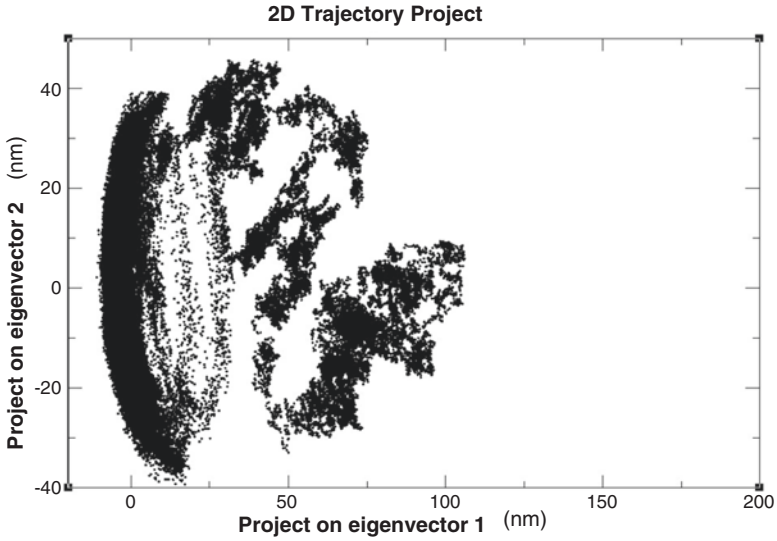

(a) The amylose complex.

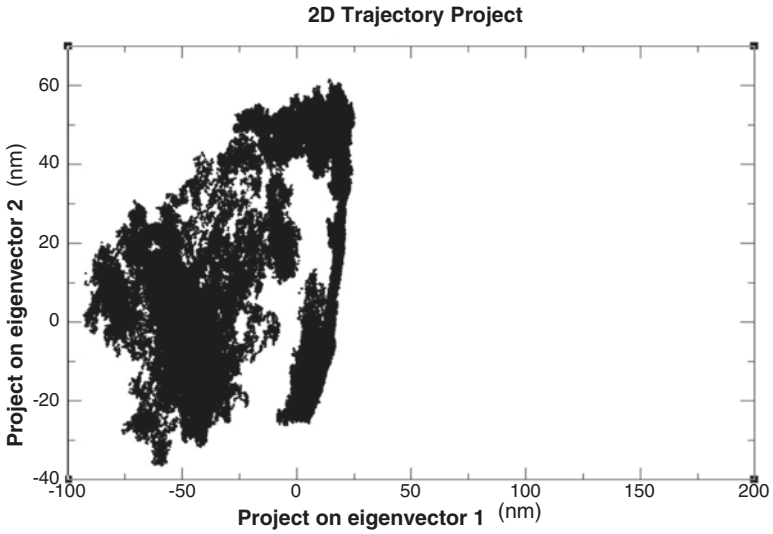

(b) Amylose alone

Fig. 7.18 PCA of the two simulation systems. (**a**) The amylose complex. (**b**) Amylose alone

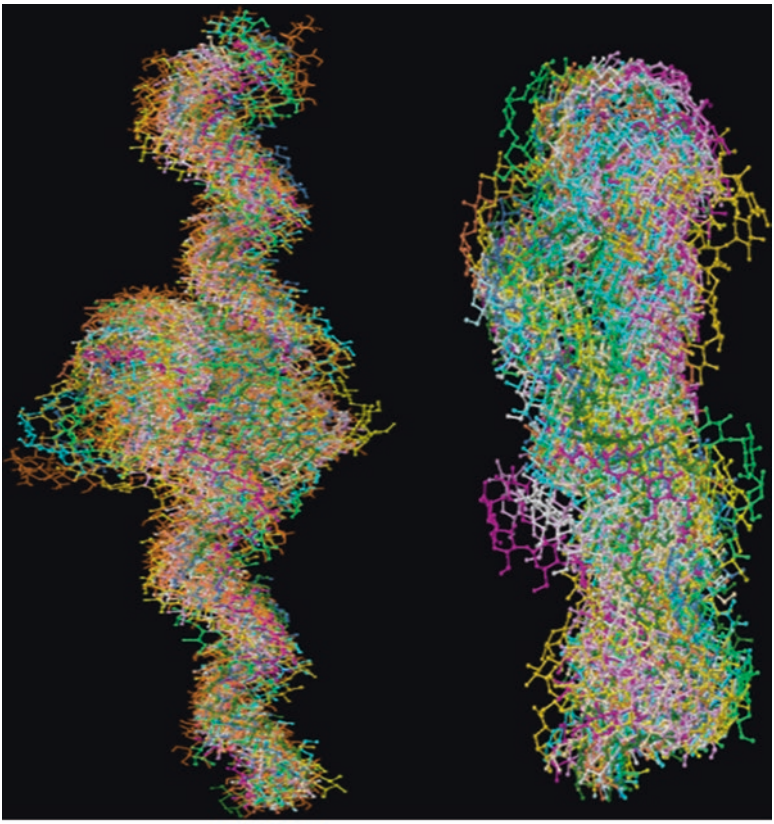

Fig. 7.19 Common conformational clusters for the amylose-linoleic acid complex and amylose alone. (**a**) The amylose complex. (**b**) Amylose alone

7.3.1.6 Common Conformational Clusters for the Amylose-α-Linoleic Acid Complex and Amylose Alone

The typical conformational clusters observed in the amylose-α-linoleic acid complex and amylose alone differed significantly (Fig. 7.19). The amylose complex showed more helical backbone groups, which increased the solvent-accessible surface area. The two conformational clusters also showed different hydration radii. The hydration radius of the amylose complex, exhibiting a stretched conformation, was 50% larger than that of amylose alone, which showed a relatively less stretched conformation. Similar conformational differences were previously reported in trialanine halide solution [31].

Conformation changes in amylose in the presence or absence of α-linoleic acid were investigated by MD simulation, during which α-linoleic acid stabilized amylose conformation relative to that observed in amylose alone. This conclusion was supported by the dynamic shift observed in the amylose backbone relative to that in

the terminal glucose residues, the displacement changes in the independent structural domains, and PCA of the amylose-α-linoleic acid complex. Furthermore, hydrogen bonding played an important role in the polymerization and structural stability of the amylose-α-linoleic acid complex. These results also confirmed the effectiveness of MD simulations for investigating the thermodynamic stability of complexes.

7.3.2 MD Simulation of the Self-Assembly Process of a Solute Nanoparticle Made from Maize Amylose/β--Lactoglobulin/α-Linoleic Acid

Many natural foods contain nanoscale ingredients often consisting of raw materials, such as proteins, starches, and lipids. Native β-lactoglobulin at ~3.6 nm can denature in conditions involving changes in pressure, temperature, and pH. In yogurt, denatured β-lactoglobulin can re-polymerize to larger fibrous and polymer structures, and heated starch granules are capable of releasing biopolymers that can recrystallize to nanostructures, such as recrystallized amylose at ~10 to ~20 nm. Lipids, such as monoglycerides, can attain a number of nano-level morphologies, including triglyceride crystals (10–100 nm), gather into clusters, undergo flocculation, and form fat crystal networks [32]. These nanomaterials are comprised of their respective individual components but can attain different structures upon complex formation.

Zhang et al. [33] found that a dilute ternary system consisting of starch, whey protein, and FFAs forms a water-soluble three-component complex after cooking. According to the high-performance size-exclusion chromatography (HPSEC) analysis, during the process of carbohydrate and iodine binding, FFAs play an important role in combining starches and proteins; however, the mechanism involved in this process remains unclear.

Previous studies reported that FFAs act as a bridge between thermodynamically incompatible amylose and protein molecules and that their functional C-terminal region is essential for complex formation [34]. Additionally, the effects of pH and salt treatment suggest that electrostatic interactions between negatively charged carboxyl groups in FFAs and positively charged proteins are the foundation for the self-assembly of complexes used as controlled-release nanocarriers and capable of maintaining the stability and biological activity of hydrophobic substances, as well as increasing their solubility. Although amylose/β-lactoglobulin/FFA nanoparticles have been studied previously, few have focused on the mechanisms associated with the formation of their ternary complex.

MD simulations offer a way to investigate the self-assembly behavior of complex systems, including processes involving micellar formation in aqueous solution. Lee at al. [35] used MD simulations to study the self-assembly of peptide amphiphiles (PAs) into a cylindrical micelle fiber starting from a homogeneous mixture of PAs in water, finding that the PA molecules first formed spherical micelles, followed by

the formation of a 3D network via van der Waals interactions, disappearance of the network, and formation of a fiber with an 800-nm diameter.

To investigate the mechanism associated with encapsulation of paclitaxel encapsulated by COS/SA, Wang et al. [30] performed all-atom MD simulations to analyze the aggregation of COS/SA molecules, revealing that van der Waals and hydrophobic interactions are the major driving forces during the encapsulation process. Additionally, analyses of the radial distribution function and the solvent-accessible surface area indicated that the COS/SA nanoparticles are highly water soluble and that the nanoparticles significantly enhanced the solubility of the hydrophobic drug. Here, we used MD simulations to investigate ternary nanoparticle formation using Gromacs software.

7.3.2.1 Preparation and MD Simulation of Ternary Nanoparticles

Preparation and Imaging by Transmission Electron Microscopy (TEM)

Nanoparticle suspensions were prepared as described in the section "Preparation and Characterization of the Amylose/α-Linoleic Acid/β-Lactoglobulin Triplex." Hot water-extracted amylose supernatant was mixed with a β-lactoglobulin solution (10 mg/mL) and α-linoleic acid, maintaining a weight ratio among the three components of 20:5:1. The mixture was then heated for 20 min in a boiling water bath with continuous stirring at 450 rpm, followed by cooling to room temperature for 4 h.

Purification of the nanoparticle was monitored using HPSEC coupled with multi-angle light scattering (MALS) and refractive index (RI) detectors. The obtained suspension was passed through a 0.45-μm filter and injected (100 μL) into a Sephacryl HR-500 column (GE Healthcare, Piscataway, NJ, USA) with 0.02% sodium azide in purified water as the mobile phase (1.3 mL/min flow rate). Light scattering was performed using a Dawn Heleos-II MALS detector equipped with a 658 nm GaAs laser diode and an OptilabrEx RI detector (Wyatt Technology Corporation, Goleta, CA, USA). Data collection and analysis were performed using Astra software (v5.3.4.10; Wyatt Technology Corporation). Light-scattering data were analyzed by the Zimm method, and a dn/dc value of 1.46 was used to obtain the average molecular weight and the radius of gyration (Rg).

Samples (500 μL) were injected into the HPSEC, and fractions were collected to obtain purified nanoparticles. Imaging analysis was performed, and a 3.5-μL suspension was applied to the carbon-coated grid and vitrified in liquid ethane (−135 °C). The image was magnified 38,000 using a Philips CM200 FEG transmission electron microscope (Philips, Amsterdam, Netherlands).

The Model of the Amylose/β-Lactoglobulin/α-Linoleic Acid Complex

An amylose segment of 55 glucose residues was used to form a sixfold left-handed helix with inner and outer diameters of ~54 nm and 135 nm, respectively, and a length of 738 nm. A β-lactoglobulin segment was used on the basis of the 3D structure

determined by nuclear magnetic resonance analysis (PDB: 1DV9) [36]. We choose the sequence from amino acids 67–101 according to a previous report. A lysine-rich peptide β-lactoglobulin segment was generated using the PRODRG server (http://davapc1.bioch.dundee.ac.uk/prodrg/) [37]. The PDB file for α-linoleic acid was downloaded from http://xray.bmc.uu.Se/hicup/EIC/. The starting structure of α-linoleic acid was generated using the PRODRG server (http://davapc1.bioch.dundee.ac.uk/prodrg/) [37].

Generation of the Force Field

The glucose force field was parameterized according to previously described methods [28, 38], and all simulations were performed using this force field. Due to the differences in glycosidic linkages, the "GLC," "GLM," and "GLK" were used to represent different amylose domains as described previously. "LA" and "LGP" were used to represent α-linoleic acid and β-lactoglobulin peptides, respectively.

MD Simulation Procedure

Gromacs version 4.6.1 was used for MD simulations, which were performed using the leapfrog motion routine, with a 2-fs time step. A total of 250,000,000 simulation steps (for a total simulation time of 500 ns) were performed. The LINCS algorithm was used to constrain all bond lengths (lincs_iter = 1; and lincs_order = 4), and system temperature was set to 100 °C using modified Berendsen thermostat coupling between the different groups, with a relaxation time of 0.1 ps. Pressure was maintained at 1.0 bar, with a relaxation time of 2 ps. Nonbonded interactions were handled using a neighboring grid cell cutoff scheme. Within a short-range neighbor list cutoff of 0.9 nm, interactions were evaluated at every time step based on a pair list. A short-range electrostatic cutoff radius of 0.9 nm and a long-range van der Waals cutoff of 1.4 nm were evaluated simultaneously with each pair-list update [21].

Simulations and Analysis of Ternary Nanoparticles

The ternary nanoparticles consisted of a 55-mer amylose chain, a β-lactoglobulin peptide chain, and α-linoleic acid. The system was embedded in a rectangular box (volume, $10 \times 6 \times 6$ nm^3) and filled with 11,272 water molecules. The behavior of the water molecules was defined using a TIP4P model. The amylose chain was precomplexed with α-linoleic acid or the β-lactoglobulin peptide, which was located near the α-linoleic acid molecule. Because the entire system exhibited a net charge of +4, four chloride ions were added for charge neutralization. The starting structure of the simulation is shown in Fig. 7.20. Simulation and analysis of the model are performed on the Gromacs 4.6.1 software.

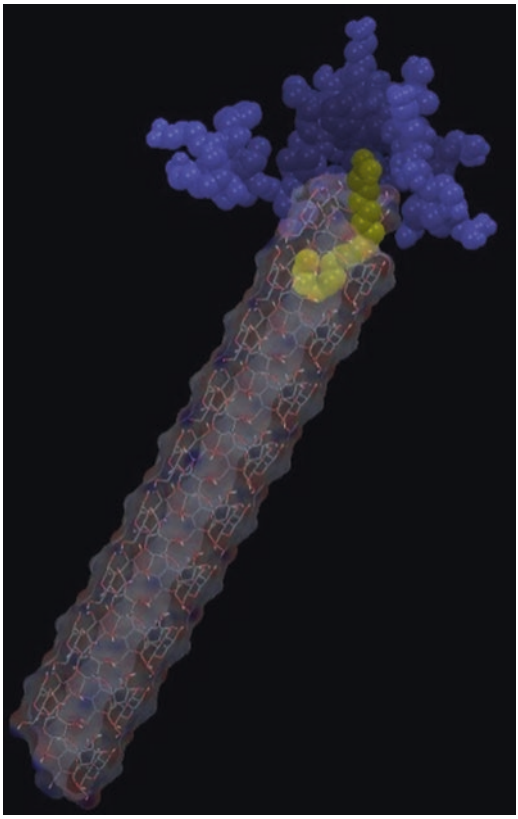

Fig. 7.20 A ternary model of the amylose/β--lactoglobulin/α-linoleic acid complex. The XRD test of the model shows that the head region of the amylose molecule exhibited a typical conformation similar to that observed in the ternary nanoparticle. In the amylose structure, red, white, and blue represent oxygen atoms, carbon atoms, and hydrogen atoms, respectively

Analysis of the Free-Energy Surface Map

The free-energy surface map of the system was fabricated using the RMSD and R (g) values for α-linoleic acid and the main chain of amylose. The RMSD and R (g) values were derived from time points 0, 100, 200, 300, 400, and 500 ns, respectively, following graph generation. Therefore, we derived the 500 N system within the free-energy curve according to a previously described method [39].

7.3.2.2 Transmission Electron Microscopy (TEM) of Ternary Nanoparticles

Figure 7.21a shows the frozen transmission electron microscopic view of the purified nanoparticles, where the dense nanoparticles within the circle represent less embedded and individual nanoparticles. The structure of the nanoparticles on the graphs is different, but when they see the full horizontal field of view, they exhibit uniform morphology and size (rod, width 10 nm, length 40 nm). Although the amylose, protein, and fatty acid self-assembled nanocomposites (Rg20–40 nm) have

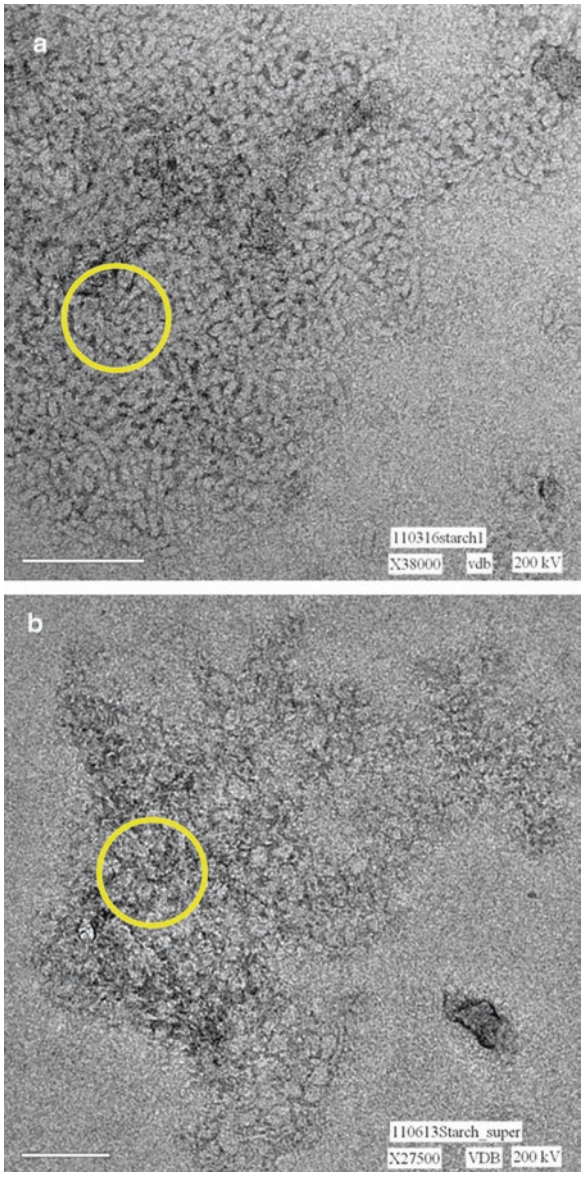

Fig. 7.21 Frozen TEM image. (**a**) Ternary nanoparticles. Discrete and homogeneous rodlike structures within the yellow circle. (**b**) Starch supernatant containing amorphous aggregates. The lower left bar represents 100 nm

been shown in our previous experiments, whether homogeneous nanoparticles are formed by their nonspecific aggregation or self-assembly is not clear. Using frozen transmission electron microscopy, it was found that nanoparticles showed uniform size, a phenomenon that showed a high degree of specific self-assembly conclusion of these macromolecules under specified conditions. Figure 7.21b shows nonspecific aggregation in only amylose solution.

7.3.2.3 Preparation and MD Simulation of Ternary Nanoparticle Formation

We used a 500-ns simulation as a starting point for determining the theoretical conformation of the cylindrical 3D structure (composed of a three-dimensional glucose cylindrical helix structure of six glucose molecules per turn). The basis for the selection of this column structure was as follows: (1) the conformation of amylose in water consists of >100 glucose units, and (2) the structure provided a template for amylose simulation in the complex. This is of great importance to allow elucidation of the role of β-lactoglobulin and α-linoleic acid in the self-assembly of ternary nanoparticles. β-Lactoglobulin and α-linoleic acid were pre-complexed in the presence of amylose. The simulation process covered all atoms.

Figure 7.22a shows a self-assembled snapshot of the ternary nanoparticles after a 500-ns simulation. Substantial reorganization of all structures occurred, resulting in the structure differing significantly from that the cylindrical 3D structure (Fig. 7.20). In the first 100 ns, the LA domain separated from amylose, and at 200 ns, LA again entered amylose from the other side of the molecule, whereas the LGP domain surrounded the LA domain and amylose. At 300 ns, LA was wrapped in a straight chain, and LGP separated from LA and amylose. At 400 ns, LA remained wrapped in the middle of the starch fragment, and LGP was located within close proximity to amylose and LA. At 500 ns, LA remained in its original position, and LGP surrounded LA and amylose, forming a rodlike conformation. This structure was consistent with the nanoparticle map shown in Fig. 7.22a.

(GLC-GLM-GLK), LA, and LGP (Fig. 7.22b) were quantitatively analyzed to assess conformational transformation. The distance between the main chain and LA was reduced from ~3.5 to ~2.5 nm, the distance between the main chain and LGP was reduced from ~5.0 to ~2.0 nm, and the distance between LA and LGP was reduced from ~3.0 to ~2.0 nm. The inter-locus distance trajectory (Fig. 7.22b) showed a turning point at 200 ns relative to the movement of the LA domain in the amylose chain, indicating that LA reentered the amylose spiral structure. The LGP domain was present at 100 ns relative to amylose, and LA moved closest to the LGP domain at the 100-ns time step, followed by increases in distance until 150 ns before approaching one another again at 220 ns. At 500 ns, the distance between the domains increased by 2 nm, indicating that the LA domain was more involved in stabilizing the system relative to the LGP domain. These data indicated that 500 ns was sufficient to reach equilibrium and that the simulated trajectories were consistent with the experimental observations.

7.3.2.4 Hydration Radius of the Ternary System

The hydration radius is a primary feature of interactions within ternary complexes. Changes in the hydration radius of ternary nanoparticles can clarify information concerning the ternary system. Figure 7.23 shows variations in the hydration radius according to simulation time in the aqueous solution. To assess the effects of water

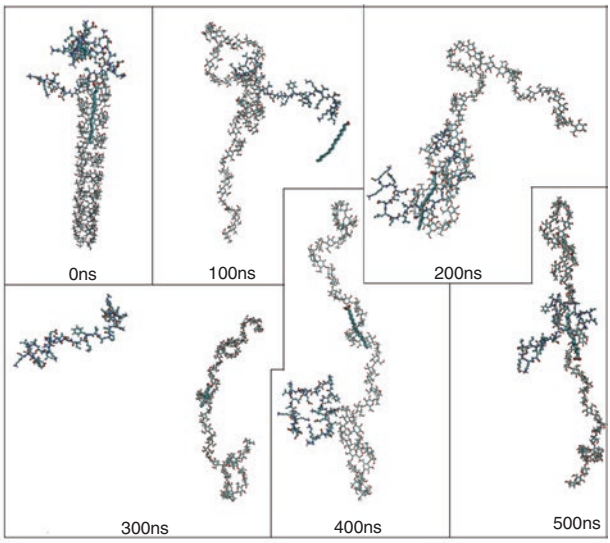

(a)

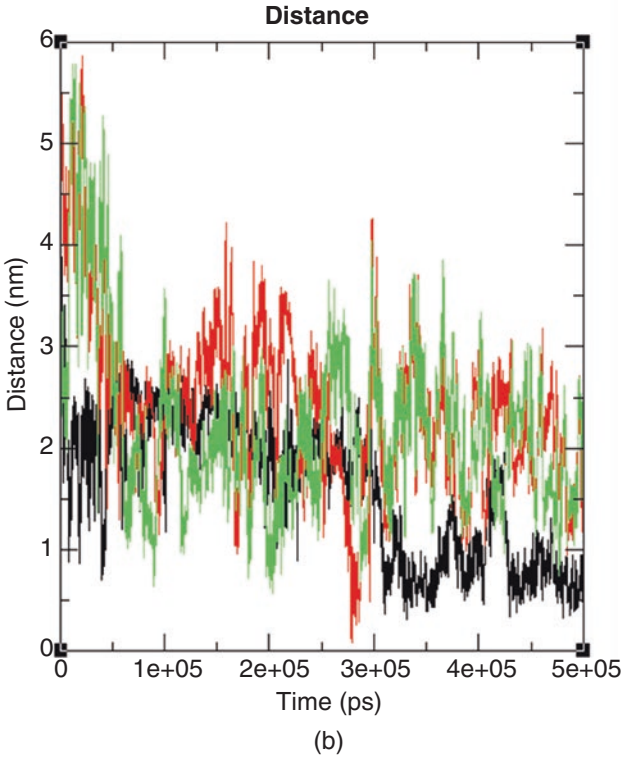

(b)

Fig. 7.22 Conformation changes in the amylose/β-lactoglobulin/α-linoleic acid complex. (**a**) Snapshots of the ternary nanoparticles over a 500-ns MD simulation. (**b**) The distance between the backbone and LA domain (black), the backbone and the LGP domain (red), and the LA and LGP domains (green)

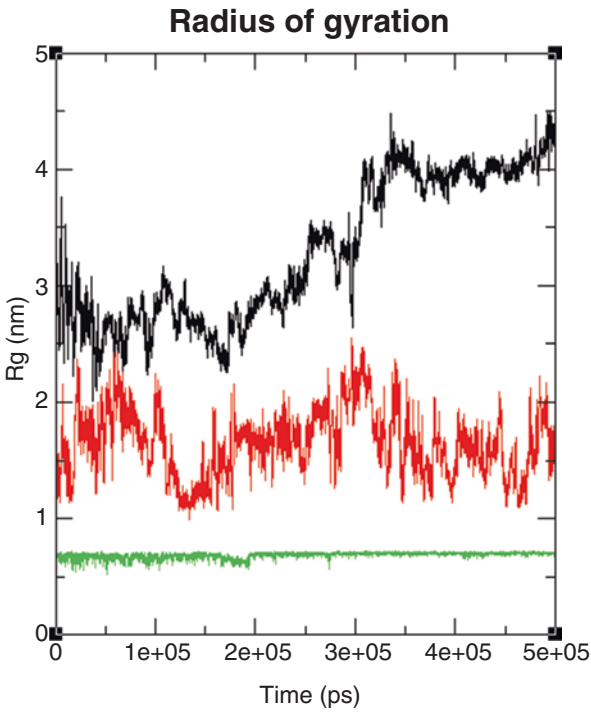

Fig. 7.23 Variations in the hydration radius of the ternary nanoparticle. Black, red, and green curves represent amylose, LGP, and LA, respectively

on the size of the amylose main chain, as well as LGP and LA hydration radii, Fig. 7.23 shows trends for the domains in aqueous solution. The hydration radius of the amylose chain was divided into three stages corresponding to the conformational changes. In the first stage ($0 < t < 200$ ns), the hydration radius in the ternary nanoparticle reduced to its lowest point (Rg = 2.25 nm), possibly due to the separation of LA and LGP from the main chain, thereby resulting in shrinkage of the main chain. The second stage ($200 < t < 350$ ns) indicated greater forces between LA and the main chain relative to that between LA and LGP; therefore, when the main chain came in contact with LA, this resulted in main-chain expansion and gradual increases in the amylose hydration radius to a maximum of 4.13 nm. In the third stage ($350 < t < 500$ ns), the hydration radius of the main chain fluctuated around 4 nm, with no significant changes. During the equilibrium phase, the mean value of the main-chain hydration radius remained at ~4 nm, indicating that the ternary nanoparticle was elongated in water. The experimental results were consistent with the MD self-assembly results in aqueous solution [40].

For the LA domain, the hydration radius did not change from ~0.7 nm, indicating that regardless of simulation time, the LA-domain hydration radius remained unaffected by other domains in the system. This value for the LGP domain was more complex, with a hydration radius between 1.0 and 2.5 nm and possibly related to different conformational changes.

7.3.2.5 The Solvent-Accessible Surface Area of the Ternary Nanoparticle System

The driving force of amylose in aqueous solution is not conducive to the contact between water and hydrophobic groups, whereas the degree of unfavorable contact is approximately proportional to the solvent-accessible surface area. At the beginning of the simulation, the hydrophobic region of the ternary nanoparticle immediately decreased and remained at ~42.5 nm^2. The reason for this change was likely that the ternary structure promoted interactions between the main chain and water molecules. The reduction in hydrophobic surface area affected overall hydrophobicity, thereby releasing the water molecules surrounding this region into the bulk solution (Fig. 7.24).

7.3.2.6 The Free-Energy Surface Map of the Ternary System

Figure 7.25 shows the free energy of the three components during the self-assembly process from the initial state (0 ns) to the final state (500 ns), with a snapshot interval of 100 ns. According to the composition shown in Fig. 7.1, the free energy of the

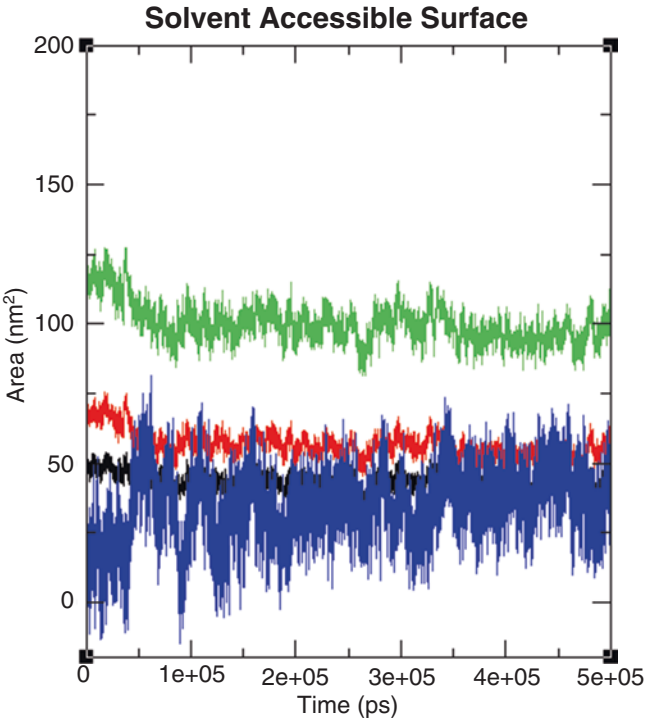

Fig. 7.24 Solvent-accessible surface area of the ternary nanoparticle. Hydrophobic area (black), hydrophilic area (red), total area (green), and ΔGsolv (blue)

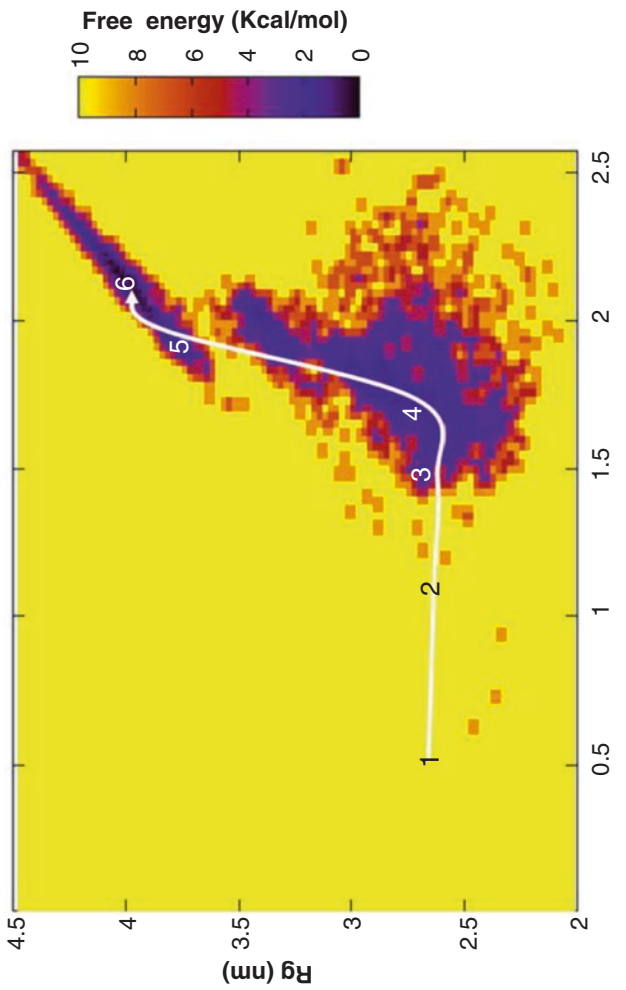

Fig. 7.25 The free energy of the amylose/LGP/LA ternary complex. The numbers represent snapshots of each 100 ns as shown in Fig. 7.22a

initial state at 0 ns (Fig. 7.25, region 1) was 9.8 kcal/mol, which is thermodynamically unfavorable. The free energy in the second region (Fig. 7.25, region 2) rapidly became 7.8 kcal/mol (Fig. 7.25, region 3) and reduced to 5.0 kcal/mol. In the third region (Fig. 7.25, region 3), the composite was separated into amylose main chain LGP and LA domain. At a free energy of 2.1 kcal/mol, LA and amylose were linked, and LGP was separated from the ternary system (Fig. 7.25, region 4), followed by self-assembly of the three components and a further reduction in free energy (Fig. 7.25, region 5). At 500 ns, the free energy was 0.03 kcal/mol (Fig. 7.25, region 6), LA was located in the helical structure of the amylose molecule, and LGP surrounded the LA carboxyl group. The reductions in the free energy following the spontaneous self-assembly of the three components indicated a thermodynamically favorable process. These results were consistent with a previous report [41] and resembled the more stable tetracyclic structure of RNA.

Previous studies described MD simulations of amylose and lipid complexes; however, their durations were generally between 100 and 200 ns, and the amylose fragments contained only 26 glucose residues. Here, out amylose fragments contained twice as many glucose fragments and a longer simulation time. One study focused on complex formation based on time, contacts, and amylose-folding conformation [21]. In the present study, we found that the LA domain altered the conformation of the ternary nanostructure and confined the movement of the amylose main chain to allow formation of a stable complex. These results supported the existence of a stable complex structure and confirmed XRD observations that the ternary complex represents the most stable form.

MD simulations reveal large-scale conformational transformations in ternary structures. Although this these changes occur naturally in amylose alone, the presence of the LA domain was necessary for the formation of a stable helical conformation, which is important for structural stability and establishing a pathway between complex formation and non-conjugation. According to the observed LA-dependent changes in the amylose structure, we speculated that the stable structure between V-amylose and FFA occurs independent of small changes in specific complexation sites and directions. LGP is attracted by LA, thereby increasing nanoparticle stability in this case.

In summary, MD simulations confirmed the importance of dynamic structural changes during stable complex formation of ternary nanoparticles. These results provided valuable insight into the formation of amphipathic ternary nanoparticle structure at the atomic level.

7.4 Applications for Starch-Lipid and Starch-Protein Complexes

7.4.1 Encapsulation of Flavor Compounds

Encapsulation of flavor compounds is an important application of starch complexes. Wulff et al. [42] optimized the formation of helical inclusion compounds of amylose with different typical flavor compounds, most of which were linear or cyclic aldehydes and ketones. There were multiple factors affecting encapsulation efficiency of the guest molecules, including molecular weight, steric structure, and solubility [42, 43]. Heptanol exhibits a typical green odor, with fruity aromas of apple and banana, and is generally used in the manufacture of hard candies. Menthone has a fresh, green, herbal, and minty flavor usually introduced into the production of gum. Therefore, heptanol and menthone were selected as flavor compounds [44].

As the most common method used for preparation of amylose flavor inclusion complexes, the melting method was performed as previously described, with minor modifications [45, 46]. A 10-mL dispersion of amylose solution (0.8%, w/v) was placed in a pressure vessel (20 mL; Parr Instrument Company, Moline, IL, USA) and subsequently heated to 150 °C for 75 min. The temperature was naturally cooled to 80 °C in the vessel, and the contents were transferred to a flask placed in an 80 °C water bath for 15 min prior to flavor compound addition. Dispersed amylose (60 mL) was pipetted into a screw cap test tube containing 60 mg of flavor compound. After vortexing, the mixture was stored in a water bath at 80 °C for 1 h before cooling to room temperature, after which amylose flavor inclusion complexes were maintained at room temperature for 18 h. The wet precipitates were quickly washed with pure anhydrous alcohol and collected after centrifugation at 1700× g for 15 min. The precipitates were then freeze-dried (Freezemobile; Vitris, Warminster, PA, USA). Dispersed amylose in the absence of flavor additive was used as a control.

An XRD analyzer (D8 ADVANCE; Bruker, Karlsruhe, Germany) was used to confirm the amylose flavor inclusion complex formation according to a previously described method [19]. Freeze-dried samples were compressed into disks of 1–2 mm thickness and a diameter of 13 mm. The pressed samples were mounted on a sample holder, and measurements were performed under ambient conditions in transmission mode on a powder diffractometer (X'Pert Pro; Pan Analytical, Almelo, Netherlands) using CuKα radiation (0.154 nm) with 35 mA and 40 kV. A divergence slit of 2 mm and a receiving slit of 1° were selected. A nickel filter was used for detection. The relative intensity was recorded in a scattering-angle range (2θ) of 5–30° using a scintillation counter at a scanning speed of 0.04°/min. Diffractograms were reduced by Fourier filtering.

Well-dispersed potato amylose in the absence of flavor additives served as a reference, and the corresponding XRD patterns are shown in Fig. 7.26. Analysis of amylose yielded an amorphous halo, indicating the absence of the pre-existing complex and retrograde effects. An analysis of both the amylose-menthone and amylose-

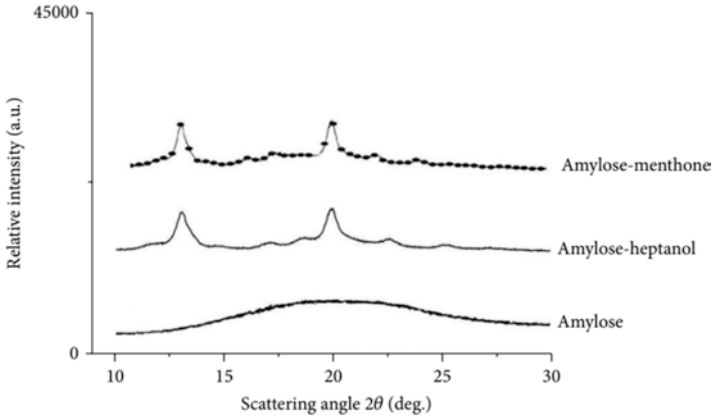

Fig. 7.26 XRD diffractograms of amylose (thick solid line), as well as amylose-menthone (-●-) and amylose-heptanol (thin solid line) complexes

heptanol complexes yielded a typical V6I amylose pattern, with scattering angles (2θ) of 13° and 20° and suggesting the presence of crystal structures of the two complexes. The diffraction diagram was characteristic for a single-amylose helix containing six D-glucose units per turn. It is most likely that the ligand was included in the helix cavity.

Encapsulation efficiency was evaluated using three different analytical methods: TGA, headspace solid-phase microextraction gas chromatography (HS-SPME-GC), and potentiometric titration (PT). For the TGA method, the change in mass varies according to different inclusion complexes. When a secondary factor related to mass loss, such as moisture, is neglected, the difference in weight ratio between the control and the inclusion complex can be regarded as the weight ratio of the included compounds. Therefore, the difference in weight ratio is generally employed to calculate encapsulation efficiency [43, 47]. For HS-SPME-GC, the amylose flavor inclusion compounds are hydrolyzed by α-amylase at an ambient temperature, followed by determination of the flavor released from the amylose helical cavity [42, 45, 48]. For PT, iodine was used as the ligand to form inclusion compounds with amylose. When the spiral cavity is occupied by a guest molecule, iodine is unable to be included into the cavity; therefore, differences in transition values between amylose and amylose in the presence of flavor additives can be compared. Subsequently, the potential transition value is used to calculate the encapsulation efficiency of flavor molecules.

7.4.2 Carriers for Low-Soluble Small Molecules

A range of low-soluble small molecules with efficacious properties relevant to the pharmaceutical and nutraceutical industries are limited in their applications due to poor dispensability and absorption efficiency [49]. There are various ways to

improve these properties, including by physicochemical modifications and the use of emulsions. However, a nanotechnology approach might be the best choice to the improve delivery characteristics of these compounds due to the high dispersion stability or solubility of the nanoparticles [50].

Amylose assembles under specific conditions of shear stress and temperature to form a nanoparticle [33, 34, 51–53]. This involves complexation of amylose and a fatty acid, such as α-linoleic acid, and its electrostatic interaction with a soluble protein [34]. Additionally, amylose can form complexes with low-soluble small molecules through hydrophobic interactions in the lumen of the amylose helix, with the inclusion complexes forming crystals that precipitate [5, 45, 54]. Lui et al [53] showed that soluble food-based nanoparticles contain empty spaces in the lumen of the amylose helix to accommodate low-soluble small molecules.

An example of amylose used as a carrier of low-soluble small molecules [55] involved dilute nanoparticle suspensions prepared as described by Zhang et al. [33], whereby a hot-water-extracted amylose-rich supernatant was mixed with a β-lactoglobulin solution (10 mg/mL) and α-linoleic acid at a weight ratio of 20:2:1. The mixture was then heated for 20 min in a boiling water bath with continuous stirring at 450 rpm, followed by cooling to room temperature for 4 h. Different concentrations of 1-naphthol (1, 2.5, 5, and 10 mM) were added to the nanoparticle suspension, and the mixtures were then heated to 75 °C for 20 min with continuous stirring at 450 rpm to facilitate 1-naphthol incorporation, followed by cooling to room temperature with stirring. The solubility of 1-naphthol and its loaded nanoparticle are shown in Fig. 7.27 and indicate that the self-assembled nanoparticle improved the solubility of the low-soluble small molecules.

7.4.3 An Approach to Improve Bioavailability

Numerous phytochemicals are of great importance in health-related applications; however, their biological activities are limited due to their low bioavailability. The creation of inclusion complexes represents an approach to improving the bioavailability of some bioactive compounds, and ternary nanoparticles consisting of amylose, α-linoleic acid, and β-lactoglobulin could constitute a good choice such complexes. Naringin (4′,5,7-trihydroxyflavanone-7-β-L-rhamnoglucoside-(1,2)-α-D-glucopyranoside), one of the most abundant bioflavonoids in grapefruit juice, is an example of the use of ternary nanoparticles for improving bioavailability [56].

To prepare ternary nanoparticles, dilute nanoparticle suspensions were prepared as previously described [55], with slight modification. Briefly, the water-extracted amylose-rich supernatant was used as the amylose solution for interacting with β-lactoglobulin and α-linoleic acid. Interactions between amylose, α-linoleic acid, and β-lactoglobulin were promoted by adding 10 mg β-lactoglobulin (dissolved in purified water; 10 mg/mL) and 50 mg α-linoleic acid (dissolved in petroleum ether; 10 mg/mL) at a weight ratio of 20:5:1. The mixture was then heated for 20 min in a boiling water bath with continuous stirring at 500 rpm, followed by cooling to room

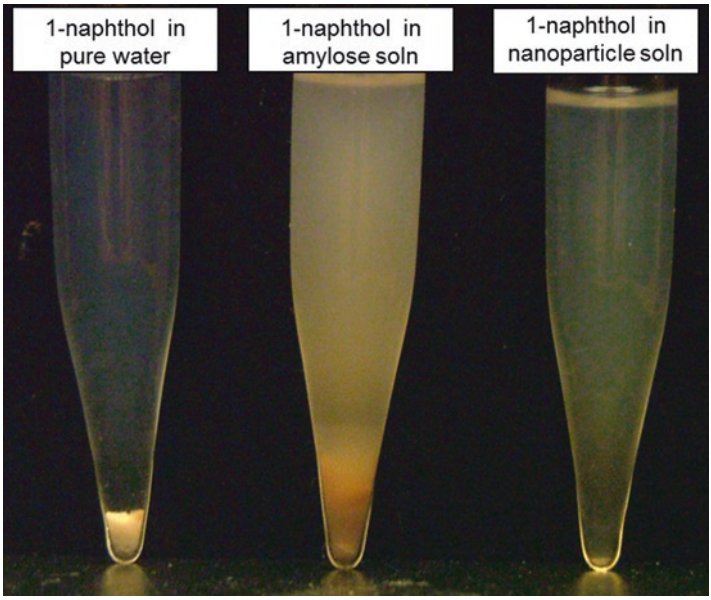

Fig. 7.27 Photograph showing solubility of the 1-naphthol-loaded nanoparticle (right tube) as compared with 1-naphthol in pure water (left tube) and incorporated with amylose (middle tube)

temperature for 4 h. To prepare the ternary nanoparticle-naringin inclusion complex, naringin was dissolved in absolute ethanol (5 mg/mL) and added to suspensions containing the ternary nanoparticle. Subsequently, the mixtures were heated for 20 min at 121 °C, followed by cooling to room temperature with stirring at 500 rpm for 4 h. The mixtures were then filtered through a 0.45-μm microporous membrane, and the supernatant was freeze-dried.

In vitro release of naringin was conducted in simulated gastric fluid (SGF) and simulated intestinal fluid (SIF) to simulate the fate of naringin in the gastrointestinal tract. Based on the release profiles in Fig. 7.28a, the ternary nanoparticle-naringin inclusion complex exhibited a progressive release process as compared with that observed for raw naringin in a gastric environment. After a 3-h incubation, the release rate of raw naringin increased to 80 ± 0.05%, whereas only 16 ± 3.02% of the incorporated naringin molecules was released. Therefore, the ternary nanoparticle-naringin inclusion complex was stable under SGF conditions. The stability of the inclusion complex is also beneficial for decreasing gastrointestinal metabolism [57], and slow release in the stomach is desirable for oral carriers, as it enables additional naringin to be available for intestinal adsorption [58]. Both raw naringin and the ternary nanoparticle-naringin inclusion complex displayed an initial burst release in SIF (Fig. 7.28b). It was hypothesized that the penetration of bile salts and pancreatin caused rapid leakage of the encapsulated compounds [59]. After a 2-h incubation, the release rate of raw naringin and encapsulated naringin increased to 55 ± 2.21% and 43 ± 0.13%, respectively, and improved to 89 ± 3.53%

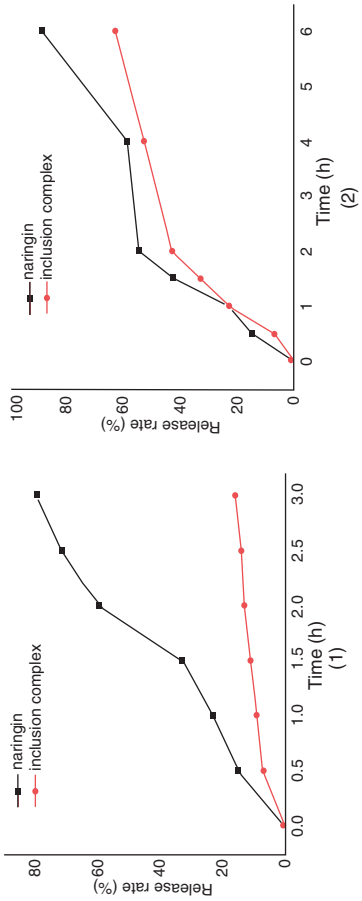

Fig. 7.28 In vitro release of the ternary nanoparticle-naringin inclusion complex in SGF (**a**) and SIF (**b**) as compared with naringin alone

and 63 ± 2.45%, respectively, after 6 h. These results demonstrated that encapsulation of naringin in the ternary nanoparticles contributed to its sustained release.

Delivery of sensitive bioactive ingredients to the colon is another major challenge to the pharmaceutical industry, and the use of enteric coatings is an approach to overcome these challenges [60, 61]. In these studies, the ternary nanoparticle-naringin inclusion complex showed strong release in SIF, allowing additional naringin molecules to be absorbed by the intestine. However, Zhang et al. [62] reported that amylose was susceptible to pancreatic enzyme digestion, leading to inefficient delivery of bioactive ingredients to the colon. However, Dimantov et al. [63] concluded that high-amylose cornstarch in combination with resistant starch considerably improved the resistance of the coating to enzymatic digestion.

In conclusion, amylose in complex with lipids and proteins is of great importance to the protection of bioactive or aromatic compounds by its ability to increase solubility and bioavailability. These findings indicate that starch-lipid and starch-protein complexes have broad applications in the food, cosmetics, and pharmaceutical industries.

References

1. Brisson J, Chanzy H, Winter WT. The crystal and molecular structure of VH amylose by electron diffraction analysis. Int J Biol Macromol. 1991;13(1):31–9.
2. Godet MC, Buléon A, Tran V, Colonna P. Structural features of fatty acid-amylose complexes. Carbohydr Polym. 1993;21(2–3):91–5.
3. Godet MC, Bizot H, Buléon A. Crystallization of amylose-fatty acid complexes prepared with different amylose chain lengths. Carbohydr Polym. 1995;27(1):47–52.
4. Le Bail P, Bizot H, Pontoire B, Buléon A. Polymorphic transitions of amylose-ethanol crystalline complexes induced by moisture exchanges. Starch Stärke. 1995;47(6):229–32.
5. Le Bail P, Rondeau C, Buléon A. Structural investigation of amylose complexes with small ligands: helical conformation, crystalline structure and thermostability. Int J Biol Macromol. 2005;35(1):1–7.
6. Cardoso MB, Putaux JL, Nishiyama Y, Helbert W, Hytch M, Silveira NP, Chanzy H. Single crystals of V-amylose complexed with alpha-naphthol. Biomacromolecules. 2007;8(4):1319–26.
7. Mira I, Persson K, Villwock VK. On the effect of surface active agents and their structure on the temperature-induced changes of normal and waxy wheat starch in aqueous suspension. Part I. Pasting and calorimetric studies. Carbohydr Polym. 2007;68(4):665–78.
8. Lauro M, Poutanen K, Forssell P. Effect of partial gelatinization and lipid addition on α-amylolysis of barley starch granules. Cereal Chem J. 2000;77(5):595–601.
9. Eliasson AC, Carlson TLG, Larsson K. Some effects of starch lipids on the thermal and rheological properties of wheat starch. Starch Stärke. 1981;33(4):130–4.
10. Hoover R, Hadziyev D. Characterization of potato starch and its monoglyceride complexes. Starch Stärke. 1981;33(9):290–300.
11. Helbert W, Chanzy H. Single crystals of V amylose complexed with n-butanol or n-pentanol: structural features and properties. Int J Biol Macromol. 1994;16(4):207–13.
12. Yang Y, Gu Z, Xu H, Li F, Zhang G. Interaction between amylose and beta-cyclodextrin investigated by complexing with conjugated linoleic acid. J Agric Food Chem. 2010;58(9):5620–4.
13. Putaux J-L, Nishiyama Y, Mazeau K, Morin M, Cardoso MB, Chanzy H. Helical conformation in crystalline inclusion complexes of V-amylose: a historical perspective. Macromol Symp. 2011;303(1):1–9.

14. Ades H, Kesselman E, Ungar Y, Shimoni E. Complexation with starch for encapsulation and controlled release of menthone and menthol. LWT Food Sci Technol. 2012;45(2):277–88.
15. Nakamura Y, Yuki K, Park S-Y, Ohya T. Carbohydrate metabolism in the developing endosperm of rice grains. Plant Cell Physiol. 1989;30(6):833–9.
16. Roger P, Colonna P. Molecular weight distribution of amylose fractions obtained by aqueous leaching of corn starch. Int J Biol Macromol. 1996;19(1):51–61.
17. Fertig CC, Podczeck F, Jee RD, Smith MR. Feasibility study for the rapid determination of the amylose content in starch by near-infrared spectroscopy. Eur J Pharm Sci. 2004;21(2–3):155–9.
18. Polaczek E, Starzyk F, Maleńki K, Tomasik P. Inclusion complexes of starches with hydrocarbons. Carbohydr Polym. 2000;43(3):291–7.
19. Nuessli J, Sigg B, Conde-Petit B, Escher F. Characterization of amylose-flavour complexes by DSC and X-ray diffraction. Food Hydrocoll. 1997;11(1):27–34.
20. Tapanapunnitikul O, Chaiseri S, Peterson DG, Thompson DB. Water solubility of flavor compounds influences formation of flavor inclusion complexes from dispersed high-amylose maize starch. J Agric Food Chem. 2008;56(1):220–6.
21. López CA, De Vries AH, Marrink SJ. Amylose folding under the influence of lipids. Carbohydr Res. 2012;364:1–7.
22. Heinemann C, Conde-Petit B, Nuessli J, Escher F. Evidence of starch inclusion complexation with lactones. J Agric Food Chem. 2001;49(3):1370–6.
23. Karkalas J, Ma S, Morrison WR, Pethrick RA. Some factors determining the thermal properties of amylose inclusion complexes with fatty acids. Carbohydr Res. 1995;268(2):233–47.
24. Buléon A, Delage MM, Brisson J, Chanzy H. Single crystals of V amylose complexed with isopropanol and acetone. Int J Biol Macromol. 1990;12(1):25–33.
25. Zabar S, Lesmes U, Katz I, Shimoni E, Bianco-Peled H. Studying different dimensions of amylose–long chain fatty acid complexes: molecular, nano and micro level characteristics. Food Hydrocoll. 2009;23(7):1918–25.
26. Tusch M, Krueger J, Fels G. Structural stability of V-amylose helices in water-DMSO mixtures analyzed by molecular dynamics. J Chem Theory Comput. 2011;7(9):2919–28.
27. Quiñonero D, Tomàs S, Frontera A, Garau C, Ballester P, Costa A, Deyà PM. OPLS all-atom force field for squaramides and squaric acid. Chem Phys Lett. 2001;350(3):331–8.
28. Kony D, Damm W, Stoll S, Van Gunsteren WF. An improved OPLS-AA force field for carbohydrates. J Comput Chem. 2002;23(15):1416–29.
29. Daura X, Gademann K, Jaun B, Seebach D, Vangunsteren WF, Mark AE. Peptide folding: when simulation meets experiment. Angew Chem Int Ed. 1999;38(1–2):236–40.
30. Wang X-Y, Zhang L, Wei X-H, Wang Q. Molecular dynamics of paclitaxel encapsulated by salicylic acid-grafted chitosan oligosaccharide aggregates. Biomaterials. 2013;34(7):1843–51.
31. Fedorov MV, Goodman JM, Kolombet VV, Schumm S, Socorro IM. Conformational changes of trialanine in sodium halide solutions: an in silico study. J Mol Liq. 2009;147(1–2):117–23.
32. Sekhon BS. Food nanotechnology – an overview. Nanotechnol Sci Appl. 2010;3:1–15.
33. Zhang G, Maladen MD, Hamaker BR. Detection of a novel three component complex consisting of starch, protein, and free fatty acids. J Agric Food Chem. 2003;51(9):2801–5.
34. Zhang G, Maladen M, Campanella OH, Hamaker BR. Free fatty acids electronically bridge the self-assembly of a three-component nanocomplex consisting of amylose, protein, and free fatty acids. J Agric Food Chem. 2010;58(16):9164–70.
35. Lee O-S, Cho V, Schatz GC. Modeling the self-assembly of peptide amphiphiles into fibers using coarse-grained molecular dynamics. Nano Lett. 2012;12(9):4907–13.
36. Uhrinova S, Smith MH, Jameson GB, Uhrin D, Sawyer L, Barlow PN. Structural changes accompanying pH-induced dissociation of the beta-lactoglobulin dimer. Biochemistry. 2000;39(13):3565–74.
37. Lemkul JA, Allen WJ, Bevan DR. Practical considerations for building GROMOS-compatible small-molecule topologies. J Chem Inf Model. 2010;50(12):2221–35.

38. Damm W, Frontera A, Tirado-Rives J, Jorgensen WL. OPLS all-atom force field for carbohydrates. J Comput Chem. 1997;18(16):1955–70.
39. Felts AK, Harano Y, Gallicchio E, Levy RM. Free energy surfaces of β-hairpin and α-helical peptides generated by replica exchange molecular dynamics with the AGBNP implicit solvent model. Proteins: Struct Funct Bioinformas. 2004;56(2):310–21.
40. Wang H, Zhang H, Liu C, Yuan S. Coarse-grained molecular dynamics simulation of self-assembly of polyacrylamide and sodium dodecyl sulfate in aqueous solution. J Colloid Interface Sci. 2012;386(1):205–11.
41. Cheng X, Cui G, Hornak V, Simmerling C. Modified replica exchange simulation methods for local structure refinement. J Phys Chem B. 2005;109(16):8220–30.
42. Wulff G, Avgenaki G, Guzmann MSP. Molecular encapsulation of flavours as helical inclusion complexes of amylose. J Cereal Sci. 2005;41(3):239–49.
43. Gunning YM, Gunning PA, Kemsley EK, Parker R, Ring SG, Wilson RH, Blake A. Factors affecting the release of flavor encapsulated in carbohydrate matrixes. J Agric Food Chem. 1999;47(12):5198–205.
44. Feng T, Liu F, Wang X, Zhuang H, Ye R, Rong Z, Liu Y. Evaluation of different analysis methods for the encapsulation efficiency of amylose inclusion compound. Int J Polym Sci. 2015;2015:1–8.
45. Condepetit B, Escher F, Nuessli J. Structural features of starch-flavor complexation in food model systems. Trends Food Sci Technol. 2006;17(5):227–35.
46. Jouquand C, Ducruet V, Bail PL. Formation of amylose complexes with C6-aroma compounds in starch dispersions and its impact on retention. Food Chem. 2006;96(3):461–70.
47. Ozturk S, Koksel H, Kahraman K, Pkw N. Effect of debranching and heat treatments on formation and functional properties of resistant starch from high-amylose corn starches. Eur Food Res Technol. 2009;229(1):115–25.
48. Arvisenet G, Le Bail P, Voilley A, Cayot N. Influence of physicochemical interactions between amylose and aroma compounds on the retention of aroma in food-like matrices. J Agric Food Chem. 2015;50(24):7088.
49. Savjani KT, Gajjar AK, Savjani JK. Drug solubility: importance and enhancement techniques. Isrn Pharm. 2012;2012(3):195727.
50. Meriskoliversidge EM, Liversidge GG. Drug nanoparticles: formulating poorly water-soluble compounds. Toxicol Pathol. 2008;36(1):43.
51. Zhang G, Hamaker BR. Starch-free fatty acid complexation in the presence of whey protein. Carbohydr Polym. 2004;55(4):419–24.
52. Shah A, Zhang G, Hamaker BR, Campanella OH. Rheological properties of a soluble self-assembled complex from starch, protein and free fatty acids. J Food Eng. 2011;105(3):444–52.
53. Liu J, Fei LC, Maladen M, Hamaker BR, Zhang GY. Iodine binding property of a ternary complex consisting of starch, protein, and free fatty acids. Carbohydr Polym. 2009;75(2):351–5.
54. Clays K, Olbrechts G, Munters T, Persoons A, Kim OK, Choi LS. Enhancement of the molecular hyperpolarizability by a supramolecular amylose-dye inclusion complex, studied by hyper-Rayleigh scattering with fluorescence suppression. Chem Phys Lett. 1998;293(5–6):337–42.
55. Bhopatkar D, Tao F, Feng C, Zhang G, Carignano M, Park SH, Zhuang H, Campanella OH, Hamaker BR. Self-assembled nanoparticle of common food constituents that carries a sparingly soluble small molecule. J Agric Food Chem. 2015;63(17):4312.
56. Tao F, Ke W, Liu F, Ran Y, Xiao Z, Zhuang H, Xu Z. Structural characterization and bioavailability of ternary nanoparticles consisting of amylose, α-linoleic acid and β-lactoglobulin complexed with naringin. Int J Biol Macromol. 2017;99:365–74.
57. Wang J, Ma W, Tu P. The mechanism of self-assembled mixed micelles in improving curcumin oral absorption: in vitro and in vivo. Colloids Surf B Biointerfaces. 2015;133:108.
58. Tan C, Xie J, Zhang X, Cai J, Xia S. Polysaccharide-based nanoparticles by chitosan and gum arabic polyelectrolyte complexation as carriers for curcumin. Food Hydrocoll. 2016;57:236–45.

59. Andrieux K, Forte L, Lesieur S, Paternostre M, Ollivon M, Grabielle-Madelmont C. Solubilisation of dipalmitoylphosphatidylcholine bilayers by sodium taurocholate: a model to study the stability of liposomes in the gastrointestinal tract and their mechanism of interaction with a model bile salt. Eur J Pharm Biopharm. 2009;71(2):346.
60. Milojevic S, Newton JM, Cummings JH, Gibson GR, Botham RL, Ring SG, Stockham M, Allwood MC. Amylose as a coating for drug delivery to the colon: preparation and in vitro evaluation using 5-aminosalicylic acid pellets. J Control Release. 1996;38(1):75–84.
61. Nykanen P, Lempaa S, Aaltonen M, Jurjenson H, Veski P, Marvola M. Citric acid as excipient in multiple-unit enteric-coated tablets for targeting drugs on the colon. Int J Pharm. 2001;229(1–2):155–62.
62. Zhang L, Cheng H, Zheng C, Dong F, Man S, Dai Y, Yu P. Structural and release properties of amylose inclusion complexes with ibuprofen. J Drug Deliv Sci Technol. 2016;31:101–7.
63. Dimantov A, Greenberg M, Kesselman E, Shimoni E. Study of high amylose corn starch as food enteric coating in a microcapsule model system. Innov Food Sci Emerg Technol. 2004;5(1):93–100.